CONFORMATIONS OF IMPORTANT HUMAN SERUM APOLIPOPROTEIN SEGMENTS. HIGH RESOLUTION NMR OF APOA-I

by

Guangshun Wang
B.Sc., Yangzhou University, 1985
M.Sc., Chinese Academy of Sciences, 1988

Thesis submitted in partial fulfillment of the requirements
for the degree of Doctor of Philosophy

in the Department of Chemistry and
Institute of Molecular Biology and Biochemistry

SIMON FRASER UNIVERSITY
July 1997

APPROVAL

Name: GUANGSHUN WANG

Degree: Ph.D., Chemistry

Title of Thesis: Conformations of Important Human Serum Apolipoprotein Segments. High Resolution NMR of ApoA-I

Examining Committee:

Chair: Dr. B.M. Pinto, Professor

Dr. R.J. Cushley, Professor
Senior Supervisor

Dr. R.B. Cornell, Associate Professor
Committee Member

Dr. D. Sen, Assistant Professor
Committee Member

Dr. J. L. Thewalt, Assistant Professor
Internal Examiner

Dr. G. Kotovych, Professor
External Examiner
Department of Chemistry
University of Alberta
Edmonton, AB T6G 2G2

Date Approved: July 28, 1997

ABSTRACT

The conformations of the lipid-binding segments from human apoE, apoA-II and apoA-I have been determined by two-dimensional NMR spectroscopy and distance geometry calculations in the presence of sodium dodecyl sulfate (SDS). ApoE(267-289) was found to be a two-domain amphipathic helical structure and apoE(263-286) a curved helix-bend-helix structural motif with a bend angle of ~150°. Enhanced lipid binding of apoE(263-286) compared to apoE(267-289) was attributed to the formation of a second hydrophobic cluster at the N-terminus of the former in addition to the aromatic-aromatic interactions. Thus, aromatic residues and hydrophobic pairs are essential lipid-binding elements in anchoring apolipoproteins to lipid. The lipid binding of apoA-II(18-30) was enhanced by adding a hydrophobic-pair-containing pentamer EWLNS to the C-terminus of the peptide. The structure of apoA-II(18-30)+ in SDS was found to be a class A2 amphipathic helix.

Circular dichroism studies indicate that association of apoA-I(166-185), apoA-I(142-187) and apoA-I(122-187) with SDS or dodecylphosphocholine (DPC) induces a conformational change from random to helical. The lipid binding of apoA-I(142-187) is also suggested by fluorescence spectroscopy. The structure of apoA-I(166-185) is more helical at physiological pH than at acidic pH. Similar class A1 amphipathic helix structures were found for the region 168-182 in SDS, DPC, or lysophosphatidylcholines.

The conformation of apoA-I(142-187) was found to be a curved helix-hinge-helix in either SDS or DPC with all the hydrophobic side chains, on average, on the concave face. The averaged interhelical structure is a half-turn in DPC and a helical bend in SDS. Side chains of M148, H155, Y166, H162, K182, and seven arginines in apoA-I(142-187) showed intermolecular NOEs with SDS, indicating that all of the helix-hinge-helix binds SDS. These NOEs also indicate that cationic side chains in class A amphipathic helices enhance anionic lipid binding. A model is proposed for apoA-I(142-187), wherein the curved peptide structure straddles the micelle.

The helix-hinge-helix motif found in apoA-I(142-187) is retained in apoA-I(122-187), and most likely in intact apoA-I (243 residues) based on peptide-aided signal assignments. Due to the periodicity in the primary sequences, such a peptide-aided signal assignment strategy may be useful for multidimensional NMR studies of exchangeable apolipoproteins.

DEDICATION

To my family,

especially Xia Li and Sophie Wang

ACKNOWLEDGMENTS

I would like to thank my supervisor, Prof. Robert J. Cushley, for his idea of "paddle model", encouragement, guidance, support, and high enthusiasm in apolipoprotein structural determination. Also, I extend my gratitude to my committee members, Drs. R. Cornell and D. Sen, for their comments.

I am greatly indebted to Prof. James T. Sparrow, Baylor College of Medicine, for synthesizing numerous peptides studied in the thesis and invaluable scientific discussions. Thank Dr. R. Anthony Shaw for FT-IR measurements. I also thank Prof. Yves L. Marcel, University of Ottawa Heart Institute, and Dr. Jan Eva Doran, the Swiss Red Cross, for ^{15}N-labeled and unlabeled human apoA-I, respectively.

The author would like to thank Drs. W. Dale Treleaven, Gregory K. Pierens, Alan Tracey, and Mrs. Marcey Tracey for NMR and computing assistance; Dr. Gregory K. Pierens for collecting NMR spectra of apoE(267-289); Dr. Garry W. Buchko for structural calculation and fluorescence spectroscopy of apoA-II(18-31)+ and purification of intact apoA-II by FPLC; Annett Rozek, Rasmus Stojorhann, David G. Naugler, Patrick Chin, Jenny Lum, John C. Cramer, and Dr. Mark Okon in the group for useful discussions, friendship, and routine assistance; David G. Naugler for the MINSQ program to calculate pKa; Dr. Cornell's lab for sharing lipids, and many others for assistance during my research at Simon Fraser University.

Financial support from the grant of the Natural Sciences and Engineering Research Council of Cananda for Dr. Cushley, from Simon Fraser University Graduate Fellowship, and from MacMillan-Bloedel I.M.B.B. Graduate Scholarship is appreciated.

TABLE OF CONTENTS

LIST OF TABLES

LISTS OF FIGURES

ABBREVIATIONS

apoA-I	apolipoprotein A-I
CCA	convex constraint analysis
CD	circular dichroism
cDNA	complementary deoxyribonucleic acid
CMC	critical micelle concentration
CSI	chemical shift index
DMPC	dimyristoylphosphatidylcholine
DPC	dodecylphosphocholine
DQF-COSY	double-quantum filtered correlation spectroscopy
DSS	sodium 2,2-dimethyl-2-silapentane-5-sulfonate
EDTA	ethylenediamine tetraacetic acid
FPLC	fast protein liquid chromatography
FT-IR	Fourier transform infrared
HDL	high density lipoproteins
HMQC	heteronuclear multiple quantum coherence correlation spectroscopy
HPLC	high performance liquid chromatography
LCAT	lecithin-cholesterol acyltransferase
LDL	low density lipoproteins
LP	lipoproteins
LPL	lipoprotein lipase
lysoPC	lysophosphatidylcholines

NMR	nuclear magnetic resonance
NOE	nuclear Overhauser enhancement
NOESY	nuclear Overhauser enhancement spectroscopy
PDB	protein data bank
PFG	pulsed field gradients
ppb/K	ppm × 10^{-3}/degree
ppm	parts per million
rf	radio frequency
RMSD	root mean square deviation
SDS	sodium dodecyl sulfate
SDS-PAGE	SDS-polyacrylamide gel electrophoresis
TFE	trifluoroethanol
TG	triglyceride
TGRL	triglyceride-rich lipoproteins
TMA	tetradecyltrimethyl ammonium chloride
TOCSY	total correlation spectroscopy
UV	ultraviolet
VLDL	very low density lipoproteins
$[\theta]$	mean residue molar ellipticity
τ_m	mixing time in ms in nD NMR experiments

CHAPTER 1: INTRODUCTION

1.1 Lipoproteins

The interest in lipoprotein research originates mainly from the clinical observation that HDL cholesterol levels are negatively correlated with ischemic heart disease whereas LDL cholesterol levels are positively correlated (Miller, 1987). Recently, Luc *et al.* (1997) found that there is a correlation between small LDL and apoA-II-free HDL. The level of apoA-I is correlated well with the plasma HDL cholesterol level (Cheung & Albers, 1977). In addition, apoA-I transgenic mice have much less atherosclerosis susceptibility than the control (Rubin *et al.*, 1991; Breslow, 1996; Castro *et al.*, 1997) and such a protective effect associates only with apoA-I-containing particles (Warden *et al.*, 1993). Thus, it has been proposed that apoA-I be regarded as a more accurate predictor of the risk of heart disease than HDL cholesterol (De Backer *et al.*, 1982).

Human serum lipoproteins are complexes of lipid and proteins. Formation of lipoprotein complexes is the first step in the transport of otherwise water-insoluble lipid between the tissues of human body. The common lipoprotein particles are given in Table 1.1. Note that these particle classes are inhomogeneous. For example, HDL can be further fractionated to HDL_1 (1.063-1.070), HDL_2 (1.070-1.125) and HDL_3 (1.125-1.21 g/mL) due to variations in protein content and protein/lipid ratios (Osborne & Brewer, 1977). HDL_3, one of the smallest HDL particles, contains more protein than HDL_2. HDL has also been divided into LpA-I (particles containing apoA-I without apoA-II) and LpA-I/A-II (particles containing both apoA-I and apoA-II) (Cheung *et al.*, 1987; Nichols, 1990).

The model of HDL was delineated as a spherical particle with a monolayer of phospholipids and cholesterol, and apolipoproteins, on the surface and cholesterol esters and triglycerides in the hydrophobic core (Morrisett *et al.*, 1977; Shen *et al.*, 1977; Edelstein *et al.*, 1979). Other lipoproteins (Table 1.1) share a similar oil-droplet model (Segrest *et al.*, 1994).

Table 1.1: Lipoprotein Properties and Composition[a]

Particles	HDL	LDL	VLDL	Chylomicrons
Density (g/mL)	1.063-1.21	1.019-1.063	0.93-1.006	0.93
Particle size (Å)	50-120	180-250	300-800	750-12,000
Electrophoresis	α-LP	β-LP	pre-β-LP	ω-LP
Composition				
Protein (%)	50	20	10	1
	AI, AII, E	B	AI, B, CI, CII, CIII, E	
Phospholipid	30	24	19	4
Cholesterol	18	45	19	6
TG	5	10	50	90

[a]Gofman *et al.*, 1949; Zubay, 1993; Segrest *et al.*, 1994; Alaupovic, 1996

The protein components of lipoproteins, apolipoproteins, are listed in Table 1.2. Apolipoproteins have been classified into three groups (Pownall & Gotto, 1992; Alaupovic, 1996). The first group is water soluble and exchangeable apolipoproteins (apoA's, C's, and E). Lipid binding of these proteins is proposed to be due to amphipathic helices. The representatives of the second group are apoB. Different from the first group, the repeating proline-rich sequences may be responsible for lipid binding by forming β-sheets (Yang *et al.*, 1986a; Yang and Pownall, 1992). The minor proteins such as apoD constitute the third group. They have no sequence similarity to either the first or second group.

In addition to the major function of lipid transport, apolipoproteins modulate the lipid metabolism by interacting with various lipolysis enzymes and receptors. The metabolism of lipoproteins is complex and there are many excellent reviews on the subject (for example, Nichols, 1990; Barter & Rye, 1996; Barrans *et al.*, 1996).

Table 1.2: Members in the Apolipoprotein Family

Protein name	Molecular weight[a]	Amino acid number[b]	C-terminal 3 residues	Putative function[b]
apoA-I	28,400	243	NTQ[c]	Structural, LCAT+, ligand for HDL receptors, cholesterol efflux+
apoA-II	17,400	2 × 77	ATQ[d]	Structural, hepatic lipase+
apoA-IV	44,500	377	LES[e]	LPL±, LCAT+
apoB-100	512,000	4536	IIL[f,g]	Structural, secretion of VLDL, Ligand for LDL receptor
apoB-48	240,000	2152	YMI[f,g]	Structural, secretion of chyromicrons
apoC-I	6600	57	IDS[h]	LCAT+, removal of TGRL by LDL receptor-related protein-
apoC-II	9000	79	GEE[i]	LPL+
apoC-III	9000	79	VAA[j]	LPL-, uptake of TGRL by liver-
apoC-IV	11200	97	DQD[k]	Not known
apoD	20,000	169	KLS[l]	Not known
apoE	35,000	299	DNH[m]	Ligand for various receptors

[a]Pownall & Gotto, 1992; Segrest *et al.*, 1994; [b]Patsch & Gotto, 1996; [c]Brewer *et al.*, 1978; [d]Brewer *et al.* 1972; [e]Elshourbagy *et al.*, 1986; [f]Yang *et al.*, 1986a; [g]Chen *et al.*, 1986; [h]Shulman *et al.*, 1974; [i]Jackson *et al.*, 1977; [j]Brewer *et al.*, 1974; [k]Zhang *et al.*, 1996; [l]Drayna *et al.*, 1986; Yang *et al.*, 1994; [m]Rall *et al.*, 1982. In the Table, "+" denotes activation or promotion, "-" means inhibition; "±" implies modulation.

Atherosclerosis results from over-accumulation of cholesterol in peripheral cells. This does not occur in healthy people probably due to the benefit of reverse cholesterol transport by HDL (Glomset, 1968). ApoA-I is a potential ligand for HDL receptors, the first of which was characterized by Acton *et al.* (1996). It is also active in promoting cholesterol efflux from peripheral tissues to HDL complexes (Castro *et al.*, 1988; Barkia *et al.*, 1991; Yancey *et al.*, 1995; Zhao *et al.*, 1996). ApoA-I is the principal cofactor of the key enzyme lecithin-cholesterol acyltransferase (LCAT) (Fielding *et al.*, 1972), which esterifies cholesterol. The esterified cholesterol is then transferred from the particle

surface to the core of HDL with the assistance of cholesterol ester transfer protein (CETP) and finally degraded in the liver or recycled. In addition, apoA-I also has other beneficial effects such as inhibiting virus-induced cell fusion (Srinivas *et al.*, 1991; Segrest *et al.*, 1994).

ApoA-II, the second major protein in HDL, has been shown to enhance the activity of hepatic lipase (Jahn *et al.*, 1983; Mowri *et al.*, 1996) but inhibit LCAT activity (Soutar *et al.*, 1975).

Upon association with lipid, apoE and apoB are ligands for the LDL receptor (apoE/B receptor) (Innerarity *et al.*, 1979; for a review on apoE, see Weisgraber, 1994). Also, apoE isoforms are involved in Alzheimer's disease (Poirier *et al.*, 1995; Weisgraber & Mahlay, 1996). Consequently, apoE is another apolipoprotein that plays a crucial role in lipid metabolism.

1.2 Protein structures

The amino acid sequence of a protein is the primary structure. The secondary structure describes the local structure of a peptide chain such as α-helices, turns, and β-strands. The packing of the secondary structural units in space constitutes a tertiary structure of a protein while a quaternary structure results from co-folding of several tertiary structural domains, each folded from a separate peptide chain (Linderström-Lang & Schellman, 1959; Shulz & Schirmer, 1979; Branden & Tooze, 1991).

Anfinsen (1973 and references cited therein) showed that the protein structural information is contained in the amino acid sequence. Prediction of the protein structure based on the amino acid sequence has since been one of the ultimate goals for structural biochemists. The new impetus for the prediction originates from rapid increase of protein sequences deduced from cDNAs. Except for transmembrane α-helical segments, which can be predicted up to an accuracy between 75 and 99.9% (Aloy *et al.*, 1997), the residue predictive accuracy of the secondary structure of globular proteins is 60-75% (Branden & Tooze, 1991; Frishman & Argos, 1997).

1.3 Features of the primary structures of the exchangeable apolipoproteins

ApoA-I, A-II, C-II, C-III, and E share the same genomic structure, namely four exons (expressed gene segments) separated by three introns (silent gene segments), suggesting that they were evolved from a common ancestor (Li *et al.*, 1988). All the mature apolipoproteins, except apoA-IV, are encoded by exon III and exon IV while Exon II encodes the signal peptide and Exon I is one of the non-translated regions. The primary structures of exchangeable apolipoproteins have been deduced by peptide sequencing or from the corresponding nucleic acid sequences (for references, please see the legend of Table 1.2).

```
1     5          10         15         20         25         30         35
DEPPQ SPWDR VKDLA TVYVD VLKDS GRDYV SQFEG (helix 0)
      40         45         50         55         60         65
SALGK QLNLK LLDNW DSVTS TFSKL REQLG P (helix 1)
      70         75         80         85         90         95
VTQE FWDNL EKETE GLRQE MSKDL EEVKA KVQP (helix 2)
100        105        110        115        120
Y LDDFQ KKWQE EMELY RQKVE P (helix 3)
     125        130        135        140
LRAE LQEGA RQKLH ELQEK LSP (helix 4)
 145        150        155        160        165
LG EEMRD RARAH VDALR THLAP (helix 5)
      170        175        180        185
YSDEL RQRLA ARLEA LKENGG (helix 6)
      190        195        200        205
ARLA EYHAK ATEHL STLSE KAKP (helix 7)
210        215        220        225        230        235        240
A LEDLR QGLLP VLESF KVSFL SALEE YTKKL NTQ (helix 8)
```

Fig. 1.1: The primary sequence of human apoA-I (mature) (Brewer *et al.*, 1978). The Brookhaven Protein Data Bank uses the preproapoA-I sequence, which contains additional 24 residues at the N-terminus, which are MKAAVLTLAVLFLTGSQARHFWQQ.

The sequence of apoA-I was first reported by Baker *et al.* (1974) and later by Brewer *et al.* (1978). The Brewer's sequence is consistent with the sequence deduced from cDNA except that Q146Q147 should be E146E147 (Cheung & Chan, 1983; Karathanasis *et al.*, 1983). ApoA-I contains a single polypeptide chain of 243 amino acid residues (Brewer *et al.*, 1978) (Fig. 1.1). The publication of the sequence in 1974 led to

the discovery of the sequence periodicity in apoA-I in 1977 simultaneously by three research groups (McLachlan, 1977; Fitch, 1977; Barker & Dayhoff, 1977). ApoA-I contains 22 amino acid residue repeating units, each consisting of two 11mers. Subsequently, it was found that this is also true of other exchangeable apolipoproteins such as apoA-IV (Elshourbagy *et al.*, 1986; Segrest *et al.*, 1994).

1.4 The amphipathic helix

A significant structural model of apolipoproteins was the amphipathic helix proposed by Segrest *et al.* (1974) based on CD data and model building. An amphipathic helix possesses two distinct faces: hydrophilic and hydrophobic. Amphipathic helices have been grouped into several classes, of which the most important are class A, G*, and Y (Segrest *et al.*, 1990; 1994). The class A helix is characterized by clustering of cationic side chains in the interface separating the hydrophobic and hydrophilic faces. Class A helices can be further categorized into class A1 and A2. One of the major differences between these two classes lies in the content of cationic side chains: mainly lysines in class A2 but arginines in class A1. The class G* helix is characterized by random distribution of cationic side chains on the hydrophilic face. In the class Y helix, cationic side chains are not only located in the interface but also in the center of the hydrophilic face in a pattern resembling a "Y". Fig. 1.2 gives the helical wheel representation (Shiffer and Edmundson, 1967) of typical amphipathic helices from apoA-I, apoA-II and apoE. The amphipathic helical regions in apolipoproteins have been predicted based on hydrophobic moment calculations (Eisenberg *et al.*, 1982) and summarized in Segrest *et al.* (1994). The number of the putative amphipathic helices in apolipoproteins A-I, E, and A-IV was found to determine the particle size and functional properties (Jonas *et al.*, 1993). Proteins with more amphipathic helices tend to form larger particles with lipids.

Brasseur *et al.* (1992) calculated hydrophobic and hydrophilic contour lines around an 18-residue putative helical peptide. The most interesting finding of such calculations is that the putative helices in apoA-I, A-IV, and E have similar hydrophobic (angle pho) and hydrophilic faces (angle phi) whereas the hydrophobic faces in the

helices of apoA-II, C-I, and C-III are larger than the hydrophilic faces. This calculation has been employed to classify amphipathic helices into two groups based on the pho and phi angles. The higher stability of the complexes of apoA-II, C-I, and C-III with lipid may be attributed to larger pho than phi in the amphipathic helices.

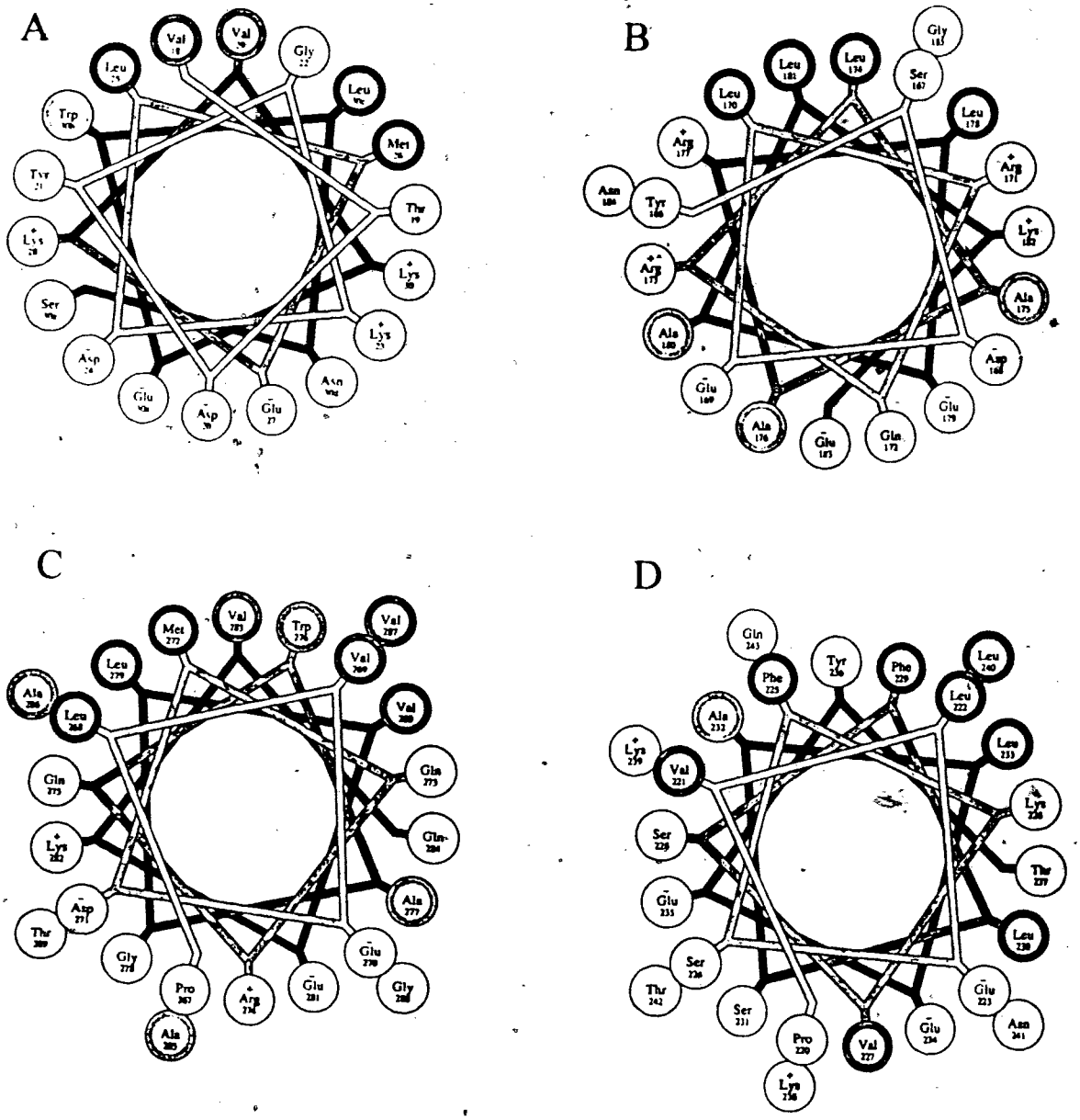

Fig. 1.2: Helical wheel representation of typical amphipathic helices in apolipoproteins. (A) Class A2 helix from apoA-II residues 18-30 plus EWLNS at the C-terminus, (B) class A1 helix from apoA-I corresponding to residues 166-185, (C) class G* helix from apoE residues 267-289, and (D) class Y helix from apoA-I residues 220-243.

1.5 Apolipoprotein peptides and site-directed mutagenesis

Solid-state peptide synthesis plays an important role in testing the amphipathic helix hypothesis and in understanding apolipoproteins because of the flexibility it offers in obtaining protein fragments otherwise unavailable. In addition, some larger peptide fragments can be obtained by selective digestion of the protein chemically or enzymatically. For example, CNBr reacts with three methionines (M86, M112, and M148) in apoA-I and produces two large fragments of 86 and 95 residues, respectively. Using restricted proteolysis, Ji & Jonas (1995) obtained apoA-I(1-192). Another important technique is site-directed mutagenesis, which made available various protein mutants to test either lipid binding or the predicted apolipoprotein structures. A frequent observation is that these protein mutants usually yield complementary information to that deduced from synthetic peptide studies. For example, apoA-I(145-185) was shown to activate LCAT (Sparrow & Gotto, 1980) while deletion of either 143-164 or 165-186 from the protein resulted in reduction of apoA-I ability to activate LCAT by 97-98% (Sorci-Thomas *et al.*, 1993).

1.5.1 Peptides

The first attempt to model the amphipathic helix with small peptides was made by J.T. Sparrow (Sparrow & Gotto,1982 and references cited therein). Two types of peptides have been studied, some corresponding to part of the apolipoprotein sequence and others having no relationship to the protein sequence (*de novo* peptides). The synthetic peptide work on apoA-I, A-II, C-I, C-II, and C-III has been reviewed by Sparrow and Gotto (1982). A summary of the lipid-binding studies on the synthetic peptides of apoE is presented in Section 4.1 of this thesis. These peptide studies indicate that hydrophobicity, peptide chain length, and helix-forming potential are important in lipid binding (Sparrow and Gotto, 1982). Lipoprotein peptides as short as 10-12 residues have been shown to bind lipid (McLean *et al.*, 1991). Note that others have shown that an (ant)agonist dipeptide (Carpenter *et al.*, 1996) or a model tripeptide (O'Neil & Sykes,

1989) interacts with micelles. The lipid affinity of amphipathic helices determines the rates of clearance of the lipid-peptide complexes from testing animals (Pownall *et al.*, 1987; Schmidt *et al.*, 1995).

There have been numerous studies on the function of the interfacial cationic side chains in class A amphipathic helices (Segrest *et al.*, 1994 and the references cited therein). In one set of experiments, the relative position of cationic and acidic side chains in the peptide sequence was switched, leading to a "reversed class A amphipathic helix". The resultant peptide, 18R, showed lower lipid affinity than the original peptide, 18A, designed to mimic a class A amphipathic helix (Kanellis *et al.*, 1980; Anantharamaiah *et al.*, 1985). In another set of experiments, the authors synthesized peptides using lysine analogues with methylene-group deletion. The peptide thus obtained showed lower lipid affinity (Segrest *et al.*, 1992; Mishra *et al.*, 1994). Based on above observations, these authors proposed that cationic side chains enhance lipid binding as epitomized in the snorkel hypothesis (Segrest *et al.*, 1990; 1994). According to this hypothesis, the hydrophobic side chains of the amphipathic helix are buried within the lipid bilayer while the cationic side chains bend by approximately 90° toward the hydrophilic face so as to hydrate the charged amino groups while the hydrophobic moieties of the amphipathic side chains are embedded in the hydrophobic phase (Segrest *et al.*, 1990; Epand *et al.*, 1995).

Various *de novo* amphipathic peptides were designed to study the amphipathic helices in activating LCAT. Pownall *et al.* (1980) showed that lipid-associating peptide LAP-20 activates LCAT although it has no sequence homology with apoA-I. Ponsin *et al.* (1986) found that inserting a proline in the middle of LAP-20 caused a decrease in helicity, lipid binding and LCAT activation. Fukushima *et al.* (1980) reasoned that the penetration depth of an amphipathic helix in lipid may determine the LCAT activation. While reversing the charges of the class A amphipathic helix led to a decrease in both lipid binding and LCAT activation (Segrest *et al.*, 1994), Subbarao *et al.* (1988) demonstrated that a peptide lacking cationic side chains activates LCAT well. Another paper suggests that in the consensus peptide sequence mimicking apoA-I Glu13 is important (Anantharamaiah *et al.*, 1990). Recent peptide analogues designed with fewer

acidic residues on the hydrophilic face were found to promote cholesterol efflux but not to activate LCAT (Labeur *et al.*, 1997). These authors proposed that the acidic residues in the center of the hydrophilic face are critical for LCAT activation.

1.5.2 Site-directed mutagenesis

Site-directed mutagenesis studies have mainly focused on human apoA-I (Minnich *et al.*, 1992; Sorci-Thomas *et al.*, 1993; 1997; Holvoet *et al.*, 1995; Frank *et al.*, 1997). According to Minnich *et al.* (1992), the region from residues 148-186 may be involved in LCAT activation since apoA-I mutants with the deletions Δ(148-186), Δ(212-233), and Δ(212-243) were much less active toward LCAT (0.5%, 28%, and 13% of wild type activation, respectively). Sorci-Thomas *et al.* (1993) have narrowed the 148-186 domain even further showing that deletion of residues 143-164 and 165-186 from apoA-I led to decrease in LCAT activity by 97 and 98%, respectively. Their finding is supported by the work of Holvoet *et al.* (1995). More recently, Sorci-Thomas *et al.* (1997) showed that substitution of residues 143-164 by another copy of residues 220-241 in apoA-I caused a 5-6-fold decrease in LCAT activation. These studies suggest that the middle region of apoA-I is most important in LCAT activation. The same truncation strategy has also been applied to apoA-IV and the LCAT activating domain was located to residues 117-160 (Emmanuel *et al.*, 1994).

1.6 Structural studies of apolipoproteins

Because of the complexity of lipoprotein systems, biochemical and biophysical studies are usually carried out using reproducible, more homogeneous, and well-defined model lipid systems. The most commonly used models include vesicles (or liposomes), emulsions, monolayers, and detergent micelles (for a review, see Jonas, 1992). The detergent micelles have been employed mainly to prepare reconstituted HDL (Jonas, 1986). For the studies using these lipid systems, interested readers are referred to

volumes 128, 129 and 263 in the "Methods in Enzymology" and a monograph on the "Structure and Function of Apolipoproteins" (Rosseneu, 1992).

1.6.1 Low resolution techniques

CD is based on the absorption difference of right- and left-polarized light upon passing through a medium containing chiral molecules such as proteins. It has been the major technique in the studies of the secondary structures of apolipoproteins. The helix content can be estimated from the 222 nm band (Chen *et al.*, 1972; Jackson *et al.*, 1973) or by deconvolution techniques such as convex constraint analysis (Perczel *et al.*, 1991). Almost all exchangeable apolipoproteins become more helical upon association with lipid such as DMPC (Morrisett *et al.*, 1977; Jonas, 1992). For example, the helix content of apoA-I increased from ~50% in aqueous solution to ~70% in DMPC (Morrisett *et al.*, 1977; Wald *et al.*, 1990; Sorci-Thomas *et al.*, 1997). Such observations played a pivotal role in the proposal of the amphipathic helix model (Segrest *et al.*, 1974). Based mainly on CD data, the structure of apoA-I in reconstituted HDL was proposed to contain several helices separated by β-turns (Jonas *et al.*, 1989; Nolte & Atkinson, 1992; for a review, see Brouillette & Anantharamaiah, 1995).

The protein IR band of major interest is the amide I, ranging from 1600 to 1700 cm^{-1}, resulting from C=O stretching vibration coupled with the other atoms in the peptide bond (Elliot & Ambrose, 1950). The most widely used method to extract the structural information from the broad amide I band involves deconvoluting the band into underlying components and then fitting the generated bands to the raw band (Byler & Susi, 1986; Surewicz & Mantsch, 1988; 1996). Based on this approach, Yang *et al.* (1991) found 40% helix and 50% β-structures in apoA-I bound to DMPC, which differs from the secondary structures found by CD (above). In addition, polarized Fourier transform attenuated total reflectance infrared spectroscopy (ATR-IR) was applied to the determination of the orientation of the putative helices of proteins relative to the bilayer of the DMPC discs. The 90° and 0° polarized light absorption difference between the

helical bands of apoA-I/DMPC discs was positive, suggesting that the helices in apoA-I are parallel to the acyl chains (Lins *et al.*, 1992).

1.6.2 High resolution techniques

1.6.2.1 X-ray crystal structures

Lipoproteins, like membrane proteins, are notoriously resistant to crystallization. To date no human apolipoprotein structure has been solved by X-ray diffraction. The structure for the N-terminus of human apoE was determined as a four-helix bundle (Wilson *et al.*, 1991), which has been assessed as a milestone in the understanding of apolipoprotein structures. A similar five-helix bundle structure was reported for apolipophorin-III from *L. migratoria* (Breiter *et al.*, 1991). Also, human apoC-I has been crystallized (Weisgraber *et al.*, 1994) and the structure is expected to appear soon. These structures provide a good basis for the understanding of the solubility, helicity, and aggregation properties of apolipoproteins in aqueous solutions. However, it is not obvious how the helix bundle structure will associate with lipid. It has been proposed that the helix bundle of apolipophorin-III (Breiter *et al.*, 1991) will open in a manner similar to the hinge model, which was proposed for apoA-I to explain the different sizes of HDL particles (Cheung *et al.*, 1987). In such a model, two helices flip by 180° and stick out into solution whereas others remain on the lipoprotein particle (Segrest *et al.*, 1994). Although a similar open mode was also put forward for the apoE bundle structure (Weisgraber, 1994), De Pauw *et al.* (1995) proposed that the long helices (~35 residues) in the bundle may break into two helices of 17 residues each.

1.6.2.2 NMR spectroscopy

Apart from X-ray crystal diffraction, NMR is the only technique that offers high resolution structural details of proteins (Wüthrich, 1986; Clore & Gronenborn, 1989; Cavanagh *et al.*, 1996). In addition, structures of membrane proteins are amenable to

NMR investigation in model lipid systems such as micelles, bicelles, and bilayers (Opella *et al.*, 1997).

1.6.2.2.1 Reconstituted lipoprotein models

As protein signals in biological membranes were too broad to observe (Austin *et al.*, 1975), ^{13}C-, ^{2}H-, ^{31}P-NMR studies of reconstituted lipoproteins focused on lipids (Stoffel *et al.*, 1974; Forrest & Cushley, 1977; Reijngoud *et al.*, 1982; Treleaven *et al.*, 1983; Parmar *et al.*, 1985; Thewalt *et al.*, 1986; 1987; Fenske *et al.*, 1990; Spuhler *et al.*, 1994). These studies indicate that the interactions between zwitterionic phospholipid head groups and apolipoproteins are not significant (Stoffel *et al.*, 1974; Reijngoud *et al.*, 1982) but the acyl chain order of lipids increases by 3-5 fold in reconstituted HDL than in vesicles (Parmar *et al.*, 1985). Spuhler *et al.* (1994) found that the positive moiety of the lipid head group moves toward the water phase presumably due to interactions with cationic side chains. By ^{13}C-labeling lysine side chains of the protein, the conformation of apoA-I or apoE in reconstituted discoidal particles was found to be different from that in spherical particles (Lund-Katz *et al.*, 1988; 1993; Sparks *et al.*, 1992;1993; Paananen *et al.*, 1995).

1.6.2.2.2 Use of lipid micelles to mimic the lipoprotein environments

Small phospholipid unilamellar vesicles (SUV) are large in size (≥ 220 Å) and have correlation time of ~10^{-6} s, thereby not very useful for high resolution NMR studies because of severe line broadening (Brown & Wüthrich, 1977; Feigenson *et al.*, 1977; Opella & Marassi, 1996). Micelles, however, are small enough (~50-60 Å) and have correlation time on the order of 10^{-8} s, giving sharp NMR lines (Brown, 1979; Lauterwein *et al.*, 1979; Brown and Wüthrich, 1981; Gierasch *et al.*, 1982). As a consequence, micelle models, consisting of perdeuterated DPC or SDS, have been extensively employed to study conformations of membrane proteins and peptides (Inagaki *et al.*, 1989; Rizo *et al.*, 1993; Henry and Sykes, 1994; Opella & Marassi, 1996; Dune *et al.*,

1996; Sejbal *et al.*, 1996a; Williams *et al.*, 1996; Opella *et al.*, 1997). The first high resolution NMR studies of apolipoprotein peptides Lycksell *et al.* (1992) and Zhong (1992). The work of Lycksell *et al.* (1992) was carried out on the C-terminal 30 residues of apoC-II in 1,1,1,3,3,3-hexafluoro-2-propanol (HFE) and the NMR structure for the peptide appeared one year later (Öhman *et al.*, 1993). However, organic solvents are not ideal mimicks of lipid environment and HFE and TFE are known to promote helix formation (Nelson & Kallenback, 1989; Macquaire *et al.*, 1993; Luidens *et al.*, 1995; Opella & Marassi, 1996; for a review, see Rajan & Balaram, 1996). The Cushley group was the first to employ perdeuterated micelle models to study apolipoprotein structures by high resolution NMR (Zhong, 1992; Cushley *et al.*, 1994). Using sodium dodecyl sulfate (SDS) and dodecylphosphocholine (DPC), the group has recently determined the structures of synthetic peptides from human apoC-I (Rozek *et al.*, 1995, 1997), apoE (Wang *et al.*, 1996a), apoA-II (Buchko *et al.*, 1996a), and apoA-I (Wang *et al.*, 1996b; 1997b). In addition, high resolution NMR spectra of intact apoA-II (collected in 1993, see Chapter 8), apoC-I (Rozek *et al.*, 1996), apoA-I (Wang *et al.*, 1997a,b), and apoC-III (Buchko *et al.*, 1997) have been obtained in SDS or DPC. A preliminary structure for apoC-I has been reported (Rozek *et al.*, 1996).

In the thesis, 2D NMR, CD, fluorescence, and FT-IR are used to investigate the conformations of apolipoprotein segments from apoA-I, apoA-II, and apoE in lipid-mimetic environments such as SDS, DPC, and lysophosphatidylcholines (lysoPC). The chemical structures of these model lipids are given below:

SDS $CH_3(CH_2)_{11}OSO_3^-Na^+$

DPC $CH_3(CH_2)_{11}OPO_3^-CH_2CH_2N^+(CH_3)_3$

LysoPC $CH_3(CH_2)_nC{=}OOCH_2\text{-}CH(OH)\text{-}CH_2OPO_3^-CH_2CH_2N^+(CH_3)_3$

Where n = 14 or 16. These lipids or detergents have the potential to form micelles. For properties of DPC and SDS, please refer to Wang *et al.* (1997b).

Chapter 2: THEORY

2.1 Introduction

In this chapter, we will first cover some basic principles necessary to understand the 2D NMR experiments employed in the thesis and then describe the procedure for protein structure determination. Exhaustive treatises on NMR theory can be found in several monographs (Abragam, 1961; Ernst *et al.*, 1987; Poole & Farach, 1987; Friebolin, 1991; van de Ven, 1995). There are also several books dealing with biomolecules in general or protein structure determination in particular (Dwek, 1973; Jardetzky & Roberts, 1981; Wüthrich, 1986; Evans *et al.*, 1995; Cavanagh *et al.*, 1996). The book by Wüthrich (1986) summarizes the protein structure elucidation by 2D NMR while the book by Cavanagh *et al.* (1996) emphasizes the theory and practice of homonuclear and heteronuclear multidimensional NMR of proteins. Crippen and Havel (1988) have written the mathematics for distance geometry and its use in molecular conformation calculation.

2.2 Nuclear magnetic resonance

Nuclear magnetic resonance (NMR), established in 1945 by F. Bloch at Stanford and E.M. Purcell at Harvard, is a technique based on the Zeeman splitting of a nucleus (spin quantum number $I \neq 0$) in the magnetic field into $(2I + 1)$ different energy states and the transition of spins between the states determined by the selection rule (magnetic quantum number $\Delta m = \pm 1$) when irradiated by B_1 at the resonance frequency. Thus, the NMR equation is:

$$\Delta E = h\nu = h\gamma B(1-\sigma)/2\pi, \qquad (2.1)$$

where ΔE is the energy resulting from the interaction between the magnetic field and the nucleus, ν is the resonance frequency where transition occurs, γ is the gyromagnetic ratio of the nucleus, B is the magnetic field, and σ is the shielding constant, which depends on

the chemical environment in which a nucleus is located. NMR is an insensitive spectroscopy since the population difference in the two states of interest is very small (1 in 10^4-10^6) obeying the Boltzmann distribution. As ΔE is proportional to the magnetic field, both sensitivity and resolution increase with increase of the field strength. Another important approach to increase sensitivity is isotope enrichment of nuclei of low natural abundance such as ^{13}C and ^{15}N.

2.2.1 The Bloch vector model and relaxation mechanisms

2.2.1.1 The classical description

The spin angular momentum of a nucleus is a vector quantity with both direction and magnitude quantized. A spin-1/2 nucleus (I = 1/2) such as ^1H, ^{13}C, ^{15}N, and ^{31}P adopts two orientations in the magnetic field: parallel (+ 1/2) or antiparallel (- 1/2). The net population difference of an ensemble of these spins, or macroscopic magnetization, can be expressed by a vector, normally placed along the z-axis (Fig. 2.1, left). The vector can be tilted by a 90° rf pulse, B_1 (Fig. 2.1, right). The evolution of the magnetization in the statie magnetic field (B_0) can be described by the Bloch equations (Bloch, 1946):

$$\begin{aligned} dM_z/dt &= -\gamma(M_x B_1 \sin\omega t + M_y B_1 \cos\omega t) - (M_z - M_0)/T_1 \\ dM_y/dt &= \gamma(M_z B_1 \cos\omega t - M_x B_0] - M_y/T_2 \\ dM_x/dt &= \gamma(M_z B_1 \sin\omega t + M_y B_0) - M_x/T_2, \end{aligned} \qquad (2.2)$$

where M_i is the i axis magnetization at time t, M_0 is the initial M_z magnetization at the equilibrium state, T_1 is the longitudinal relaxation time, and T_2 is the transverse relaxation time. The first term in above equations on the right describes the motion of the magnetization due to interaction with the magnetic field. The magnetization precesses at the Larmor frequency ($\omega = 2\pi\nu$) and induces a current in the receiving coil, namely the NMR signal. Such a process can be repeated n times after re-establishment, at least partially, of the Boltzmann distribution to improve the signal to noise ratio by the square root of n (Jardetzky *et al.*, 1963).

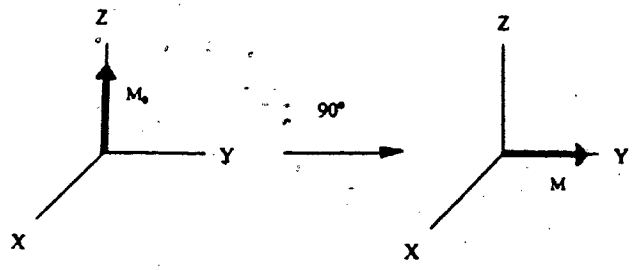

Fig. 2.1: Vector model description of 1D NMR. In the rotating frame, the initial magnetization, M_0, along the z axis is flipped to the y axis by a 90° pulse applied along x axis.

2.2.1.2 Relaxation mechanisms

The second term on the right of Eq. 2.5 assumes an exponential decay of the magnetization with time, that is, magnetization relaxation. The time required for the magnetization to relax along the z axis to the equilibrium state is called T_1, the spin-lattice relaxation time. Similarly, the time measuring the decay of magnetization in the xy plane is called T_2, the spin-spin relaxation time. The corresponding relaxation rates are $R_1 = 1/T_1$ and $R_2 = 1/T_2$. The perturbed spin system will resume the Boltzmann equilibrium state at R_1. Neglecting the effect of the rf field, the total Hamitonian of the system contains the following terms:

$$H = H_Z + H_{DD} + H_{CS} + H_J + H_Q + H_O, \qquad (2.3)$$

where H_Z is the Zeeman term, describing the interaction between the magnetic field and the nucleus, H_{DD} is the dipole-dipole interaction, H_{CS} is the chemical shift anisotropic effect, H_J is the spin-spin coupling interaction, H_Q is the quadrupolar interaction, and H_O is other interactions. The total relaxation rate (R) is a sum of the relaxation rates owing to these interactions (Eq. 2.3), i.e.,

$$R = \Sigma R_i \qquad (2.4)$$

The relaxation is most efficient when the frequency of the fluctuating local field matches the appropriate Larmor frequency as depicted in Eq. 2.1. Thus, electronic motions and

molecular vibrations are unimportant whereas Brownian motion (rotational and diffusional) is efficient. The fluctuating local fields have different effects on R_1 and R_2. Any of such fields can be decomposed into three principal components, e.g.,

$$B_{loc} = iB_x + jB_y + kB_z. \quad (2.5)$$

R_1 by definition depends only on the k component whereas R_2 is influenced by both i and j components. In general, the spectral density function describing the nuclear relaxation due to Brownian motion has the form (Shaw, 1984):

$$R_1 = B_{loc}^2[C_1\tau_c/(1 + \omega^2\tau_c^2)] \quad (2.6)$$

$$R_2 = B_{loc}^2[C_2\tau_c + C_3\tau_c/(1 + \omega^2\tau_c^2)], \quad (2.7)$$

where τ_c is the correlation time that measures the time required for the molecule to tumble around by 1 radian. For spherical proteins the isotropic rotational τ_c can be estimated from the Stokes-Einstein Law:

$$\tau_c = \eta V/(kT), \quad (2.8)$$

where η is the viscosity of the solvent, V is the volume of the protein molecule, k is the Boltzmann's constant, and T is the absolute temperature in K.

2.2.1.2.1 Dipolar relaxation

Dipole-dipole interactions are the predominant relaxation mechanism for spin-1/2 nuclei. For a spin pair I = S = 1/2, the local fluctuating field (B_{loc}) that causes relaxation is

$$B_{loc}^2 = (h\gamma_I\gamma_S/2\pi)^2 I(I + 1)/r^6_{IS}. \quad (2.9)$$

Therefore, dipole-dipole relaxation is influenced by gyromagnetic ratios, the distance between nuclei I and S (r_{IS}), and the spectral density function (Eqs. 2.6 & 2.7) (Shaw, 1984).

2.2.1.2.2 Chemical shift anisotropy

Motion of electrons in the molecules generates different local fields. Due to anisotropy, the local fields vary with the molecular reorientation in solution, that is,

$$B_{loc}^2 = \gamma^2 B^2 (\sigma_p - \sigma_\perp)^2 \qquad (2.10)$$

where σ_p and $\sigma_\perp$ are the parallel and perpendicular components of the chemical shift tensor, respectively (Shaw, 1984). Such a chemical shift anisotropy (CSA) is more pronounced for nuclei with larger chemical shift ranges such as ^{13}C, ^{15}N, and ^{31}P, especially at higher magnetic field (Eq. 2.10). For protons, spin relaxation due to CSA is negligible.

2.2.1.2.3 Scalar spin-spin coupling

The J-related coupling provides a fluctuating magnetic field, which is

$$B_{loc}^2 = 2/3S(S + 1)\pi^2 J^2 \qquad (2.11)$$

This mechanism depends on the properties of bonded nucleus. It is most efficient when chemical exchange is fast (the first kind) or the lifetime for the excited state of the nucleus is short (the second kind) (Abragam, 1961; Shaw, 1984).

2.2.2 Building blocks of multidimensional NMR

Two-dimensional NMR was discovered by exploiting the time domain (Ernst *et al.*, 1996). The information in the time domain can be extracted by a combination of pulses and time delays followed by detection. Fig. 2.2 gives the basic pulse sequences for 1D, 2D, 3D, and nD experiments. A multidimensional NMR experiment is composed of four building blocks: excitation, evolution, mixing, and detection. There is no evolution and mixing unit in 1D NMR experiments. Two-dimensional experiments contain one such unit whereas 3D NMR experiments contain two such units.

1D:

$$\mathbf{D\text{-}P_1\text{-}Acq\ (t_1)}$$

2D:

$$\mathbf{D\text{-}P_1\text{-}t_1\text{-}P_2\text{-}\tau_1\text{-}P_3\text{-}Acq\ (t_2)}$$

3D:

$$\mathbf{D\text{-}P_1\text{-}t_1\text{-}P_2\text{-}\tau_1\text{-}P_3\text{-}t_2\text{-}P_4\text{-}\tau_2\text{-}P_5\text{-}Acq\ (t_3)}$$

nD:

$$\mathbf{D\text{-}P_1\text{-}\{t_i\text{-}P_j\text{-}\tau_i\text{-}P_k\}_{(n-1)}\text{-}Acq\ (t_n)}$$

Fig. 2.2: Pulse sequences for multidimensional NMR experiments. In the Figure, D = relaxation delay in sec; P_j = pulse j (j can also stand for the flip angle); τ_i is the mixing time in ms, for example, in NOESY. It can be zero, for example, in COSY; Acq = acquisition time; t_i = incremental time delay. Four-dimensional NMR has been performed (Kay *et al.*, 1990; Clore *et al.*, 1991).

2.2.3 Density matrix description

In quantum mechanics, the state of a system can be expressed either by the wave function $\Psi(t)$ (Lowe, 1993) or by the density operator $\rho(t)$ (Poole & Farach, 1987). The time evolution of density operators can be described by the Liouville-von Newmann equation or density operator equation:

$$d\rho/dt = -i[\mathcal{H}(t), \rho(t)], \qquad (2.12)$$

where $\mathcal{H}$ is the reduced (divided by $\hbar/2\pi$) total energy Hamitonian of the system. Assuming $\mathcal{H}$ is time-independent, the solution to Eq. 2.12 is simply

$$\rho(t) = \exp(-i\mathcal{H}t)\ \rho(0)\ \exp(i\mathcal{H}t), \qquad (2.13)$$

where $\rho(0)$ is the initial density operator. For example, the Hamitonian is $\mathcal{H} = B\gamma I_z$ for a single spin system. The density operator description of the 1D pulse in Fig. 2.2 at different stages is given below (van de Ven, 1995; Cavanagh *et al.*, 1996).

At the thermal equilibrium state:

$$\rho_0 = \mathbf{I}_z \qquad (2.14)$$

After the 90° pulse applied along x:

$$\rho_1 = \exp(-i\omega \mathbf{I}_x t_1)\, \rho_0 \exp(i\omega \mathbf{I}_x t_1)$$

$$= \exp(-i\pi/2\mathbf{I}_x)\, \mathbf{I}_z \exp(i\pi/2\mathbf{I}_x) = \mathbf{I}_z \cos 90° - \mathbf{I}_y \sin 90° = -\mathbf{I}_y \qquad (2.15)$$

The last line in Eq. 2.15 is true because of the commutation $[\mathbf{I}_x, \mathbf{I}_y] = i\mathbf{I}_z$. Similarly, the density matrix for a 2D COSY pulse sequence (Fig. 2.2, 2D, where $\tau = P_3 = 0$) is

$$\rho(t) = \exp(-i\mathcal{H}_4 t_2) \exp(-i\mathcal{H}_3 P_2) \exp(-i\mathcal{H}_2 t_1) \exp(-i(\mathcal{H}_1 P_1) \times$$

$$\rho_0 \exp(i\mathcal{H}_1 P_1) \exp(i\mathcal{H}_2 t_1) \exp(i\mathcal{H}_3 P_2) \exp(i\mathcal{H}_4 t_2), \qquad (2.16)$$

where P_1 and P_2 are the pulse lengths in μs for the two 90° pulses and t_1 and t_2 are the two time delays. From the derived density operator $\rho(t)$, the expectation value for the observable is calculated by finding the trace of the matrix product of the observable operator $\mathbf{I}_y$ and the density operator, namely

$$\langle I_y \rangle = \mathrm{tr}\{\mathbf{I}_y \rho(t)\}. \qquad (2.17)$$

Once the matrix has been calculated, the trace is the sum of the diagonal terms.

2.2.4 Product operator formalism

The density matrix calculation is tedious and not very informative in understanding pulse sequences. Therefore, a simplified notion called product operator formalism was proposed (Sørensen *et al.*, 1983; Ernst *et al.*, 1987). In this formalism, the density matrix is decomposed into a set of basis operators. The coefficients for the basis operators are directly proportional to the expectation value of the observable quantity. As the matrix size for N spins with quantum number I = S = 1/2 is $2^N \times 2^N$, a two spin system can be expressed by linear combination of 16 basis operators:

$$1/2E \text{ (E = unitary operator)},$$

$$I_x, I_y, I_z, S_x, S_y, S_z \qquad (2.18)$$

$$2I_xS_x, 2I_xS_y, 2I_xS_z, 2I_yS_x, 2I_yS_y, 2I_yS_z, 2I_zS_x, 2I_zS_y, 2I_zS_z$$

The effects of pulses, chemical shifts, and spin couplings on the operators are easy to follow since the transformations obey the right-hand rule. In the right-hand rule, let the thumb co-phase with the direction along which the pulse is applied. The rotational

direction of the operator (as if it were a vector) corresponds to the direction the other four fingers are pointing at.

2.2.4.1 Pulses

The Hamitonian for a pulse of phase x can be expressed as $H = \beta I_x$, where β is the flip angle of the pulse. The transformation of I_z by β-pulse is

$$I_z \rightarrow I_z\cos\beta - I_y\sin\beta. \qquad (2.19a)$$

Similarly, the transformation of I_z by a $-I_y$ pulse of the same flip angle is $I_z \rightarrow I_z\cos\beta - I_x\sin\beta$. A pulse along the i axis (i = x, y, and z) does not affect the operator along the same axis.

2.2.4.2 Chemical shifts

The Hamitonian of a chemical shift has the form $H = \Omega I_z$. The magnetization evolves as follows:

$$I_x \rightarrow I_x\cos(\Omega t) + I_y\sin(\Omega t);$$
$$I_y \rightarrow I_y\cos(\Omega t) - I_x\sin(\Omega t)$$
$$I_z \rightarrow I_z \qquad (2.19b)$$

2.2.4.3 Spin coupling

The Hamitonian for evolution under a spin coupling is $H = 2\pi J I_z S_z$. Hence, the operators I_x, I_y, and I_z will evolve according to the following equations:

$$I_x \rightarrow I_x\cos(\pi Jt) + 2I_yS_z\sin(\pi Jt);$$
$$I_y \rightarrow I_y\cos(\pi Jt) - 2I_xS_z\sin(\pi Jt);$$
$$I_z \rightarrow I_z. \qquad (2.19c)$$

The second term, e.g., $2I_yS_z\sin(\pi Jt)$ will further evolve and contain forbidden higher quantum coherences. Thus, it is a key step for multiple-quantum coherence experiments such as DQF-COSY and HMQC.

2.2.5 Product operator description of 2D NMR

Assuming a two-spin system with spin 1/2, the operator evolution of the two spins (I-S, chemical shifts Ω_I and Ω_S with a weak coupling constant of J, neglecting relaxation) is identical and here only the change of I_z will be followed. Refer to the 2D pulse sequence in Fig. 2.2. Let us start from the equilibium state with initial operator of I_z.

a. After $90°_x$ pulse

$$I_z \rightarrow -I_y \qquad (2.20a)$$

b. During t_1 the magnetization corresponding to the $-I_y$ operator evolves under both the chemical shift (Ω_I) and spin coupling (Eq. 2.19, b & c) and leads to four terms

$$-I_y\cos(\Omega_I t_1)\cos(\pi Jt_1) + 2I_xS_z\cos(\Omega_I t_1)\sin(\pi Jt_1)$$
$$+ I_x\sin(\Omega_I t_1)\cos(\pi Jt_1) + 2I_yS_z\sin(\Omega_I t_1)\sin(\pi Jt_1). \qquad (2.20b)$$

c. After the second $90°_x$ pulse, we have

$$-I_z\cos(\Omega_I t_1)\cos(\pi Jt_1) - 2I_xS_y\cos(\Omega_I t_1)\sin(\pi Jt_1)$$
$$+ I_x\sin(\Omega_I t_1)\cos(\pi Jt_1) - 2I_zS_y\sin(\Omega_I t_1)\sin(\pi Jt_1). \qquad (2.20c)$$

For **COSY**, $P_1 = P_2 = 90°$ and $\tau_1 = P_3 = 0$ in the 2D sequence in Fig. 2.2. Only terms 3 and 4 in Eq. 2.19c will further evolve into observable magnetization during acquisition time t_2 under the chemical shifts and J (Eq. 2.19, b & c):

$$\text{term 3: } \underline{I_x\sin(\Omega_I t_1)\cos(\pi Jt_1)\cos(\Omega_I t_2)\cos(\pi Jt_2)} + 2I_yS_z\sin(\Omega_I t_1)\cos(\pi Jt_1)\cos(\Omega_I t_2)\sin(\pi Jt_2)$$
$$+ \underline{I_y\sin(\Omega_I t_1)\cos(\pi Jt_1)\sin(\Omega_I t_2)\cos(\pi Jt_2)} - 2I_xS_z\sin(\Omega_I t_1)\cos(\pi Jt_1)\sin(\Omega_I t_2)\sin(\pi Jt_2). \qquad (2.21)$$

term 4: $-2I_zS_y\sin(\Omega_I t_1)\sin(\pi Jt_1)\cos(\Omega_S t_2)\cos(\pi Jt_2) + \underline{S_x\sin(\Omega_I t_1)\sin(\pi Jt_1)\cos(\Omega_S t_2)\sin(\pi Jt_2)}$

$+ 2I_zS_x\sin(\Omega_I t_1)\sin(\pi Jt_1)\sin(\Omega_S t_2)\cos(\pi Jt_2) - \underline{S_y\sin(\Omega_I t_1)\sin(\pi Jt_1)\sin(\Omega_S t_2)\sin(\pi Jt_2).}$

(2.22)

The underlined terms in Eq. 2.21 give diagonal peaks as seen from the same chemical shift at (Ω_I, Ω_I). The underlined terms in Eq. 2.22 lead to off-diagonal cross peaks at (Ω_I, Ω_S). The fine structure of the cross peaks due to the coupling between spins I and S becomes evident by performing the following trigonometric conversions

$$\sin(\Omega_I t_1)\cos(\pi Jt_1) = 1/2[\sin(\Omega_I t_1 - \pi Jt_1) + \sin(\Omega_I t_1 + \pi Jt_1)] \qquad (2.23)$$

and

$$\sin(\Omega_I t_1)\sin(\pi Jt_1) = 1/2[\cos(\Omega_I t_1 - \pi Jt_1) - \cos(\Omega_I t_1 + \pi Jt_1)]. \qquad (2.24)$$

Hence, cross peaks have anti-phase line shape (Eq. 2.24) while diagonal peaks are in phase (Eq. 2.23).

For **DQF-COSY** (Rance *et al.*, 1983), $P_1 = P_2 = P_3 = 90°$ and τ_1 = very short delay in the 2D sequence in Fig. 2.2. Only term 2, $-2I_xS_y\cos(\Omega_I t_1)\sin(\pi Jt_1)$, in Eq. 2.20c will be chosen. This term is the superimposition of the double quantum (DQ) and zero-quantum (ZQ) coherences, namely,

$$-2I_xS_y = -2I_{1x}S_{2y} = -1/2[(2I_{1x}S_{2y} + 2I_{1y}S_{2x}) + (2I_{1x}S_{2y} - 2I_{1y}S_{2x})]$$
$$= DQ + ZQ. \qquad (2.25)$$

The first double quantum term above is chosen by phase cycling. The last $90°_x$ pulse will generate $-1/2[(2I_{1x}S_{2z} + 2I_{1z}S_{2x})\cos(\Omega_I t_1)\sin(\pi Jt_1)$. Further evolution of I_{1x} and S_{2x} leads to diagonal and cross peaks, respectively. Both are antiphase cross peaks. Therefore, DQF-COSY does not have the problem of COSY, where phasing of cross peaks leads to dispersive diagonal peaks, which blur cross peaks there.

In an **NOESY** experiment (Jeener *et al.*, 1979), $P_1 = P_2 = P_3 = 90°$ and τ_1 = mixing time in ms in the 2D sequence in Fig. 2.2. Term 1 (Eq. 2.21c), $-I_z\cos(\Omega_I t_1)\cos(\pi Jt_1)$, corresponding to the inverted magnetization in a transient 1D NOE experiment (Noggle & Schirmer, 1971), is chosen. However, the zero quantum coherence term in Eq. 2.25 remains as well, which can be identified at a shorter mixing time as dispersive peaks

(Cavanagh *et al.*, 1996). During the mixing time τ_m, the magnetization I_z transfers to k spins according to the Solomon equation (Section 2.2.8.3.1):

$$-\Sigma I_{kz} a_{lk}(\tau_m)\cos(\Omega_l t_1)\cos(\pi J t_1), \qquad (2.26)$$

where $a_{lk} = [\exp(-\mathbf{R}\tau_m)]$ is the (1, k)th element of the matrix exponential and **R** is the matrix of relaxation rate constants (ρ_{ij} and σ_{ij}). In the matrix, the diagonal terms results from the transfer of the magnetization to the same spin (ρ_{ij}). All other non-diagonal terms (σ_{ij}) produce NOE cross peaks, which contain the distance information required for structural elucidation. The exponential relaxation matrix $\exp(-\mathbf{R}\tau_m)$ can be expanded in a power series (van de Ven, 1995):

$$a_{lk} = [\exp(-\mathbf{R}\tau_m)]_{lk} = 1 - \mathbf{R}_{lk}\tau_m + (1/2)\tau_m^2 \Sigma \mathbf{R}_{lj}\mathbf{R}_{jk} + \cdots. \qquad (2.27)$$

When τ_m is very short, $\mathbf{R}_{lk}\tau_m$ is dominant and other higher terms above can be neglected. The NOE intensity is proportional to $\sigma_{ij} \times \tau_m$, which builds up linearly with τ_m.

The most efficient correlated spectrum in identifying the spin systems is TOCSY (Braunschweiler *et al.*, 1983) or HOHAHA (homonuclear Hartman-Hahn spectroscopy, Bax and Davis, 1985). The magnetization transfer in TOCSY is achieved under Hartman-Hahn conditions via strong scalar coupling Hamitonian.

2.2.6 Phase cycling and pulsed field gradients

As pointed out above, certain experiments usually focus on a specific type of coherence and other unwanted coherences or artifacts will be removed using either phase cycling or pulsed field gradients (PFG). In phase cycling, the phase of the detector follows the required coherence whereas the phases of other coherences will be cycled so as to cancel each other by summing or subtraction operations. For examples, see Wüthrich (1986) and Ernst *et al.* (1987).

PFG works by dephasing unwanted coherences. The dephasing rate is both coherence- and gyromagnetic ratio-dependent (Cavanagh *et al.*, 1996). As PFG reduces phase cycles and artifacts, it is expected to find wide use in nD experiments (Keeler *et al.*,

1994; Kay, 1995). In addition, PFG is also used to improve solvent suppression (see Section 2.2.7).

2.2.7 Water suppression

Biological samples are normally analyzed in aqueous solution. In deuterium oxide the amide protons become weak or even disappear due to exchange with D_2O. It is therefore necessary to run protein samples in water, where the NOEs from amide protons to other protons can be seen. Relative to water, where the proton concentration is 110 M, the solute signals (~1-5 mM peptides) are much weaker. Hence, water signal must be suppressed. Most commonly used techniques include presaturation, 1-1 Jump and return (Plateau & Guéron, 1982), and PFG WATERGATE (Piotto *et al.*, 1992). Presaturation during recycling delay leads to water signal saturation and no transition will occur. The disadvantage is that signals near water are also saturated. In the more recent WATERGATE technique (Piotto *et al.*, 1992), signals near water in t_1-direction are maintained.

2.2.8 NMR structural information

2.2.8.1 Chemical shifts

The relationship between chemical shift and protein structure is not well understood (Ösapay & Case, 1991; Szilágyi, 1995). The chemical shifts for amino acids in unstructured model peptides have been tabulated by Wüthrich (1986) and are given in Table 2.1. Statistical analysis of the accumulated body of chemical shifts from peptides and proteins revealed that α-protons in a helical conformation shift upfield by 0.39 ppm, on average, relative to the value in the random structure whereas they shift to lower field by 0.37 ppm in β-strands (Markley *et al.*, 1967; Jimenez *et al.*, 1987; Szilágyi & Jardetzky, 1989; Williamson, 1990; Pastore & Saudek, 1990; Wishart *et al.*, 1991; Szilágyi, 1995).

The secondary shifts have been utilized to predict protein secondary structures when a full assignment is achieved (Wishart *et al.*, 1992). The amide proton chemical shifts of amphipathic helices were shown to present a periodicity (Bruix *et al.*, 1990; Kuntz *et al.*, 1991; Zhou *et al.*, 1992). Ösapay and Case (1991) showed that there is a good correlation between the calculated chemical shifts and the measured ones. They suggested that such calculated chemical shifts may find use in protein structure refinement.

2.2.8.2 Spin-spin coupling constants

The isotropic scalar (or spin-spin) coupling Hamitonian, $H_J = 2\pi J_{IS}\mathbf{IS}$ between spin I and S slightly affect the Zeeman energy levels of the coupled spins. Hence, coupled spins show splitting as described, for example, in Eqs. 2.19 & 2.20. The J values are a valuable structural parameter as reflected in the Karplus equation (Karplus, 1963):

$$^3J = a\cos^2\theta + b\cos\theta + c, \qquad (2.28)$$

where θ is the dihedral angle formed by the three covalent bonds. Values obtained for the constants are a = 6.0-6.7, b = -1.3-1.76, and c = 1.5-2.4 for $^3J_{HNH\alpha}$ (Cavanagh *et al.*, 1996). However, such J values are not available from micelle-bound peptides or proteins as a result of association with lipid (Henry and Sykes, 1994; Wang *et al.*, 1996b; 1997b).

Table 2.1: Proton Chemical Shifts (ppm) of Amino Acid (X) Residues in Model Peptides GGXA at pH 7 and 35 °C (Wüthrich, 1986)

Residue	H^N	H^α	H^β	H^γ	Others
Gly	8.39	3.97			
Ala	8.25	4.35	1.39		
Val	8.44	4.18	2.13	0.97, 0.94	
Ile	8.19	4.23	1.90	1.48, 1.19	δCH_3 0.95; γCH_3 0.89
Leu	8.42	4.38	1.65, 1.65	1.64	H^δ 0.94, 0.90
Met	8.42	4.52	2.15, 2.01	2.64, 2.64	εCH_3 2.13
Trp	8.09	4.70	3.22, 3.19		2H 7.24, 4H 7.65
					5H 7.17, 6H 7.24
					7H 7.50, $1H^N$ 10.22
Tyr	8.18	4.60	3.13, 2.92		2,6H 7.15; 3,5H 6.86
Phe	8.23	4.66	3.22, 2.99		2,6H 7.20, 3,5H 7.29
					4H 7.24
Pro[a]		4.44	2.28, 2.02	2.03, 2.03	H^δ 3.68, 3.65
Cys	8.31	4.69	3.28, 2.96		
Arg	8.27	4.38	1.89, 1.79	1.70, 1.70	H^δ 3.22, 3.22
					εH^N 7.17, 6.62
Lys	8.41	4.36	1.85, 1.76	1.45, 1.45	H^δ 1.70, 1.70
					H^ε 3.02, 3.02
His	8.41	4.63	3.26, 3.20		2H 8.12, 4H 7.14
Glu	8.37	4.29	2.09, 1.97	2.31, 2.28	
Asp	8.41	4.76	2.84, 2.75		
Gln	8.41	4.37	2.13, 2.01	2.38, 2.38	δH^N 6.87, 7.59
Asn	8.75	4.75	2.83, 2.75		γH^N 7.59, 6.91
Ser	8.38	4.50	3.88, 3.88		
Thr	8.24	4.35	4.22	1.23	

[a]Data for *trans*-Pro.

2.2.8.3 Nuclear Overhauser effect (NOE)

Both chemical shifts and J constants are structural parameters. However, the nuclear Overhauser effect (Solomon, 1955; Noggle & Schirmer, 1971) provides the most abundant and useful information for the structural determination of biomolecules.

2.2.8.3.1 Solomon equation

From Fig. 2.3, the Solomon equation can be derived for a pair of spins with spin quantum number S = I = 1/2 (Solomon, 1955; Cavanagh *et al.*, 1996):

$$d\Delta I_z(t)/dt = -\rho_I \Delta I_z(t) - \sigma \Delta S_z(t)$$
$$d\Delta S_z(t)/dt = -\rho_S \Delta S_z(t) - \sigma \Delta I_z(t), \qquad (2.29)$$

where $\rho_I = W_0 + 2W_1 + W_2$ is referred to as autocorrelation rate constant and $\sigma = W_2 - W_0$ denotes cross relaxation rate (refer to the legend of Fig. 2.3). The important result is that dipole-coupled spins do not relax independently. The influence of spin I on the relaxation of another nucleus S nearby leads to the signal enhancement (nuclear Overhauser effect).

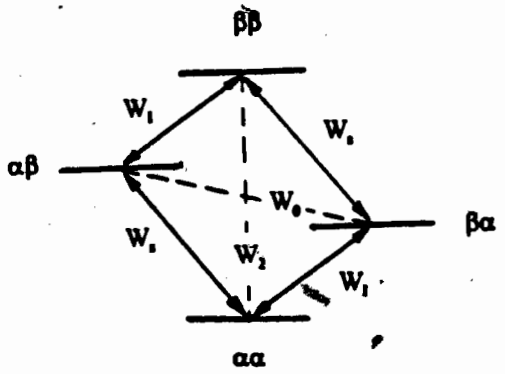

Fig. 2.3: Spin transitions for a two-spin system, with I = S =1/2. W_I and W_S are the single-quantum transitions of spins I and S whereas W_2 and W_0 are the double-quantum and zero-quantum transitions, respectively. The overall relaxation rates are a combination of all the possible paths.

2.2.8.3.2 Steady state and transient NOEs

There are two types of NOE experiments: *steady state* and *transient*. Under the steady-state condition, $d\Delta I_z(t)/dt = 0$ in Eq. 2.29. When spin I is irradiated by rf (B_2) and saturated, the population for I_z is equalized, namely $I_z = 0$. Then, we have (Freeman, 1994)

$$S_z = S_0 + I_0\sigma/\rho_S. \qquad (2.30)$$

Therefore, nuclear Overhauser enhancement:

$$NOE = (S_z - S_0)/S_0. \qquad (2.31)$$

Substituting Eq. 2.30 into Eq. 2.31 gives

$$NOE = (\gamma_I/\gamma_S)\,(W_2 - W_0)/(W_0 + 2W_S + W_2). \qquad (2.32)$$

It is evident that for small molecules W_2 is dominant and positive NOE is obtained assuming $\gamma > 0$. For large molecules such as proteins W_0 is dominant, leading to negative NOEs.

Measurement of transient NOEs can be made by both 1D and 2D experiments. The NOE is characterized by the cross relaxation rate. Using the isotropic rotor spectral density function, the cross relaxation rate between spins I and S for a homonuclear spin system is given by the following equation (Cavanagh *et al.*, 1996):

$$\sigma = [(h^2\mu_0^2\gamma^4\tau_c)/(40\pi^2r^6)]\,\{6/(1 + 4\omega^2\tau_c^2) - 1\}. \qquad (2.33)$$

That is to say, NOE is related to both the distance and the spectral density function. Eqs. 2.27 & 2.33 thus form the basis for structural determination.

2.2.9 Assignment of protein signals

The key step before structure determination is to completely assign all proton signals of proteins. The sequential assignment method was first demonstrated for a cyclic peptide using 1D NMR (Gibbons *et al.*, 1976). The elegance of the method, however, was not fully appreciated until the application of 2D NMR to proteins (Wüthrich, 1986). For homonuclear NMR work, three types of 2D experiments are required to fully assign the spectra. They are TOCSY, DQF-COSY, and NOESY. The first two are through-

bond correlated experiments whereas the third is through-space correlated experiment (Section 2.2.5). The sequential assignment strategy consists of two basic steps. First, TOCSY is used to find amino acid spin systems. Second, NOESY is used to link these spin systems. Another assignment strategy, main-chain-directed method (MCD), differs slightly from the sequential strategy in that the MCD does not fully assign the spin systems first (Englander & Wand, 1987). Identification of the NOE patterns for helices or β-sheets is the main step in the assignment.

The use of homonuclear 2D NMR spectra is limited to proteins with molecular weight <10 kD under favorable conditions. For all helical proteins bound to micelles, the limit drops to ~5 kD or ~50 residues (Wang *et al.*, 1997b) as a result of spectral overlap. It is natural to extend the 2D technique to higher dimensions (Griesinger *et al.*, 1989; Clore & Gronenborn, 1989; Ernst, 1994; Gronenborn & Clore, 1995). Although the first 3D NMR spectrum is homonuclear (Oschkinat *et al.*, 1988), almost all 3D work at present is heteronuclear-edited or triple resonance experiments. In an ^{15}N-edited 3D HMQC-NOESY experiment (Clore & Gronenborn, 1989), the overlapped NOE peaks are now scattered onto a series of 2D slices, where there is a great chance to be resolved. The 2D assignment methods (Wüthrich, 1986; Englander & Wand, 1987) are applicable to heteronuclear-edited experiments such as HMQC-NOESY (Marion *et al.*, 1989; Clore and Gronenborn, 1989). A J-related assignment approach was developed for the heteronuclear triple-resonance experiments to assign backbone signals (Ikura *et al.*, 1990; Kay *et al.*, 1990; Clore & Gronenborn, 1991; Bax & Grzesiek, 1993; Oschkinat *et al.*, 1994).

2.3 Distance geometry and protein structure calculation

Distance geometry is a study of geometric problems with an emphasis on distance between points (Crippen, 1981; Kuntz *et al.*, 1989). The calculation can be either carried out in real space (Niles *et al.*, 1988) or in distance space (Havel, 1991). The DGII program used by the author belongs to the latter, which is detailed below. In principle, there is no solution to an incomplete distance set (Crippen & Havel, 1988). However,

atomic coordinates can be estimated from a set of incomplete distances (simulated NMR restraints measured from X-ray structures). The folding of the protein BPTI was successfully reproduced using the simulated NMR restraints, indicating that the systematic error from distance geometry calculation is not significant (Havel & Wüthrich, 1984; 1985; Wagner *et al.*, 1987; Berndt *et al.*, 1996). In 1985, the first NMR-derived protein structure appeared (Williamson *et al.*, 1985) and the method was soon summarized in a monograph (Wüthrich, 1986). The attempt to determine protein structure from NOE data obtained from 1D NMR, however, commenced slightly earlier, for example, in Jardetzky's laboratory using model building (Ribeiro *et al.*, 1981). The development of heteronuclear 3D and 4D NMR (Oschkinat *et al.*, 1988; Vuister *et al.*, 1988; Kay *et al.*, 1991; Boucher *et al.*, 1992) and deuteration (Markley *et al.*, 1968; Crespi *et al.*, 1968; LeMaster *et al.*, 1988; Torchia *et al.*, 1988) techniques enabled signal assignment of proteins with a single polypeptide chain up to 269 residues (Remerowski *et al.*, 1994; Fogh *et al.*, 1994) and protein/oligonucleotide complex as large as 64 kD (Shan *et al.*, 1996). Recently, the structure for a peptide of 259 residues has been determined (Garrett *et al.*, 1997). The largest protein complex with structure solved so far by NMR is 37 kD (Zhang *et al.*, 1994) whereas the largest protein complex determined by X-ray diffraction to date is 700 kD (Stuart & Jones, 1997). Attempt has also been made to refine the protein structure by combining NMR restraints and x-ray diffraction data (Schiffer *et al.*, 1994).

2.3.1 Upper bound distance generation from NOEs

The most efficient experiment that leads to a large quantity of NOEs is multidimensional NOESY. Normally, a series of NOESY spectra are collected at different mixing times under identical conditions. The cross relaxation rates can then be estimated from the NOE build-up curves. As shown in Eq. 2.33, such a cross relaxation rate (σ) is proportional to both distance between protons (r) and the correlation time (τ_c) (Wüthrich, 1986). For globular proteins it can be assumed that the protein tumbles

isotropically with the same τ_c. This assumption leads to the cancellation of the other terms in Eq. 2.33 by calculating the ratio of cross relaxation rates

$$\sigma_m = \sigma_s(r_m/r_s)^{-6}, \qquad (2.34)$$

where σ_s and r_s are the cross relaxation rate and distance between a pair of protons with known distance such as well resolved methylene protons, σ_m and r_m are the cross relaxation rate and the distance of an unknown proton pair, respectively (Wüthrich, 1986). Eq. 2.34 is also known as isolated spin-pair approximation (ISPA). The signal to noise ratio is bad at very short mixing times and NOE volumes are difficult to measure accurately. As a result, accurate distances are not readily obtained. On the other hand, Eq. 2.34 becomes invalid for mobile parts in the molecules (Doucet & Weber, 1996) or at a long mixing time due to potential indirect NOE effect (spin diffusion) with big biomolecules. Spin diffusion results from the transfer of the magnetization from spin A to a third spin C via spin B (Eq. 2.27). As a result, the cross peak between B and C shows a lagged NOE build-up and can be identified and discarded (Wüthrich, 1986). The common practice in structural calculation, however, is to deduce *approximate* distances from NOE cross peaks. These distances are employed conservatively by treating them as the upper bounds and further grouping them into three or four classes such as strong (1.80-2.80), medium (1.80-3.50), and weak (1.80-5.00 Å) (Clore & Gronenborn, 1989) with 1.8 Å being the lower bound set for a pair of protons. Such a classification leaves uncertainty only in the boundary, thus significantly reducing the effect of potential spin diffusion, uncertainty in the integration of cross peaks due to overlap or classification, and internal mobility of molecules. It has been shown that the most important factor in determining the quality of the protein structure is the number of useful restraints rather than accurate distances (Clore & Gronenborn, 1991; Gronenborn and Clore, 1995; Havel, 1996).

2.3.2 Holonomic restraints

NMR data alone are not adequate to determine the conformation of biomolecules (Jardetzky & Roberts, 1981). The covalent structure of the peptide with known bond

lengths, angles, and chiralities must be provided. The extended peptide structure can be constructed from the standard amino acid library of the empirical conformation energy program for peptides (ECEPP) (Momany *et al.*, 1975; for a list of bond lengths and angles, see Wolfe *et al.*, 1988). The choice of extended peptide chain is necessary to prevent initial bias toward specific conformation. Many holonomic restraints such as chiral and planar covalent constraints are created to ensure a correct geometry. The chiral constraints are indispensable since the handedness of a molecule can not be determined mathematically by the distance restraints (Crippen & Havel, 1988). The distinction between D and L (or R and S) configuration is made by the signed determinant consisting of the Cartesian coordinates of the four points (or atoms) around the chiral center. Multiplying the determinant by -1 leads to the mirror image. L-isomers have positive determinant volumes. As a special case, the planarity of the peptide bonds and aromatic rings are enforced by equating volumes to zero (Crippen & Havel, 1988; Kuntz *et al.*, 1989). Lower bounds are also imposed as the sum of van der Waals radii to prevent steric inconsistency. For example, the lower bound between a pair of protons is usually set to 1.80 Å.

2.3.3 Bound smoothing

Because NOE-derived distances involve only protons and are thus incomplete, smoothing is conducted in combination with geometric restraints to compute more precise restraints. In other words, smoothing reduces the allowed conformation space of the molecule by lowering the upper bounds and increasing the lower bounds. The following relation is the basis for triangle smoothing:

$$d_{ik} - d_{jk} \leq d_{ij} \leq d_{ik} + d_{jk}. \qquad (2.35)$$

It is simply the law of triangle inequality borrowed from Euclidean geometry, where i, j, and k denote the three atoms in consideration.

Development and use of tetrangle smoothing (Crippen & Havel, 1988) stem from the poor approximation of triangle smoothing to the distance upper ranges. Using tetrangle inequality, tighter distance limits can be calculated (Easthope & Havel, 1989).

The problem lies in the computing time required, which is proportional to N^4 (N is the number of atoms in a molecule), indicating a thorough search is impractical. As a consequence, in the DGII package, only a restricted tetrangle smoothing was programmed by scanning four atoms or quadruples (1) with two pairs of covalently bonded atoms; (2) with two pairs of atoms, where each pair is taken from the same amino acid group; and (3) with two pairs of atoms from consecutive amino acid groups in the sequence (Havel, 1991).

2.3.4 Embedding

Embedding is the key step that converts the distance matrix to the coordinates yet consumes the least computing time. The distance matrix is constituted by randomly choosing distances between all upper and lower limits. The main steps are summarized below (Crippen, 1977; Crippen and Havel, 1978; Havel *et al.*, 1983).

Step 1. Construct a trial distance matrix $D = (d_{ij})$ by randomly sampling distances from the ranges set by all upper and lower bounds. The procedure metrization is included at this step to maximize the sampling in all the conformation space (Havel, 1990). The metrization is also based on the law of triangle inequality. The shortest-paths tree data structure is utilized to efficiently calculate the distances from one atom to all its neighbors and then extend further (perspective). The starting atom is randomized by the program to prevent biased calculation. The sampling of distances from between the lower and upper bounds determines that there is no unique solution to the distance restraint file deduced from NMR NOESY data. That is why NMR structures are always reported as an ensemble by sampling m times from the same distance set or restraint file. The number of conformations (m) reported in literature varies from 10 to 50 (Wüthrich, 1986; Dunne *et al.*, 1996; Rozek *et al.*, 1995; Wang *et al.*, 1996a).

Step 2. From the distance matrix D, calculate the distances from each atom or point i of the molecule to the mass center or centroid O by

$$d^2_{iO} = n^{-1}\Sigma d^2_{ij} - n^{-2}\Sigma\Sigma d^2_{jk}, \qquad (2.36)$$

where n is the number of points (Crippen and Havel, 1978).

Step 3. Establish the metric matrix $G = (g_{ij})$ using the law of cosine:

$$2g_{ij} = 2\,\mathbf{iO}\cdot\mathbf{jO} = d^2_{iO} + d^2_{jO} - d^2_{ij}, \qquad (2.37)$$

where g_{ij} is the dot product of the two vectors **iO** and **jO**. This is central to the entire program, which is why the method is called metric matrix distance geometry.

Step 4. Find the largest three eigenvalues, λ_1, λ_2, and λ_3, and eigenvectors w_{ij} for matrix G.

Step 5. Calculate the coordinates for each of the n atoms in the matrix as below:

$$v_{ij} = \lambda^{1/2}_j w_{ij} \qquad (2.38)$$

Step 6. Improve a weighted least squares fit between the trial distances and the coordinates, a procedure called majorization in the program (Havel, 1991).

Note that normally more than three eigenvalues are found. Taking only the first three largest eigenvalues leads to the truncation of data. Such a "shrinking" effect is one of the reasons why optimization is always conducted (Kuntz *et al.*, 1989).

2.3.5 Optimization

The purpose of optimization is to reduce the violations of restraints to an acceptable level. Different protocols can be applied for this step depending on the complexity of the problem. For small molecules (less than 100 atoms), conjugate gradient algorithms are satisfactory. For peptides or proteins, such simple algorithms always fail because of the existence of multiple mimima. To achieve the global minimum and structure convergence, simulated annealing is included in the distance geometry program (DGII, Havel, 1991).

DGII advises that annealing be done in 4D for molecules with more than 200 atoms. The error function is scaled to an equivalent energy (in kcal) that is adequate to heat the system up to the initial upper bound T^0_{max}, typically 200 K. The upper bound T_{max} is thus defined as

$$T_{max} = T^0_{max}\{3[(S_{max} - i)/S_{max})^2 - 2[(S_{max}-i)/S_{max}]^3\}, \qquad (2.39)$$

where S_{max} is the total number of annealing steps. The larger the steps the lower the energy of the system. The initial energy is usually found using "previewing" by watching the distribution of fast atoms. The error function in 4D is defined as (Havel, 1991)

$$F(\mathbf{P}) = \Sigma A^2_{ij}(\mathbf{P}) + \Sigma B^2_{ij}(\mathbf{P}) + \Sigma C^2_{ijkm}(\mathbf{P}) + \Sigma D^2_i(\mathbf{P}), \qquad (2.40)$$

where

$$A_{ij}(\mathbf{P}) = \alpha \cdot \max\{0, 2(r_i + r_j)^2/[(r_i + r_j)^2 + \|\mathbf{p}_i - \mathbf{p}_j\|^2] - 1\}$$

$$B_{ij}(\mathbf{P}) = \beta \cdot \max\{0, 2l_{ij}^2/[(l_{ij}^2 + \|\mathbf{p}_i - \mathbf{p}_j\|^2] - 1\} +$$

$$\beta \cdot \max\{0, [\varepsilon^2 + \|\mathbf{p}_i - \mathbf{p}_j\|^2]/(\varepsilon^2 + u_{ij}^2) - 1\}$$

$$C_{ijkm}(\mathbf{P}) = \gamma \cdot \max[0, l_{ijkm} - v_{ijkm}(\mathbf{P})] + \gamma \cdot \max[0, v_{ijkm}(\mathbf{P}) - u_{ijkm}]$$

$$D^2_i(\mathbf{P}) = \delta \Sigma d_i^2.$$

The three terms A_{ij}, B_{ij}, and C_{ijkm}, enforce the hard sphere lower bounds, the remaining lower and upper bounds, and the chirality constraints, respectively. The parameters α, β, and γ are the weight coefficients of the first three terms relative to the upper distances. The fourth term, D^2_i, is the dimensionality error, where the fourth coordinate, d_i, is driven to zero. The coefficient δ is a dimensionality weight. The computation of distances in 4D and the use of heavy atoms are additional procedures to avoid local minima in the annealed structures although they do not have physical meaning. The use of 4D not only fixes the problem with local chirality of the molecule at lower temperatures and a shorter calculation time but also improves the final structural convergence. The use of heavy atoms renders annealing in a larger contour of the energy surface, thus providing extra stability to the process. This in turn allows many more step-sizes (Eq. 2.39). For small molecules, a full matrix analysis of the error function could be conducted. For large molecules such as the peptides studied in this thesis, the sparse matrix was employed, which considers only input restraints or distances from smoothing. It is evident that the "simulated annealing" protocol used in DGII program is different from others such as Niles *et al.* (1988). The dynamic simulation of others was performed at 1000 K in order to either try to eliminate residual violations or to calculate structures from random coordinates by adjusting force fields. However, both procedures were derived from metallurgy, where annealing is performed to remove "brittleness" of alloys and obtain materials of higher quality.

Although the coordinates obtained above are almost a minimum, further minimization was programmed to minimize the error function to a precise minimum. The protocol adopted in DGII (Havel, 1991) is Shanno's conjugate gradient method (Shanno, 1978), which is an iterative procedure to approach the minimum.

CHAPTER 3: MATERIALS AND METHODS

3.1 Materials

Protonated SDS (> 99%) was purchased from BDH (Poole, UK). Perdeuterated DPC (98.9% D) and SDS (98% D) were purchased from CDN Isotopes (PQ, Canada) and Cambridge Isotope Laboratories (MA, USA), respectively. Deuterium oxide (99.9% D) was from Isotec Inc. (OH, USA). TMA and lysoPC (Sigma) were kindly provided by Dr. Cornell (Simon Fraser University).

3.1.1 Peptides

ApoE(267-289), PLVEDMQRQWAGLVEKVQAAVGT, apoA-II(18-30)+, VTDYGKDLMEKVKEWLNS, and apoA-I(166-185), YSDELRQRLAARLEALKENG, were purchased from Dr. Ian Clark-Lewis (University of British Columbia) and synthesized as described elsewhere (Clark-Lewis *et al.*, 1986).

ApoE(263-286), SWFEPLVEDMQRQWAGLVEKVQAA, apoA-I(142-187), apoA-I(122-187), apoA-I(114-142) and other peptides mentioned herein were synthesized by Dr. James T. Sparrow (Baylor College of Medicine) on an Applied Biosystems 430A synthesizer using solid-phase method (Barany and Merrifield, 1980) as detailed in Sparrow & Monera (1996) and also the co-authored papers (Wang *et al.*, 1996a; 1997b).

3.1.2 Apolipoprotein isolation and purification

Apolipoproteins (A-I, A-II, and C-I) were purified from human blood plasma provided by the Canadian Red Cross. Briefly, HDL was isolated by sequential isopycnic ultracentrifugation (Havel *et al.*, 1955; Schumaker and Puppione, 1986) for 20 h or longer

between density 1.063 and 1.21 g/mL in a Beckman 50.2 Ti rotor at 42,000 rpm and 4°C. Density was adjusted using KBr. A third spin was performed to remove the remnants of albumin. Lipids in HDL were removed by extraction with a mixed solvent of diethyl ether and ethanol (2:3, v/v) (Scanu and Edelstein, 1971). The delipidated HDL or apoHDL (~70-100 mg) was then dissolved in the 25 mM imidazole buffer containing 7.2 M urea and 25 mM dithiothreitol, pH 7.4, to a protein concentration of 10-15 mg/mL. The protein solution was applied to a PBE-94 column (1.4 × 40 cm) (Pharmacia) and proteins were fractionated with the elution buffer containing 111 mL of polybuffer®74 (Pharmacia) plus 889 mL of 8 M urea, pH 4 (Mcleod *et al.*, 1989). The urea (electrophoresis grade) was deionized prior to use by chromatography on a Rexyn 1-300 (Fisher Scientific) column (3 × 100 cm). UV spectroscopy (280 nm) was employed to locate protein fractions and the purity was checked by SDS-PAGE before pooling the fractions. The pooled pure protein fractions were then run through the column (1.0 × 10 cm) packed with 2.0 g of hydroxylapatite (HTP) to remove polybuffer. These protein fractions were finally dialyzed against 4 L of the standard buffer (0.15 M NaCl, 0.04% EDTA, 0.03% NaN_3, pH 7.0) with two changes. Alternatively, apoC-I was eluted first from PBE-94 column using the equilibration buffer (0.025 M imidazole, 1 mM EDTA, 7.2 M urea, pH 7.4) followed by eluting apoA-I & A-II with the normal elution buffer. The detected apoC-I fractions were then pooled and dialyzed against 10-mM NH_4HCO_3 buffer directly. During dialysis, the monomer apoA-II isolated can be oxidized back by 0.023% H_2O_2 to the native dimer form. A second method employed to isolate intact apoA-II from delipidated HDL (above) was FPLC (Mezdour *et al.*, 1987).

The apoA-I (90 ± 5%) (Letter from Dr. J. E. Doran), provided by the Swiss Red Cross, was purified by the cold ethanol fractionation procedure (Peitsch *et al.*, 1989). Sucrose in apoA-I was removed by dialysis against 10-mM NH_4HCO_3 buffer with two changes. Finally, the protein solution was dialyzed against water once. For NMR studies, such a dialysis protocol is required to remove the majority of the salts such as EDTA in proteins purified by other procedures (below).

The ^{15}N-labeled apoA-I was provided by Dr. Marcel, expressed in *E. coli* (Bergeron *et al.*, 1997).

3.1.3 Peptide or protein assay

The peptide or protein concentration in the stock solution was assayed by the method of Lowry *et al.* (1951) using bovine serum albumin as standard or measured by UV spectroscopy at 280 nm (Gill & von Hippel, 1989). Synthetic peptides were judged pure by analytical HPLC, automatic amino acid sequencing and mass spectroscopy (Sparrow & Monera, 1996; Wang *et al.*, 1997b). The purity of apolipoproteins was checked by SDS-PAGE (Raymond & Weinstraub, 1959; Maguire *et al.* 1989) and NMR spectroscopy. The protein electrophoresis gels were Coomassie blue or silver stained (Heukeshoven and Dernick, 1985), the latter having sensitivity 5 times higher than the former. For NMR samples, 1-2 μL was taken directly and loaded to the gel wells after mixing with 1 μL of glycerol (1:1, v/v). The protein ladder contains bovine serum albumin, carbonic anhydrase, lysozyme, aprotinin, and somatostatin (all Sigma products).

3.2 Fluorescence spectroscopy

Fluorescence measurements were conducted on an SLM4800C spectrofluorometer at 20°C. Tryptophans in the peptides were excited at 280 nm and emission spectra were observed from 300 to 450 nm. Samples of apoA-I(142-187) and the standard, tyrosine (Narayanaswami *et al.*, 1993), were excited at 277 nm and emission was recorded from 270 to 350 nm. The excitation and emission bandwidths were both 8 nm. The relative quantum yield (Q_x) was calculated according to the equation (Freifelder, 1976):

$$Q_x = (Q_s I_x A_s)/(I_s A_x), \qquad (3.1)$$

where Q_x and Q_s are the quantum yield of the unknown and standard samples, respectively; I_x and I_s are the integrated intensities of the unknown and standard samples; and A_x and A_s are the optical density of the unknown and standard at 277 nm.

3.3 Circular dichroism

CD spectra were recorded on a Jasco J710 spectropolarimeter with a Neslab RTE-110 temperature controller and interfaced to a personal computer. The instrument was calibrated using *d*-(+)-camphorsulfonate at 290.5 nm (Yang *et al.*, 1986b; Johnson, 1990). The pH (± 0.1) of the sample was measured by inserting a glass electrode into the CD cell (0.1-cm path length). Each spectrum was the result of the average of two scans, collected from 190 to 260 nm every 0.5 nm at a scan speed of 20 nm per minute and the response time of 0.25 s. After smoothing and background subtraction, the recorded degrees were converted to molar ellipticity per residue, $[\theta]$, in $deg.cm^2.dmol^{-1}$:

$$[\theta] = \theta/[10dcn], \qquad (3.2)$$

where θ is an angular measure in degree, d is the light path in centimeter, and c is the molar concentration (mol/L) of the peptide or protein, and n is the number of residues in the peptide or protein.

The helix content was calculated using convex constraint analysis (Perczel *et al.*, 1991, 1992). Alternatively, the helix content was estimated based on the 222-nm band using the formula below (Jackson *et al.*, 1973):

$$\text{Helix\%} = [(|\theta_{222}| + 3000)/39000] \times 100, \qquad (3.3)$$

where $|\theta_{222}|$ is the absolute value of the molar ellipticity of proteins at 222 nm.

3.4 Fourier transform infrared spectroscopy

The FT-IR samples were aliquots of NMR samples (Chapters 4-6), which were lyophilized and dissolved in the same volume of D_2O. The IR procedure was detailed in the co-authored paper (Shaw *et al.*, 1997).

3.5 Nuclear Magnetic resonance

3.5.1 NMR sample preparation

The apoE(267-289) (2.9 mM) or apoE(263-286) (5 mM) peptides were co-dissolved with SDS-d_{25} in 0.6 mL of 90% H_2O and 10% D_2O solution and filtered into a 5 mm NMR tube. The final peptide/SDS ratio was 1:90 (mol/mol). The ratio refers to molar ratio hereafter in the thesis unless otherwise indicated. NMR samples for other peptides (5 mM) were prepared similarly. The pH (meter reading without isotope effect correction) of the samples was measured directly in the NMR tube with a glass electrode (Broadley James Inc., CA, USA), calibrated using two standard buffers at pH 4.0 and 7.0, and adjusted using a small fractions of NaOH or HCl solutions. The difference in pH before and after data collection was within ± 0.1-pH unit.

To the freshly purified yet still dilute apoA-II or apoA-I solution immediately after the final dialysis against water (Section 3.1.2), perdeuterated SDS was added at a protein/SDS ratio of 1:80 for apoA-II and 1:140 for apoA-I (Reynolds, 1982). The SDS-containing protein solution was then freeze-dried and dissolved in 0.5 mL of H_2O/D_2O (9/1, v/v) solution. The solution was filtered into the NMR tube, filled with nitrogen gas and sealed.

3.5.2 Data acquisition and processing

NMR spectra were initially recorded to optimize the spectral resolution in the amide region (~6-11 ppm) by changing pH, temperature, or both. The stability of the sample was routinely followed by NMR spectra before and after 2D experiments. All NMR spectra such as TOCSY (Braunschweiler *et al.*, 1983; Bax and Davis, 1985), NOESY (Jeener *et al.*, 1979), and DQF-COSY (Rance *et al.*, 1983) were acquired at the same ^1H resonance frequency of 600.13 MHz on a Bruker AMX 600 spectrometer

equipped at Simon Fraser University. The spectral width in both dimensions was 6250-7246.3 Hz with the carrier frequency set at the water resonance. The water signal was suppressed by the WATERGATE technique (Piotto *et al.*, 1992) using 3-9-19 pulse sequence (Sklenár *et al.*, 1993) for TOCSY and NOESY experiments. In DQF-COSY experiments in 10% or 99.9% D_2O the water signal was suppressed by a presaturation pulse during the recycling delay. All spectra were collected in the time proportional phase incrementation (TPPI) mode (Redfield and Kuntz, 1975; Marion & Wüthrich, 1983) with 2K data points in t_2 and 512-640 increments (32-64 scans each) in t_1. NOESY spectra were recorded at a series of mixing times such as 50, 75, 100, 150 and 200 ms. TOCSY experiments were performed at the mixing time of 45 to 125 ms with a trim pulse before the MLEV-17 spin-locking sequence.

NMR data were processed using the commercial software FELIX (v. 2.30 or v. 95, Biosym Technologies, Inc.) on the Silicon Graphics workstation. The residual water signal was removed by the convolution difference low-pass filter technique (Marion *et al.*, 1989). The first data point was scaled by a factor of 0.5 to reduce t_1 ridges and baseline distortions (Otting *et al.*, 1986). The FID was apodized by a shifted squared sine-bell window function 90° in F_2 and 0° in F_1 for the spectra of apoE(263-286) and 60° in both dimensions for the spectra of apoE(267-289). After zero-filling, the time domain data were Fourier transformed to give a 2K × 2K matrix. The frequency-domain data, or NMR spectra, were baseline corrected using a fifth order polynomial function in both dimensions. Chemical shifts were referenced to external DSS for signal assignments but to the methyl signal (0.00 ppm) of internal DSS to facilitate pH titration or temperature coefficient measurements (Section 3.5.3). Other proton signals from DSS resonate at 2.90, 1.75, and 0.63 ppm, respectively.

3.5.3 Temperature coefficients of amide protons

To measure temperature coefficients ($\Delta\delta/\Delta T$) for amide protons, NOESY and TOCSY spectra were collected from 22 to 47 °C in steps of 5 °C. Temperature was controlled by a variable temperature (VT) unit on the spectrometer with the precision of ± 0.1 °C. A minimum of 0.5 h was allowed for the sample to reach a new equilibrium state each time when the temperature was changed. The chemical shifts of each amide signal read from NOESY at various temperatures were linearly regressed against temperature. The rate of chemical shift change per degree of temperature, in units of ppb/°C, is the temperature coefficient of the specific amide proton.

3.5.4 Intermolecular NOE experiment

Intermolecular NOEs (Kaiser, 1965) between apoA-I peptides and SDS were observed in the presence of protonated SDS or a mixture of 50% SDS-d_{25} and 50% protonated SDS.

3.5.5 Measurement of pKa

The change of chemical shifts of the protons nearest to the ionizable groups with pH was followed by 2D NMR (Khoda *et al.* 1992) as key cross peaks were not resolved on 1D NMR spectra. The chemical shifts at various pHs were then fitted to the modified Henderson-Hasselbalch equation

$$\delta_{ob} = [\delta_A + \delta_B(10^{pH-pKa})/(1+10^{pH-pKa})], \qquad (3.4)$$

where δ_{ob} is the chemical shift observed at specific pH, δ_A and δ_B are the chemical shifts of the acidic and basic forms, respectively.

3.6 Structure calculation

Three-dimensional structures of apolipoprotein peptides in micelles were calculated from NOE distance restraints using DGII (Havel, 1991) of InsightII (Biosym

Technologies, Inc.). The NOE peaks were integrated using FELIX (v. 2.30). They were grouped into three classes: strong (1.8-2.8), medium (1.8-3.8), and weak (1.8-5.0 Å) according to NOE volumes (Gronenborn and Clore, 1995) under the consistent valence force field (CVFF) upper and lower force constants at 10 kcal·mol^{-1}·Å^{-2} for apoE(263-286) and 32 kcal·mol^{-1}·Å^{-2} for apoE(267-289) with a maximum force constant of 100 kcal·mol^{-1}·Å^{-2} for both. For apoA-I(166-185) (Chapter 6) and apoA-II(18-30) (Buchko *et al.*, 1996a), cross-peaks on the NOESY spectra, mixing times of 100-150 ms, were classified into three intensity levels: strong (1.80-2.50), medium (2.51-3.50), and weak (3.51-5.00 Å) according to the peak volume (Wüthrich, 1986). Distance restraints for apoA-I(142-187) were generated from the NOESY spectra (80 ms in DPC and 100 ms in SDS) and classified into 1.8-2.8, 1.8-3.8, and 1.8-5.0 Å based on the intensity of cross peaks. The upper distance bounds were calibrated using the known distance between pairs of well-resolved methylene protons (1.74 Å) for apoA-I(166-185) or based on the known distances in an α-helix structure for apoA-I(142-187) (Wüthrich, 1986; Cavanagh *et al.*, 1996; Johnson *et al.*, 1996) such that normally H^N_i-H^N_{i+1} should be strong (1.8-3.0 Å) and H^α_i-H^N_{i+3} should be medium (1.8-3.8 Å) (Wüthrich, 1986). Pseudoatom corrections were made for unresolved methylene, methyl, aromatic protons and 2 methyls by adding 1.0, 1.5, 2.0 and 2.4 Å, respectively, to the upper bounds of pertinent restraints (Wüthrich *et al.*, 1983) using the NMR-Refine Module of InsightII. An additional 0.5 Å was added to the distance upper bounds involving methyl group protons (Clore *et al.*, 1987). In addition to these distance restraints, the chiral and geometry restraints were generated from the corresponding extended covalent peptide structure.

Distance geometry calculations include three major steps: smoothing, embedding, and optimization (Chapter 2). The optimization step contains a simulated annealing protocol and an energy minimization program based on the conjugate gradient algorithm. The initial energy for annealing was found using the PREVIEWING protocol and 800 and 1700 kcal/mol were found to be proper for ~20mers and the 46mer, respectively. Simulated annealing was performed by converting the error function to an equivalent energy (in kcal) that is adequate to "cook" the system to 200 K, the initial upper bound on

temperature. The structures were then cooled gradually to 0 K at 2.1×10^{-13} s per step. Initially, 10 structures were calculated. When the final optimization error is greater than the fail level (0.5) the mirror image of the structure will be re-annealed. No optimization will be performed if the final error of the mirror image is again greater than the fail level. Such structures were discarded. The fail level reflects the distance, chirality, and contact violations. Upon completion of the calculation, the distances with violations greater than 0.1 Å were listed and examined. When the upper distance bound violations in ~20% of the structures are greater than 0.2 Å, these bounds were relaxed to an upper class to reflect the uncertainty in classification or integration due to spectral overlap. When no further improvements were achieved after iterative refinements, 20-50 structures were calculated in the final run. Structures accepted have fail level less than 0.1 and contact error below 0.1 Å. No distance violations greater than 0.5 Å were observed.

CHAPTER 4: CONFORMATIONS OF APOE(267-289) AND APOE(263-286) IN SDS MICELLES

4.1 Introduction

Human serum apoE (M_r = 34,200) consists of a single polypeptide chain of 299 amino acid residues (Rall *et al.*, 1982; Breslow *et al.*, 1982). When associated with lipid, apoE modulates the lipid metabolism via binding to LDL receptors (Innerarity *et al.*, 1979; Mahley and Innerarity, 1983; Weisgraber, 1994).

Thrombin digestion of apoE yields two segments: residues 1-191 and 216-299. The N-terminal fragment only weakly interacts with lipid (De Pauw *et al.*, 1995). The X-ray crystal structure for apoE(1-191) is an anti-parallel four-helix bundle structure with all the hydrophobic side chains oriented toward the center forming a hydrophobic core (Wilson *et al.*, 1991). These helices contain 19, 28, 36, and 35 amino acids; among them helix 3 (residues 87-120) is kinked at G105. The N-terminal fragment is purported to contain the LDL receptor-binding domain in the region corresponding to residues 140-150 (Innerarity *et al.*, 1983). Dyer *et al.* (1995) found that the dimer of synthetic peptide 141-155 binds to the LDL receptor. Sparrow *et al.* (1985) found that synthetic peptide 129-169 bound DMPC whereas the segments 139-169 or shorter did not. The C-terminal fragment is proposed to contain the major lipid-binding domain (Wetterau *et al.*, 1988) and to be responsible for LCAT activation (De Pauw *et al.*, 1995). Using synthetic peptides, Sparrow *et al.* (1992) showed that segments 202-243, 211-243, 267-286 did not associate with DMPC while 263-286 did. The importance of 263-286 was subsequently confirmed by truncation mutagenesis studies (Westerlund and Weisgraber, 1993). Segment 263-286 has thus been recognized as one of the primary lipid-binding regions of apoE (Sparrow *et al.*, 1992; Weisgraber, 1994; De Pauw *et al.*, 1995).

In order to elucidate the structural details of the apoE(263-286) and apoE(267-289), the author has performed fluorescence and CD spectroscopy and 2D NMR studies of both peptides in SDS micelles.

4.2 RESULTS

4.2.1 Circular dichroism

Fig. 4.1 depicts the CD spectra of apoE(263-286) (A) and apoE(267-289) (B). In the absence of lipid, both peptides are mainly random as indicated by the strong negative band at 198-200 nm (Woody, 1995). Convex constraint analysis (Perczel *et al.*, 1991) yields 68% and 62% random coil and 7% and 2% α-helix for apoE(263-286) and apoE(267-289), respectively. The addition of SDS induced a dramatic change in the spectra of both peptides. At a peptide/SDS ratio of 1:5 or greater, the CD spectra for both peptides possess a positive band at 192-193 nm and double minima at 208 nm and 222 nm (Fig. 4.1), features that are characteristic of helical structures (Holzwarth and Doty, 1965; Woody, 1995). The content of helix is listed in Table 4.1. The increase in the helix content for both peptides with the addition of SDS is apparent according to either CCA (Perczel *et al.*, 1991) or simply the 222 nm band estimation using Eq. 3.3 (Jackson *et al.*, 1973). Furthermore, similar helix percentages were found by the two methods for these peptides in the SDS-bound state (Table 4.1). The Table also suggests that all of apoE(267-289) was bound to SDS (Bairaktari *et al.*, 1990) at a lower peptide/SDS ratio (1:10) than apoE(263-286) (1:40). The final helix content at 1:90 is 67% for apoE(263-286) and 51% for apoE(267-289), indicating a longer helical segment in the former (16 out of 24 residues) than the latter (12 out of 23 residues). The longer helix in apoE(263-286) is also suggested by the ratio of the molar ellipticity at 222 nm to that at 208 nm, 1.09 for apoE(263-286) and 0.82 for apoE(267-289) (Rizo *et al.*, 1993; Fasman, 1996). The correlation between the helix length and lipid affinity supports the notion that amphipathic helices are responsible for lipid binding (Sparrow & Gotto, 1982; Ponsin *et al.*, 1986; Segrest *et al.*, 1994). The increase of temperature from 25 to 37 °C caused a decrease in the helix content of apoE(263-286) in SDS by 11%. The peptide was found to be most helical at pH 6-7. The helix content decreased by 5% with the decrease of the pH by 3 units but by 13% when the pH was increased by 3 units.

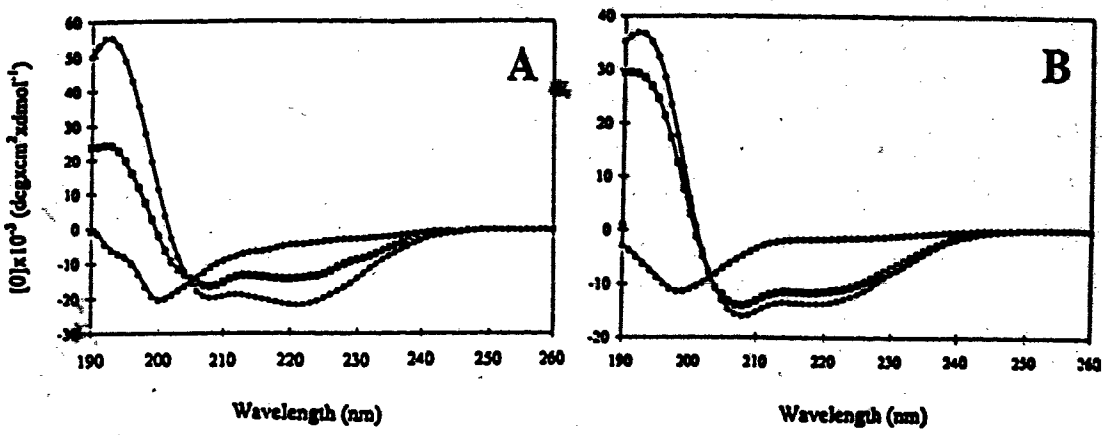

Fig. 4.1: CD spectra of apoE(263-286) (A) and apoE(267-289) (B) in the absence and presence of SDS. The peptide concentration is 0.10 mM and SDS concentrations are: (Δ) 0; (□) 0.5; and (●) 9 mM at 25 ± 0.5°C, pH 5-6 [Adapted from Wang *et al.* (1996a)].

Table 4.1: Helix Percentage of ApoE(263-286) and ApoE(267-289) with Titration of SDS

Peptide/SDS ratio	ApoE(263-286)			ApoE(267-289)		
	CD[a]	CD[b]	NMR[c]	CD[a]	CD[b]	NMR[c]
1:0	18	7		11	2	
1:5	44	37		35	44	
1:10	50	52		39	51	
1:40	62	61		40	49	
1:90	63	6[illegible]	60	40	51	58

[a]Helix contents estimated using the 222-nm band (Jackson *et al.*, 1973). [b]Helix contents from convex constraint analysis (Perczel *et al.*, 1991). [c]Calculated using Eq. 4.2.

4.2.2 Fluorescence spectroscopy

In the absence of lipid, both peptides fluoresce at 350 nm (Fig. 4.2), indicating the exposure of the Trp to the aqueous solution (Jonas, 1992). The fluorescence of apoE(263-286) is stronger than that of apoE(267-289) since there are two Trp residues in the former yet only one in the latter. The maximum emission for both peptides was found to shift to a shorter wavelength (blue shift) with the addition of SDS. At the saturating levels of SDS a 19 nm blue shift was measured for both peptides although more SDS was required for apoE(263-286) (Fig. 4.2). Such a shift in the maximum of the Trp fluorescence arises from the movement of the Trp aromatic ring(s) from an aqueous to a hydrophobic milieu (Lakowicz, 1983; Jonas, 1992; Mishra *et al.*, 1996), indicating the association of the apoE peptides with SDS. A similar blue shift was observed for apoE(263-286) bound to DMPC (Sparrow *et al.*, 1992).

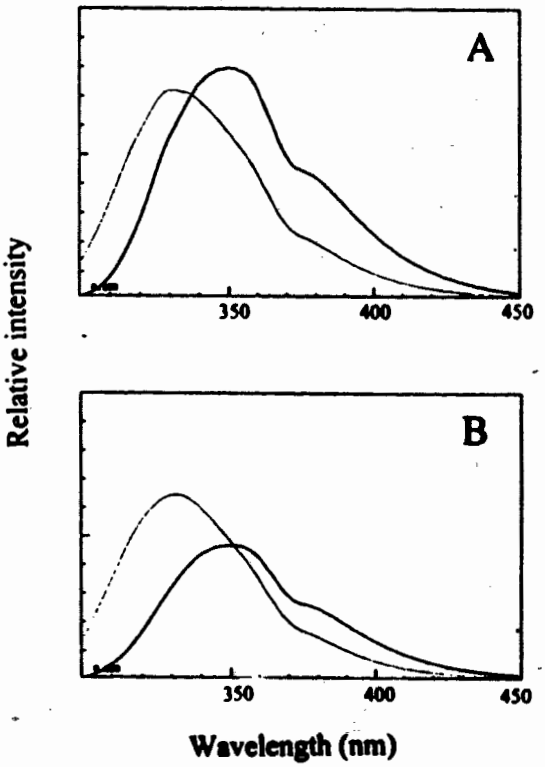

Fig. 4.2: Fluorescence spectra of 0.01 mM apoE(263-286) (A) and apoE(267-289) (B) before and after the addition of SDS. Spectra in the absence of SDS are depicted in thicker lines and thinner lines in the presence of SDS at the peptide/SDS ratios of 1:230 and 1:80, respectively, at pH 5-6 and 20 °C.

4.2.3 NMR resonance assignment

The NMR resonances of apoE(267-289) in water were found to shift considerably with the addition of SDS at a peptide/SDS ratios of 1:5 or greater, indicating a conformational change. At the peptide/SDS ratios of 1:5 or lower, the spectral lines were broad due to exchange between the free and lipid-bound states. However, a single set of well resolved, sharp peaks was found at a peptide/SDS ratio of 1:90. The spectral linewidths, approximately 10 Hz, made it impossible to obtain spin-spin coupling constants between H^{α}_{i}-H^{N}_{i} (~5 Hz in a helical structure) (Wüthrich, 1986). This is consistent with the association of the peptide with lipid (Henry and Sykes, 1994; Rozek *et al.*, 1995; Wang *et al.*, 1996b). Optimal resolution of H^{N} resonances in the presence of SDS was obtained at pH 4.8 for apoE(263-286) and pH 6.0 for apoE(267-289). Further increase in pH from 7 to 10 gave rise to a selective decay of amide signals of apoE(267-289) in SDS without noticeable signal shift. At pH 10, only amide signals from residues L279 to V287 were observed (Fig. 4.3). Comparison of NOESY spectra from pH 4 to 7 indicates no measurable conformation change for both peptides.

Two-dimensional NMR spectra of apoE(267-289) were assigned to one set of resonances using the sequential assignment strategy (Wüthrich, 1986). This was achieved by identifying spin systems on the TOCSY spectrum. Each vertical line in Fig. 4.4 shows the cross peaks of the amide proton to its side chain, corresponding to one spin system or one amino acid residue. These spin systems were mapped onto the amino acid sequence of the known peptide via NOE connectivities such as H^{N}_{i}-H^{N}_{i+1} (Fig. 4.5A) and H^{α}_{i}-H^{N}_{i+1} (B). The complete assignment of spin systems such as aromatic, N, and Q residues were achieved with the aid of the NOESY spectra. The assignment for side chains was confirmed by DQF-COSY.

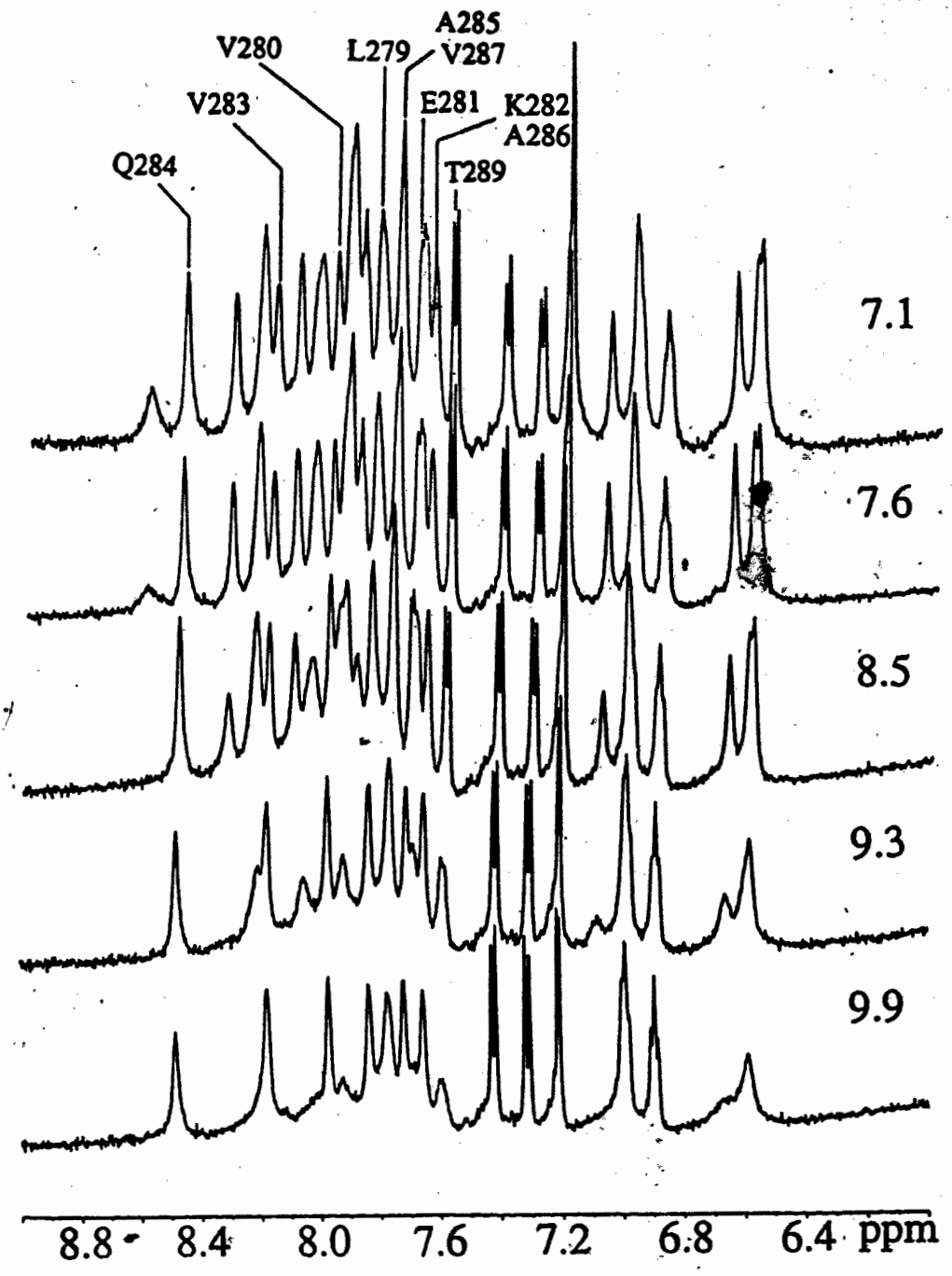

Fig. 4.3: NMR spectra of apoE(267-289) in SDS at various pH values. Spectra were followed from pH 7 to 10 at 37 °C. Each spectrum is the accumulation of 128 scans over a spectral width of 7352.9 Hz .

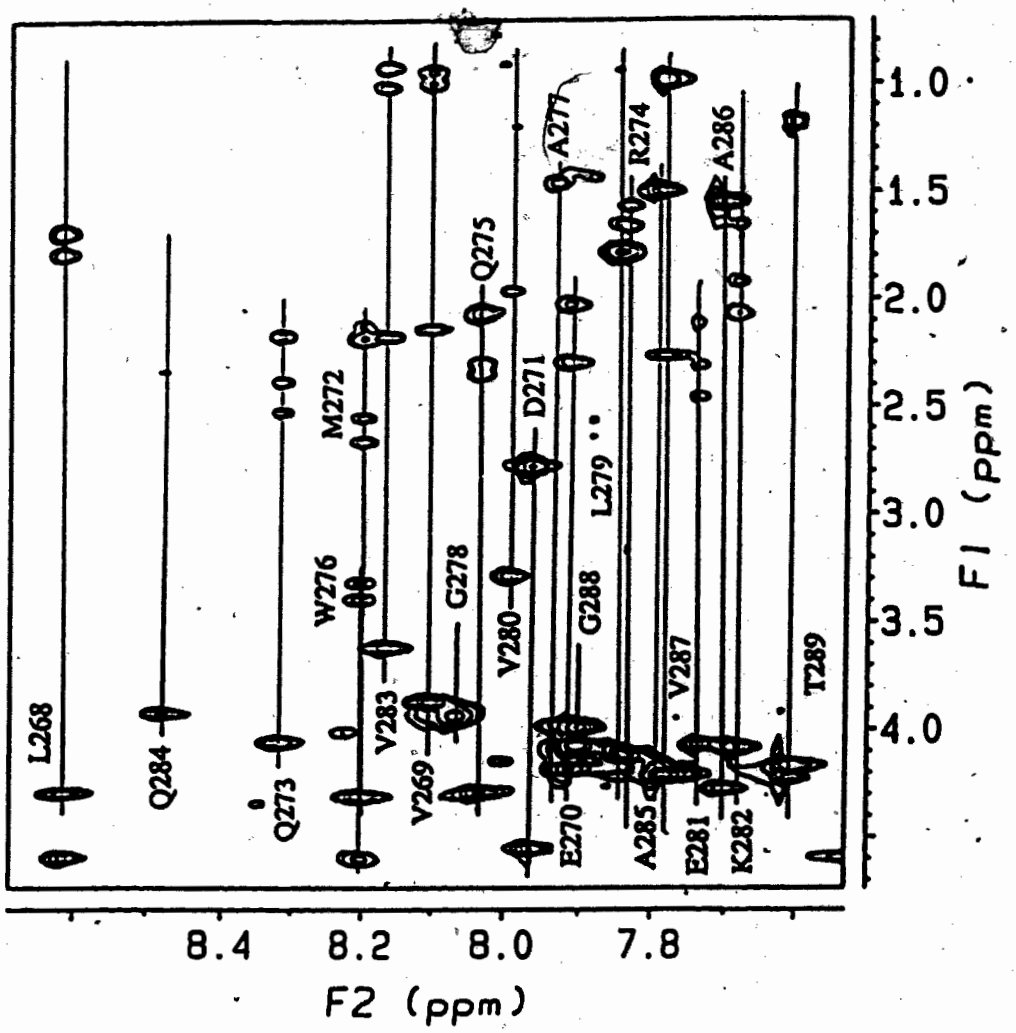

Fig. 4.4: Fingerprint region of the TOCSY spectrum of apoE(267-289) in SDS. The spectrum was collected by Dr. Pierens for a 2.9 mM sample (peptide/SDS, 1:90) in H_2O/D_2O (9:1, v/v) solution at pH 6.0 and 37 °C. Each labeled vertical line corresponds to one spin system identified and assigned using the NOESY spectrum (Fig. 4.5).

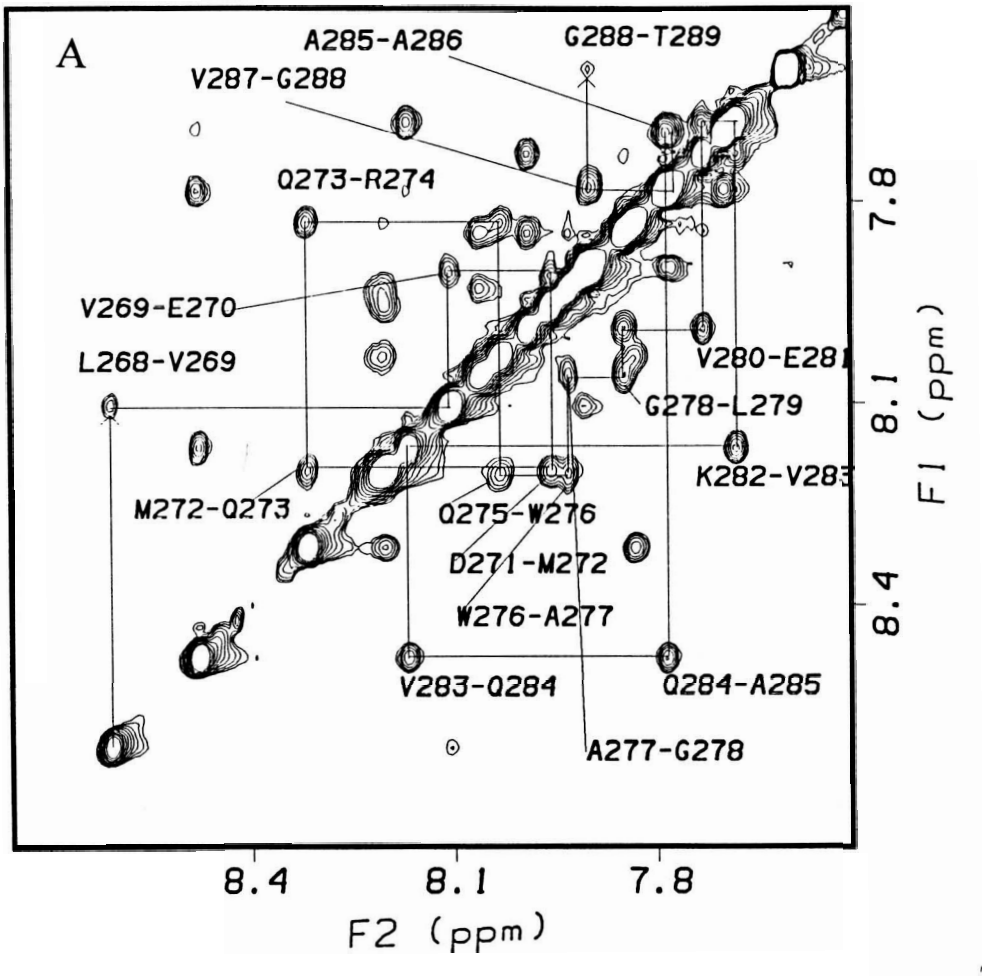

Fig. 4.5. Portions of the NOESY spectrum of apoE(267-289) in SDS. Shown in (A) is the amide region and in (B) (NEXT PAGE) the fingerprint region recorded for a 2.9 mM peptide sample at a mixing time of 150 ms in aqueous solution (H_2O/D_2O, 9:1, v/v) of SDS-d_{25} (peptide/SDS, 1:90) at pH 6.0 and 37 °C. The constructs follow the sequential NOE connectivities with H^N_i-H^α_i (A) and H^N_i-H^N_{i+1} (B) cross peaks labeled (This spectrum was collected by Dr. Pierens).

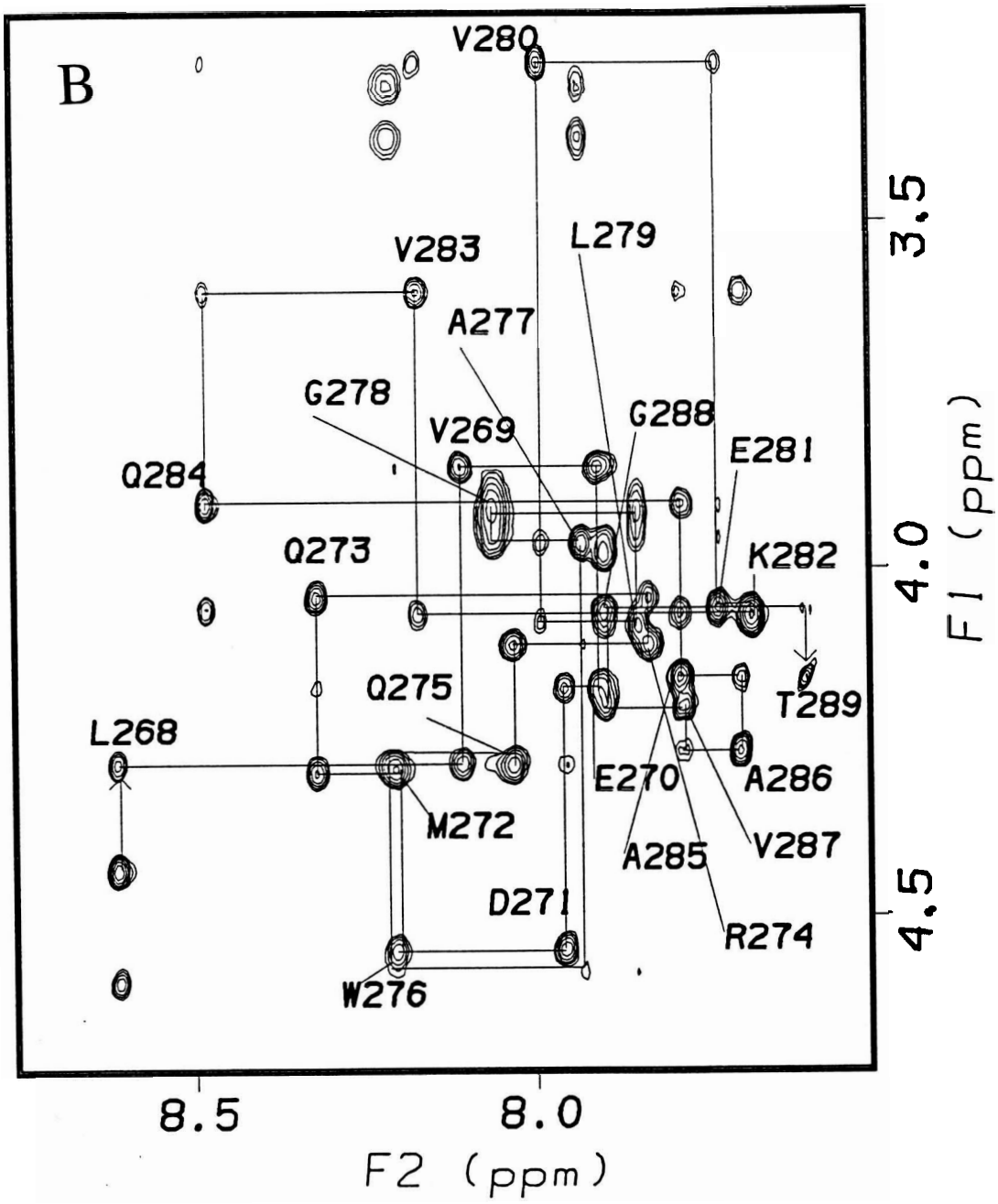

Fig. 4.5 (Continued)

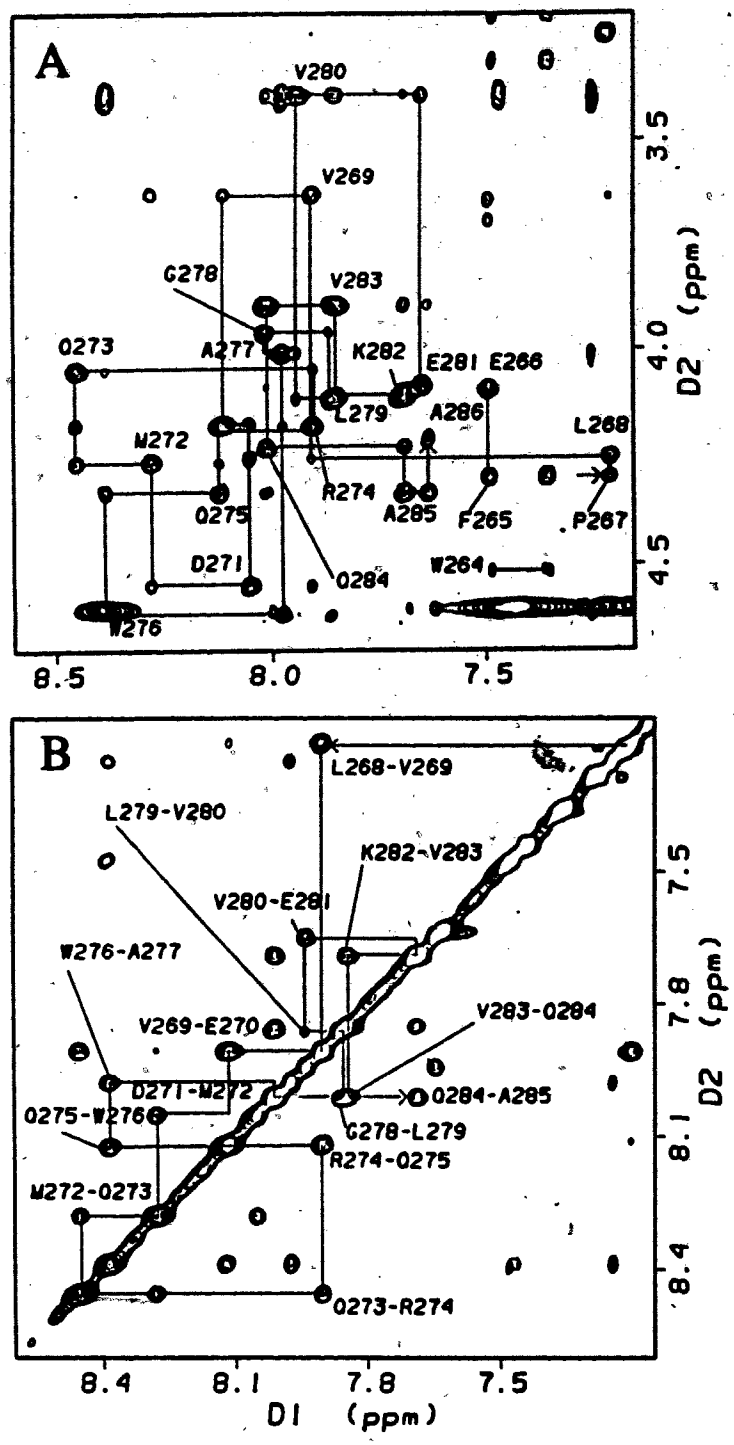

Fig. 4.6: Portions of the NOESY spectrum of apoE(263-286) in SDS. Shown in (A) is the amide proton region and in (B) the fingerprint region collected at a mixing time of 150 ms in aqueous solution (H_2O/D_2O, 9:1, v/v) of SDS-d_{25} (peptide/SDS, 1:90) at pH 4.8 and 37 °C

Table 4.2: Proton Chemical Shifts (ppm) of ApoE(267-289) in SDS-d_{25} Micelles at the Peptide/SDS Molar Ratio of 1:90, pH 6.0 and 37 °C[a]

Residue	H^N	H^α	$\Delta H\alpha$[b]	H^β	H^γ	Others
Pro267		4.45	+0.01	2.59, 2.56	2.13, 2.07	H^δ 3.43
Leu268	8.62	4.29	-0.09	1.78, 1.68	1.66	H^δ 0.98, 0.93
Val269	8.09	3.86	-0.32	2.12	0.99, 0.94	
Glu270	7.91	4.18	-0.11	2.02	2.29	
Asp271	7.96	4.55	-0.21	2.77		
Met272	8.19	4.31	-0.21	2.17, 2.10	2.66, 2.54	εCH_3 2.02
Gln273	8.31	4.05	-0.32	2.16	2.52, 2.38	δH^N 7.24, 6.67
Arg274	7.83	4.12	-0.26	1.78	1.66, 1.56	H^δ 3.17; εH^N 7.19
Gln275	8.03	4.29	-0.08	2.06	2.34, 2.29	δH^N 7.10, 6.60
Trp276	8.19	4.60	-0.10	3.38, 3.31		2H 7.19; 4H 7.43; 5H 6.90; 6H 7.00; 7H 7.33; HN 9.78
Ala277	7.93	3.97	-0.38	1.45		
Gly278	8.06	3.93	-0.04			
Leu279	7.85	4.09	-0.29	1.78	1.64	H^δ 0.93, 0.87
Val280	7.99	3.28	-0.90	1.95	0.81, 0.64	
Glu281	7.73	4.06	-0.23	2.10	2.45, 2.31	
Lys282	7.68	4.07	-0.29	2.06, 1.91	1.48	H^δ 1.71, 1.65
Val283	8.16	3.61	-0.57	2.15	1.01, 0.91	
Gln284	8.48	3.91	-0.46	2.16	2.55, 2.33	δH^N 7.01, 6.58
Ala285	7.79	4.16	-0.19	1.49		
Ala286	7.70	4.27	-0.08	1.55		
Val287	7.78	4.21	+0.03	2.26	0.97	
Gly288	7.90	3.98	+0.06[c]			
		4.07				
Thr289	7.60	4.22	-0.13	4.16	1.18	

[a]Chemical shifts are referenced to external standard DSS (0.00 ppm). [b]$\Delta H\alpha$ is calculated according to Eq. 4.1. H^α, was taken from Wüthrich (1986). [c]Relative to the average value of the H^α chemical shift.

Table 4.3: Proton Chemical Shifts (ppm) of ApoE(263-286) in SDS-d_{25} Micelles at the peptide/SDS Molar Ratio of 1:90, pH 4.8 and 37 °C[a]

Residue	H^N	H^α	$\Delta H\alpha^b$	H^β	H^γ	Others
Ser263	--	4.31	-0.19	3.85, 3.76		
Trp264	8.41	4.52	-0.18	3.31, 3.20		2H 7.48; 4H 7.35; 5H 7.01; 6H 7.10; 7H 7.44; HN 10.00
Phe265	6.77	4.30	-0.36	2.76, 2.23		2,6H 6.78; 3,5H 7.27; 4H 7.22
Glu266	7.49	4.09	-0.20	2.11	2.39	
Pro267		4.30	-0.14	2.39, 1.80	2.12, 2.00	H^δ 3.69, 3.64
Leu268	7.20	4.25	-0.13	1.91, 1.79	1.64	H^δ 1.07, 0.99
Val269	7.90	3.62	-0.56	2.22	0.97, 0.94	
Glu270	8.11	4.17	-0.12	2.12	2.56, 2.43	
Asp271	8.04	4.55	-0.21	3.16, 2.93		
Met272	8.28	4.25	-0.27	2.28, 2.13	2.76, 2.58	εCH_3 2.03
Gln273	8.45	4.04	-0.33	2.25, 2.16	2.60, 2.41	δH^N 7.10, 6.64
Arg274	7.91	4.18	-0.20	1.93	1.77, 1.63	H^δ 3.25; εH^N 7.21
Gln275	8.12	4.33	-0.04	2.10, 2.05	2.43, 2.26	δH^N 7.07, 6.58
Trp276	8.39	4.61	-0.09	3.39		2H 7.24; 4H7.46; 5H 6.93; 6H 7.02; 7H 7.36; HN 9.80
Ala277	7.98	4.00	-0.35	1.48		
Gly278	8.01	3.96 3.89	-0.02[c]			
Leu279	7.86	4.11	-0.27	1.78	1.69	H^δ 0.95, 0.87
Val280	7.94	3.39	-0.79	1.91	0.79, 0.64	
Glu281	7.64	4.07	-0.21	2.12	2.53, 2.44	
Lys282	7.69	4.10	-0.26	2.04, 1.96	1.63, 1.50	H^δ 1.71; H^ε,3.00; εH^N 7.41
Val283	7.84	3.89	-0.29	2.20	1.02, 0.97	
Gln284	8.00	4.23	-0.14	2.09	2.53, 2.39	δH^N 7.16, 6.65
Ala285	7.69	4.33	-0.02	1.44		
Ala286	7.62	4.21	-0.14	1.42		

[a,b, & c]Same as in Table 4.2.

Because of the overlap of H^N signals for M272 and W276 in apoE(267-289), their side-chain connectivities were corroborated by comparison with the NOESY spectra at other temperatures. The chemical shifts for apoE(267-289) are listed in Table 4.2. The spectra of apoE(263-286) were assigned similarly to apoE(267-289) and the sequential assignment is depicted for both the fingerprint (Fig. 4.6A) and the amide proton (B) regions of the NOESY spectra of apoE(263-286) in SDS-d_{25}. The chemical shifts for apoE(263-286) are presented in Table 4.3. At 37 °C, the H^N signal of W264 was very weak and the assignment was confirmed by NOESY at 27 °C. Also, at a lower temperature H^N and H^δ of F265 were completely resolved. As a result of the shift of the water signal to high field with increase of temperature, the assignment of the resonances near water was verified. S263 was identified by DQF-COSY (Fig. 4.7).

4.2.4 Secondary shifts

The H^α secondary shifts were calculated and are plotted in Fig. 4.8A. The secondary shift ($\Delta H\alpha$) is defined as

$$\Delta H\alpha = H^\alpha_m - H^\alpha_r, \qquad (4.1)$$

where H^α_m is the H^α chemical shift measured and H^α_r the corresponding residue in the random coil (Wüthrich, 1986). The secondary shifts for both apoE peptides are plotted in Fig. 4.8A. A grouping of three or four secondary shifts less than -0.1 ppm is indicative of a helical structure whereas a dense grouping of secondary shifts greater than 0.1 ppm indicates β-strand (Wishart *et al.*, 1992; 1995). For apoE(267-289) the region V269 to A285 is most likely helical whereas for apoE(263-286) the region S263 to Q284 appears to be a helical structure. For both peptides, secondary shifts for most of the residues in the region Q275-G278 are close to zero, suggesting that the structure around that region is less helical (Wishart *et al.*, 1992; Rizo *et al.*, 1993; Chupin *et al.*, 1995).

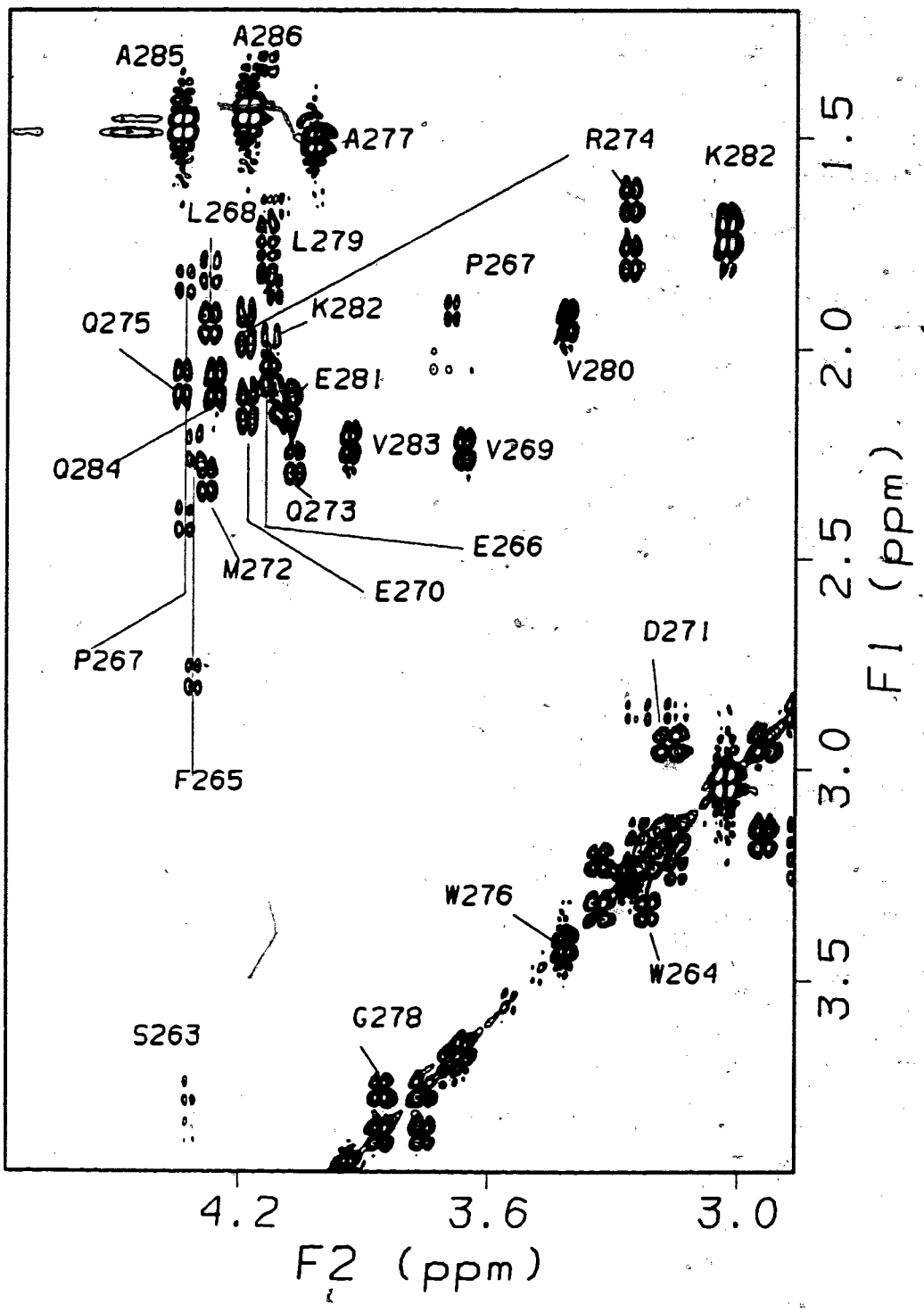

Fig. 4.7: Portion of the DQF-COSY spectrum of apoE(263-286) in SDS. The spectrum was collected for a 5 mM peptide in the presence of SDS-d_{25} (peptide/SDS, 1:90) in D_2O at pH 5.5 and 37 °C.

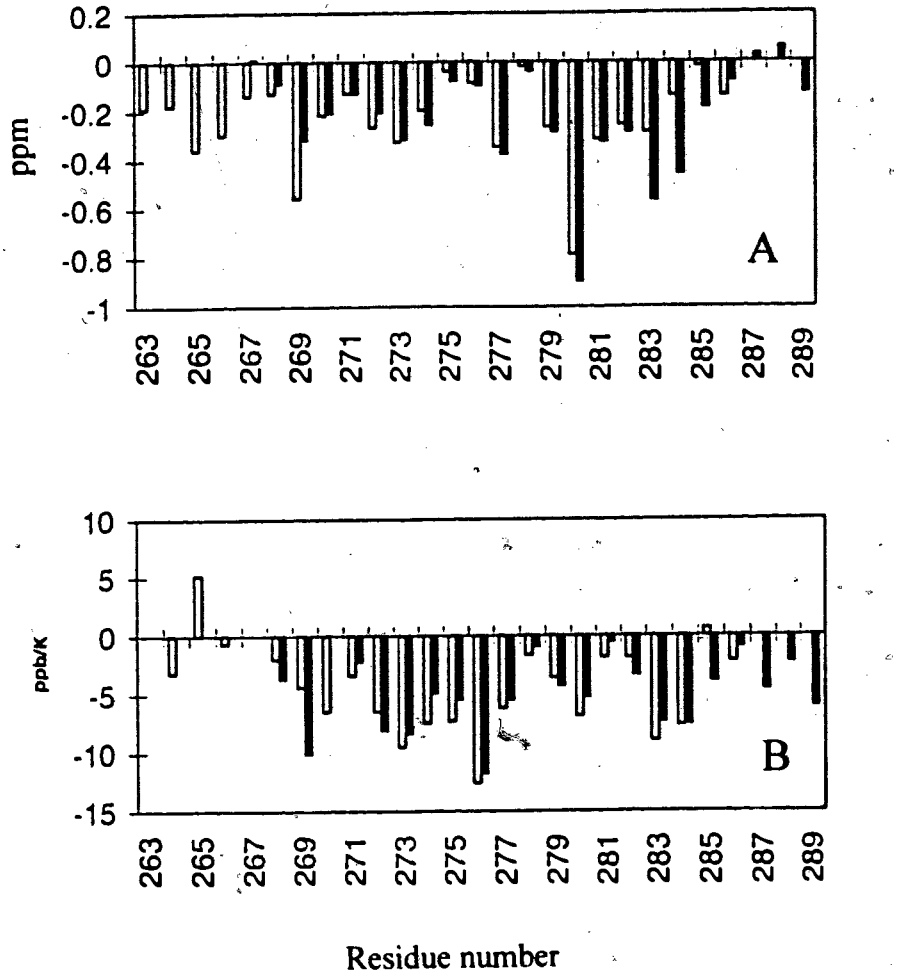

Fig. 4.8: Plots of the secondary shifts or temperature coefficients *versus* the residue number of apoE(267-289) or apoE(263-286) in SDS. (A) Secondary shifts of the α-protons of apoE(263-286) (white column) and apoE(267-289) (black column). (B) Temperature coefficients of amide protons of apoE(263-286) (white column) and apoE(267-289) (black column). Data were read from the NOESY spectra (τ_m = 100 ms) collected with 2K data points in t_2 and 400 increments (16 scans each) in t_1.

From Fig. 4.8A, the periodicity of the secondary shifts is evident, suggesting amphipathic helical structure (Bruix *et al.*, 1990; Szilágyi, 1995). Based on the secondary shifts, the helix content can be estimated using the following formula (Bruix *et al.*, 1990; Rizo *et al.*, 1993):

$$\text{Helix}\% = (\Sigma|\Delta H\alpha|/n/0.35) \times 100, \qquad (4.2)$$

where $\Sigma|\Delta H\alpha|$ is the sum of the absolute values of the secondary shifts, n is the number of residues in the peptide, and the constant 0.35 is an average secondary H^{α} shift value where 100% helix is assumed. The helix content thus obtained is 60% for apoE(263-286) and 58% for apoE(267-289) in SDS. In the calculations, 0.5 ppm was deducted from the sum to reflect the ring current effect of W276 on the H^{α} of V280 (see below) (Johnson and Bovey, 1958). These helix percentages are similar to those found by CD for the two peptides (Table 4.1).

4.2.5 Temperature dependence of amide proton chemical shifts

Temperature coefficients for the H^{N} protons of apoE(263-286) and apoE(267-289) in SDS micelles are presented in Fig. 4.8C. Temperature coefficients have been utilized as evidence for hydrogen bonds or solvent accessibility, and to determine the secondary structures in peptides (Basu *et al.*, 1991; Liu *et al.*, 1993; Raj *et al.*, 1994; Yee *et al.*, 1995; Sejbal *et al.*, 1996a). Temperature coefficients ranging from -3.0 to 0 ppb/K are indicative of hydrogen-bonded; -3 to -4.5 ppb/K of weak hydrogen-bonded, and -5 to -12 ppb/K of solvent exposed amide protons (Liu *et al.*, 1993; Yee *et al.*, 1995; Sejbal *et al.*, 1996a). In apoE(263-286) amide protons of residues W264, E266, L268, D271, G278, E281, K282, A285, and A286 are probably hydrogen-bonded whereas for apoE(267-289) amide protons of residues E270, D271, G278, E281, K282, A286, and G288 may be hydrogen-bonded. While hydrogen bonds were found along almost the entire sequence of apoE(263-286), in apoE(267-289) most were located at the C-terminus, indicating that the N-terminus of apoE(267-289) is less structured (Fig. 4.8C).

In both peptides, the backbone amide protons of residues 272-277 are most sensitive to temperature, indicating that the region is highly solvent accessible.

4.2.6 NOE connectivities and secondary structures

Fig. 4.9A is a summary of interresidue NOEs of apoE(263-286) in the presence of SDS-d_{25}. Medium to strong H^N_i-H^N_{i+1}, H^α_i-H^N_{i+1}, H^α_i-H^N_{i+3}, H^α_i-H^β_{i+3} and weak to medium H^α_i-H^N_{i+4}, H^α_i-H^N_{i+2}, H^N_i-H^N_{i+2} NOE connectivities were found for the region L266 to A286, indicating a helical structure (Wüthrich, 1986). In addition, the N-terminus contains many (i, i+3) and (i, i+4) NOE connectivities between aromatic rings of W264 or F265 and the side chains of L268 or V269, suggesting that the helical structure extends to W264. NOE cross peaks between P267 H^δ and E266 H^N as well as P267 H^δ and E266 H^α, but not between P267 H^α and E266 H^α, indicate the E266-P267 peptide bond is predominantly in the *trans* conformation (Wüthrich *et al.*, 1984). Inclusion of a proline in a helical region has been reported for several peptides (Barlow and Thornton, 1988; Yun *et al.*, 1991; Johnson *et al.*, 1994; Yuan *et al.*, 1995).

Interresidue NOEs for apoE(267-289) in SDS are summarized in Fig. 4.9B. These NOE connectivities support an α-helix structure for the region 277-288 (Wüthrich, 1986). A combination of strong H^α_i-H^N_{i+1}, weak H^α_i-H^N_{i+2}, H^α_i-H^N_{i+3}, H^N_i-H^N_{i+2} and weak to medium H^α_i-H^β_{i+3} NOEs (Fig. 4.9B) was found for residues 267-276 of apoE(267-289), suggesting an unstable helical structure in that region. This is further supported by strong TOCSY relayed peaks from amide protons to side chains for residues 267-276 but weak relays for the region 277-288 (Fig. 4.4). The former is similar to what was observed for apoC-I(35-53) (Buchko *et al.*, 1995), apoA-II(18-30)+ (Chapter 5), and other peptides in water (Dyson *et al.*, 1988 & 1992) while the latter resembles the well-defined helical regions of apoA-I peptides in micelles (Chapter 6). Therefore, the N-terminus of apoE(267-289) is probably weakly bound to SDS (Pierens *et al.*, 1995).

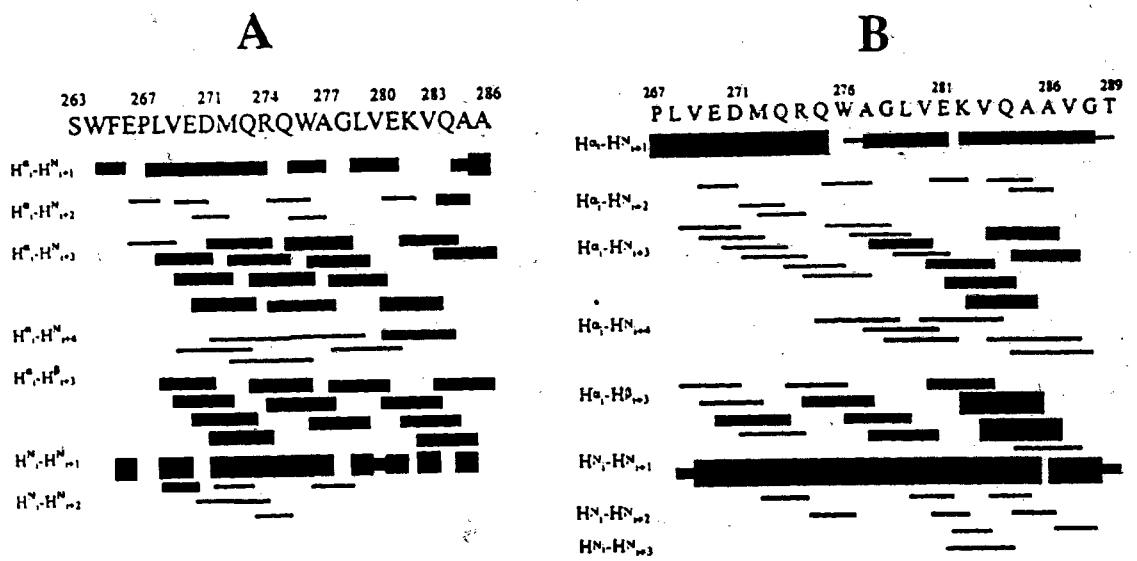

Fig. 4.9: Summary of interresidue NOEs for apoE(267-289) (A) and apoE(267-289) (B) in SDS. NOEs were derived from the spectra collected in an aqueous solution of SDS-d_{25} (peptide/SDS, 1:90) at a mixing time of 100-150 ms. NOE intensities are indicated by the height of the bar [From Wang *et al.*(1996a)].

4.2.7 Three-dimensional structures of apoE(263-286) and apoE(267-289) in SDS

For the final DGII calculations, 370 NOE distance restraints (194 inter- and 176 intra-residue) for apoE(263-286) and 276 NOE restraints (143 inter- and 133 intra-residue) for apoE(267-289) were used. The number of NOEs per residue for both peptides is plotted in Fig. 4.10. More NOE restraints were obtained for the aromatic residues (W264, F265, and W276) and L268, V269 and V280 than other residues. Therefore, the larger number of NOEs for apoE(263-286) than for apoE(267-289) arises mainly from the N-terminus in the former. Fig. 4.11A shows an ensemble of 41 structures of apoE(263-286) and Fig. 4.11B an ensemble of 37 structures of apoE(267-289), where the backbone atoms (N-C^{α}-C=O) have been superimposed. From the ensemble of structures, the RMSD for superimposing residues 265-284 of apoE(263-286)

is 0.64 ± 0.17 Å for backbone atoms and 1.51 ± 0.13 Å for all atoms. The backbone RMSDs of apoE(267-289) are 0.75 ± 0.21 Å for superimposing residues 268-275 and 0.34 ± 0.10 Å for residues 276-286, respectively.

Fig. 4.12 is a plot of pairwise RMSD *versus* residue number in the sequence. The RMSD for superposition of all atoms for both peptides is generally below 1.5 Å. Increased RMSDs at the termini for both peptides indicate end fraying (Shoemaker *et al.*, 1987; Rozek *et al.*, 1995). Backbone atoms in the N-terminus of apoE(267-289), e.g., from residues 267-275, are less well defined than those at the C-terminus and the N-terminus of apoE(263-286) is better defined than that of apoE(267-289) (refer to Figs. 4.9 & 4.10). For apoE(263-286), the RMSDs for residues Q273 to Q275 are as large as those of terminal residues (Fig. 4.12A), suggesting that this middle part of the helix is distorted.

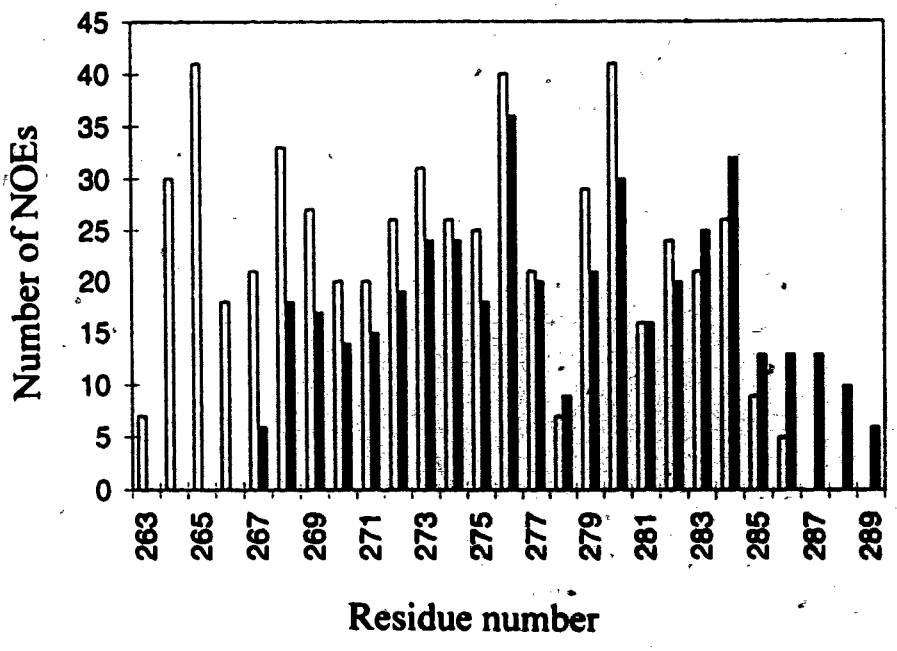

Fig. 4.10: Number of NOE restraints per residue found for apoE(263-286) (white columns) and apoE(267-289) (black columns) bound to SDS. Data were obtained from the statistical analysis of the restraint files employed in the calculations.

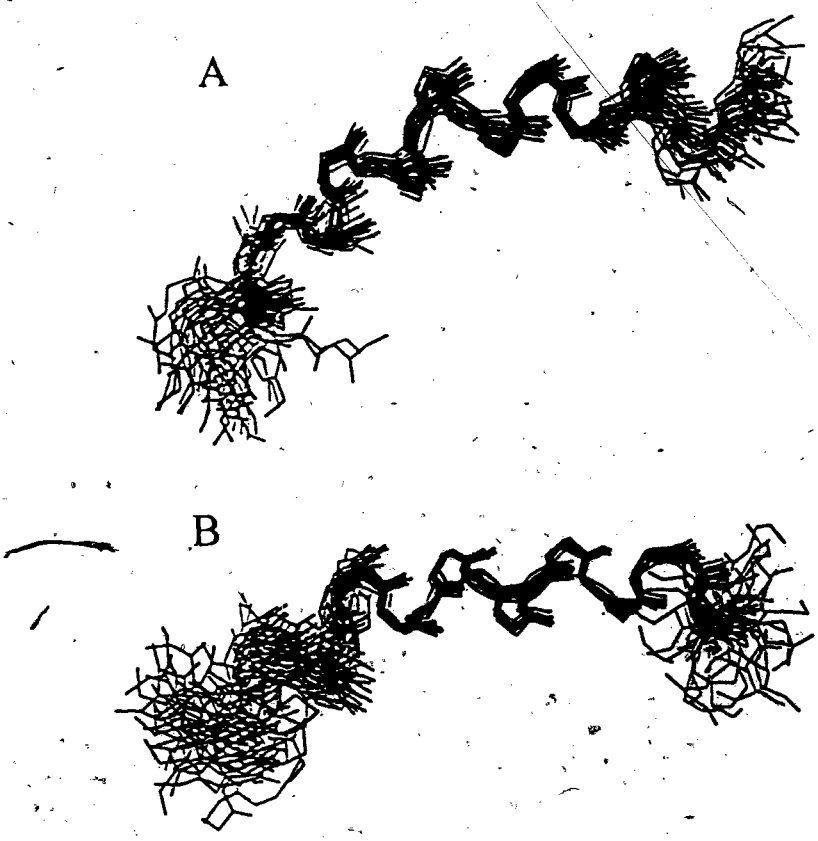

Fig. 4.11: Superimposed backbone view of an ensemble of the structures for apoE(263-286) (A) and apoE(267-289) (B). A total of 41 structures for apoE(263-286) (A) and 37 structures for apoE(267-289) bound to SDS-d_{25} (B) was calculated based on NOE-derived distance restraints using the DGII program. The backbone atoms (N-C^{α}-C=O) of residues E266 to Q284 for apoE(263-286) and residues Q275 to Q286 for apoE(267-289) have been superimposed [From Wang *et al.* (1996a)].

A stereoview of side-chain orientations for both peptides is shown in Fig. 4.13, from which the hydrophobic (medium grey), hydrophilic (light grey), and interfacial (dark) faces can be seen. Side chains, especially hydrophilic ones, are less well defined than backbone atoms due to fewer interresidue restraints and quenching of NOEs by side-chain mobility (Berndt *et al.*, 1996; Doucet & Weber, 1996). In Fig. 4.14, we show the average orientation for side chains of apoE(263-286) (A) and apoE(267-289) (B) with the backbone atoms replaced by ribbons. For apoE(263-286), an amphipathic helix-bend-helix structural motif was found with a bend angle of ~150°. This helical bend around residues 273-278, also evident from Figs. 4.11A and 4.13A, is consistent with near zero secondary shifts as well as large temperature coefficients for the region (Fig. 4.8). All hydrophobic side chains in apoE(263-286) are clustered on the concave face and E266, P267, E270, R274, E281, and A283 on the convex hydrophilic face. Residues D271, Q273, Q275, A277, K282, and Q284 are found at the interface. Similar side-chain orientations can be seen in the structure of apoE(267-289) (Figs. 4.13B and 4.14B). The colored amphipathic helical structures for apoE(263-286) and apoE(267-289) can be viewed at: http://pdb.pdb.bnl.gov/. The PDB identification number is 1oef for the former and 1oeg for the latter.

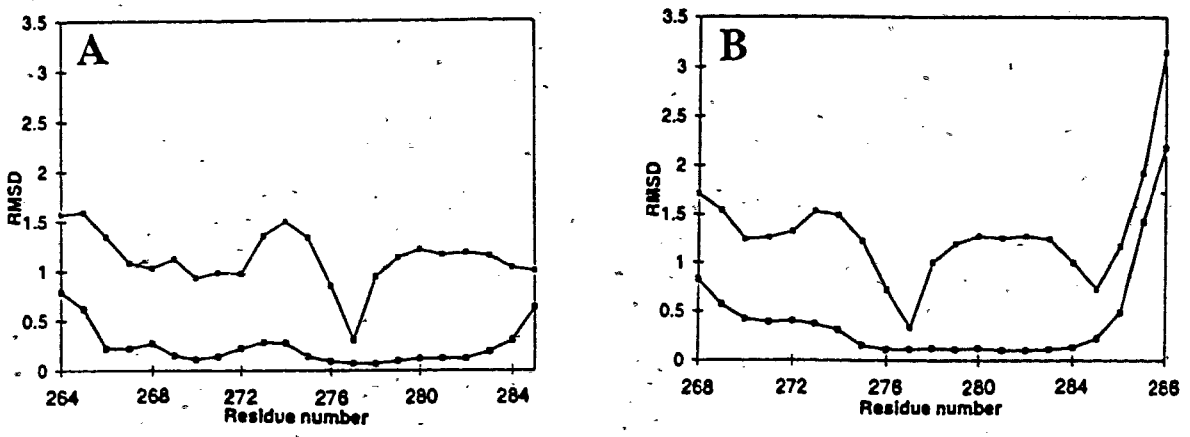

Fig. 4.12: Plots of pairwise RMSDs for the structures of apoE(263-286) (A) and apoE(267-289) (B) bound to SDS. RMSDs are relative to the mean structure for superposition of all atoms (solid squares) and backbone atoms N-C^{α}-C=O (open squares) of each residue of apoE(263-286) (A) and apoE(267-289) (B). Data were smoothed in a three-residue window [From Wang *et al.* (1996a)].

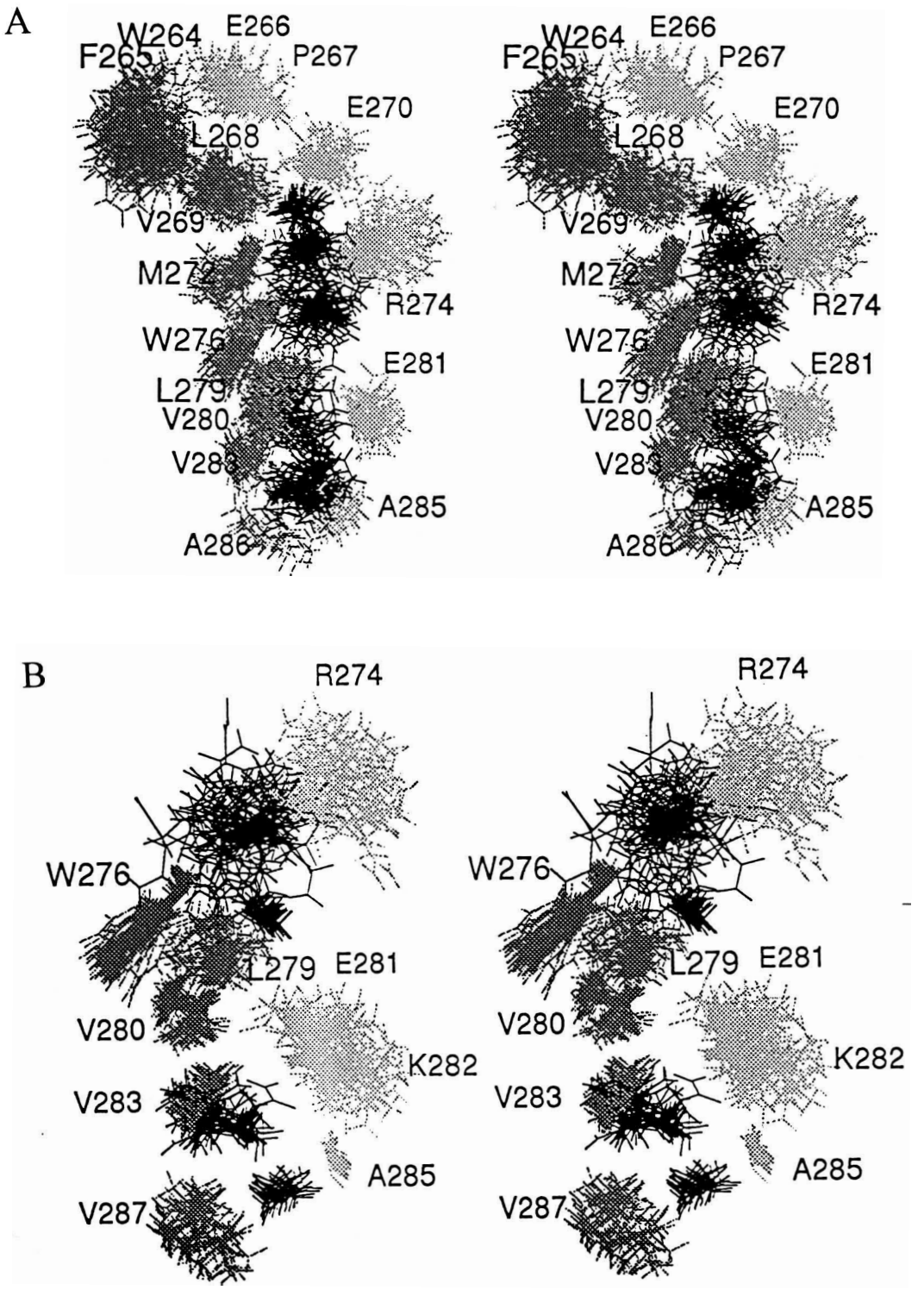

Fig. 4.13: Stereoview of the side chains of apoE(263-286) (A) and apoE(267-289) (B) in SDS-d_{25}. The backbone atoms are omitted for clarity. Hydrophobic side chains are shown in medium grey, hydrophilic side chains in light grey, and interfacial side chains in dark grey. Side chains are selectively labeled. In (A), interfacial side chains from top to bottom are D271, Q273, Q275, A277, K282, and Q284. In (B), side chains of residues 267-273 and 288-289 are not shown due to fraying [From Wang *et al.* (1996a)].

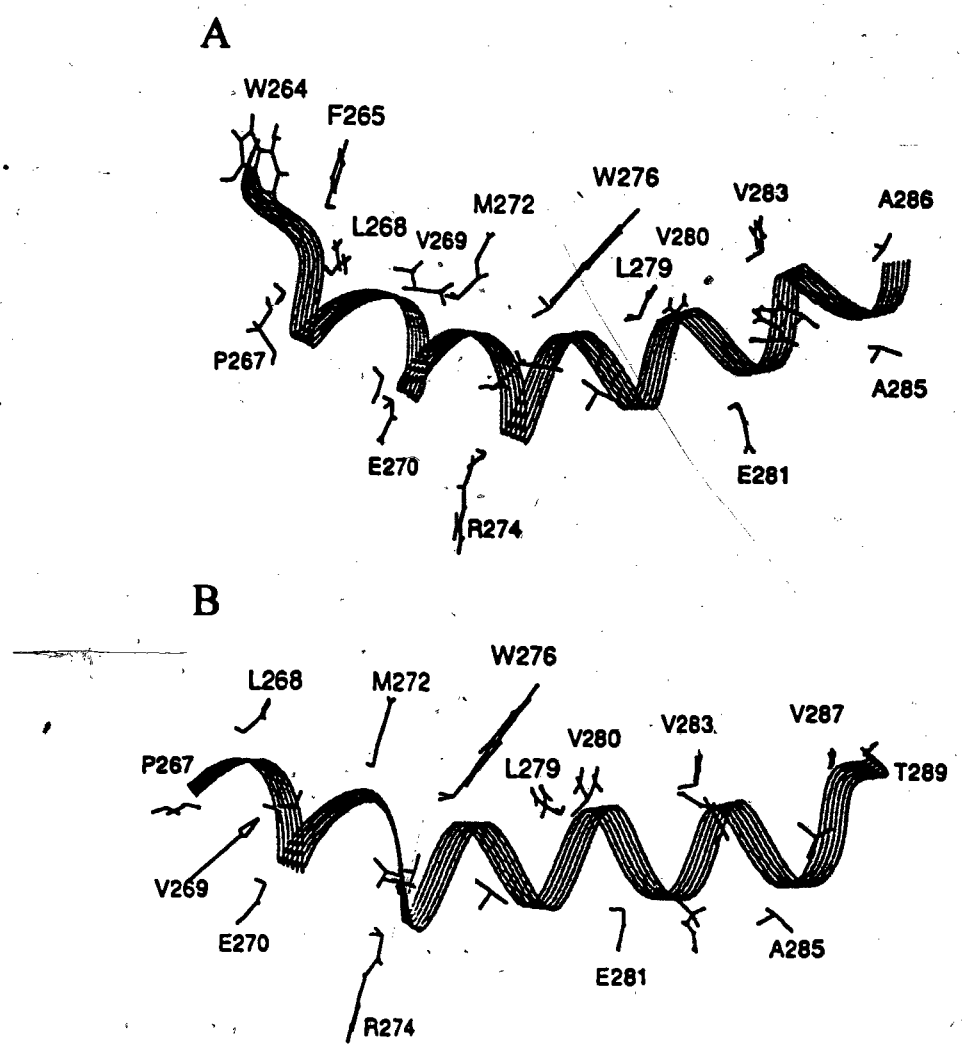

Fig. 4.14: Side view of the average structures of apoE(263-286) (A) and apoE(267-289) (B) in SDS-d_{25}. The backbone atoms are replaced by ribbons. Hydrophobic side chains are clustered on the same side forming the hydrophobic face whereas hydrophilic side chains are distributed on the opposite side. Interfacial side chains, D271, Q273, Q275, A277, K282, and Q284, are not labeled for clarity. Excursions of longer side chains such as R274 and K282 were defined by a cone (Fig. 3.13) with the average orientation corresponding to the axis of the cone [From Wang *et al.* (1996a)].

As shown in Fig. 4.14, the aromatic side chain of W276 in the average structures of both peptides forms a 30-50° angle with the helix long axis and lies close to V280. As a result of the ring current effect, the chemical shifts of H^{α}, H^{β}, and one of the H^{γ} of V280 are shifted to higher field (Johnson and Bovey, 1958; Plesniak *et al.*, 1996) compared to other valines in Tables 4.2 and 4.3. This ring current effect between residue i (W276) and residue i+4 (V280) further supports a helical structure for that part of the molecule and indicates hydrophobic side-chain interaction in the helix. In apoE(263-286), Fig. 4.14A, F265 forms an 85° angle with the N-terminal helix long axis. In addition, W264 lies close to L268 and F265. This accounts for the upfield shift of H^{N}, H^{β}, H^{δ} of F265, and H^{N} of L268 (Table 4.2). Successful interpretation of these ring current effects on proton chemical shifts indicates that an accurate geometry has been obtained for these apoE peptide structures in the lipid-bound state.

4.3. DISCUSSION

4.3.1 ApoE(263-286) has a helix-bend-helix structure

In the lipid-bound state, CD and H^{α} secondary shifts suggest helical conformations for these apoE peptides. The detailed 3D structures, shown in Figs. 4.11, 4.13 & 4.14, confirmed the amphipathic helical structures. While K282 lies in the interface, R274 is located at the center of the hydrophilic face (Fig. 3.14). Such a "random" orientation of cationic side chains on the hydrophilic face of both peptide structures elucidated in the micelle model fits the definition for the class G* amphipathic helix (refer to Section 1.4 and Fig. 1.2). However, the helices determined are not "ideal" as predicted. ApoE(267-289) is a two-domain structure with a flexible N-terminal helix. As a result, V269, on average, is not located on the hydrophobic face (Fig. 4.14B). In addition, apoE(263-286) was found to be a curved helix-bend-helix motif with a bend angle of approximately 150° (Figs. 4.11A and 4.14A). Based on sequence prediction

algorithms and CD data, Nolte and Atkinson (1992) proposed a helix from residues 264-271, a β-strand from 273-277 and a helix from 279-285 of apoE. While we see no evidence of β-strand, the helical bend we find in the vicinity of residues 273-278 corresponds exactly to Nolte and Atkinson's proposed β-region. A similar curved helical structural motif was reported for melittin bound to DPC micelles (Inagaki *et al.*, 1989), in methanol (Bazzo *et al.*, 1988), and in the crystal structure, where the peptide is in the tetramer state (Terwilliger *et al.*, 1982). Interestingly, these structures all bend at G12 with a proline in the vicinity. Chupin *et al.* (1995) found that the signal peptide adopts similar secondary structures in SDS, DPC, or TFE with a break again at G12. As apoE(263-286) showed near zero H^{α} secondary shifts at G278 in either TFE (not shown) or in SDS, it appears that the secondary structure of apoE(263-286) is determined primarily by the peptide sequence (Inagaki *et al.*, 1989; Cordier-Ochsenbein *et al.*, 1996). In addition, the chemical shift differences in different environments (Fig. 4.8B) indicate that the lipid also modulates the peptide conformation to some extent as apoE(263-286) is more helical at the N-terminus in SDS than in TFE probably due to the peptide-lipid interactions (Section 4.3.3). These interactions may have caused near zero secondary shifts for two more residues, Q275 and W276, in SDS (Fig. 4.8B) but not in TFE. In this sense, the helix-bend-helix motif may be said to better conform to the micelle. In conclusion, the peptide sequence, lipid, and the peptide-lipid interactions all play a role in determining the final conformation of the peptide in lipid.

4.3.2 Factors that stabilize class G* amphipathic helices

From the average structure, the (i, i+4) hydrogen bond between the carbonyl group and the amide proton can be measured using the program HBond in the NMR-Refine module of Insight II. A hydrogen bond satisfies the following conditions: $H^{N}\cdots O$ distances less than 2.5 Å and N-H···O bond angles between 120 and 180°. According to these criteria, nine hydrogen bonds involving amide protons of L279 to V287 were found

for apoE(267-289), all at the C-terminus. This finding is consistent with the two-domain structure of apoE(267-289) (Fig. 4.11A). The existence of these hydrogen bonds only at the C-terminus may explain, at least in part, the selective decay of amide signals with increase of pH at the N-terminus of apoE(267-289) (Fig. 4.3) (Englander & Kallenbach, 1983; Perrin *et al.*, 1990; Déméné *et al.*, 1994; Finucane & Jardetzky, 1996).

Recently, Wang *et al.* (1996b) found that all interfacial arginine side chains of apoA-I(166-185) showed intermolecular NOEs with SDS alkyl chains, thus enhancing the binding of the class A amphipathic helix to the micelle. The association of these apoE peptides with SDS is supported by CD (Fig. 4.1), fluorescence spectroscopy (Fig. 4.2), and chemical shift change and line broadening of peptide resonances (Section 4.2.3). As only K282 was found in the interface, electrostatic interactions between negatively charged SDS head groups and positively charged peptide side chains do not appear to be essential in the binding of these apoE peptides to the micelles. Instead, these G* helices bind to lipid predominantly by exposing a large hydrophobic surface due to the existence of hydrophobic pairs in the sequence such as W264F265, L268V269 and L279V280. Hence, these structures substantiate the notion that the hydrophobic effect dominates in stabilizing the peptide structure complexed with the micelle (Buchko *et al.*, 1996a,b; Wang *et al.*, 1996b;1997b).

Since the hydrophobic effect plays the major role, we may neglect other factors here and calculate the hydrophobic binding energy for solely comparative purpose. On the basis of the transfer free energies for amino acids (Nozaki & Tanford, 1971; Tanford, 1980), Karplus (1997) has tabulated the estimated hydrophobic effect for side chain burial (δG_i) (Table 4.4). We may estimate hydrophobic binding free energy (ΔG_{hb}) for an amphipathic helix by summing the transfer free energy of all hydrophobic side chains, viz.,

$$\Delta G_{hb} = \Sigma(\delta G_i). \qquad (4.3)$$

From the residues found on the hydrophobic faces of the structures (Figs. 4.13 and 4.14) ΔG_{hb} was calculated to be −22.8 kcal/mol for apoE(263-286) and −17.6 kcal/mol for apoE(267-289). Since the fragments are of similar length (24 *versus* 23 residues), we

attribute the more favorable ΔG_{hb} for apoE(263-286) to the additional hydrophobic pair of aromatic residues, W264 and F265. This may explain, in part, why apoE(263-286) binds to DMPC and apoE(267-286) (ΔG_{hb} = -15.4 kcal/mol) does not (Sparrow *et al.*, 1992).

Table 4.4: Transfer Free Energies (kcal/mol) for Atoms, Hydrophobic Side Chains[a], hydrophobic Pairs and Some Hydrophobic Clusters[b]

Side chain	δG_i	Hydrophobic pair	ΔG_p	Hydrophobic cluster	ΔG_c
W	-2.9	WF	-5.2	WFLV	-10.3
F	-2.3	WL	-5.8	WLVV	-10.2
L	-2.9	LI	-5.6	LLLL	-11.6
I	-2.9	LL	-5.8		
M	-2.3	LM	-5.2		
Y	-1.6	YF	-3.9		
V	-2.2	LV	-5.1		
A	-1.0	VV	-4.4		
K	-1.9				
R	-1.1				

[a]Karplus (1997). [b]Hydrophobic pairs are defined as a pair of residues that are adjacent in sequence such as W264F265 while a hydrophobic cluster is a lipid binding unit characterized by the packing of a group of hydrophobic side chains (Section 4.3.3). ΔG_p and ΔG_c are calculated similar to ΔG_{hb} by summing the component side chains.

4.3.3 Aromatic-aromatic interactions, hydrophobic pairs and hydrophobic clusters are lipid-binding elements

Like cationic side chains, the indole ring of Trp is amphipathic. As can be seen from Fig. 4.14, W264 adopts an orientation with the hydrophobic six-membered ring

facing inward and the five-membered ring outward. On the other hand, W276 is on the hydrophobic face near the helical bend region, which may account for the large negative temperature coefficients of the amide protons (Fig. 4.8B). A statistical analysis of membrane proteins revealed that most of the aromatic residues (Trp, Phe, and Tyr) appear to prefer the interfacial regions (Landolt-Marticorena *et al*, 1993), where Trp and Tyr residues may form hydrogen-bonds with the lipid head groups or water (Haltia & Freire, 1994). Such orientations of Trp side chains are believed to be energetically favorable (Jacobs & White, 1989; Cowan *et al.*, 1992) and would explain the blue shift in the fluorescence spectroscopy of apoE peptides (Fig. 4.2).

In proteins, aromatic rings are frequently found to be perpendicular to one another, approximately 4.5-7 Å apart. This is believed to result from favorable partial charge interactions between δ+ hydrogen atoms on the edge of one ring and δ- π-electrons on the face of the other ring (Burley and Petsko, 1985;1988; Serrano *et al.*, 1991). As can be seen from Fig. 4.14A, the aromatic rings of W264 and F265 in the average structure are oriented more or less perpendicular to each other. The distances between aromatic H^{δ} or H^{ε} protons of F265 and the six-membered ring of W264 were calculated to be 4-6 Å. Such an edge-to-face aromatic-aromatic interaction may explain the lower fluorescence for apoE(263-286) than apoE(267-289) in SDS (Fig. 4.2) owing to quenching (Siemion *et al.*, 1994). It caused ring current shifts for H^{δ}, H^{β}, and H^{N} of F265 (Johnson and Bovey, 1958). A large upfield shift of H^{N} of L268 (1.42 ppm) is also observed. These ring current effects are a good indication of the packing of hydrophobic side chains in the amphipathic helix. Taken together with the NOEs found between W264, F265, L268, and V269, a hydrophobic cluster of these four residues is proposed (ΔG_c = -10.3 kcal/mol). While such aromatic-aromatic interactions (-1 to -2 kcal/mol) have been found to stabilize protein tertiary and quaternary structures (Burley and Petsko, 1985; Serrano *et al.*, 1991), we propose that the hydrophobic cluster, including the aromatic-aromatic interaction in apoE(263-286), creates a new lipid binding site and plays a crucial role in the stabilization of the amphipathic helix structure at the N-terminus of apoE(263-286) via intercalating the hydrophobic cluster into the hydrophobic core of SDS micelle (Figs. 4.13 and 4.14). A similar N-terminus stabilization has been

observed with apoA-I(166-185) in the presence of SDS, wherein the terminal Y166 aromatic ring orients toward the hydrophobic face due to interaction with SDS (Chapter 6). As a consequence of intercalation into the micelle interior, the W276 side chain in both apoE peptides has very restricted motion (Fig. 4.13), resulting in ring current shifts of H^{α}, H^{β}, and one of the H^{γ} of V280 (Tables 4.2 and 4.3). Hence, W276, hydrophobic pair L279V280, and V283 constitute another hydrophobic cluster (ΔG_c = -10.2 kcal/mol, Table 4.4). The fact that apoE(263-286) contains two hydrophobic clusters whereas apoE(267-289) only one would further explain why apoE(263-286) binds to DMPC "avidly" and apoE(267-286) does not (Sparrow *et al.*, 1992). In addition, the hydrophobic packing and formation of hydrophobic clusters may be the direct reason for the curved helix structure of apoE(263-286). Interestingly, a similar ring current effect of the Trp (i) on residue (i+4) has been observed with one of the apoC-I fragments (Rozek *et al.*, 1995; Buchko *et al.*, 1995) and the LCAT-activating peptide LAP-20 (Buchko *et al.*, 1996b) in both SDS and DPC. Therefore, hydrophobic packing involving aromatic residues appears to be general. We propose that aromatic and paired hydrophobic residues are especially important in anchoring apolipoproteins to lipid.

4.3.4 Biological Implications

We have elucidated the detailed structures for the primary lipid binding segment at the C-terminus of apoE (Sparrow *et al.*, 1992; Westerland & Weisgraber, 1993; De Pauw *et al.*, 1995). The molecular basis for high lipid affinity of apoE(263-286) was attributed to several aromatic residues and hydrophobic pairs in the sequence by forming hydrophobic clusters. Scanning through the entire apoE sequence revealed that there are only two such regions that are rich in aromatic and paired hydrophobic residues. They are residues 29-40 and 260-290, the latter corresponding to apoE(263-286). Therefore, such a sequence analysis may be useful in locating strong lipid binding segments in apolipoproteins. Indeed, sequence analysis found that such strong lipid binding domains exist at the carboxyl termini of all human exchangeable apolipoproteins except apoC-II,

consistent with the deduction from peptide studies as stated in Wang *et al.* (1996a). However, the similarity between the C-terminus of apoA-I and that of apoE is more striking. Deletion of the C-terminal segment from either protein reduces not only the lipid affinity but also the propensity to aggregate in the absence of lipid (Westerlund and Weisgraber, 1993; Holvoet *et al.*, 1996; Ji & Jonas, 1995). In addition, such an apoA-I mutant has a much higher catabolic rate *in vivo* than the wild type (Schmidt *et al.*, 1995). Therefore, the significance of these hydrophobic amphipathic helices may be to anchor apolipoproteins to lipid, to stabilize the lipoprotein structures, and to determine the lifetime of these proteins in metabolism. They may also determine the lipid carrier capacity of the protein and particle size of lipoproteins (please also refer to Wang *et al.*, 1996a).

CHAPTER 5: SOLUTION STRUCTURES OF APOA-II(18-30)+ IN THE PRESENCE OF SDS

5.1 Introduction

Human apoA-II is the second major protein of HDL particles. Its primary structure contains two identical polypeptide chains of 77 residues each, linked at Cys6 via a disulfide bond (Brewer *et al.*, 1972). The reduction and alkylation of the disulfide bond of apoA-II led to complete conversion of the dimer to the monomer without affecting the structure, composition and particle size distribution of HDL_3 (Calabresi *et al.*, 1996). Such a treatment of apoA-II does not impair its lipid affinity significantly (Jackson *et al.*, 1973). Segrest *et al.* (1974) predicted that two regions, residues 17-30 and 39-47, of apoA-II are amphipathic helices. Based on the lipid-binding studies on synthetic peptides, segment 50-77 was found to be the minimum C-terminal lipid-binding region (Mao *et al.*, 1981). On the other hand, Chen *et al.* (1979) found that the N-terminal synthetic peptide apoA-II(17-31) did not bind to DMPC but apoA-II(12-31) or (7-31) did. These data illustrate that the N-terminal lipid-binding domain of apoA-II should be slightly longer than predicted. Therefore, apoA-II contains at least two lipid-binding regions, which are at the C- and N-termini (Sparrow and Gotto, 1982).

In Chapter 4, we showed that aromatic residues and hydrophobic pairs are key lipid-binding elements. Here we attempt to enhance the lipid affinity of the segment, apoA-II(18-30), by adding to the C-terminus five more residues EWLNS, which contains a hydrophobic pair WL. ApoA-II(18-30, EWLNS) is herein referred to as apoA-II(18-30)+, where the sign "+" denotes our effort to increase the lipid affinity. The amphipathic potential of apoA-II(18-30)+ has been maintained (Fig. 1.2). Introduction of a Trp residue to the peptide facilitates fluorescence measurement. The binding of apoA-II(18-30)+ to SDS, DPC, and TMA was also investigated by CD. Based on CD and fluorescence spectroscopy, 2D NMR studies of the peptide were performed in the

presence of SDS. The solution structures of the peptide bound to SDS were determined using NOE restraints and distance geometry calculations in cooperation with Dr. Buchko (Buchko *et al.*, 1996a).

5.2 Results

5.2.1 Optical spectroscopy

In the absence of lipid, the CD spectrum of apoA-II(18-30)+ showed a strong negative band at 200 nm, suggesting that the major conformation is random (Woody, 1995). With the addition of SDS, CD spectra exhibited a strong positive band at 192 nm and two minima at 208 and ~220 nm, respectively, indicating the formation of α-helix (Holzwarth & Doty, 1965). Similar spectral changes occurred upon the addition of dodecylphosphocholine (DPC) or tetradecyltrimethyl ammonium chloride (TMA). The helix content of apoA-II(18-30)+ in water and in various lipids was analyzed by CCA (Table 5.1). Apparently, the peptide became helical in all three lipids. Table 5.1 suggests that SDS is most effective and TMA is least effective in the promotion of helical structure of apoA-II(18-30)+.

The maximum emission of the fluorescence spectrum appeared at 350 nm in the absence of lipid, indicating that the Trp is exposed to water (Jonas, 1992). The addition of SDS, DPC, or TMA all induced a blue shift (Table 5.1), illustrating that the Trp in apoA-II(18-30)+ moves to a more hydrophobic milieu (Lakowicz, 1983; Jonas, 1992) as a result of helix formation (above). This is reminiscent of apoE peptides, where blue shifts of Trps correlate with their locations on the hydrophobic face of the amphipathic helix and intercalation into the micellar interior (Chapter 4). Both CD and fluorescence spectroscopy suggest that apoA-II(18-30)+ also binds DMPC (Buchko *et al.*, 1996a), confirming that our enhancement of the lipid affinity of apoA-II(18-30) has been successful.

Table 5.1: Helix Content and Wavelength of the Maximum Emission of ApoA-II(18-30)+ in Various Lipids[a]

Lipid	Net charge	Peptide/lipid ratio	Helix content (%)	λ_{max} (nm)
-	-	1:0	10	351
SDS	-1	1:40	55	338
DPC	0	1:40	45	336
TMA	+1	1:40	39	337

a. Adapted from Buchko *et al.* (1996a). Helix contents were estimated from CCA analysis (Perczel *et al.*, 1991). The last column is the wavelength of the maximum emission of the fluorescence spectrum of the tryptophan in the peptide.

5.2.2 NMR Structure

5.2.2.1 Signal assignment

In aqueous solution at pH 2.6, all backbone amide protons of apoA-II(18-30)+ showed clear doublets owing to spin-spin coupling with the α-protons (Fig. 5.1A). The coupling constants measured range from 5.5 to 5.8 Hz for Y21, D24, E27, and K30 but 7.6-7.7 Hz for T19 and D20. While the terminal residues of the peptide have a coupling constant typical of conformational averaging, the coupling constants for the residues in the middle region indicate some populations of "nascent helical structures" sampled by NMR (Wüthrich, 1986). Supporting this notion are the weak (i, i+3) NOEs but strong H^{α}_{i}-H^{N}_{i+1} cross peaks in the region (Buchko *et al.*, 1995). Increase of pH to 4.8, however, brought about a dramatic broadening and shift of signals and those coupling constants could no longer be measured (Fig. 5.1B). We attribute this effect to the peptide aggregation (Buchko *et al.*, 1996a). A similar phenomenon was observed for apoE(263-286) with increase of pH.

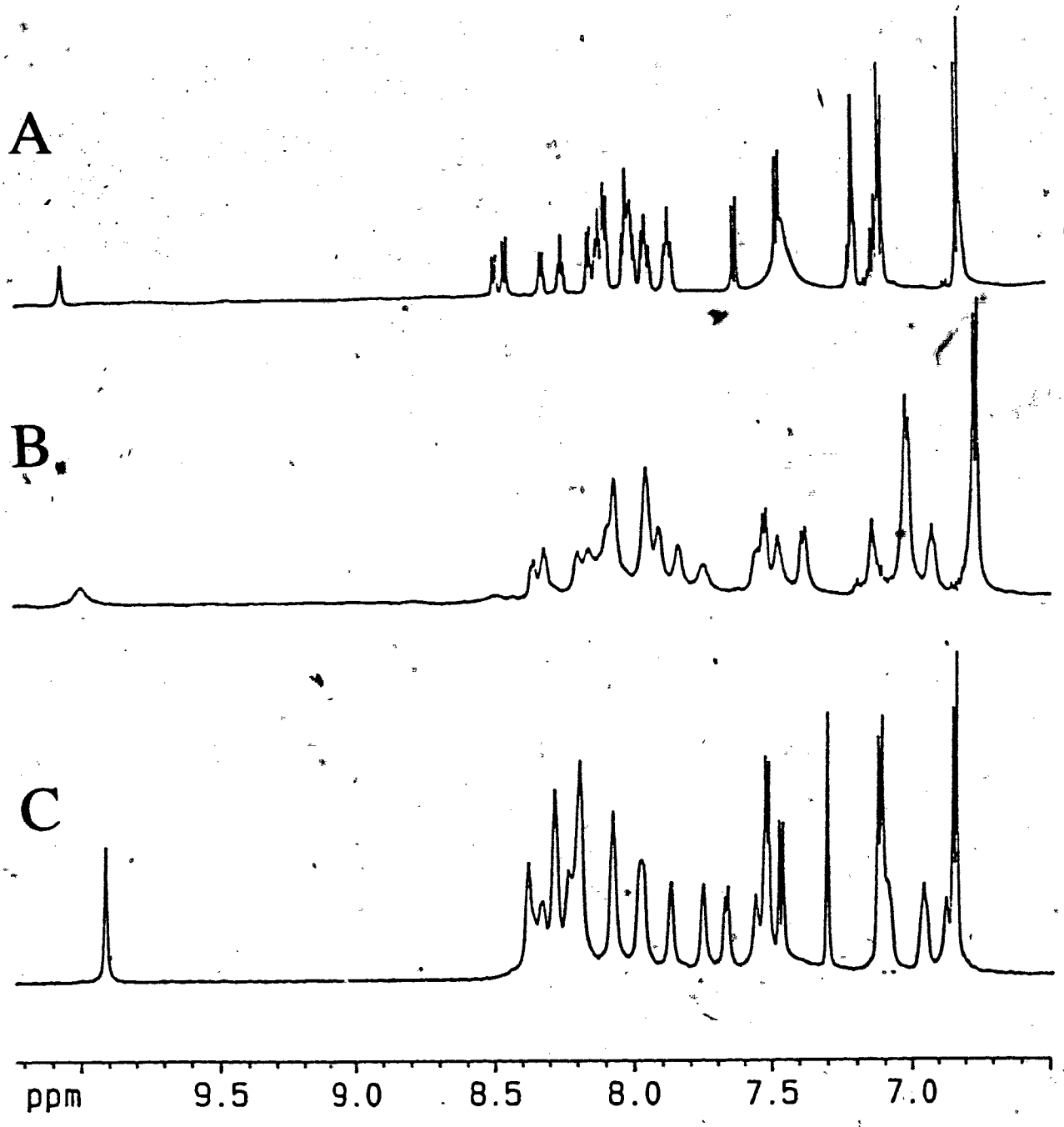

Fig. 5.1: Amide and aromatic proton regions of the NMR spectra of apoA-II(18-30)+ under different conditions. Spectra were collected for a 5.0 mM peptide (A) in water, pH 2.6; (B) in water, pH 5.6; and (C) in the presence of 200 mM SDS, pH 5.6, all at 37 °C (From Buchko *et al.*, 1996a).

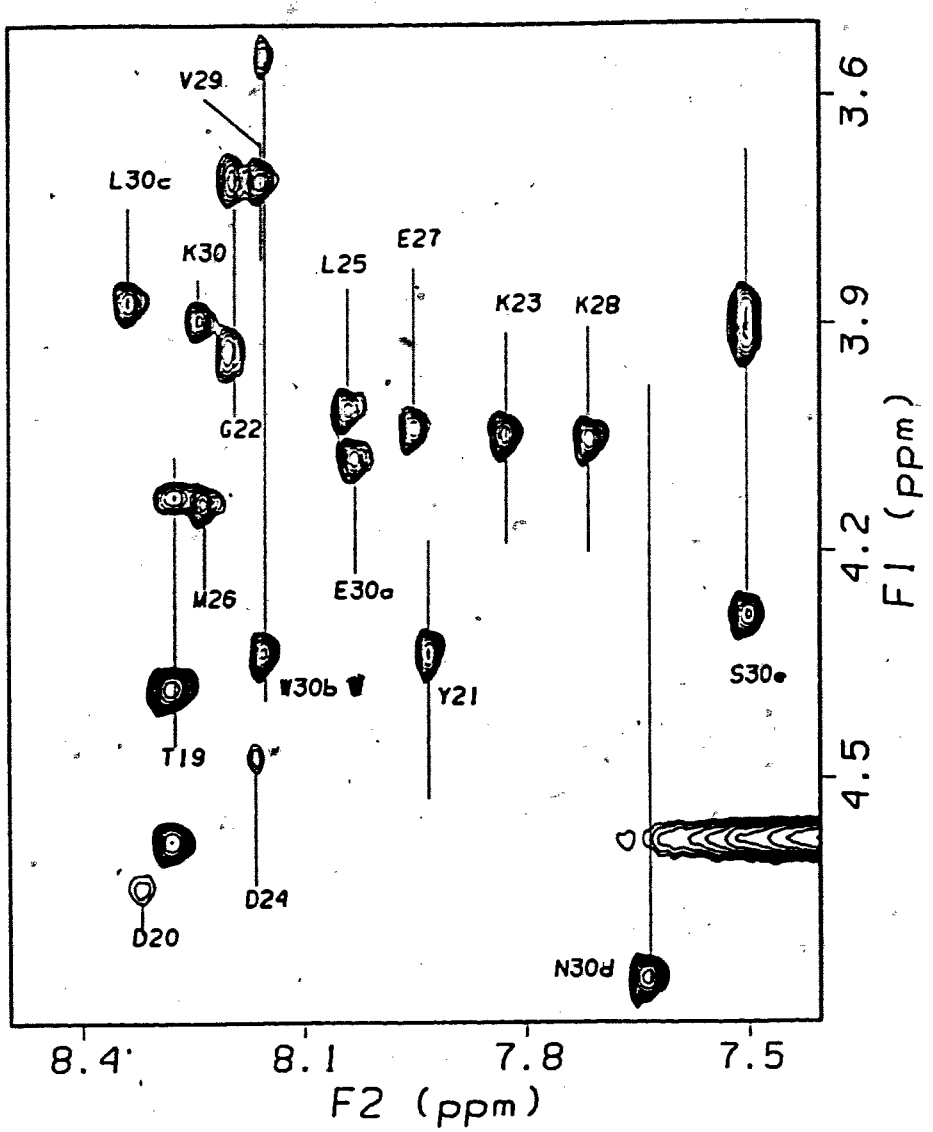

Fig. 5.2: Fingerprint region of the TOCSY spectrum of apoA-II(18-30)+ in SDS. The spectrum was collected for a 5 mM peptide in H_2O/D_2O (9:1, v/v) solution in the presence of SDS-d_{25} (peptide/SDS, 1:80) at pH 4.9 and 37 °C. The spin-locking pulse lengths in the MLEV-17 of TOCSY (τ_m = 100 ms) were 16.8, 25.1, and 50.2 μs for 60°, 90°, and 180°, respectively. The H^N-H^α cross peaks of amino acid residues are labeled.

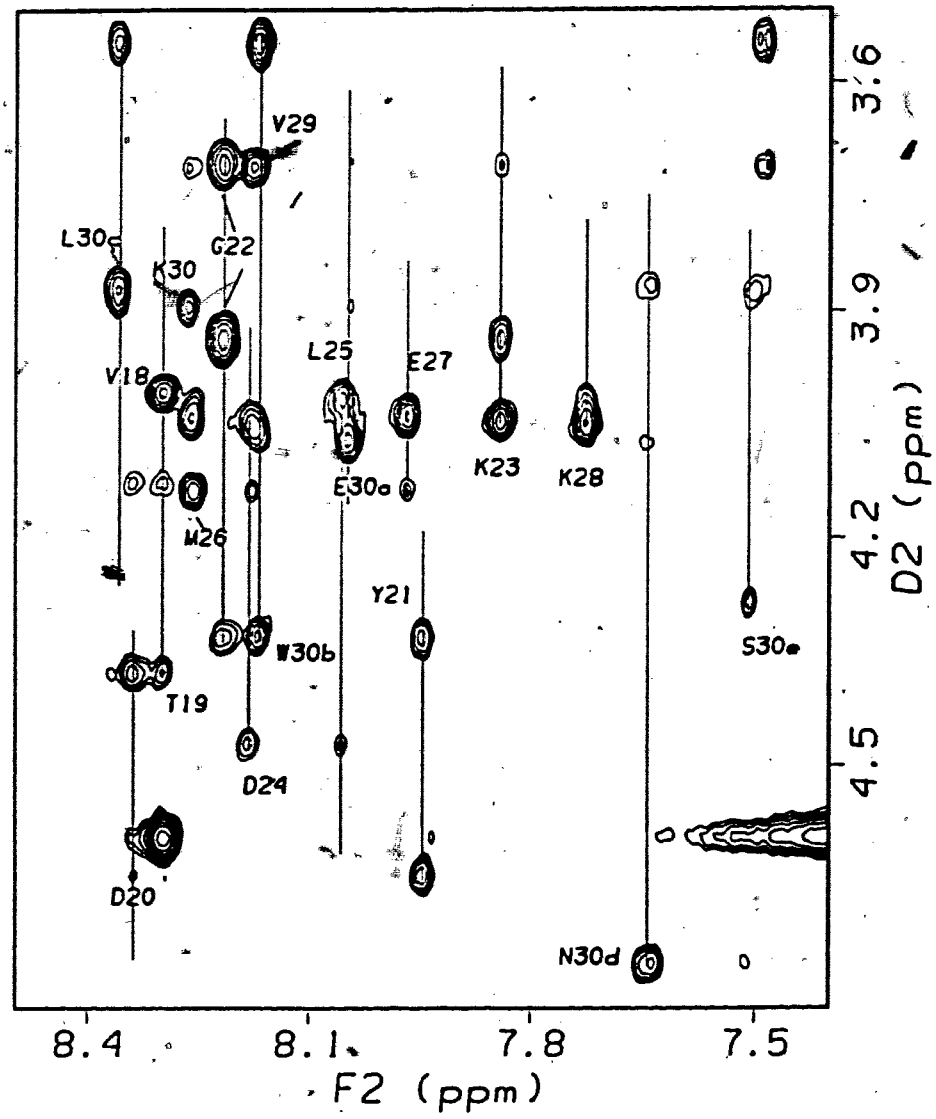

Fig. 5.3: Fingerprint region of the NOESY spectrum of apoA-II(18-30)+ in SDS. The spectrum was collected at τ_m = 100 ms for a 5 mM peptide solution (H_2O/D_2O, 9:1, v/v) in the presence of SDS-d_{25} (peptide/SDS, 1:80) at pH 4.9 and 37 °C. The H^N-H^α cross peaks of amino acid residues are labeled.

Table 5.2: Proton Chemical Shifts (ppm) of ApoA-II(18-30)+ in SDS-d_{25}[a] in H_2O/D_2O (9:1, v/v) at 37 °C and pH 5.0[b]

Residue	H^N	H^α	$\Delta H\alpha$[c]	H^β	H^γ	Others
Val18	8.33	4.04	-0.14	2.27	1.09	
Thr19	8.33	4.42	0.07	4.18	1.15	
Asp20	8.36	4.66	-0.02	2.77		
Tyr21	7.97	4.38	-0.22	3.07, 2.94		2,6H 7.13; 3,5H 6.85
Gly22	8.24	3.97				
		3.75	-0.11[d]			
Lys23	7.87	4.08	-0.28	1.89	1.54, 1.45	H^δ 1.71, H^ε 2.95
Asp24	8.21	4.51	-0.07	3.01, 2.86		
Leu25	8.07	4.05	-0.33	1.81, 1.72	1.7	H^δ 0.93, 0.89
Met26	8.28	4.17	-0.35	2.19	2.68, 2.60	H^ε 1.97
Glu27	7.99	4.07	-0.32	2.23, 2.15	2.53	
Lys28	7.75	4.08	-0.28	2.05, 1.84	1.52	H^δ 1.72, 1.66, H^ε 2.95
Val29	8.19	3.75	-0.43	2.32	1.07	
Lys30	8.29	3.93	-0.43	1.94	1.71, 1.44	H^δ 1.70, H^ε 2.98
Glu30a	8.08	4.11	-0.28	2.26, 2.21	2.68, 2.48	
Trp30b	8.19	4.37	-0.33	3.41, 3.58		2H 7.31, 4H 7.53, 5H 6.97, 6H 7.10, 7H 7.48, NH 9.92
Leu30c	8.38	3.91	-0.47	1.87, 1.59	2.01	H^δ 0.93, 0.89
Asn30d	7.68	4.81	0.09	2.91, 2.72		γH^N 6.87, 7.56
Ser30e	7.53	4.30	-0.2	3.95; 3.91		

[a]Chemical shifts are relative to external DSS (0.00 ppm). [b]Peptide/SDS ratio 1:40. [c]Calculated according to Eq. 4.2. [d]From the average measured H^α chemical shift.

The peptide signals also shifted and became broad with the addition of SDS (Fig. 5.1C). The shift of signals indicates conformational change while spectral broadening is consistent with peptide association with SDS (Lauterwein *et al.*, 1979; Rizo *et al.*, 1993; Henry & Sykes, 1994; Rozek *et al.*, 1995). The spectral lines in SDS are narrower than those in the aggregated state as manifested by the N1 proton of the Trp ring (Fig. 5.1). This may suggest that the peptide in micelles is less restrictive than in the peptide aggregates. In SDS, an optimal resolution in the amide region of the NMR spectrum of apoA-II(18-30)+ was achieved at pH ~5.0 and 37 °C. The 2D NMR spectra of apoA-II(18-30)+ were assigned to a single set of peaks using the TOCSY (Fig. 5.2) and NOESY spectra (Fig. 5.3) as demonstrated for apoE peptides previously (Chapter 4). The chemical shifts for the apoA-II(18-30)+ in SDS are listed in Table 5.2.

5.2.2.2 Chemical shifts, NOE connectivity, and secondary structure

Based on Table 5.2 and the definition in Eq. 4.1, the H^{α} secondary shifts of apoA-II(18-30)+ were calculated and also included in Table 5.2. The secondary shifts (Jimenez *et al.*, 1987; Wishart *et al.*, 1991) suggest that residues 20-30c are helical (Pierens *et al.*, 1995). The helix content of apoA-II(18-30)+ is 67% estimated by Eq. 4.2. Fig. 5.3 depicts the interresidue NOE connectivities for apoA-II(18-30)+ bound to SDS. The medium to strong H^{N}_{i}-H^{N}_{i+1} and medium H^{α}_{i}-H^{N}_{i+1} NOEs for residues 20-30d indicate a helical conformation. This is further supported by numerous weak to medium H^{α}_{i}-H^{N}_{i+3}, H^{α}_{i}-H^{β}_{i+3}, H^{α}_{i}-H^{N}_{i+4}, H^{α}_{i}-H^{N}_{i+2}, and H^{N}_{i}-H^{N}_{i+2} NOEs (Wüthrich, 1986).

5.2.2.3 Three-dimensional structures of apoA-II(18-30)+ in SDS

The helical conformation can be seen from the backbone view of the superimposed ensemble of 15 structures (Fig. 5.5A). The RMSDs for superimposing the

backbone atoms (N-C$^{\alpha}$-C=O) are 0.35 ± 0.11 Å for the region 20-30c and 0.54 ± 0.16 Å for all backbone atoms, respectively.

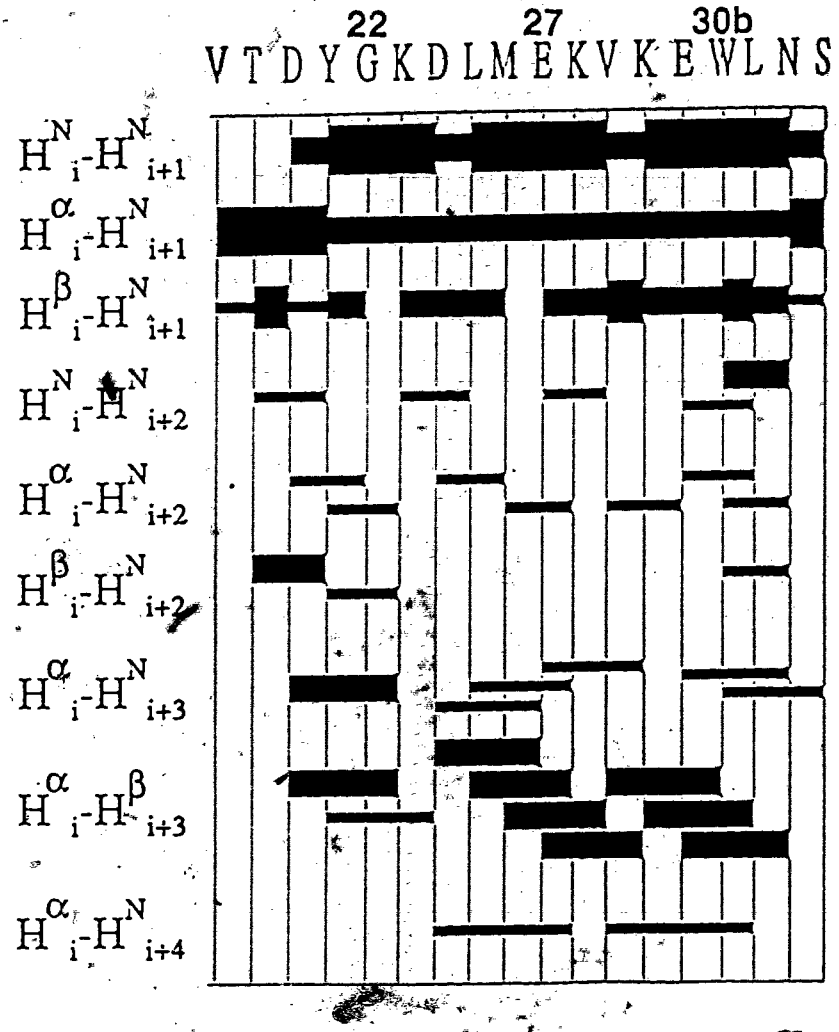

Fig. 5.4: Graphic representation of interresidue NOEs from the NOESY spectrum of apoA-II(18-30)+ in SDS. The spectrum was collected at τ_m = 150 ms, Peptide/SDS, 1:40, pH 5.0 and 37 °C. The thickness of the bar corresponds to the three classes of NOE intensities.[From Buchko *et al.* (1996a)].

Fig. 5.5B shows an end-on view of the average orientation of side chains. The hydrophobic residues are at the top and hydrophilic residues at the bottom, indicating that apoA-II(18-30)+ adopts an amphipathic helix structure when bound to SDS. The amphipathic feature of the structures is also evident in Fig. 5.6, where a stereoview of the side chains of all structures is given.

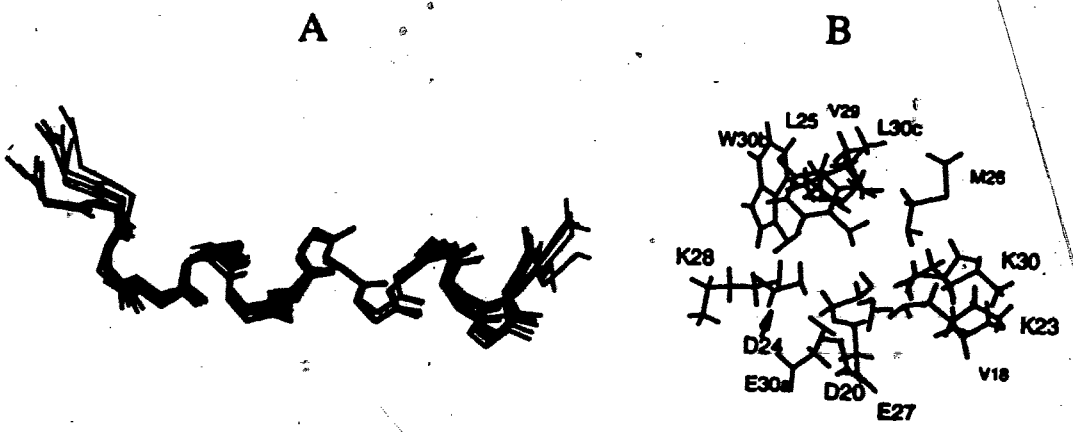

Fig. 5.5: Three-dimensional structures of apoA-II(18-30)+ bound to SDS. (A) is a backbone view where the backbone atoms (N-C^{α}-C=O) of residues 20-30c of an ensemble of 15 out of 20 structures have been superposed; (B) is an end-on view from the N-terminus of the average helical structure, where the hydrophobic (top) and hydrophilic (bottom) faces are evident from the residue labels. Note that V18 is on the hydrophilic face consistent with an unstructured N-terminus (see the text).

5.3 Discussion

5.3.1 Factors that stabilize a class A2 amphipathic helix

As apoA-II(18-30)+ binds lipids of different head groups, it strongly suggests that the hydrophobic effect dominates in the association of apoA-II(18-30)+ with lipid. In fact, Reynolds (1982) showed that both apoA-I and apoA-II even bind alkanes in addition to detergents of different head groups. The importance of hydrophobic interactions has been discussed in Chapter 4 of this thesis and also proposed by many other researchers. For example, Mao *et al.* (1981) found that substitution of K54K55 in apoA-II(50-77) by

SerSer did not affect the lipid binding affinity of the peptide. Subbarao *et al.* (1988) showed that GALA, a 30-residue peptide, lacks cationic residues but binds lipid.

The proposed intrahelix ion pairs (Segrest *et al.*, 1974) were not found in apoA-II(18-30)+ (Buchko *et al.*, 1996a), in agreement with observations for apoC-I peptides (Rozek *et al.*, 1995) and apoA-I(166-185) in both SDS and DPC (Chapter 6). Instead, interactions between anionic SDS and cationic side chains of apoA-I peptides have been observed (Chapter 6). The electrostatic interactions between SDS head groups and the cationic lysine side chains may explain the more helical structure of apoA-II(18-30)+ in SDS than in either DPC or TMA. In the presence of lipid, pH had little effect on the conformation of either apoA-II(18-30)+ or apoE(263-286) (chapter 4). In the absence of lipid, apoA-II(18-30)+ aggregated above pH 3.7 but not at pH 2.6 (Fig. 5.1). Also, apoC-I does not aggregate at pH below 3 (Osborne & Brewer, 1977). Otter *et al.* (1988;1989) showed that salt bridge forms only at physiological pH but not at acidic pH. At acidic pH, Asp and Glu side chains are protonated and there is sufficient repulsion between net positive charges to prevent peptide or protein aggregation (Buchko *et al.*, 1996a). The helix bundle structures for either apoE(1-191) (Wilson *et al.*, 1991) or apolipophorin (Breiter *et al.*, 1991) in the absence of lipid are stabilized by both hydrophobic interactions and salt bridges. These interactions have been extrapolated to apoA-I, where the helix-helix salt bridges stabilize the tertiary structure in lipid (Lins *et al.*, 1995). The interaction difference we see for the peptides in the presence and absence of lipid strongly indicates that caution should be taken in extending the observations from the lipid-free to lipid-bound states.

There has been the proposal that cationic side chains "snorkel", that is, the cationic side chains of the class A amphipathic helices bend toward the hydrophilic face by 90° (Segrest *et al.*, 1990; Epand *et al.*, 1995) (Section 1.4). All lysine side chains in the ensemble of structures were found to be extended in the interfacial region of hydrophobic and hydrophilic faces (Figs. 5.5 & 5.6). Similar orientations were seen for cationic side chains in class A1 (Chapter 6) and class A2 (Rozek *et al.*, 1995; Buchko *et al.*, 1996a,b) amphipathic helices in SDS or DPC, indicating that snorkeling of cationic side chains may not be a universal phenomenon (Rozek *et al.*, 1995).

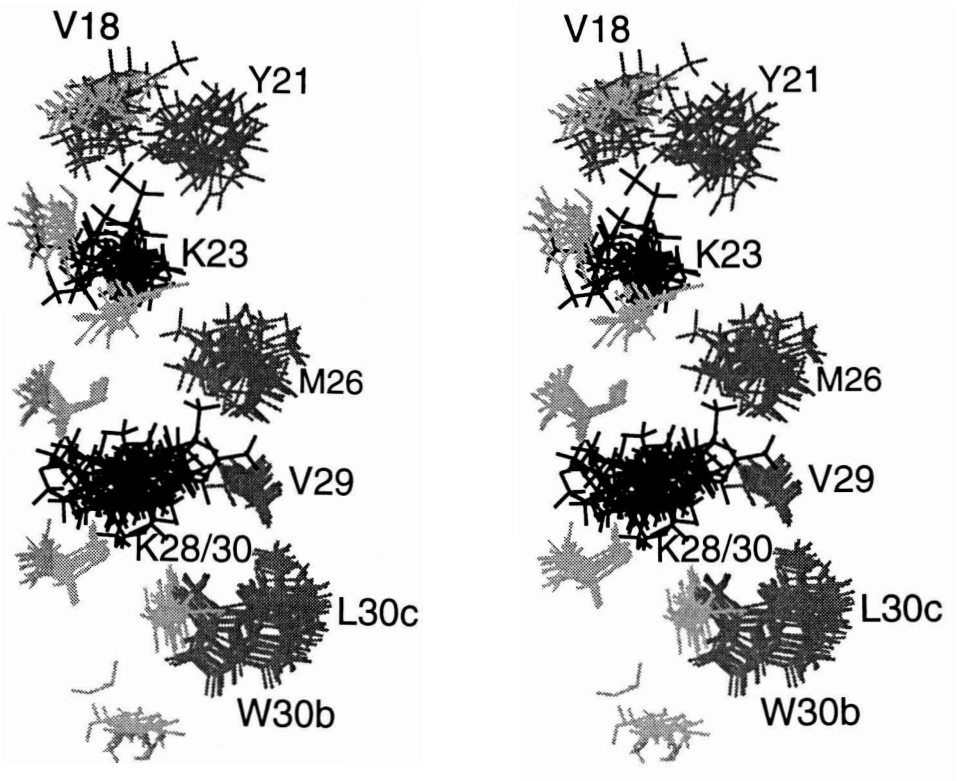

Fig. 5.6: Stereoview of the side chains of apoA-II(18-30)+ structures in the SDS-bound state. Hydrophobic (medium grey) and cationic side chains (dark grey), K23, K28, and K30, are labeled. Hydrophilic side chains (light grey) are D20, D24, E27, E30a, and N30d, respectively, from top to bottom.

However, the participation of cationic side chains in hydrophobic interactions is evident. Firstly, the δ-protons of arginine side chains of apoA-I(166-185) showed NOE cross peaks with hydrophobic leucine side chains, indicating that the cationic side chains are near the hydrophobic face (Chapter 6). Secondly, for LAP-20 in both SDS and DPC

(Buchko *et al.*, 1996b), the chemical shifts of K16 (residue i+4) side-chain protons all shifted upfield under the influence of the aromatic ring of W12 (residue i), indicating that the hydrophobic moieties of the amphipathic cationic side chain of K16 are near the hydrophobic face. A similar Trp (i) ring current effect on lysine (i + 4) in melittin occurs in DPC micelles (Inagaki *et al.*, 1989) or in methanol (Bazzo *et al.*, 1988), suggesting that the cationic side-chain orientation is not purely due to micelle environments. Thirdly, cationic side chains in class A1 amphipathic helices of apoA-I peptides showed intermolecular NOEs with SDS alkyl chains, indicating that they are sitting on the micellar surface (Wang *et al.*, 1996b). In conclusion, cationic side chains may indeed enhance lipid binding but do not "snorkel" at least in micelles.

5.3.2 The lipid affinity of apoA-II(18-30) is successfully enhanced by a hydrophobic pair

Both apoA-II(12-31) (Chen *et al.*, 1979) and apoA-II(18-30)+ (Buchko *et al.*, 1996a) bind DMPC with a similar increase in helicity. In apoA-II(12-31), a YF aromatic pair was included by elongation of the N-end of apoA-II(18-31) while in apoA-II(18-30)+ a hydrophobic pair, WL, was appended to the C-end of apoA-II(18-30). Mao *et al.* (1981) found that substitution of the pair of hydrophobic residues L52I53 of a lipid-binding segment of apoA-II with AlaAla totally abolished lipid-binding ability. Therefore, residues L52I53 are essential for lipid binding. Since inclusion of the WF pair in apoE(263-286) led to the formation of an extra hydrophobic cluster WFLV (Chapter 4), which greatly enhanced lipid-binding affinity (Sparrow *et al.*, 1992), we propose that the enhanced lipid binding of apoA-II peptides may result from the formation of an additional hydrophobic cluster, namely V29WL at the C-terminus of apoA-II(18-30)+ and Y14F15V18 at the N-terminus of apoA-II(12-31). In the NMR structures of apoA-II(18-30)+ bound to SDS micelles (Figs. 5.5B & 5.6), V18 is not located on the hydrophobic face, probably not involved in lipid binding. This is reminiscent of the N-terminus of apoE(267-289), where V269 was found on the hydrophilic face and the

several residues nearby became flexible (Chapter 4). Thus, it may be the case that deletion of a hydrophobic pair from a lipid-binding peptide disrupts a potential hydrophobic cluster. Similar arguments may be applied to many other examples collected in the excellent review on apolipoprotein peptides of various lengths (Sparrow and Gotto, 1982).

CHAPTER 6: STRUCTURES OF APOA-I SEGMENTS IN SDS, DPC, OR LYSOPC. PEPTIDE-LIPID INTERACTIONS

6.1 Introduction

As mentioned in Section 1.6.1, the secondary structure of apoA-I in lipid matrix is predicted to contain 6-9 helices linked by β-turns (Jonas *et al.*, 1989; Brasseur *et al.*, 1990; Marcel *et al.*, 1991; Nolte and Atkinson, 1992; Calabresi *et al.*, 1993; Segrest *et al.*, 1994). The putative amphipathic helices (Section 1.4) are proposed to be responsible for lipid binding (Segrest *et al.*, 1974) and likely other functions of apoA-I (Segrest *et al.*, 1990; 1992; 1994). In addition, the tertiary structure of apoA-I is proposed to be stabilized by adjacent helix-helix interactions via forming ion pairs (Brasseur *et al.*, 1990; Lins *et al.*, 1995).

As no 3-D structure of apoA-I is available, synthetic peptide analogue, antibody binding and site-directed mutagenesis studies have been performed in an attempt to confirm the predicted structure or to locate the LCAT activation domain(s). Sparrow and Gotto (1982) showed that apoA-I(197-243) bound to DMPC but did not activate LCAT. The importance of the C-terminus of apoA-I in lipid binding but not in LCAT activation is consistent with limited proteolysis of apoA-I (Ji & Jonas, 1995) and site-directed mutagenesis studies (Schmidt *et al.*, 1995; Holvoet *et al.*, 1996). Also, the region from residues 43 to 48 is susceptible to enzymatic hydrolysis (Lins *et al.*, 1993). The truncation of the N-terminal residues 1-43 from apoA-I was proposed to have little effect on LCAT activation (Brouillette & Anantharamaiah, 1995; Rogers *et al.*, 1997). Based on the finding that the consensus sequence with a Glu residue at the 13th position best activates LCAT, Anantharamaiah *et al.* (1990) proposed that the major LCAT-activating domain is within residues 66-120 (Banka *et al.*, 1991). Both apoA-I(1-86) and apoA-I(149-243) from CNBr digestion were found to activate LCAT to 25-30% of apoA-I (Soutar *et al.*, 1975), suggesting that residues 44-86 and 149-197 may be part of the LCAT activation domains. Monoclonal antibody studies (Meng *et al.*, 1993; Uboldi *et al.*, 1996) suggest that several putative helical regions covering residues 96-174 of apoA-I

are all implicated in LCAT activation. Although more recent mutagenesis studies also imply the entire middle region, the importance of residues 120-187 is more pronounced (Minnich *et al.*, 1992; Sorci-Thomas *et al.*, 1993; 1997; Holvoet *et al.*, 1995). Complementary to the site-directed mutagenesis studies, synthetic peptides apoA-I(121-164) (Fukushima *et al.*, 1980) and apoA-I(145-185) (Sparrow and Gotto, 1980) were both shown to bind DMPC, to adopt helical conformations and to activate LCAT to 30% and 25% of apoA-I, respectively. These "44mers" are believed to be the paradigm of apoA-I (Nakagawa *et al.*, 1985). In addition to LCAT activation, the region 122-187 was also shown to play a role in cholesterol efflux (von Eckardstein *et al.*, 1993; Fielding *et al.*, 1994; Sviridov *et al.*, 1996).

Because of the potential biological importance, 2D NMR was employed to study the conformations of peptides within residues 114-187 of apoA-I in micelle models. The micelles (~50-60 Å) are comparable in size with the smallest spherical HDL particle and thus should be a good approximation. As anionic detergent SDS is subject to criticism for modeling lipoprotein environments, we have also determined the structures of apoA-I(166-185) and apoA-I(142-187) in zwitterionic DPC. These two model lipids (SDS and DPC) with different head groups may mimic anionic and zwitterionic lipids, respectively, to some extent. In addition, the use of anionic SDS provides an excellent chance to test the role of cationic side chains in the class A amphipathic helices. The peptide-lipid interactions were investigated by CD, fluorescence spectroscopy, and intermolecular nuclear Overhauser effect. The signal assignment of apoA-I(122-187) was aided by the assignment of apoA-I(142-187) and apoA-I(114-142).

6.2 Results

6.2.1 Circular dichroism

ApoA-I(166-185) (20mer), apoA-I(142-187) (46mer), and apoA-I(122-187) (66mer) have net positive charges and are readily soluble in water. Fig. 6.1 shows the CD spectra of the 20mer (A), 46mer (B), and 66mer (C) in the absence and presence of

SDS. In water, the CD spectra of all three peptides showed a strong negative band at 202-203 nm (Fig. 6.1), suggesting that the major conformation is random (Woody, 1995). Convex constraint analysis gave 15% helix and 47-50% random structures for all segments. The CD spectra changed with titration of SDS and no further change was observed for the 20mer, 46mer, and 66mer above the peptide/SDS ratio of 1:10, 1:40, and 1:20, respectively, suggesting that peptides were predominantly in the bound state (Bairaktari *et al.*, 1990; Rozek *et al.*, 1995; Buchko *et al.*, 1996a,b). The CD curves for all segments in SDS are manifested by the double minima at 207-209 and ~222 nm and a strong positive band at ~195 nm (Fig. 6.1), indicating helical conformations (Holzwarth & Doty, 1965).

When the SDS titration was performed at pH < 5, all three peptide solutions became turbid at the peptide/SDS ratio approximately 1:5. As a result, the CD absorbance dropped significantly. The turbidity disappeared upon raising pH or with further addition of SDS. A similar phenomenon was observed for apoC-I fragments (Rozek *et al.*, 1995), probably due to salt formation (O'Neil and Sykes, 1989). In the SDS-bound state, the change of pH from 3.7 to 10 had little effect on the CD spectra of apoA-I(166-185) (peptide/SDS, 1:40), indicating that the helical conformation was retained throughout the pH range.

The variation of the molar ellipticity at the 222 nm for apoA-I(166-185) (A), apoA-I(142-187) (B), and apoA-I(122-187) (C) with titration of DPC or SDS at pH 6-7 is plotted in Fig. 6.2. While the 222 nm band of these peptides changed with the addition of SDS well below the CMC (8 mM, Helenius *et al.*, 1979), little change occurred with titration of DPC until the DPC concentration was near the CMC (1.1-1.2 mM, Lauterwein *et al.*, 1979; Cordier-Ochsenbein *et al.*, 1996). A plateau was reached at about peptide/DPC ratio of 1:60 for all three peptides (Fig. 6.2), suggesting that one peptide binds one micelle. The trend of the 222 nm band with titration of a mixture of DPC/SDS (1:1) to the 46mer resembles that of SDS, indicating that SDS may initiate binding. The contents of helix for the 20mer, 46mer, and 66mer at the saturating amounts of DPC (SDS) are 48% (50%), 69% (62%), and 53% (56%), respectively, suggesting that these peptides adopt similar conformations in the two micelles.

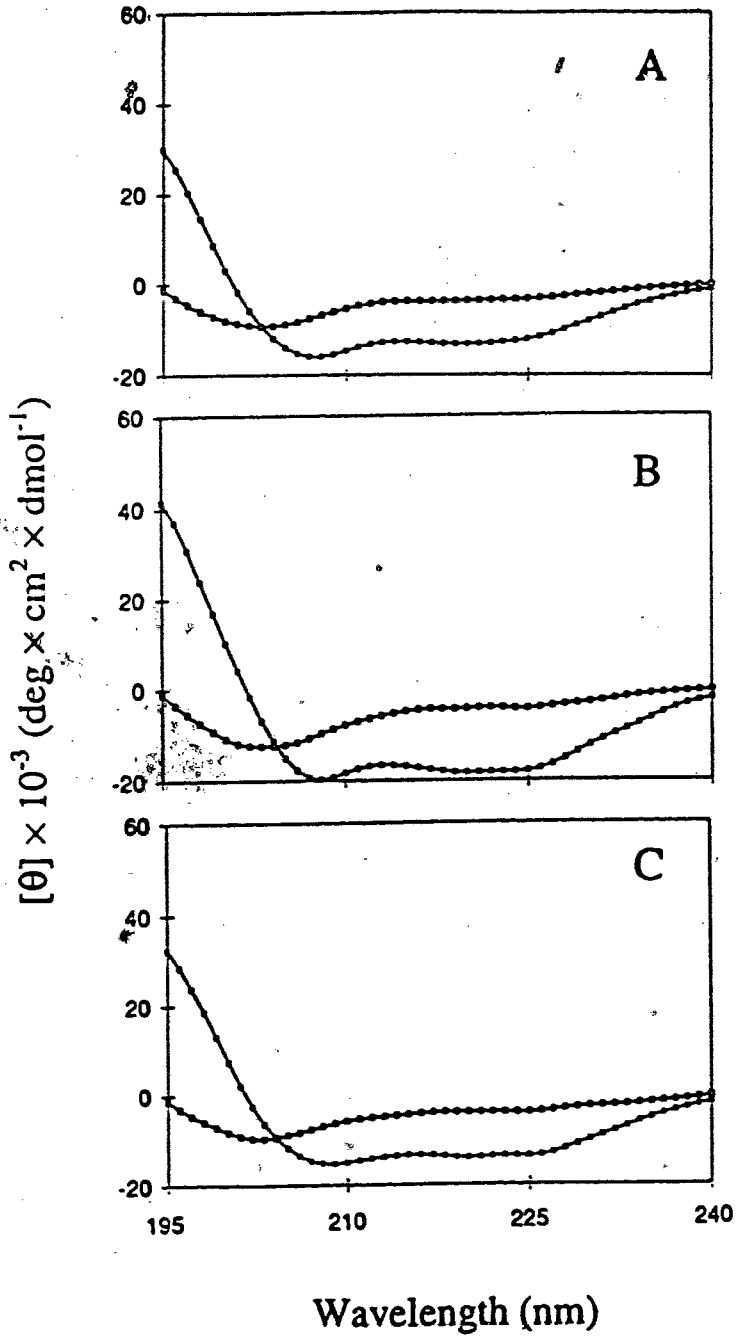

Fig. 6.1: CD spectra of 0.1 mM **apoA-I(166-185) (A),** 0.035 mM **apoA-I(142-187) (B), and** 0.035 mM **apoA-I(122-187) (C) in the absence** (open squares) **and presence** (solid squares) **of SDS at pH 6-7,** 37 ± 0.7°C.

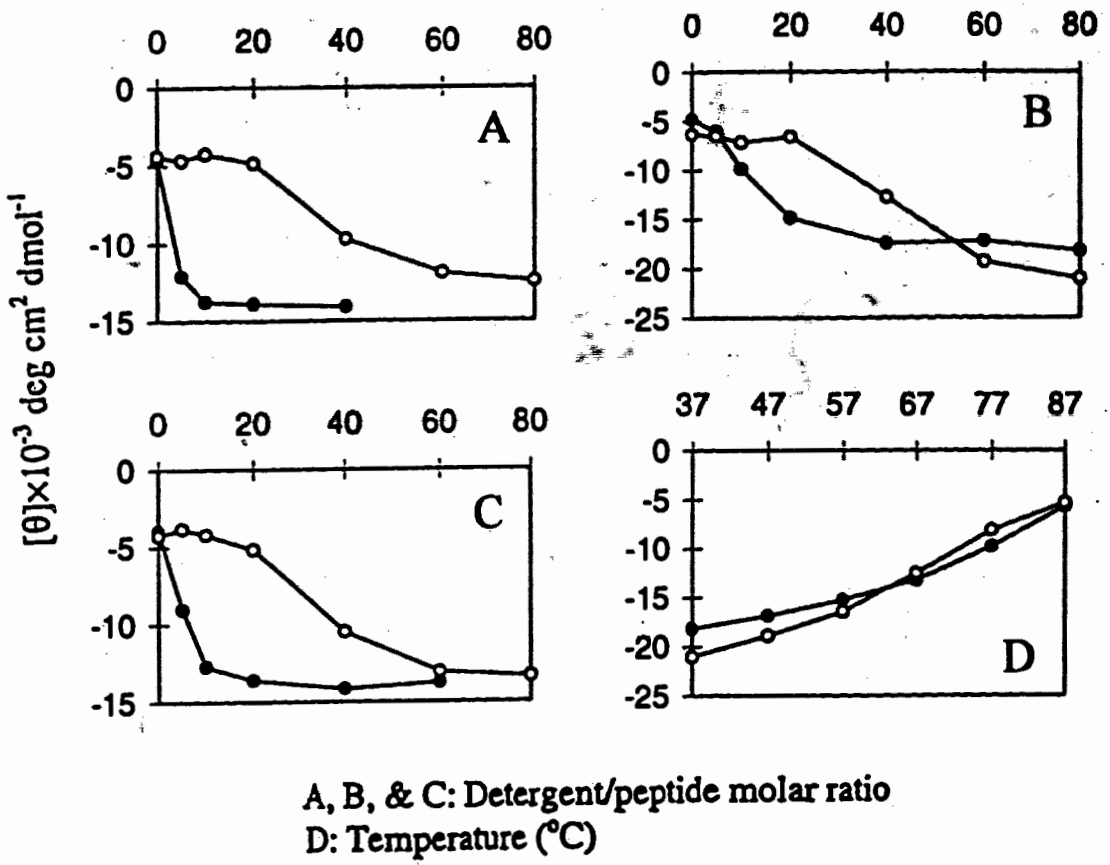

Fig. 6.2 Variation of the 222 nm band of the CD spectra of 0.1 mM **apoA-I(166-185) (A),** 0.035 mM **apoA-I(142-187) (B), and** 0.035 mM **apoA-I(122-187) (C) with the addition of SDS** (solid circles) **or DPC** (open circles) at pH 6-7, 37 °C. (D) Change of the 222 nm band of the CD spectra of apoA-I(142-187) complexed with SDS (solid circles) or DPC (open circles), peptide/lipid ratio 1:80, with the increase of temperature at pH 6-7.

To compare the stability of the helical structure in the bound state, the complexes of apoA-I(142-187) with SDS or DPC were heated from 37 °C to 87 °C in steps of 10°C (Fig. 6.2D). The decrease in the value of the molar ellipticity at 222 nm indicates less helical conformation with increase of temperature. Linear regression of the molar ellipticity values at 222 nm against temperature gave the slopes of 327 and 245 deg cm^2 $dmol^{-1}$ $°C^{-1}$ in DPC and SDS, respectively, indicating that the stability of the apoA-I(142-187)/SDS complexes is greater than the peptide/DPC complexes.

6.2.2 Fluorometric study

ApoA-I(142-187) contains a single intrinsic fluorescent probe, Y166, which is located in the putative β-turn region. Using Eq. 3.1, the relative quantum yields of Y166 in apoA-I(142-187) were calculated at various levels of SDS or DPC and the results are plotted in Fig. 6.3. Upon the addition of SDS to apoA-I(142-187) (0.01 mM) the quantum yield of Y166 doubled from 0.031 in water to 0.059 in SDS (SDS/peptide ratio 320:1), indicating that the peptide associates with the lipid (Narayanaswami *et al.*, 1993). The addition of DPC to apoA-I(142-187) gave marginal change in the quantum yield when the peptide/DPC ratio was below approximately 1:80. However, the quantum yield increased dramatically at the peptide/DPC ratio of 1:160 or the DPC concentration of 1.6 mM. When the trtration was performed at the peptide concentration of 0.020 mM, a rapid increase in the quantum yield was seen at the peptide/DPC ratio of 1:80 or 1.6 mM DPC. In both cases, when a rapid increase in the quantum yield occurred, the DPC concentration was above the CMC. These experiments here and also in previous section all demonstrate that one apoA-I(142-187) associates with one DPC micelle (Lauterwein *et al.*, 1979; Cordier-Ochsenbein *et al.*, 1996).

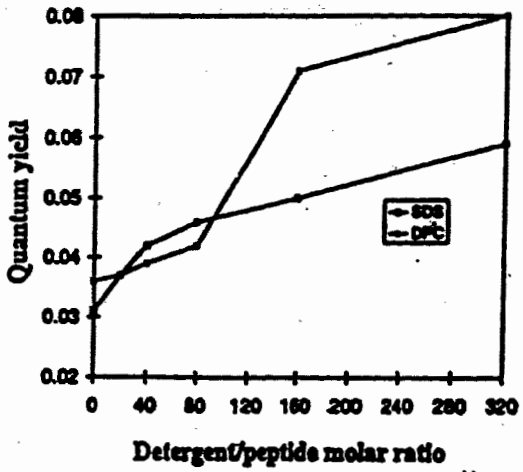

Fig. 6.3: Increase of the quantum yield of Y166 fluorescence in apoA-I(142-187) with the addition of SDS (open squares) or DPC (solid squares) at pH 6-7, 20 °C. Quantum yields were calculated by Eq. 3.1 using free Tyr in 0.1 M phosphate buffer as standard (Quantum yield 0.07, Narayanaswami *et al.*, 1993).

6.2.3 Structure of apoA-I(166-185) in micelles

6.2.3.1 NMR signal assignment

Portions of the NOESY spectra of apoA-I(166-185) in SDS, at pH 6.6 (A) and at pH 3.7 (B), in DPC at pH 6.0 (C), and in lysoPC at pH 3.7 (D) are shown in Fig. 6.4. In SDS at pH 6.6, all amide signals were resolved except the overlap between R171 and Q172. The resonance assignment of the peptide at pH 6.6 was achieved similar to the apoE peptides (Chapter 4). Due to the degeneracy in amide chemical shifts, the NOE connectivities to amide protons of R171 and Q172 were confirmed at 27 °C. The amide proton signal of S167 was not observed as a result of probably faster exchange with water at pH 6.6 (Wüthrich, 1986). The α- and β-proton signals were identified in the H^{α}–H^{β} correlation region and further confirmed by the H^{α}_{i}-H^{N}_{i+1} and H^{β}_{i}–H^{N}_{i+1} NOE connectivities to D168. The chemical shifts of apoA-I(166-185) in SDS at pH 6.6 are given in Table 6.1. The spectra of apoA-I(166-185) in SDS at pH 3.7 and in other lipids were assigned similarly. The chemical shifts of apoA-I(166-185) in SDS at pH 3.7 are listed in Table 6.2 and the chemical shifts in DPC are tabulated in Table 6.3, where the H^{α} chemical shifts of apoA-I(166-185) in lysoPC are also included. In the DPC sample, impurities in the lipid gave resonances at 8.92, 8.55, and 8.08 ppm at pH 6.0 and 37 °C. Occasionally, two sets of such impurity peaks could be seen.

6.2.3.2 Chemical shift change of the ionizable groups in apoA-I(166-185) with pH

The pH dependence of chemical shifts for the side-chain groups of Y166, D168, E169, E179 and E183 in apoA-I(166-185) bound to SDS (A) or DPC (B) micelles is depicted in Fig. 6.5. The solid lines in the Figure were calculated using the modified Henderson-Hasselbalch equation (Eq. 3.4). The calculated pKa values are given in Table 6.4. Compared to the pKa values in DPC (Fig. 6.5B), those in SDS, especially at the N-terminus of the peptide, are higher. We may attribute this difference to the electrostatic effect of SDS head groups causing a decrease in the local pH at the micellar surface. The

pKa values of the N-terminal Y166 in the two lipids differ by as large as 2 pH units (Fig. 6.5C), suggesting that the ammonium group may form a salt bridge with the SDS head group (Jardetzky and Roberts, 1981; Sem & Kasper, 1993; Pallaghy *et al.*, 1995). Using the equation (Nicholson *et al.*, 1991)

$$\Delta G = 2.3RT(\Delta pKa) \qquad (6.1)$$

the free energy (ΔG) for such a salt bridge was estimated to be 2.6 kcal/mol at T = 310 K. In addition, the pKa of Y166 in the peptide in a mixture of SDS/DPC (1:1, mol/mol) was measured to be 8.1, which is closer to the pKa in SDS than the value in DPC (Table 6.4), implying the formation of a possible anionic SDS domain by the cationic side chains of the peptide.

Fig. 6.4: (NEXT TWO PAGES) Fingerprint regions of the NOESY spectra of apoA-I(166-185) in SDS, at pH 3.7 (A) and pH 6.6 (B), in DPC, pH 6.0 (C), and in lysoPC at pH 3.7 (D), all collected at 37 °C. The peptide/lipid ratio is 1:40 except for lysoPC, where 1:11 was used. The sequential assignments in the fingerprint regions are constructed for the spectra in SDS (A & B) and DPC (C). The NOE constructs showing the sequential assignments of the amide protons of apoA-I(166-185) in both SDS and DPC can be found in Wang *et al.* (1996b) Biochim. Biophys. Acta 1301, 174-184.

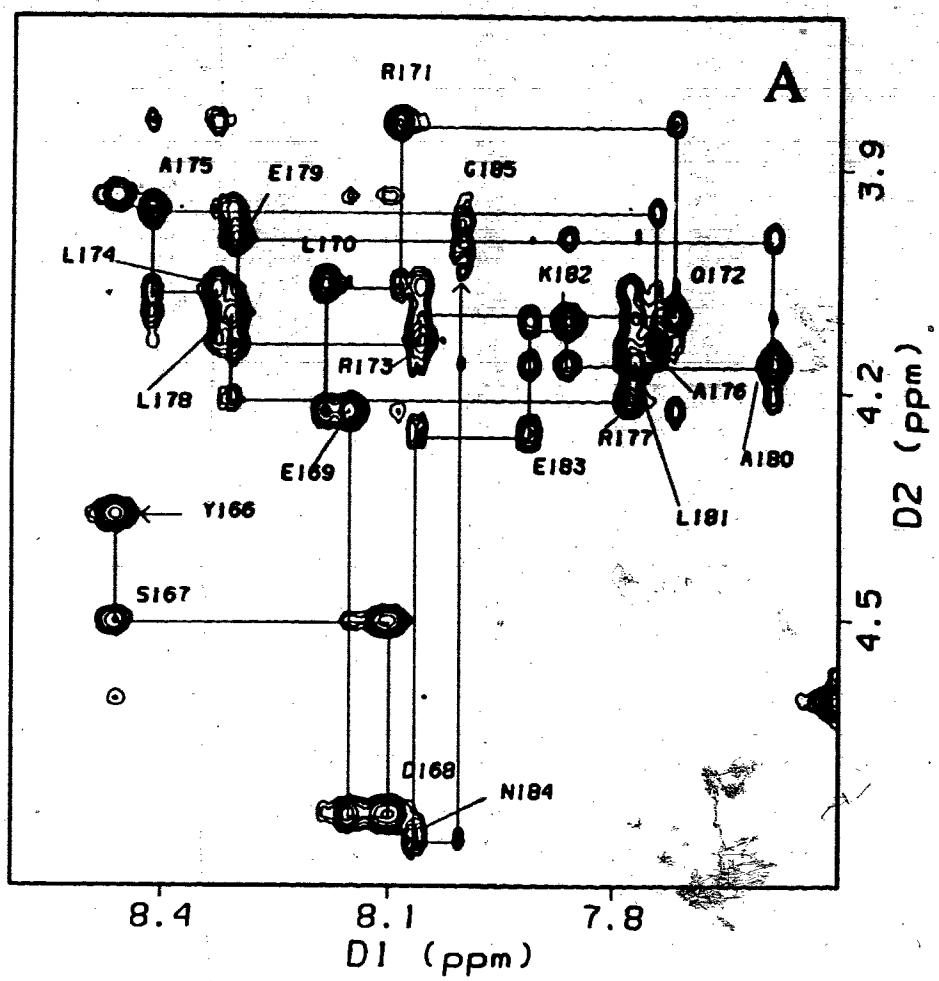
A
R171
A175
E179
G185
L174
L170
K182
Q172
R173
A176
L178
R177
A180
E169
E183
L181
Y166
S167
D168
N184
3.9
4.2
4.5
D2 (ppm)
8.4
8.1
7.8
D1 (ppm)

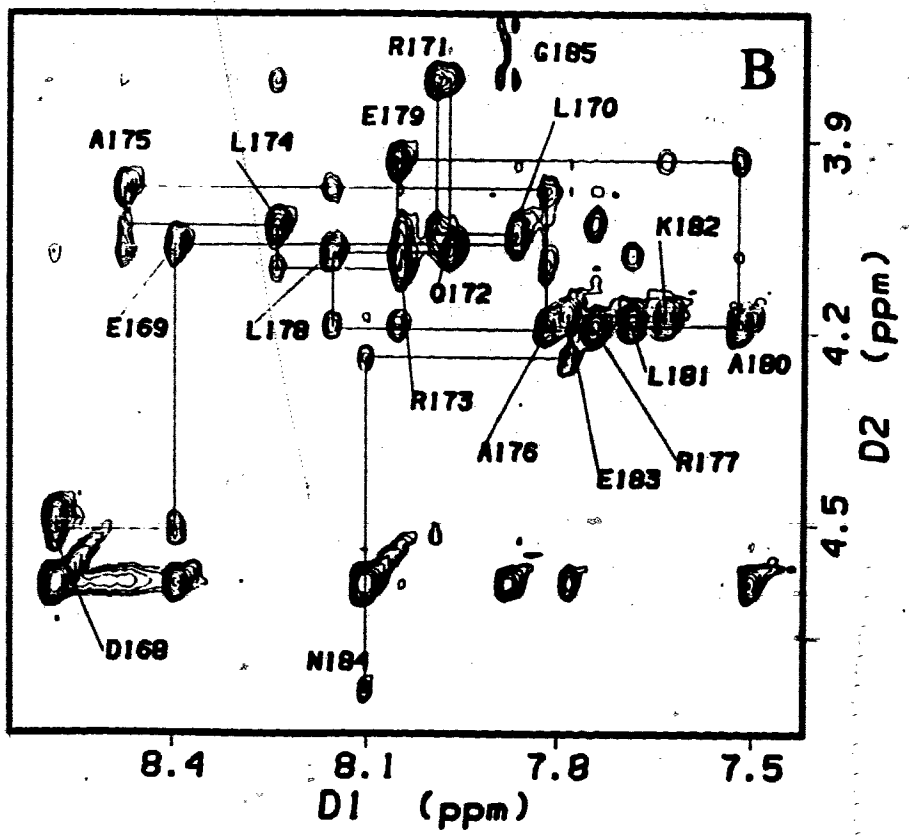
B
R171
G185
E179
L170
A175
L174
K182
Q172
E169
L178
A180
L181
R173
A176
R177
E183
D168
N184
3.9
4.2
4.5
D2 (ppm)
8.4
8.1
7.8
7.5
D1 (ppm)

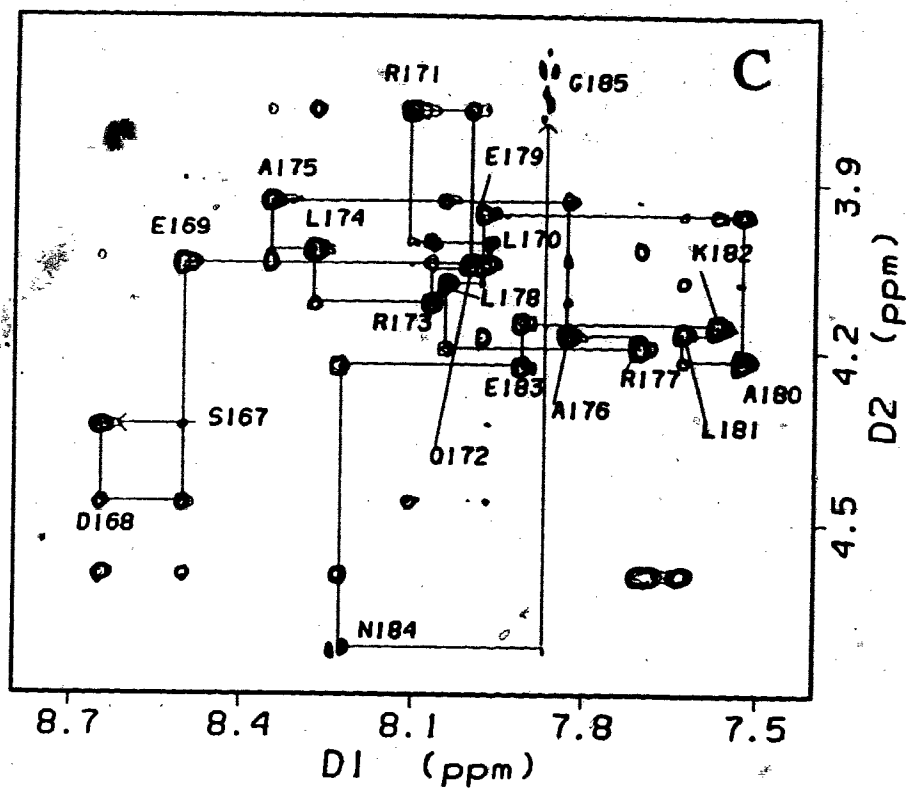
C
R171
G185
E179
A175
L174
E169
L170
K182
L178
R173
R177
A180
E183
A176
S167
L181
Q172
D168
N184
8.7
8.4
8.1
7.8
7.5
D1 (ppm)
3.9
4.2
4.5
D2 (ppm)

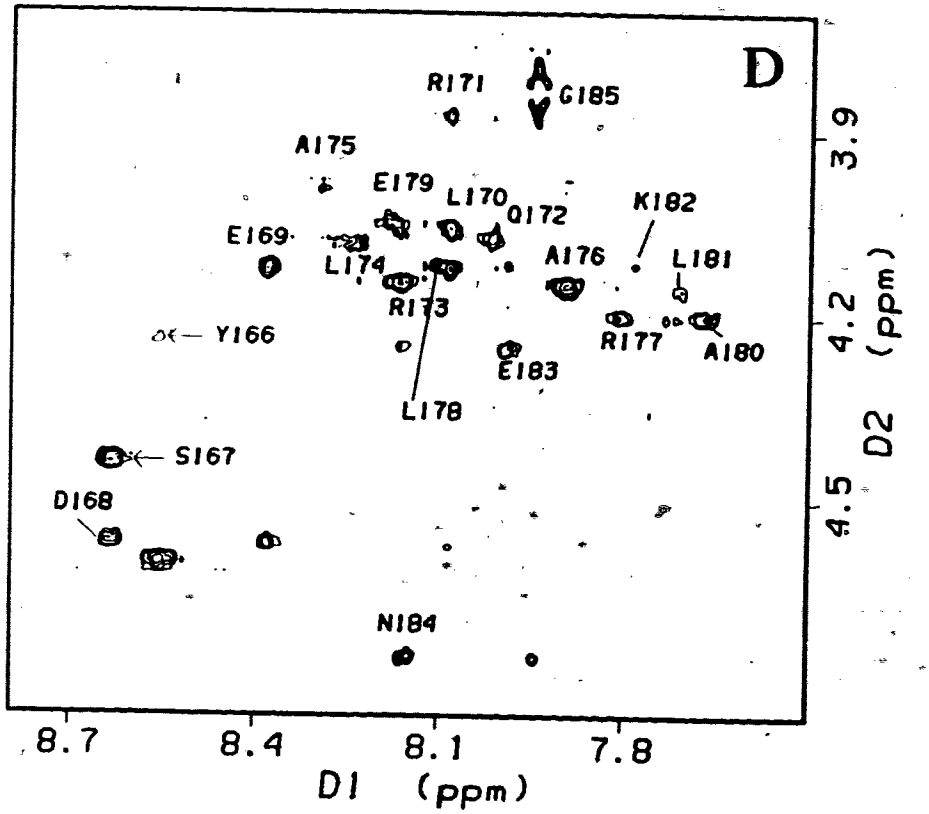
D
R171
G185
A175
E179
L170
Q172
K182
E169
A176
L181
L174
R173
Y166
R177
A180
E183
L178
S167
D168
N184
8.7
8.4
8.1
7.8
D1 (ppm)
3.9
4.2
4.5
D2 (ppm)

6.2.3.3 Chemical shifts, NOE connectivities and secondary structures

Chemical shifts are a sensitive probe for conformational change or interaction between molécules (Dwek, 1973; Jardetzky & Roberts, 1981; Sugiura *et al.*, 1987; Wishart *et al.*, 1991; Folkers *et al.*, 1989; Ösapay & Case, 1994; Szilágyi, 1995; Shuker *et al.*, 1996). Most of the residues of apoA-I(166-185) showed H^{α} chemical shift differences within 0.05 ppm with decrease of pH from 6.6 to 3.7 (Tables 6.1 & 6.2). However, the differences for residues D168, E169, and G185 are as large as 0.2 ppm. From the H^{α} secondary shifts, the region D168 to K182 is suggested to be helical at pH 6.6 (Table 6.1) whereas at pH 3.7 only the region L170 to K182 appears to be helical (Table 6.2). Using Eq. 4.2, the helix content for apoA-I(166-185) was estimated to be 71% and 57% at pH 6.6 and 3.7, respectively. Further increase of pH above 7 had little effect since H^{α} chemical shifts showed little change except that of Y166, which shifts upfield due to deprotonation (Fig. 6.5C). A similar pH effect on the N-terminal conformation of the peptide was also observed in DPC. The helix content, according to Eq. 4.2, is 79% at pH 6.0 and 67% at pH 3, respectively. Similar chemical shifts in SDS and DPC (Tables 6.1 & 6.3) suggest similar conformations in the two micelles. The peptide H^{α} chemical shifts in DPC changed little with increase of temperature from 22 to 47 °C (Fig. 6.6). In SDS, the major set of peaks suggests helical structure even at 80 °C. This is supported by CD, which showed that the helix percentage in SDS decreased slightly from 55% at 37 °C to 49% at 87 °C.

The sequential NOE connectivities for apoA-I(166-185) in SDS, at the two pHs, and in DPC are depicted in Fig. 6.7. From a combination of NOE pattern such as the numerous strong, medium and weak H^{N}_{i}-H^{N}_{i+1}, H^{α}_{i}-H^{N}_{i+1}, H^{α}_{i}-H^{N}_{i+2}, H^{α}_{i}-H^{N}_{i+3}, H^{α}_{i}-H^{β}_{i+3} and H^{α}_{i}-H^{N}_{i+4} cross peaks, a predominantly helical structure is indicated for the peptide (Wüthrich, 1986). Similar NOE connectivity patterns (Fig. 6.7, A & C) strongly support that apoA-I(166-185) adopts similar conformations in SDS and DPC at a similar pH.

Table 6.1: Proton Chemical Shifts (ppm) of ApoA-I(166-185) in SDS-d_{25} at pH 6.6, Peptide/SDS Ratio 1:40 and 37 °C[a]

Residue	H^N	H^α	$\Delta H\alpha^b$	H^β	H^γ	Others
Tyr166		4.32	-0.28	3.18, 3.13		2,6H 7.15; 3,5H 6.81
Ser167	-	4.48	-0.02	4.06, 3.92		
Asp168	8.58	4.51	-0.25	2.69		
Glu169	8.39	4.05	-0.24	2.01	2.32, 2.27	
Leu170	7.85	4.04	-0.34	1.78	1.64	H^δ 0.90, 0.96
Arg171	7.99	3.79	-0.59	2.01, 1.93	1.70, 1.63	H^δ 3.22; εH^N 7.22
Gln172	7.96	4.06	-0.31	2.15	2.44, 2.52	δH^N-
Arg173	8.05	4.09	-0.29	2.01, 1.88	1.68	H^δ 3.17; εH^N 7.24
Leu174	8.24	4.03	-0.35	1.81	1.54	H^δ 0.86
Ala175	8.47	3.96	-0.39	1.52		
Ala176	7.81	4.17	-0.18	1.51		
Arg177	7.74	4.18	-0.20	2.11, 1.94	1.82, 1.69	H^δ 3.27, 3.19; εH^N 7.28
Leu178	8.15	4.08	-0.30	1.75	1.51	H^δ 0.89
Glu179	8.05	3.93	-0.36	2.12, 2.05	2.38, 2.23	
Ala180	7.50	4.17	-0.18	1.52		
Leu181	7.67	4.17	-0.21	1.87	1.67	H^δ 0.94
Lys182	7.62	4.16	-0.20	1.90, 1.82	1.57, 1.43	H^δ 1.66; H^ε 2.94
Glu183	7.77	4.23	-0.06	2.08, 2.01	2.34, 2.26	
Asn184	8.09	4.75	0.00	2.85, 2.75		γH^N -
Gly185	7.87	3.78 3.72	-0.22[c]			

[a]Chemical shifts are relative to external DSS (0.00). [b]H^α secondary chemical shifts calculated according to Eq. 4.1. [c]Relative to the average H^α chemical shift 3.75 ppm.

As seen from Figs. 6.7A and B, fewer (i, i+3) type NOEs were found at the N-terminus of apoA-I(166-185) at pH 3.7 than at pH 6.6. In addition, the strong H^α_i-H^N_{i+1}, connectivities extend further to E169, suggesting that the structure at the N-terminus at a lower pH is more extended (Wüthrich, 1986; Cann *et al.*, 1994). Therefore, both H^α secondary shifts and NOE connectivities support that the N-terminus of apoA-I(166-185) is more helical at physiological pH than at acidic pH.

Table 6.2: Proton Chemical Shifts (ppm) of ApoA-I(166-185) in SDS-d_{25} at pH 3.7, Peptide/SDS Ratio 1:40 and 37 °C[a]

Residue	H^N	H^α	$\Delta H\alpha^b$	H^β	H^γ	Others
Tyr166		4.37	-0.23	3.33, 3.16		2,6H 7.24; 3,5H 6.89
Ser167	8.46	4.51	+0.01	3.94		
Asp168	8.11	4.75	+0.01	3.05		
Glu169	8.15	4.23	-0.06	2.03, 2.13	2.47	
Leu170	8.18	4.05	-0.33	1.83, 1.76	1.69	H^δ 0.92, 0.99
Arg171	8.09	3.84	-0.54	1.94	1.71	H^δ 3.27, 3.19; εH^N 7.10
Gln172	7.72	4.10	-0.27	2.16	2.45, 2.54	δH^N 7.27, 6.71
Arg173	8.06	4.13	-0.25	2.09, 1.99	1.90, 1.72	H^δ 3.22, 3.18; εH^N 7.11
Leu174	8.33	4.06	-0.32	1.82, 1.58	1.54	H^δ 0.89
Ala175	8.41	3.95	-0.40	1.53		
Ala176	7.74	4.14	-0.21	1.53		
Arg177	7.78	4.21	-0.17	2.12, 1.96	1.83,1.71	H^δ 3.28, 3.20; εH^N 7.29
Leu178	8.31	4.10	-0.28	1.82, 1.64	1.53	H^δ 0.90
Glu179	8.30	3.99	-0.30	2.18, 2.10	2.57, 2.60	
Ala180	7.58	4.16	-0.19	1.54		
Leu181	7.77	4.17	-0.21	1.91, 1.83	1.70	H^δ 0.94
Lys182	7.86	4.11	-0.25	1.96, 1.84	1.56, 1.47	H^δ 1.70; H^ε 2.99 εH^N 7.43
Glu183	7.91	4.26	-0.03	2.13	2.59, 2.53	
Asn184	8.06	4.79	+0.04	2.91, 2.82		γH^N 7.51, 6.86
Gly185	8.00	3.99	+0.02			

[a]Chemical shifts are relative to external DSS (0.00). [b]H^α secondary chemical shifts calculated according to Eq. 4.1.

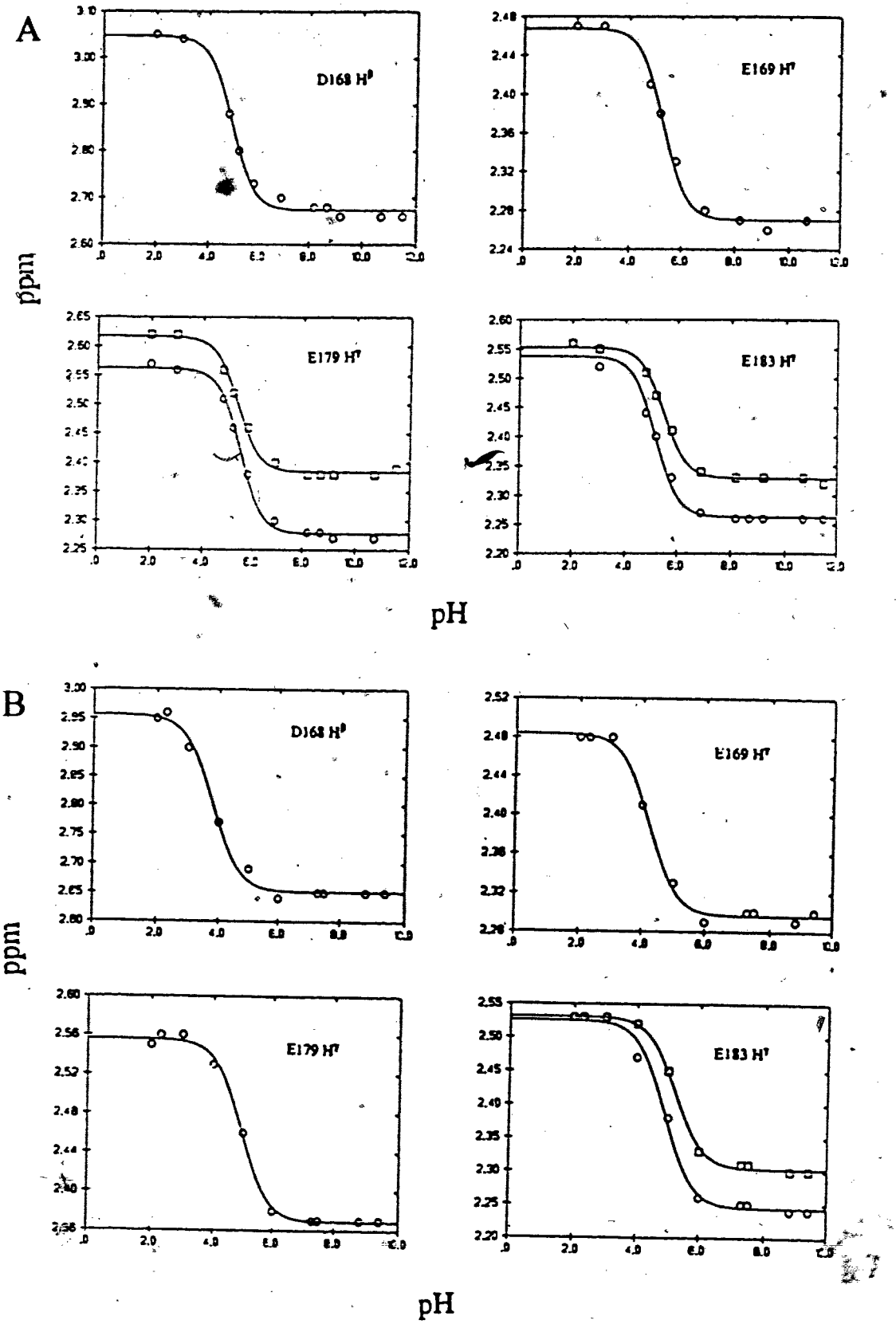

Fig. 6.5 (A,B), legend on next page.

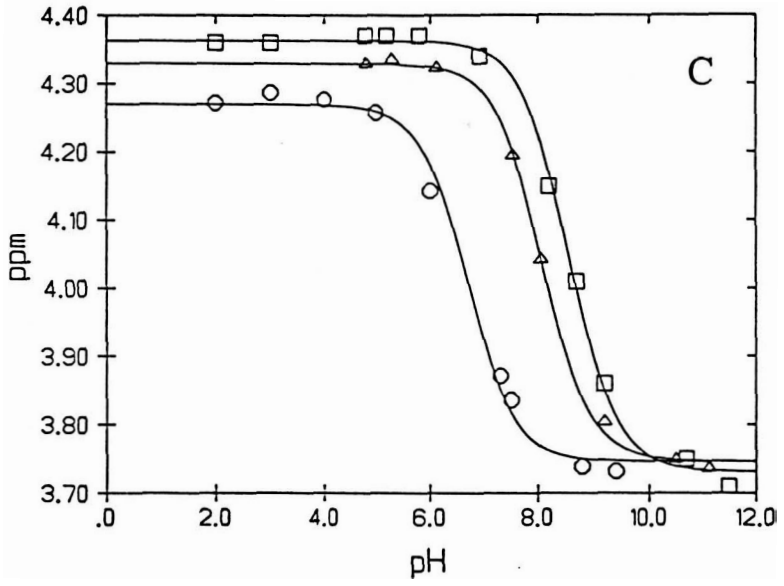

Fig. 6.5: Chemical shifts of the ionizable side chains of apoA-I(166-185) bound to SDS (A) or DPC (B) as a function of pH. (C) The pKa for the amino group of the N-terminal residue of the peptide measured in SDS (□), DPC (○), and SDS/DPC (1:1) (Δ) by following the chemical shift change of H^{α} of Y166 with pH. In all cases the peptide/lipid ratio is 1:40 at 37°C.

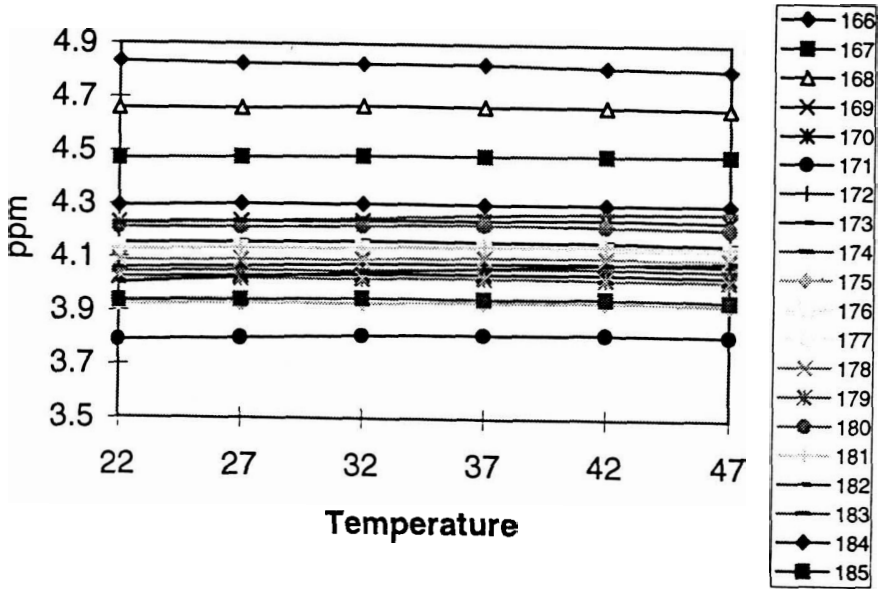

Fig. 6.6: H^{α} chemical shifts of the residues in apoA-I(166-185) bound to DPC at various temperatures from 22 to 47 °C. Data were obtained from 2D NMR spectra collected at pH 3.1 using DSS as internal standard.

Table 6.3: Proton Chemical Shifts (ppm) of ApoA-I(166-185) in DPC-d_{38} or lysoPC at 37 °C[a]

Residue	H^N	H^α	$H^{\alpha b}$	H^β	H^γ	Others
Tyr166		4.14	4.26	3.12, 3.05		2,6H 7.11; 3,5H 6.79
Ser167	-	4.33	4.45	4.04, 3.89		
Asp168	8.66	4.46	4.58	2.64		
Glu169	8.52	4.05	4.13	2.03, 1.97	2.29	
Leu170	7.98	4.02	4.06	1.73	1.64	H^δ 0.93, 0.88
Arg171	8.12	3.77	3.87	2.03, 1.93	1.70, 1.59	H^δ 3.24; εH^N 7.69,6.92
Gln172	8.01	4.06	4.07	2.15	2.41, 2.50	δH^N 7.27,6.73
Arg173	8.08	4.12	4.15	1.95	1.86, 1.68	H^δ 3.15; εH^N 7.63
Leu174	8.29	4.02	4.08	1.78	1.56	H^δ 0.83
Ala175	8.36	3.94	3.99	1.51		
Ala176	7.84	4.17	4.15	1.49		
Arg177	7.71	4.20	4.20	2.04, 1.91	1.81, 1.67	H^δ 3.19; εH^N 7.71,6.95
Leu178	8.05	4.09	4.12	1.79	1.62	H^δ 0.86
Glu179	7.99	3.96	4.05	2.09	2.38, 2.32	
Ala180	7.54	4.22	4.21	1.48		
Leu181	7.64	4.17	4.15	1.86, 1.73	1.62	H^δ 0.90,0.88
Lys182	7.58	4.15	4.12	1.88, 1.82	1.51, 1.43	H^δ 1.67; H^ε 2.93
Glu183	7.93	4.23	4.26	2.07, 1.96	2.33, 2.26	
Asn184	8.24	4.73	4.76	2.85, 2.71		γH^N 7.53, 6.84
Gly185	7.88	3.70 3.76	3.80 3.87			

[a. & c]Same as in Table 6.2. The peptide/DPC molar ratio is 1:40 at pH 6.0. [b]The α-proton chemical shifts of apoA-I(166-185) in lysoPC, peptide/lysoPC ratio 1:11, pH 3.7.

Table 6.4: Ionization Constants (pKa) of Some Side Chains of ApoA-I(166-185) in SDS-d_{25} or DPC-d_{38}[a]

		SDS		DPC		
Residue	pKa	δ_A	δ_B	pKa	δ_A	δ_B
Y166	8.56	4.36	3.73	6.69	4.27	3.74
D168	4.92	3.05	2.67	3.80	2.96	2.65
E169	5.21	2.45	2.27	4.23	2.48	2.30
E179	5.35*	2.59*	2.33	4.95	2.56	2.37
E183	5.23*	2.55	2.29*	5.06*	2.53	2.27*

[a]Calculated according to Eq. 3.4. The standard deviations of the pKa values is less than ± 0.1. Data followed by a star are averaged pKa's from two resolvable methylene protons of the side chains (Fig. 6.5).

6.2.3.4 Three-dimensional structures of apoA-I(166-185) in SDS-d_{25}

In SDS, 223 NOE distance restraints, including 101 inter- and 122 intra-residue, were found for apoA-I(166-185) at pH 6.6 whereas 259 distance restraints (141 inter- and 118 intra-residue) were obtained at pH 3.7. A comparison of the NOE restraint files at the two pHs revealed that more distance restraints at pH 3.7 than at pH 6.6 stem mainly from the N-terminus of the peptide. In Fig. 6.8, we show the NOE build-up curves for a select group of cross peaks representing different types of NOEs. Normal build-ups demonstrate that these NOEs result from proton dipolar interactions and spin diffusion plays a minor role at a mixing time less than 150 ms (Wüthrich, 1986). The ensemble of 19 out of 20 structures, calculated for apoA-I(166-185) in the presence of SDS at pH 6.6 and 3.7, respectively, is presented in Fig. 6.9. The Brookhaven PDB identification numbers for apoA-I(166-185) in SDS are 1ODP at pH 6.6 and 1ODQ at pH 3.7. The middle region of the structures is well defined at pH 6.6 while the ends are not due to dynamic fraying (Shoemaker *et al.*, 1987) as reflected in the higher RMSDs (Fig. 6.10). As shown in Fig. 6.10, the RMSDs for residues L170 through L178 are below 0.1 Å except for R173 to A175 in SDS at the lower pH, whose RMSDs are below 0.2 Å. The RMSDs for the helical region and the entire molecule relative to the average structure are given in Table 6.6. The backbone RMSDs of the structures at both pHs for superimposing the well-defined helical region R171-K182 are below 0.5 Å. The N-terminal structure of the peptide in SDS at pH 3.7 is better defined than that at pH 6 owing to a larger number of NOEs between Y166 aromatic protons and the side chains of residues 167-169.

Fig. 6.7: (On next page) NOE connectivities of apoA-I(166-185) in SDS, pH 6.6 (A) and 3.7 (B), and in DPC pH 6.0 (C), all at 37 °C. Classification of NOE intensities into strong, medium, and weak is indicated by the height of the bars [From Wang *et al.* (1996b)].

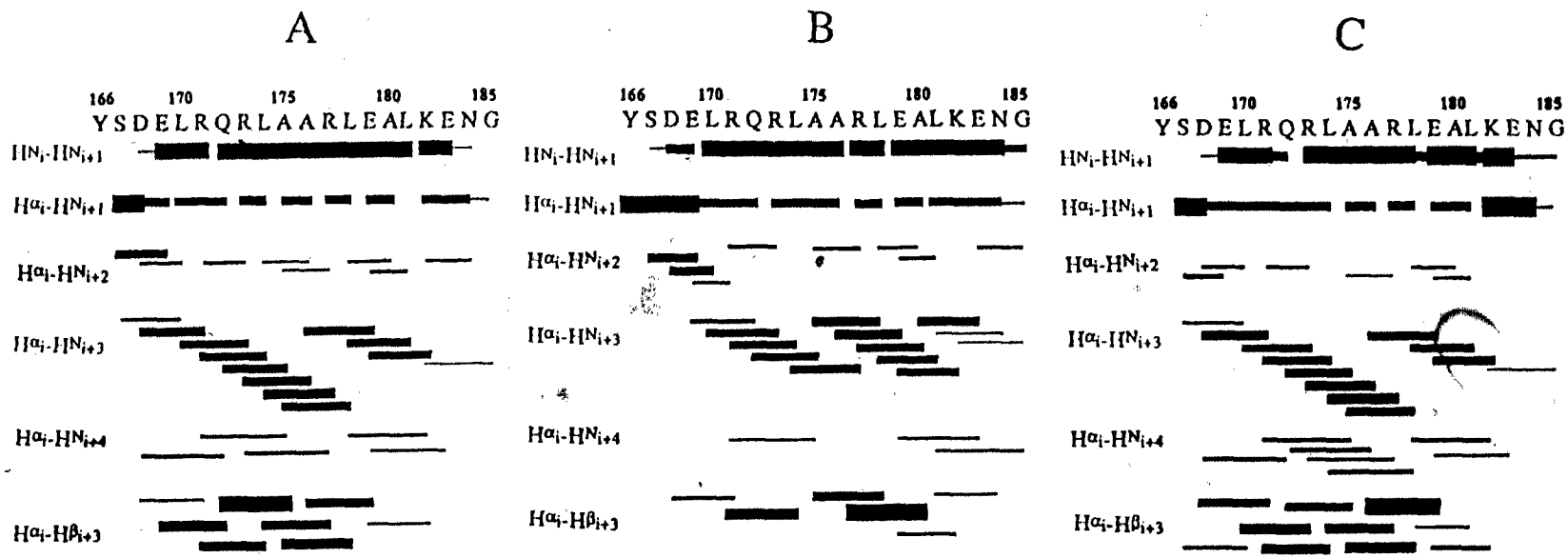
A
B
C
166 170 175 180 185
Y S D E L R Q R L A A R L E A L K E N G
HNi-HNi+1
Hαi-HNi+1
Hαi-HNi+2
Hαi-HNi+3
Hαi-HNi+4
Hαi-Hβi+3

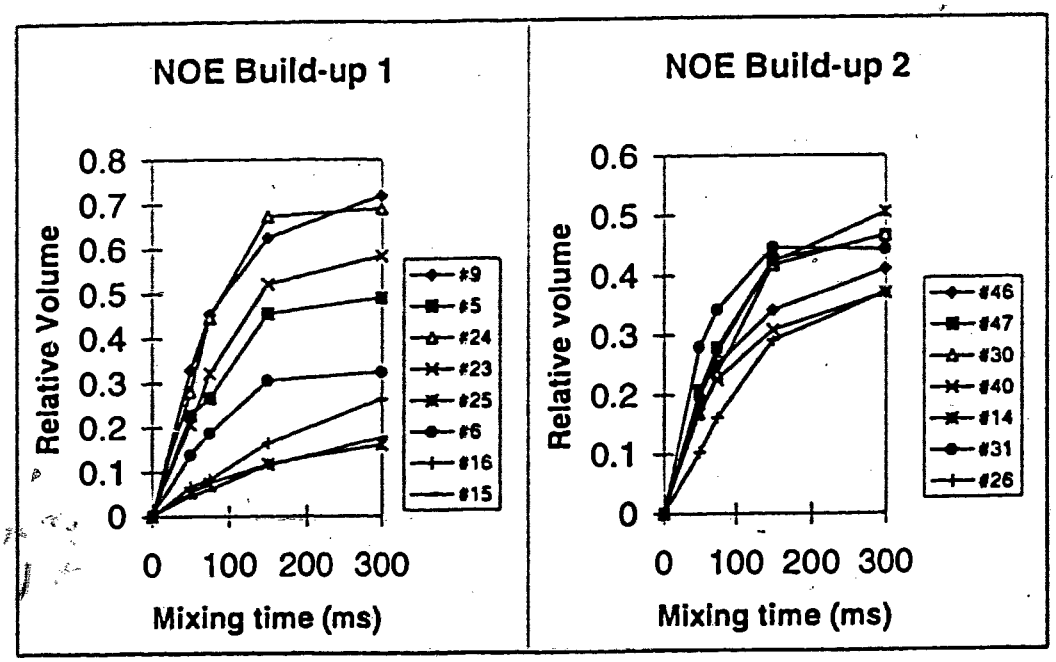

Fig. 6.8: NOE build-up curves for select cross peaks of apoA-I(166-185) in SDS at pH 3.7 and 37 °C. Mixing times are 50, 75, 150, and 300 ms. Peak idendity: (on NOE Build-up 1) #9, S167 H^N-Y166 H^α; #5, A180 H^N-E179 H^N; #24, E169 H^N-D168 H^α; #23, D168 H^N-S167 H^α; #25, R171 H^N-L170 H^α; #6, A176 H^N-A175 H^N; #16, A180 H^N-E179 H^α; #15, A176 H^N-A175 H^α; (on NOE Build-up 2) #46, L174 H^β-R171 H^α; #47, L178 H^β-A175 H^α; #30, L174 H^β-A175 H^N; #40, L178 H^β-E179 H^N; #14, S167 H^β-S167 H^N; #31, L170 H^β-L170 H^N; #26, D168 H^β-E169 H^N.

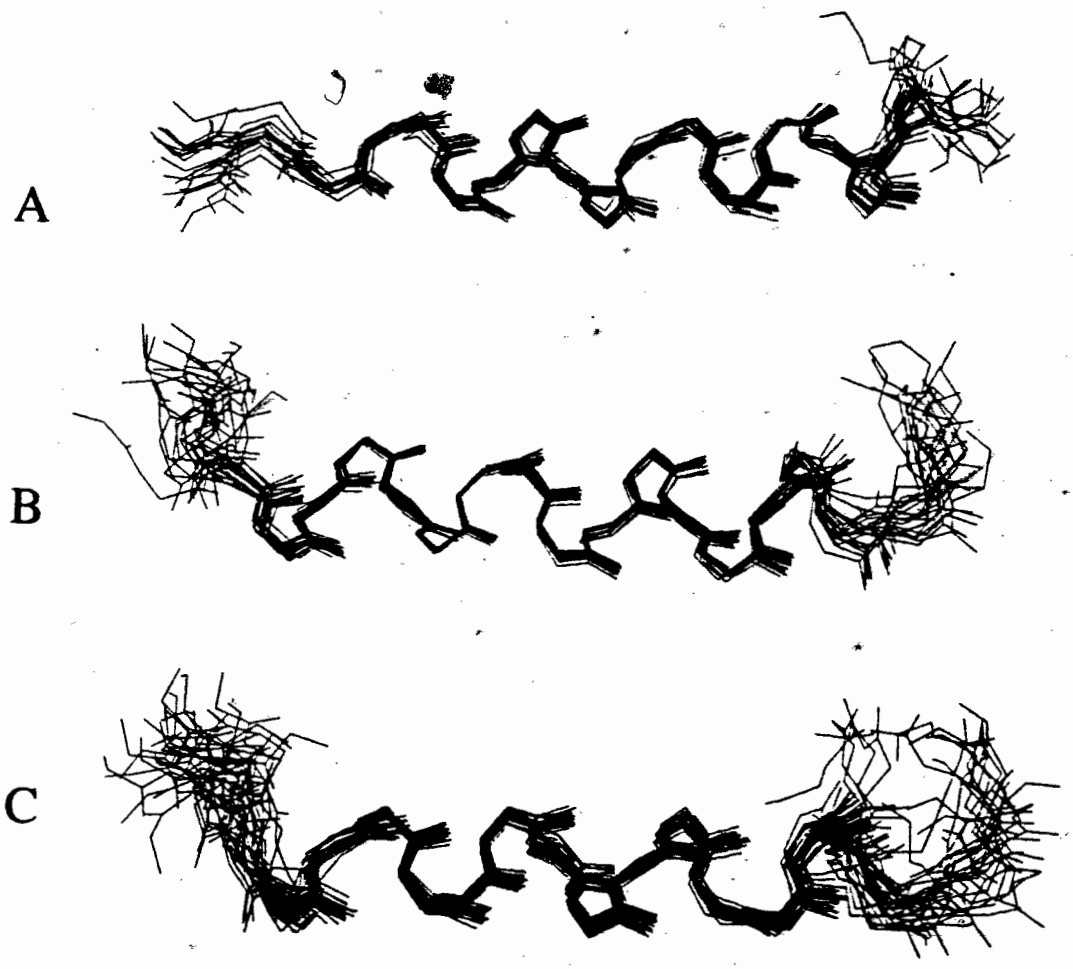

Fig. 6.9: Backbone structures of apoA-I(166-185) determined in SDS micelles at pH 3.7 (A), pH 6.6 (B), and in DPC micelles at pH 6.0 (C). The ensemble contains 19, 19, and 29 structures, respectively. In all structures, the middle helical region has been superimposed [Adapted from Wang *et al.* (1996b)].

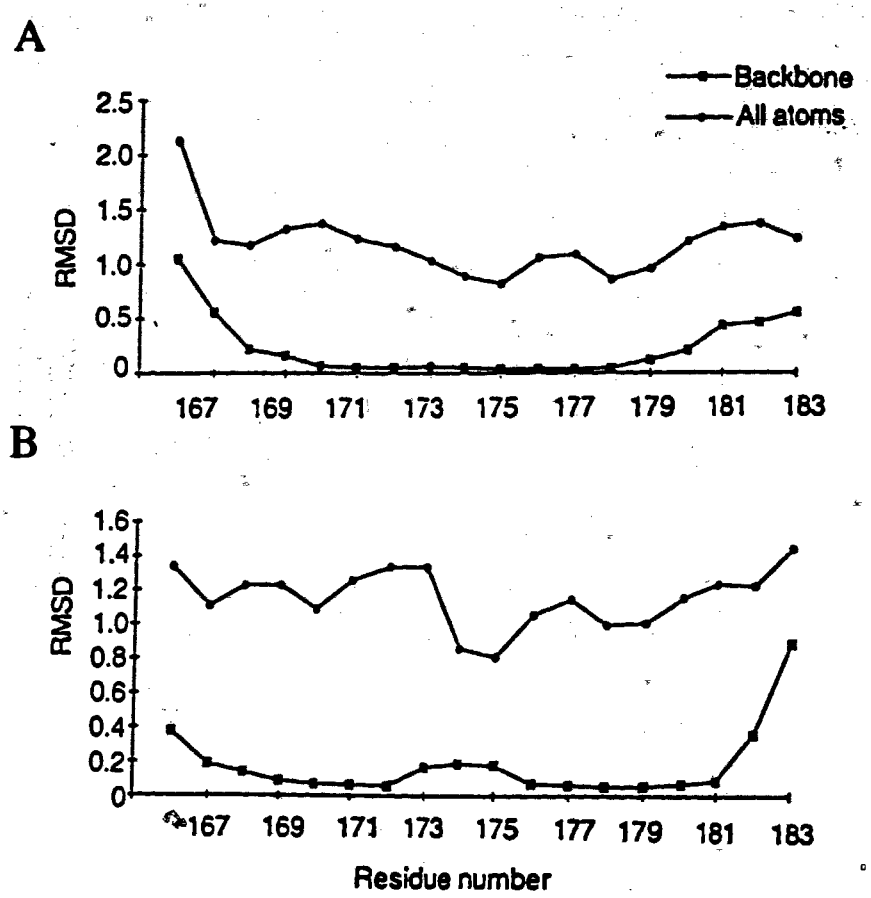

Fig. 6.10: RMSD plots of apoA-I(166-185) structures *versus* residue number. RMSDs of the structures in SDS at pH 6.6 (A) and at pH 3.7 (B) were calculated relative to the average structure. Each value was smoothed in a three-residue window.

The main body of the structures at both pHs is helical from residues R171 to K182. At pH 3.7, however, the helix levels off starting L170 to an almost extended structure whereas the helical structure extends to D168 at pH 6.6. As a result, the distance from the amide N atom of Y166 to the amide proton of L170 decreases by about 2.7 Å at pH 6.6 compared to the mean distance at pH 3.7. The more compact N-terminal structure at pH 6.6 is in accord with the observation of NOEs between Y166 and L170 at pH 6.6 but not at pH 3.7. The stereoview superposition of side chains of the structures at pH 3.7 is shown in Fig. 6.11. The ensemble of aromatic rings of Y166 all bends toward L170 and R171, probably participating in hydrophobic binding. Such an orientation of Y166 is similar to but not identical with the hydrophobic-staple motif, where residue i interacts with residue i+5 at the N-terminus (Munoz *et al.*, 1995).

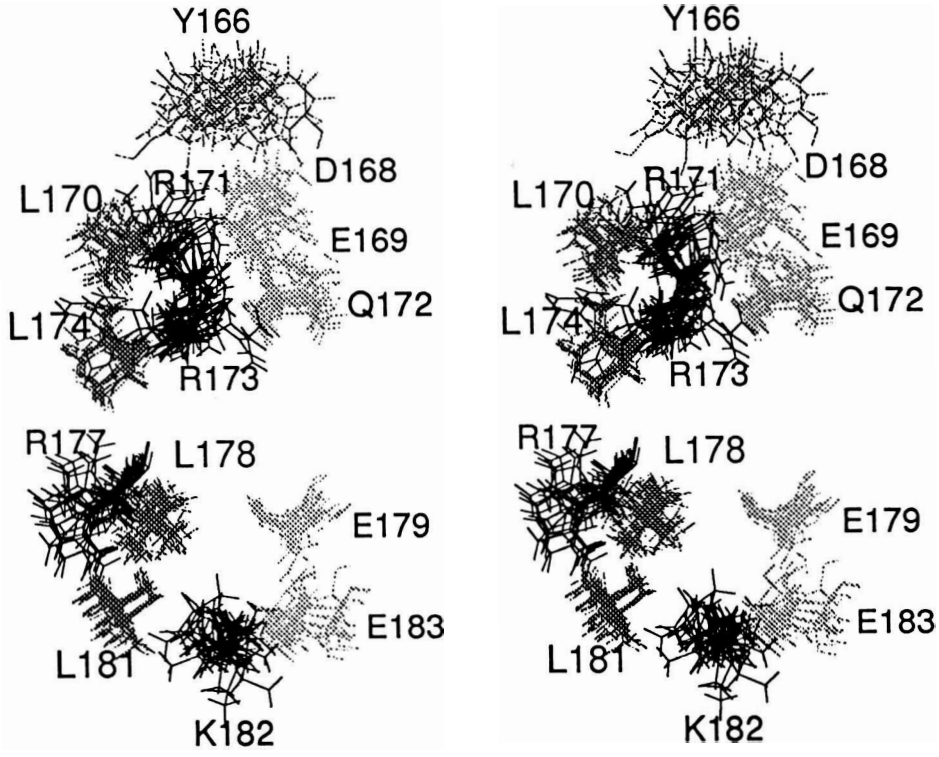

Fig. 6.11: Stereoview superposition of the side chains of the ensemble of calculated structures for apoA-I(166-185) in SDS at pH 3.7. Backbone atoms have been deleted for clarity. Hydrophobic side chains are shown in medium grey, negatively charged and polar side chains in light grey, and interfacial cationic side chains in dark grey [From Wang *et al.* (1996b)].

6.2.3.5 Three-dimensional structures of apoA-I(166-185) in DPC

Fig. 6.9C shows an ensemble of 29 structures for apoA-I(166-185) in complexes with DPC at pH 6.0. The Brookhaven PDB identification number for apoA-I(166-185) in DPC is 1ODR. Comparison of the average structures determined for the peptide in SDS at pH 6.6 and in DPC at pH 6.0 is illustrated in Fig. 6.12A, where the backbone atoms have been replaced by ribbons and overlaid. The mean structure in DPC (dark) superimposes nicely with that in SDS (grey) from R171 to K182, a region with well-defined amphipathic helices in both lipids. As shown, such a similarity in structure even extends to the majority of the side chains. The most evident Local structural difference was seen near D168 and E169. The similar structures of apoA-I(166-185) in SDS or

DPC, regardless of the lipid head group, demonstrate that hydrophobic interactions determine the final lipid-bound conformations of the peptide.

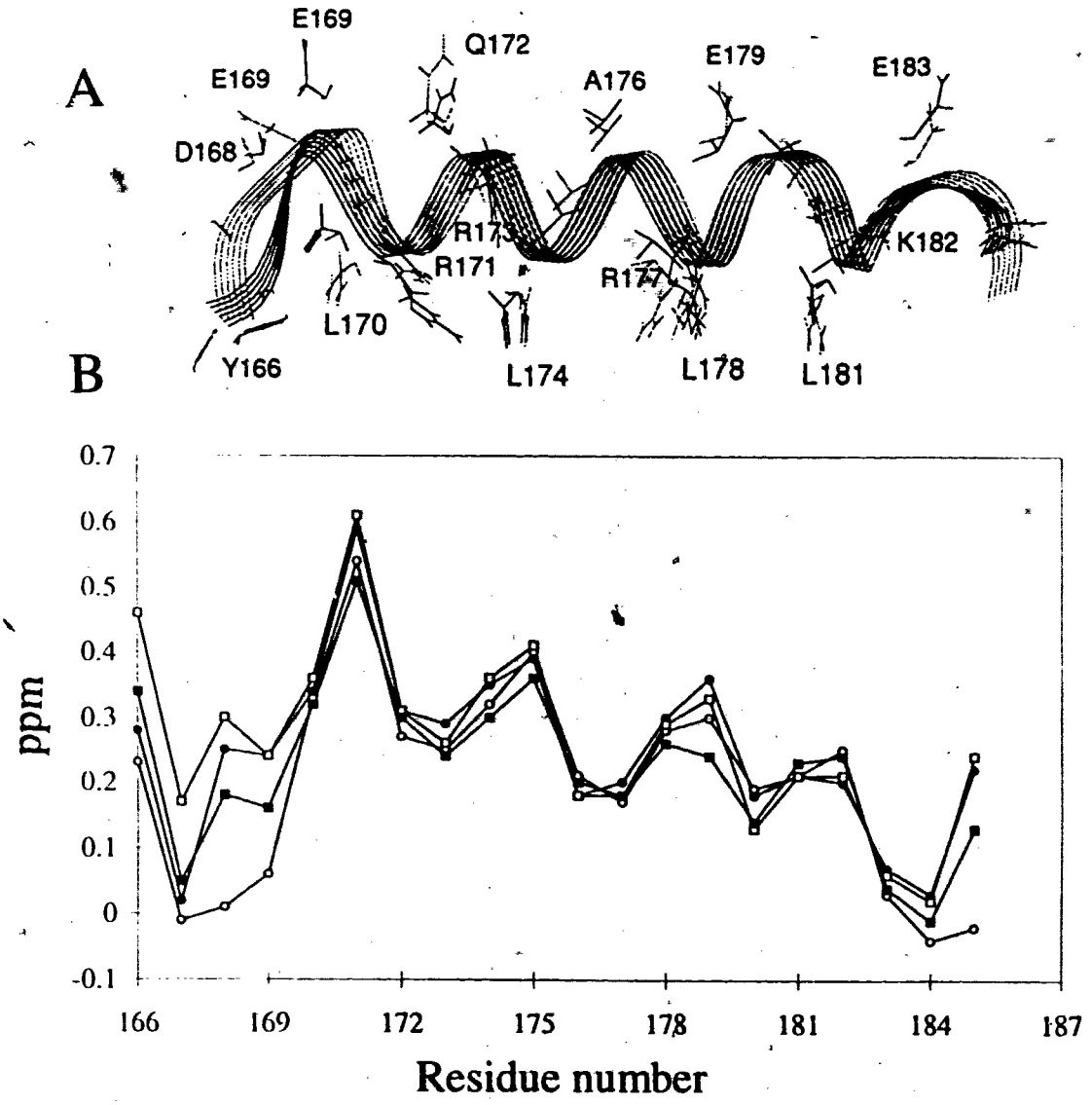

Fig. 6.12: (A) Average structures of apoA-I(166-185) in SDS (dark) **and DPC** (light) **micelles with the ribbons superimposed.** (B) Plots of secondary H^{α} chemical shifts of apoA-I(166-185) in SDS, at pH 3.7 (O) and 6.6 (●), DPC, pH 6.0 (□), and lysoPC, pH 3.7 (■) against the residue number.

Table 6.5: RMSD (Å) for the Final Sets of Structures of ApoA-I(166-185) in SDS, at pH 6.6 and 3.7, and in DPC at pH 6.0, All at 37 °C

	SDS, pH 6.6	SDS, pH 3.7	DPC, pH 6.0
Backbone N-C^{α}-C=O			
D168-K182	0.28 ± 0.07	0.35 ± 0.10	0.45 ± 0.09
Y166-G185	0.83 ± 0.19	0.77 ± 0.25	1.21 ± 0.39
All atoms			
D168-K182	1.36 ± 0.10	1.38 ± 0.21	1.60 ± 0.17

The end-on views of the average structures of apoA-I(166-185) determined in SDS and DPC are presented in Fig. 6.13. All the acidic and polar side chains are centered on the hydrophilic face at the bottom of the view, defining a hydrophilic arc of 75°, whereas leucine side chains are clustered in a hydrophobic face arc of approximate 110°. Cationic side chains are extended and located between the hydrophilic and the hydrophobic faces. Similar patterns were found in SDS and DPC for the region E169 to E183. Such overall orientations of the side chains indicate that the helical structures of apoA-I(166-185), determined in either SDS or DPC micelles, fit the definition for class A1 amphipathic helices (Segrest *et al.*, 1990).

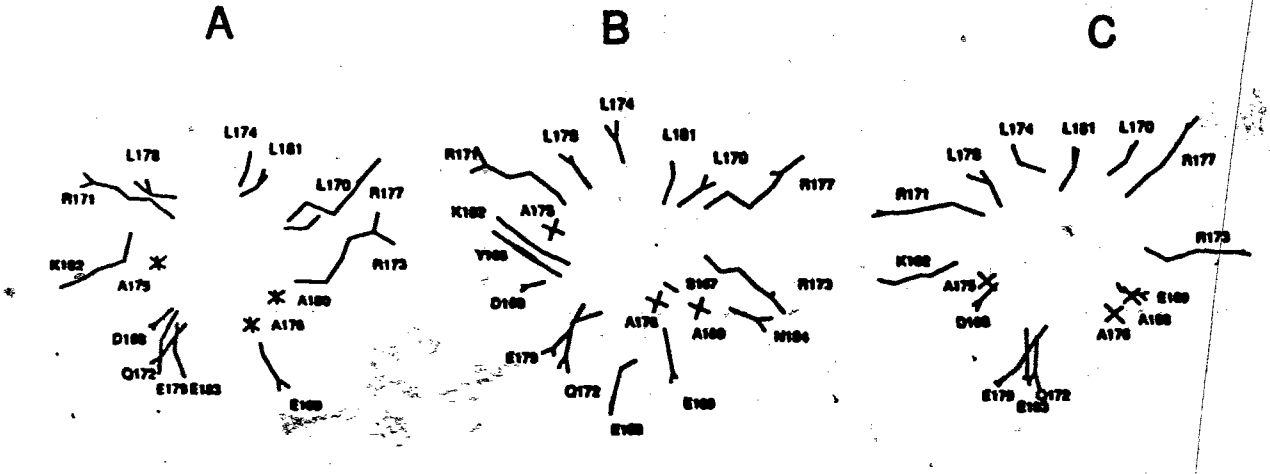

Fig. 6.13: End-on view of the average structure of apoA-I(166-185) in SDS at (A) pH 6.6 and (B) pH 3.7, and (C) in DPC at pH 6.0, all viewed from the C-terminal end of the peptide. Only side-chain heavy atoms are shown, that is, all backbone atoms and side-chain hydrogens have been omitted for clarity. Alanine methyl carbons are labeled with an asterisk. The two terminal residues at both ends in (B) and (C) are not shown because of fraying [From Wang *et al.* (1996b)].

6.2.3.6 Structure of apoA-I(166-185) in lysoPC

Among detergents, lysoPC is regarded as one of the best to solubilize membrane proteins (Tanford & Reynolds, 1976). To further test model lipids, we also investigated the possibility of lysoPC. The fingerprint region of the NOESY spectrum of apoA-I(166-185) in lysoPC is given in Fig. 6.4D. As lysoPC was not deuterated, the spectral quality is poor compared to that in deuterated SDS or DPC (Fig. 6.4). The signals were assigned by comparison with those assignments in SDS and DPC. Similar H^{α} chemical shifts (Fig. 6.12B) indicate that apoA-I(166-185) also adopts a similar conformation in lysoPC as in SDS or DPC (Fig. 6.12A). The differences in chemical shift at the N-terminus of apoA-I(166-185) suggest that this part of the peptide is sensitive to lipid as well as pH (Fig. 6.12B) (Sugiura *et al.*, 1987). Besides the chemical shifts (Tables 6.2 & 6.3), NOE connectivities at the N-terminus of apoA-I(166-185) in lysoPC at pH 3.7 were found to be similar to those in SDS at pH 3.7. In addition, intermolecular NOEs were also detected between the aromatic ring protons of Y166 and the acyl chains of lysoPC at the peptide/lysoPC ratio of either 1:1 or 1:11, indicating that Y166 is involved in lipid binding.

6.2.3.7 Intermolecular NOEs between apoA-I(166-185) and SDS

6.2.3.7.1 Interactions before helix formation

In the absence of apoA-I(166-185), SDS resonates at 4.01 (C1-H), 1.64 (C2-H), 1.33 (C3-H), 1.24 [$(CH_2)_n$] and 0.82 (CH_3) ppm (Fig. 6.14A) at 25 °C. On the other hand, in the absence of SDS, the proton signals of apoA-I(166-185) display spin-spin couplings (Fig. 6.14B). Mixing SDS with the peptide caused a shift of signals of both SDS and peptide. The shift of SDS proton signals by 0.04-0.09 ppm to higher field upon addition of apoA-I(166-185) may be ascribed to hydrophobic interactions (Dwek, 1973). The arginine εH^{N} multiplet of the peptide at 7.18 ppm in the absence of SDS split into three distinct singlets at 7.15 (R173), 7.18 (R171) and 7.22 (R177) ppm in presence of

SDS. Meanwhile, most of the spin-spin splitting of the peptide disappeared due to the line broadening (Fig. 6.14C). The shift of the peptide signals indicates conformational change while peak broadening suggests the association of apoA-I(166-185) with SDS (Dwek, 1973; Henry & Sykes, 1994; Rozek *et al.*, 1995; Buchko *et al.*, 1996a,b). Further investigation of the NMR spectrum revealed that the broadening is selective. It is more pronounced for signals less than 2 ppm (side chains of cationic residues and leucines) than for those between 2 and 2.9 ppm (hydrophilic side chains such as Glu, Gln, and Asp) (Fig. 6.14C). Such a selective interaction would suggest that anionic SDS has a much higher probability to interact with hydrophobic and positively charged side chains than with negatively charged side chains.

Fig. 6.15A, bottom, is a portion of the TOCSY spectrum of apoA-I(166-185) (peptide/SDS ratio, 1:1) showing cross peaks between protonated SDS C-1 and other protons as labeled. The NOESY spectrum (Fig. 6.15A, top) shows intermolecular cross peaks: SDS C1-H with leucine methyls, alanine methyls, and β-, γ- and δ-H of all the arginines. In addition, arginine εH^N signals, as well as the aromatic ring protons of Y166, showed NOE cross peaks with SDS C-1 and $(CH_2)n$ protons (Fig. 6.15B), consistent with the observation in lysoPC (Section 6.2.3.6). These 2D cross peaks (Fig. 6.15) and the selective broadening of NMR signals (Fig. 6.14) all support that SDS interacts specifically with hydrophobic and cationic side chains of apoA-I(166-185).

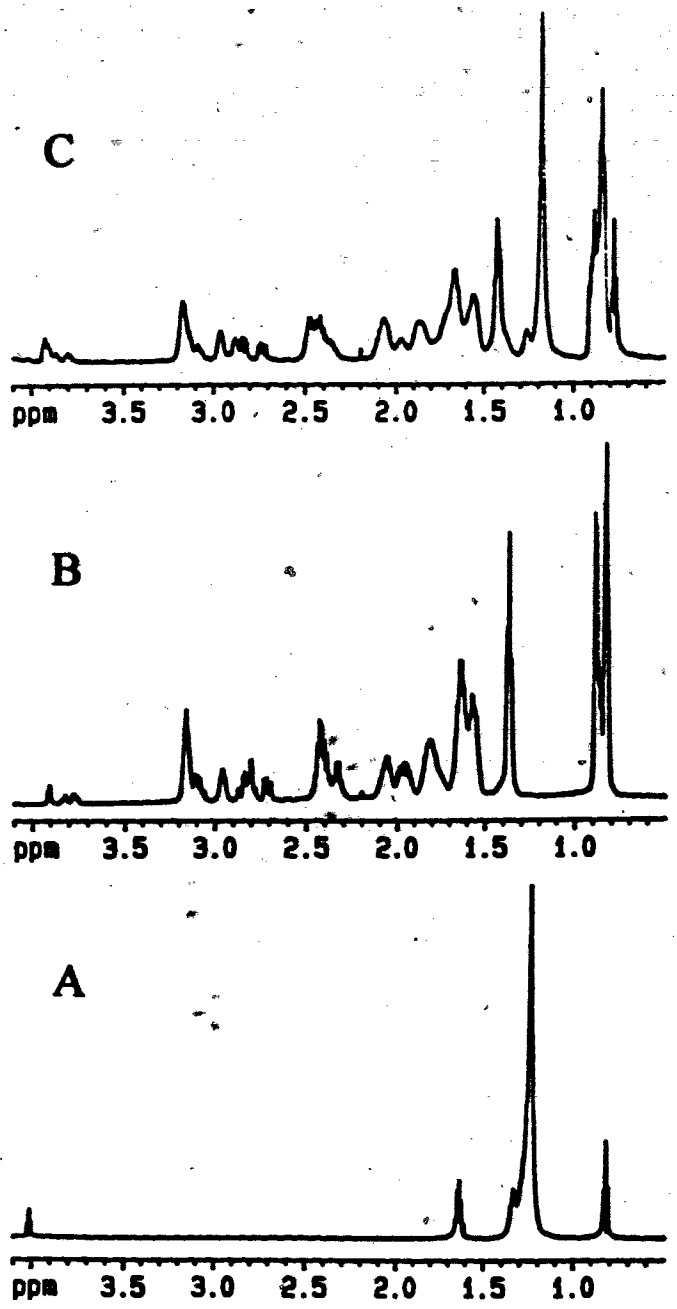

Fig. 6.14: NMR spectrum of SDS (A), side-chain region of apoA-I(166-185) in water (B) and in SDS (C). Note that the signal broadening for the cationic and hydrophobic side-chains in (C) are more pronounced.

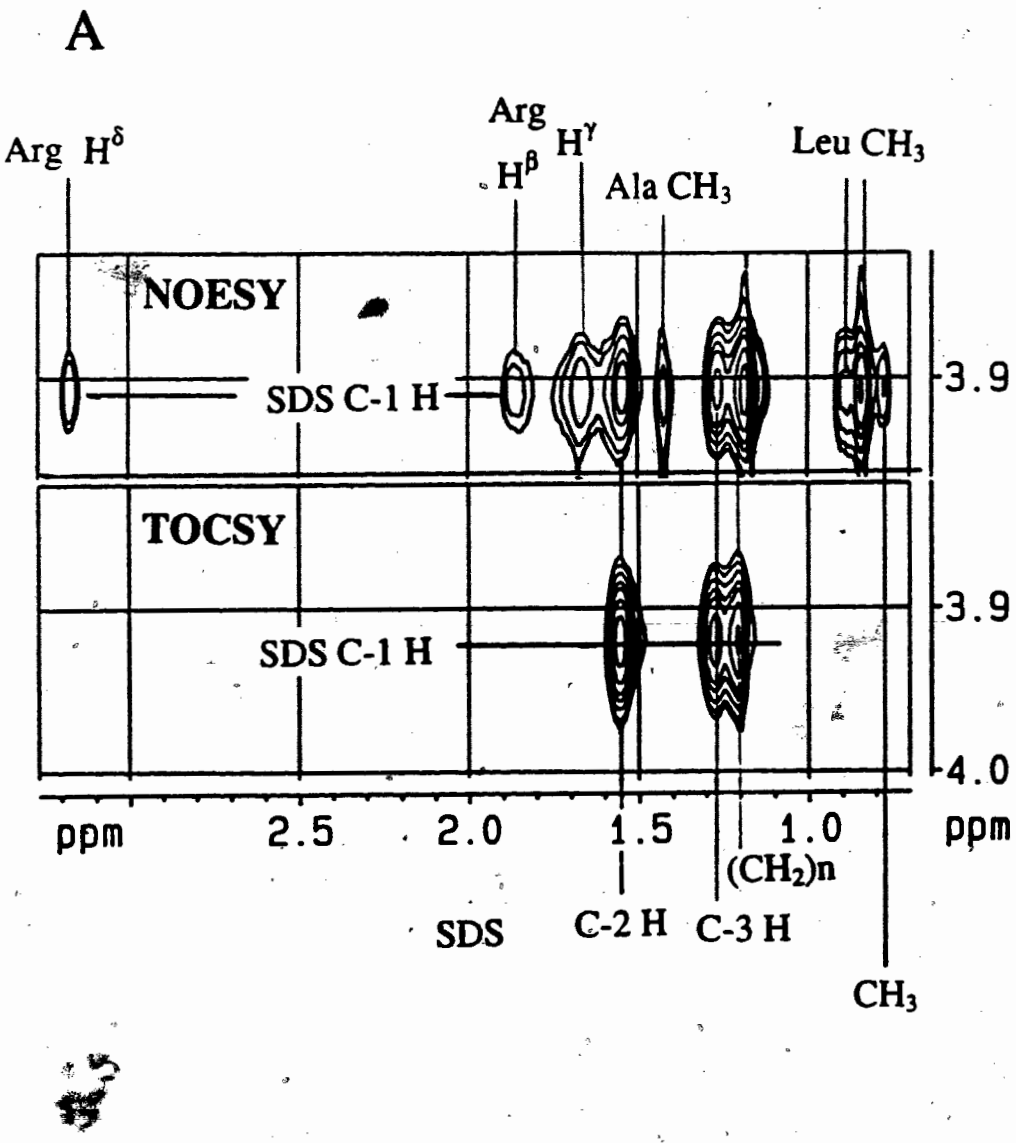

Fig. 6.15: Portions of the TOCSY and intermolecular NOESY spectra of apoA-I(166-185) at the peptide/SDS ratio of 1:1. Shown in (A) is the same H^{α}-side-chain regions of the TOCSY (bottom) and NOESY (top) spectra. The amide and aromatic side-chain region is given in (B).

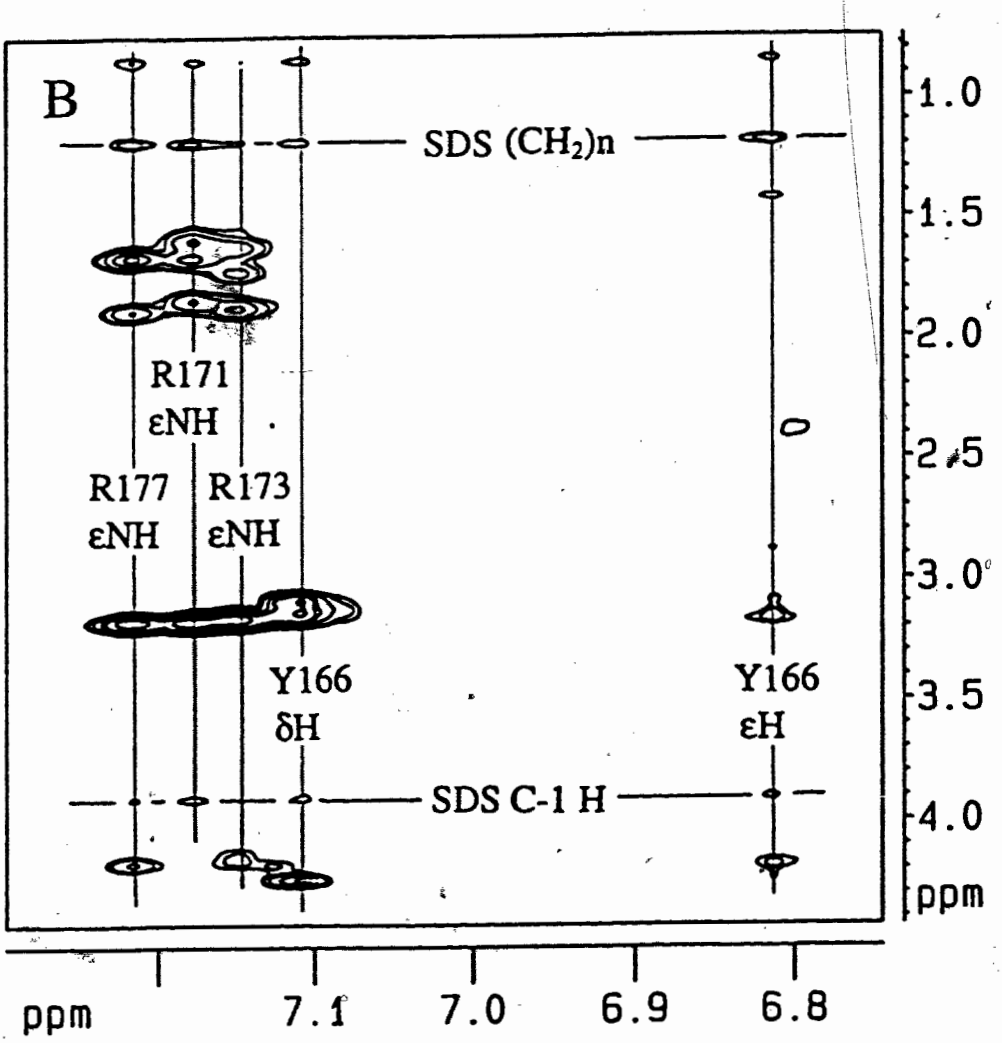

6.2.3.7.2 Interactions after helix formation

Fig. 6.16 is part of the NOESY spectrum of apoA-I(166-185) at the peptide/SDS-d_{25}/SDS ratio of 1:5:5 at 25 °C. The 1:10 ratio is the minimum ratio required for apoA-I(166-185) to adopt a helical conformation as shown in Fig. 6.2. Also, the NOE connectivity patterns in the NOESY spectra of the peptide at the peptide/SDS ratios 1:10, 1:40, and 1:80 are identical. Although the intermolecular NOEs were also observed at 37

°C they are clearer at 25 °C. By comparison with the NOESY in SDS-d_{25} at 1:40, it was found that εH^N of R177, R171 and/or R173 all showed intermolecular cross peaks with SDS $(CH_2)n$ and C-1 protons. As well, cross peaks were observed between the Y166 aromatic protons and SDS C1-H, C2-H, C3-H and $(CH_2)_n$ peaks (Fig. 6.16). These cross peaks could be seen at different mixing times ranging from 50 to 150 ms and are, therefore, due to direct dipole-dipole interactions. The detection of weak intermolecular NOE peaks indicates that the average distance between SDS C-1 protons and the εH^N protons of arginines is within 5 Å (Wüthrich, 1986).

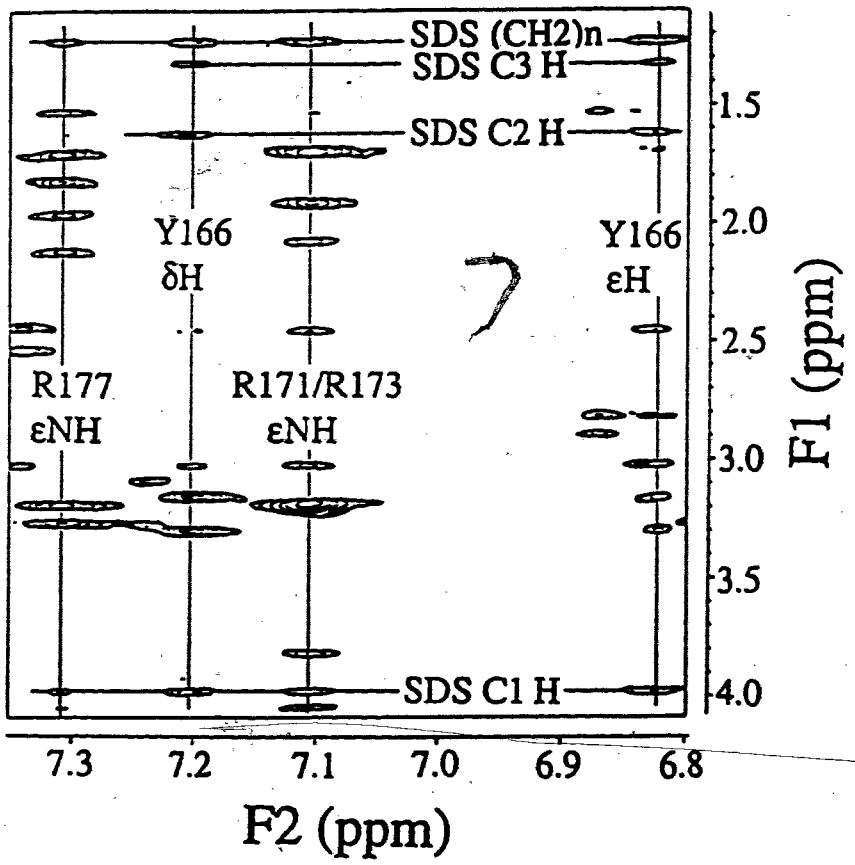

Fig. 6.16: Portion of the intermolecular NOESY spectrum of apoA-I(166-185) at the peptide/SDS ratio of 1:10 (peptide/SDS/SDS-d_{25}, 1:5:5). The peptide side-chain signals for Y166, R171, R173, and R177 as well as SDS signals are labeled. Intermolecular NOE peaks are at the cross of the SDS and peptide signals [From Wang *et al.* (1996b)].

6.2.4 Structures of apoA-I(142-187) in SDS or DPC micelles

6.2.4.1 Signal assignment

As shown in Fig. 6.17, the TOCSY cross peaks from H^N to side chains for apoA-I(142-187) in DPC are sparse. This is true of the TOCSY spectrum in SDS. As a consequence, the assignment of apoA-I(142-187) was achieved by applying the sequential assignment (Wüthrich, 1986), the main chain directed approach (MCD) (Englander & Wand, 1987; Di Stefano & Wand, 1987), and the peptide-aided signal assignment strategy (PASA) (Wang *et al.*, 1997a,b). The fingerprint (A) and amide proton (B) regions of the NOESY spectrum of apoA-I(142-187) in DPC-d_{38} micelles at 37 °C are presented in Fig. 6.18. The assignment was started from the identification of unique spin systems on the NOESY spectrum (Revington *et al.*, 1997). For example, the side chain of the single valine gave two sets of NOE connectivities. The stronger ones resulted from the H^N of V156 to its H^α, H^β, and H^γ whereas the medium to weak ones were assigned as the NOE connectivities of V156 to the H^N of D157. From D157, A158 was deduced using the H^β_i-H^N_{i+1} connectivities. Other useful starting spin systems were Y166, D150, H155, H162, and the alanines. The assignment of Y166 and histidines was facilitated by the NOE connectivities of H^β to both H^N and aromatic ring protons. The spin systems were then linked using H^α_i-H^N_{i+1}, H^α_i-H^β_{i+3}, and H^N_i-H^N_{i+1} as shown in Fig. 6.18B. The H^α and side-chain resonances were confirmed by TOCSY spin patterns and the assignment of side chains was corroborated by DQF-COSY. The very C-terminal residues such as G185, G186, and A187 were assigned using the zero-quantum dispersive peaks observed in the NOESY spectrum at 50 ms (Cavanagh *et al.*, 1996). A similar peak was observed for G185 in apoA-I(166-185) (Fig. 6.4).

As shown in Fig. 6.19A, the spectral overlap in the amide region is heavy at 37 °C and a higher temperature (50 °C) was necessary to achieve the assignments in SDS (Fig. 6.19B). The spectra of the peptide in SDS were assigned similarly. Shown in Fig. 6.20 is the fingerprint region of NOESY spectrum of apoA-I(142-187) in SDS. Since H^α signals of D150 and D157 resonated near the water signal at 50 °C in SDS, they were confirmed

at 37 °C. Comparison of the spectra in SDS and DPC confirmed the assignment for G145, E146, D168 and E169, which are weak or incomplete in SDS. In addition, the side-chain εH^N signals of arginines of apoA-I(142-187) resonate between 7.49-7.83 ppm in DPC (Fig. 6.17) but 7.08-7.26 ppm in SDS. These side-chain signals in SDS do not overlap with amide proton resonances of the peptide, thus verifying the assignments in DPC. Table 6.6 lists the chemical shifts of the peptide in SDS and the chemical shifts of apoA-I(142-187) in DPC micelles are tabulated in Table 6.7. In both SDS and DPC, two sets of peaks were found for residues E183 and N184 (Tables 6.6 & 6.7), indicating that the C-terminus of apoA-I(142-187) is flexible and exists in at least two conformers (Cavanagh *et al.*, 1996).

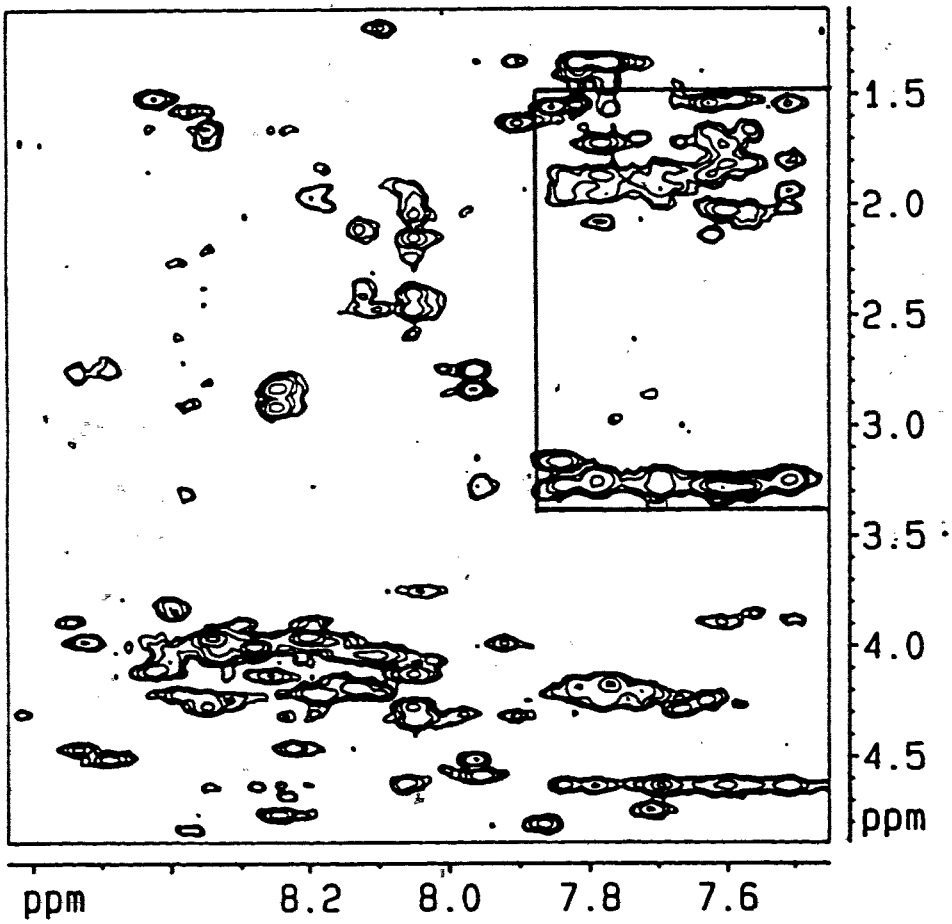

Fig. 6.17: Fingerprint region of the TOCSY spectrum of apoA-I(142-187) in DPC. The peptide/DPC ratio is 1:60, pH 4.9 and 37 °C. The boxed region contains predominantly the TOCSY relay peaks from the εH^N of arginines to side-chains. Note that these peaks in SDS do not appear in the amide region (cf., Fig. 6.16).

Table 6.6: Proton Chemical Shifts (ppm) of ApoA-I(142-187) Bound to SDS-d_{25} at the Peptide/SDS Molar Ratio of 1:60 at pH 4.9 and 50 °C[a]

Residue	H^N	H^α	CSI	H^β	H^γ	Others
Ser142	-	4.09	-1	3.79		
Pro143	-	4.50	0	2.41	2.10, 1.98	H^δ 3.84
Leu144	7.91	4.26	-1	1.72, 1.64	-	H^δ 0.96, 0.91
Gly145	7.95	3.78	-1			
Glu146	8.04	4.04	-1	2.12	2.45	
Glu147	8.13	4.22	-1	2.24, 2.13	2.49	
Met148	8.19	4.22	-1	2.24, 2.03	2.68, 2.59	εCH_3 2.03
Arg149	8.18	3.90	-1	2.02, 1.92	1.82, 1.59	H^δ 3.24, 3.20; εH^N 7.08, 6.65
Asp150	8.11	4.45	-1	2.89, 2.80		
Arg151	8.04	4.14	-1	1.98	1.87, 1.75	H^δ 3.25; εH^N 7.26
Ala152	8.38	4.12	-1	1.49		
Arg153	8.32	3.96	-1	2.01	1.83,1.72	H^δ 3.27; εH^N 7.17, 6.64
Ala154	7.74	4.22	-1	1.40		
His155	7.88	4.75	0	3.35, 3.23		2H 8.77; 4H 7.46
Val156	8.04	3.77	-1	2.28	1.11, 1.04	
Asp157	8.44	4.45	-1	2.84, 2.79		
Ala158	7.81	4.26	-1	1.60		
Leu159	8.00	4.15	-1	1.91, 1.80	-	H^δ 0.96, 0.92
Arg160	8.47	3.90	-1	2.08, 2.00	1.87, 1.67	H^δ 3.24; εH^N 7.12
Thr161	7.98	4.05	-1	4.21	1.20	
His162	7.86	4.59	-1	3.35, 3.30		2H 8.76; 4H 7.45
Leu163	7.99	4.59	+1	1.89, 1.69	-	H^δ 0.92
Ala164	7.75	4.31	0	1.56		
Pro165	-	4.35	0	2.15, 1.07	1.85	H^δ 3.67, 3.41
Tyr166	7.69	4.71	+1	3.33, 2.86		2,6H 7.15; 3,5H 6.91
Ser167	7.98	4.53	0	3.97, 3.83		
Asp168	8.33	4.51	-1	2.77, 2.70		
Glu169	7.95	4.18	-1	2.26, 2.18	2.57, 2.48	
Leu170	8.26	4.06	-1	1.85	1.67	H^δ 0.91
Arg171	8.33	3.84	-1	2.02	1.82, 1.62	H^δ 3.26; εH^N 7.13, 6.64

Gln172	7.85	4.10	-1	2.19	2.56, 2.46	δH^N 7.21,-
Arg173	8.05	4.14	-1	2.08, 1.91	1.78	H^δ 3.20; εH^N 7.13, 6.64
Leu174	8.31	4.07	-1	1.84	1.59	H^δ 0.90
Ala175	8.42	3.99	-1	1.54		
Ala176	7.72	4.17	-1	1.51		
Arg177	7.75	4.20	-1	2.15, 1.94	1.84,1.73	H^δ 3.26, 3.19; εH^N 7.25, 6.66
Leu178	8.28	4.09	-1	1.82	1.68	H^δ 0.91
Glu179	8.13	4.00	-1	2.19, 2.12	2.53	
Ala180	7.56	4.16	-1	1.53		
Leu181	7.72	4.18	-1	1.89, 1.83	1.69	H^δ 0.93
Lys182	7.80	4.14	-1	1.92, 1.86	1.59, 1.47	H^δ 1.69; H^ε 2.97
Glu183	7.82	4.28	-1	2.16, 2.09	2.54, 2.45	
Glu183'	-	4.34		2.16, 2.03	2.52, 2.46	
Asn184	8.01	4.74	0	2.92, 2.85		γH^N -
Asn184'	7.84	4.57		2.84, 2.77		
Gly185	8.06	3.97	0			
Gly186	8.14	3.95	0			
Ala187		-4.22	-1	1.35		

a. Chemical shifts are referenced to internal standard DSS (0.00).

Table 6.7: Proton Chemical Shifts (ppm) of ApoA-I(142-187) in DPC-d_{38} at the Peptide/DPC Molar Ratio of 1:60 at pH 4.9 and 37 °C [a]

Residue	H^N	H^α	CSI	H^β	H^γ	Others
Ser142	-	4.03	-1	-		
Pro143	-	4.50	0	2.41, 2.10	2.05, 1.98	H^δ 3.83, 3.77
Leu144	8.34	4.26	-1	1.70, 1.64	-	H^δ 0.95, 0.90
Gly145	8.39	3.78	-1			
Glu146	8.14	4.02	-1	2.07	2.45, 2.35	
Glu147	8.33	4.21	-1	2.19	2.43, 2.36	
Met148	8.38	4.20	-1	2.23	2.69, 2.59	εCH_3 2.03
Arg149	8.18	3.86	-1	1.93, 1.84	1.80, 1.54	H^δ 3.23; εH^N 7.49
Asp150	8.21	4.44	-1	2.85, 2.75		
Arg151	8.17	4.20	-1	2.00, 1.91	1.86, 1.71	H^δ 3.23; εH^N 7.78

Ala152	8.42	4.09	-1	1.49		
Arg153	8.29	3.87	-1	2.03	1.84, 1.71	H^{δ} 3.27; εH^{N} 7.59
Ala154	7.79	4.21	-1	1.38		
His155	7.85	4.80	0	3.32, 3.14		2H 8.60; 4H 7.21
Val156	8.02	3.72	-1	2.28	1.10, 1.03	
Asp157	8.53	4.45	-1	2.73		
Ala158	7.89	4.30	0	1.61		
Leu159	8.04	4.11	-1	1.93, 1.77	- .	H^{δ} 0.94, 0.90
Arg160	8.53	3.86	-1	2.12, 2.00	1.83, 1.67	H^{δ} 3.26; εH^{N} 7.61
Thr161	8.09	4.01	-1	4.20	1.17	
His162	7.94	4.58	-1	3.29, 3.24		2H 8.69; 4H 7.94
Leu163	8.05	4.60	+1	1.89	1.63	H^{δ} 0.91
Ala164	7.86	4.24	-1	1.59		
Pro165	-	4.36	0	2.17, 1.02	1.87, 1.83	H^{δ} 3.71, 3.38
Tyr166	7.69	4.73	+1	3.32, 2.83		2,6H 7.15; 3,5H 6.91
Ser167	7.90	-	-	3.96		
Asp168	8.48	4.50	-1	2.71		
Glu169	8.12	4.17	-1	2.25, 2.11	2.46	
Leu170	8.32	4.02	-1	1.89, 1.86	1.63	H^{δ} 0.91
Arg171	8.38	3.83	-1	2.07	1.63	H^{δ} 3.26; εH^{N} 7.55
Gln172	8.03	4.11	-1	2.21	2.57, 2.45	δH^{N} 7.25, 6.76
Arg173	8.18	4.02	-1	1.93, 1.87	1.60	H^{δ} 3.26; εH^{N} 7.68
Leu174	8.27	3.98	-1	1.83	1.63	H^{δ} 0.92, 0.88
Ala175	8.36	3.98	-1	1.55		
Ala176	7.81	4.17	-1	1.53		
Arg177	7.77	4.24	-1	2.05, 1.95	1.85	H^{δ} 3.26, 3.21; εH^{N} 7.83
Leu178	8.25	4.11	-1	1.81	1.65	H^{δ} 0.96, 0.90
Glu179	8.08	4.04	-1	2.12	2.45	
Ala180	7.60	4.22	-1	1.52		
Leu181	7.71	4.19	-1	-	-	H^{δ} 0.94
Lys182	7.75	4.14	-1	1.93, 1.87	1.55, 1.46	H^{δ} 1.71; H^{ε} 2.97
Glu183	8.03	4.26	-1	2.14, 2.04	2.47, 2.39	
Glu183'	8.04	4.32		2.15, 1.97	2.39	
Asn184	8.25	4.75	0	2.91, 2.83		γH^{N}-
Asn184'	7.96	4.51		2.83, 2.75		

Gly185	8.27	3.98	0	
Gly186	8.20	3.94	0	
Ala187	7.76	4.17		1.33
A187'	7.81	4.19	-1	1.34

a. Chemical shifts are referenced to internal standard DSS (0.00).

6.2.4.2 Chemical shift index, NOE pattern and secondary structure

Using Tables 6.6 & 6.7 and the H^{α} reference chemical shift table (Wüthrich, 1986), the CSIs for apoA-I(142-187) in SDS and DPC were obtained and are also included in the respective tables. A dense grouping of "-1"s indicates helical conformation while a dense grouping of "+1"s suggests β-strand. Zeros are indicative of random coil. Thus, in both DPC and SDS the regions corresponding to residues 144-162 and 168-183 were predicted to be helical. The extension of the first helix to at least T161 is consistent with the observation that the H^{α} chemical shift is less than H^{β}, different from the unstructured terminal threonines in apoE(267-289) (Table 4.2) and in apoA-II(18-30)+ (Table 5.2) (Doak *et al.*, 1996). A comparison of Tables 6.6 & 6.7 revealed that, except for residues S142, R153, A164, R173, and L174, whose H^{α} chemical shifts differ by 0.12 ppm or less, the differences in H^{α} chemical shifts of the 46mer in the two micelles are within ± 0.05 ppm, suggesting that apoA-I(142-187) adopts similar conformations in the two lipid environments.

Fig. 6.18: Fingerprint (A) and amide proton (B) region of the NOESY spectrum of apoA-I(142-187) (5 mM) in DPC-d_{38} (H_2O/D_2O, 9:1, v/v) (τ_m = 80 ms) at peptide/DPC ratio 1:60, pH 4.9, and 37 °C. H^{α}_i-H^N_i cross peaks for each residue (A) are labeled and the H^N_i-H^N_{i+1} cross peaks (B) are labeled. For clarity, only the sequential connectivities for the region 166-173 (B) are shown (From Wang *et al.*, 1997b)

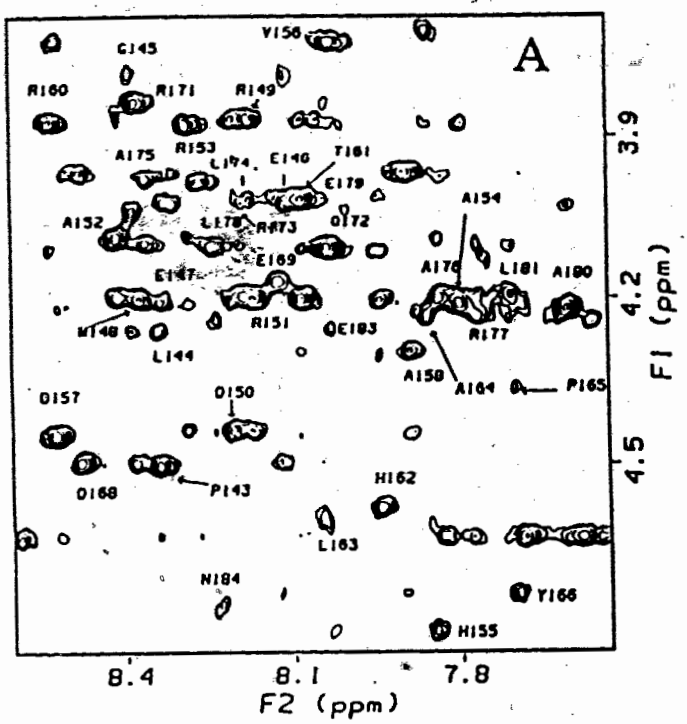
A
G145
Y156
R160
R171
R149
R153
A175
L174
E146
T181
E179
A154
A152
L178
R173
Q172
E169
E147
A176
L181
A180
M148
R151
QE183
R177
L144
A158
A164
P165
D157
D150
D168
P143
H162
L163
N184
Y166
H155
8.4
8.1
7.8
F2 (ppm)
3.9
4.2
4.5
F1 (ppm)

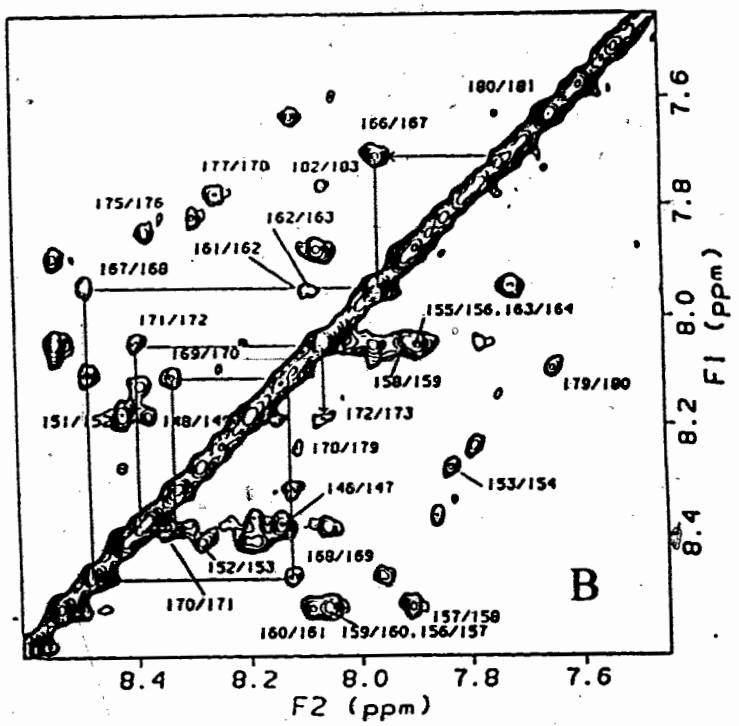
B
180/181
166/167
177/178
102/103
175/176
162/163
161/162
167/168
171/172
155/156.163/164
169/170
158/159
179/180
151/152
148/149
172/173
170/179
153/154
146/147
168/169
152/153
170/171
157/158
160/161
159/160.156/157
8.4
8.2
8.0
7.8
7.6
F2 (ppm)
7.6
7.8
8.0
8.2
8.4
F1 (ppm)

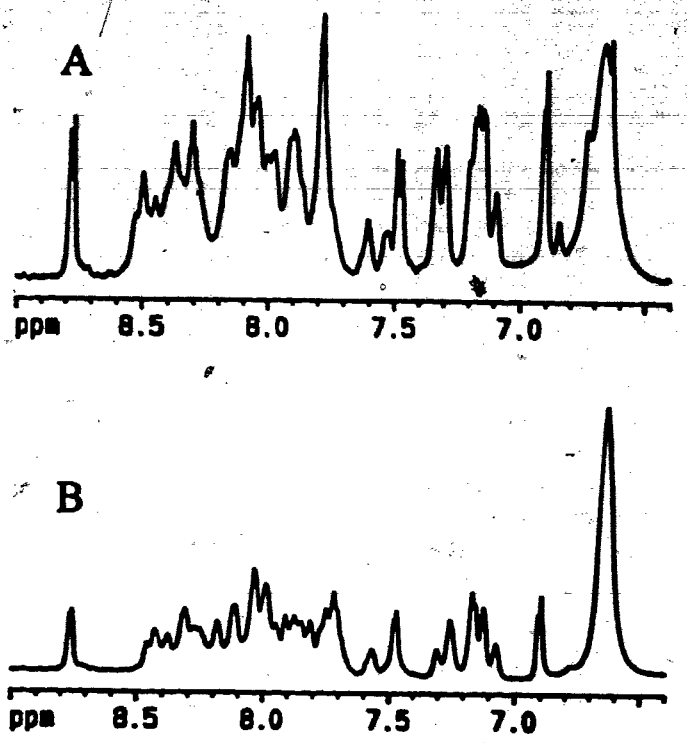

Fig. 6.19: NMR spectrum of apoA-I(142-187) (5 mM) (peptide/SDS, 1:60) in SDS at pH 4.9, (A) 37 °C and (B) 50 °C.

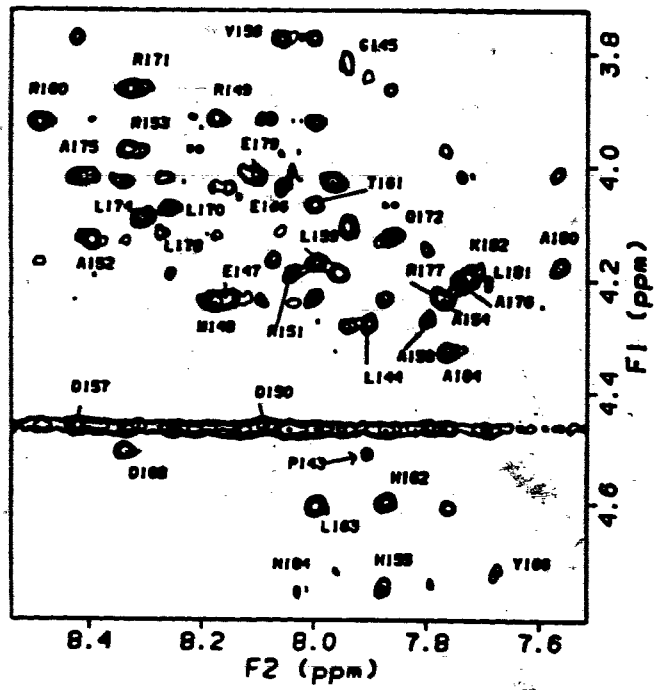

Fig. 6.20: Fingerprint region of the NOESY spectrum of apoA-I(142-187) (5 mM) in SDS-d_{25}-containing aqueous solution (H_2O/D_2O, 9:1, v/v) (τ_m = 100 ms) at a peptide/SDS ratio 1:60, pH 4.9, and 50 °C. The H^{α}_i-H^{N}_i cross peaks for each residue are labeled.

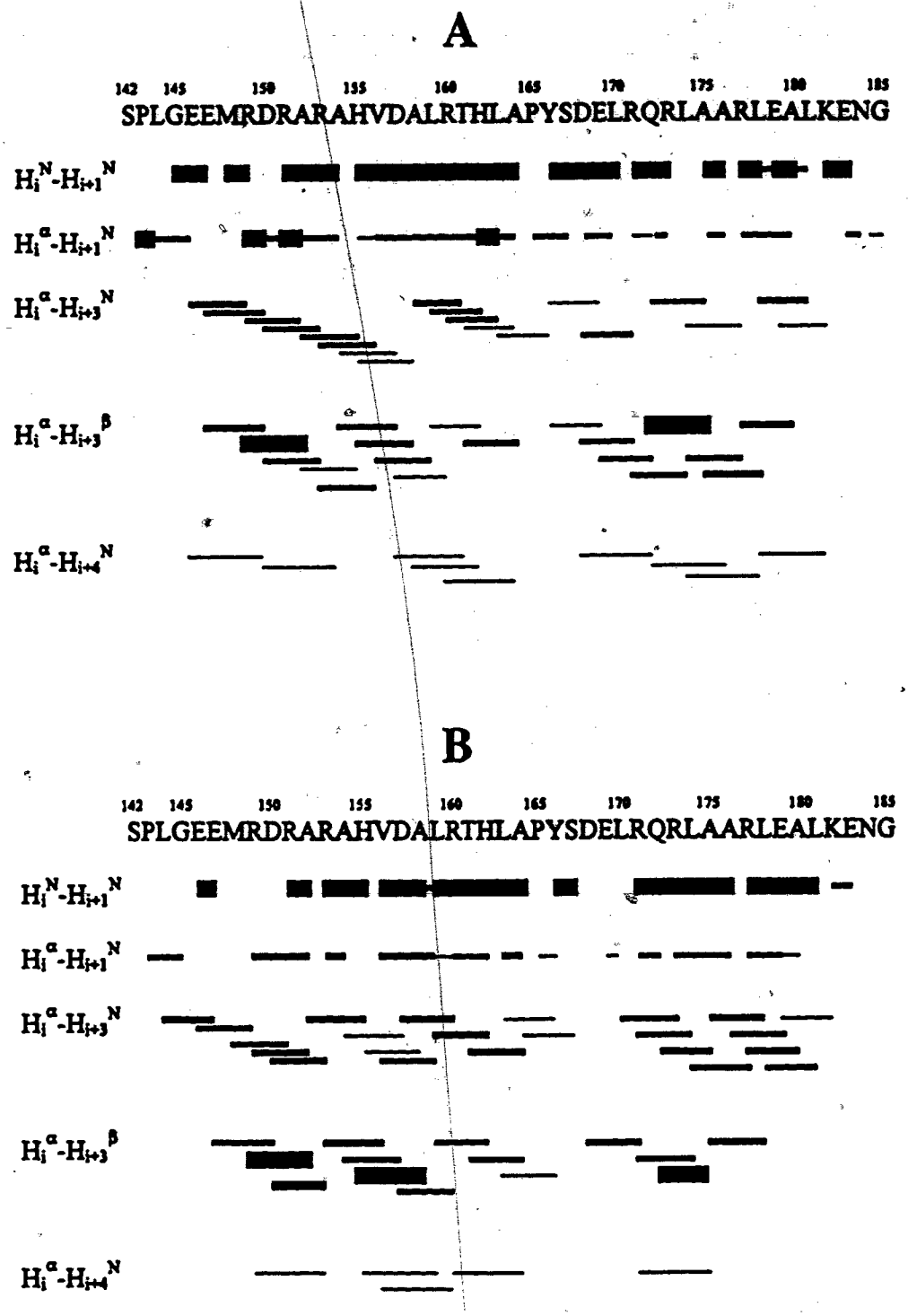

Fig. 6.21: Summary of interresidue NOE connectivities of apoA-I(142-187) bound to DPC (A) and SDS (B) micelles. Strong, medium, and weak NOEs are depicted with the height of the bars (From Wang *et al.*, 1997b).

The interresidue NOEs for apoA-I(142-187) in DPC (A) or SDS (B) micelles are summarized in Fig. 6.21. In both micelles, a combination of the NOE pattern such as medium to strong H^N_i-H^N_{i+1}, weak to medium H^α_i-H^N_{i+3}, weak to strong H^α_i-H^β_{i+3} and H^α_i-H^N_{i+1}, and weak H^α_i-H^N_{i+4} indicates helical structure in regions corresponding to residues 146-164 and 168-182. The H^N signals of both Y166 and A164 showed NOE cross peaks with the H^δ of P165, indicating a *trans* conformation for the proline (Wüthrich *et al.*, 1984). A similar proline conformation has been found in apoE(263-286) (Chapter 4).

6.2.4.3 Three-dimensional structures of apoA-I(142-187) in SDS or DPC

Fig. 6.22 shows the backbone view of the structures of apoA-I(142-187) in the presence of DPC calculated using 450 NOE distance restraints (227 intra- and 223 inter-residues). The Brookhaven PDB identification number is 1GW3. Superimposing the N-terminal helix (146-162) led to a "fraying" of the C-terminal helix (168-182) (Fig. 6.22A) and vice versa, illustrating the interhelical structure is not uniquely defined. The RMSD for superimposing the backbone atoms of the helical regions 146-162 is 0.98 ± 0.22 Å. Superimposing the backbone atoms of the helical regions 168-182 (Fig. 5B) gave a RMSD of 1.99 ± 0.42 Å. The better defined N-terminal helix can be attributed to higher resolution of proton resonances (more NOE restraints). Finally, when 29 structures of the hinge region, residues 163-168, are superimposed (Fig. 6.22C) a helical-like structure can be seen. The RMSD for superimposing the backbone atoms of the interhelical region, residues 163-168, is 1.11 ± 0.39 Å.

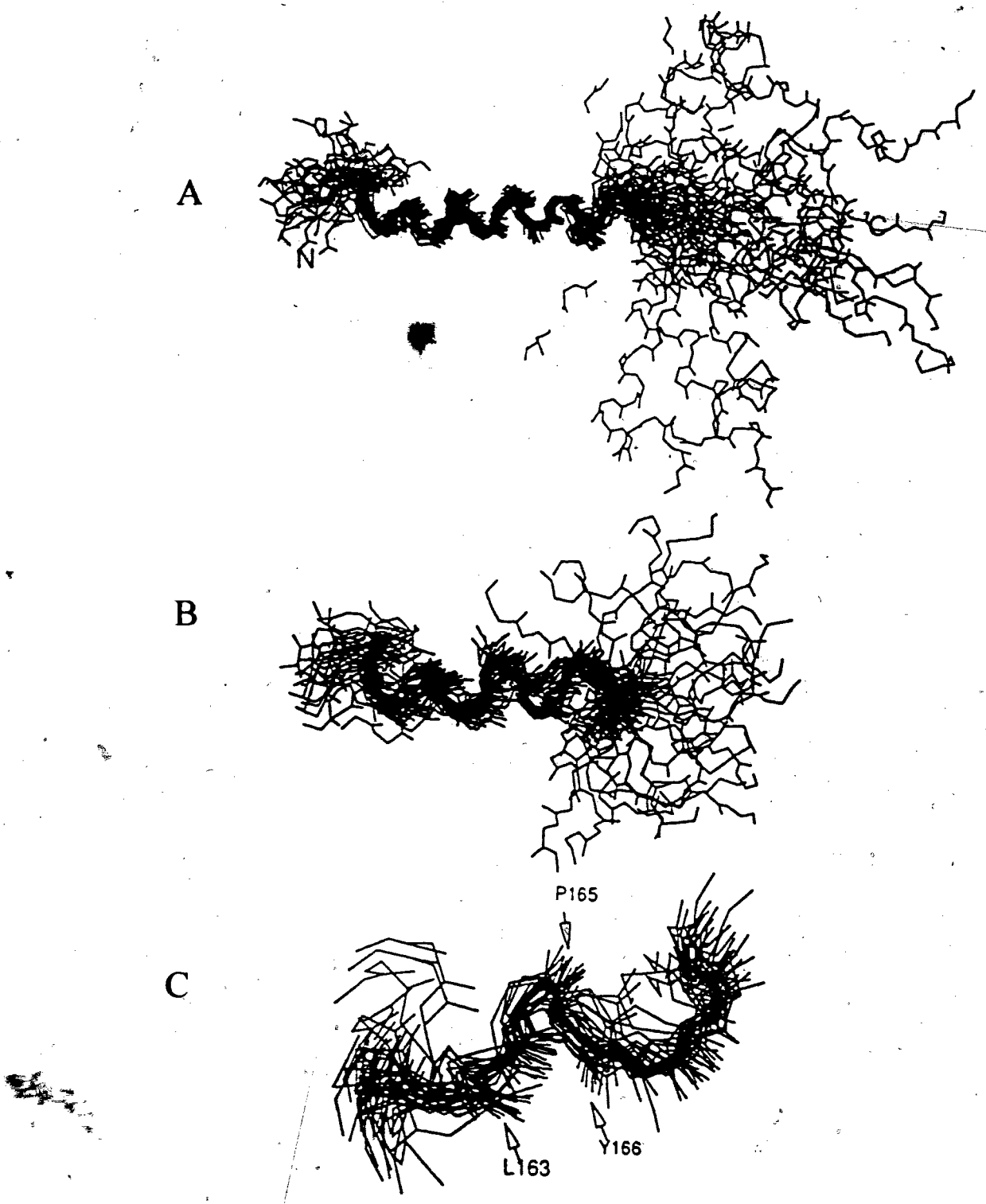

Fig. 6.22: Backbone view of an ensemble of 29 structures of apoA-I(142-187) in DPC at pH 4.9 and 37 °C (A) with residues 146-164 superimposed; (B) C-terminal helical structures, residues 169-183 with residues 170-181 superimposed; and (C) the interhelical structures, residues 161-169 with 163-168 superimposed (Form Wang *et al.*, 1997b).

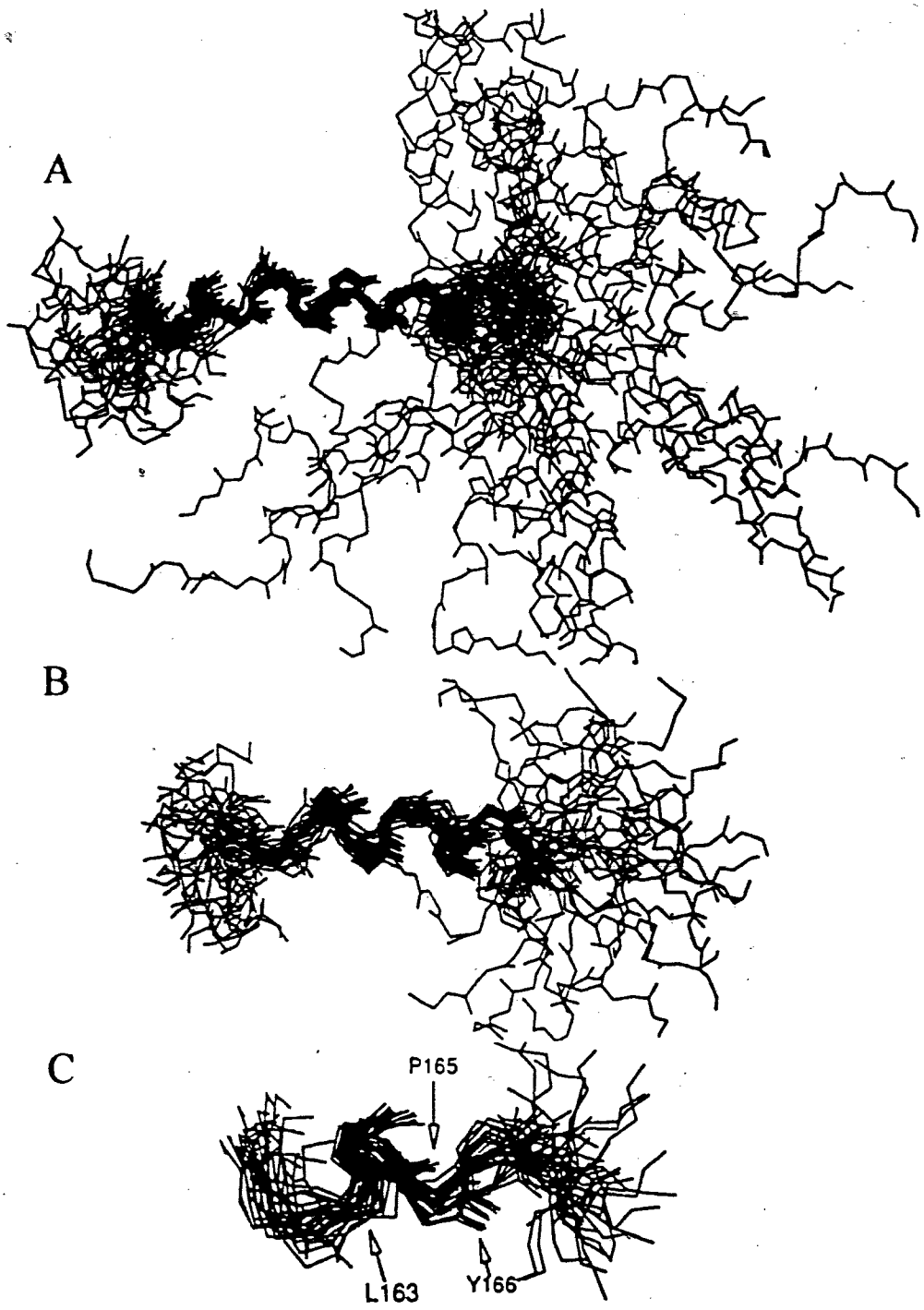

Fig. 6.23: Backbone view of an ensemble of 29 structures of apoA-I(142-187) in SDS at pH 4.9 and 50 °C (A) with the N-terminal helix, residues 146-164 superimposed; (B) The C-terminal helix, residues 169-183 with residues 170-181 superimposed; and (C) The interhelical structures, residues 161-169 with residues 163-168 superimposed (From Wang *et al.*, 1997b).

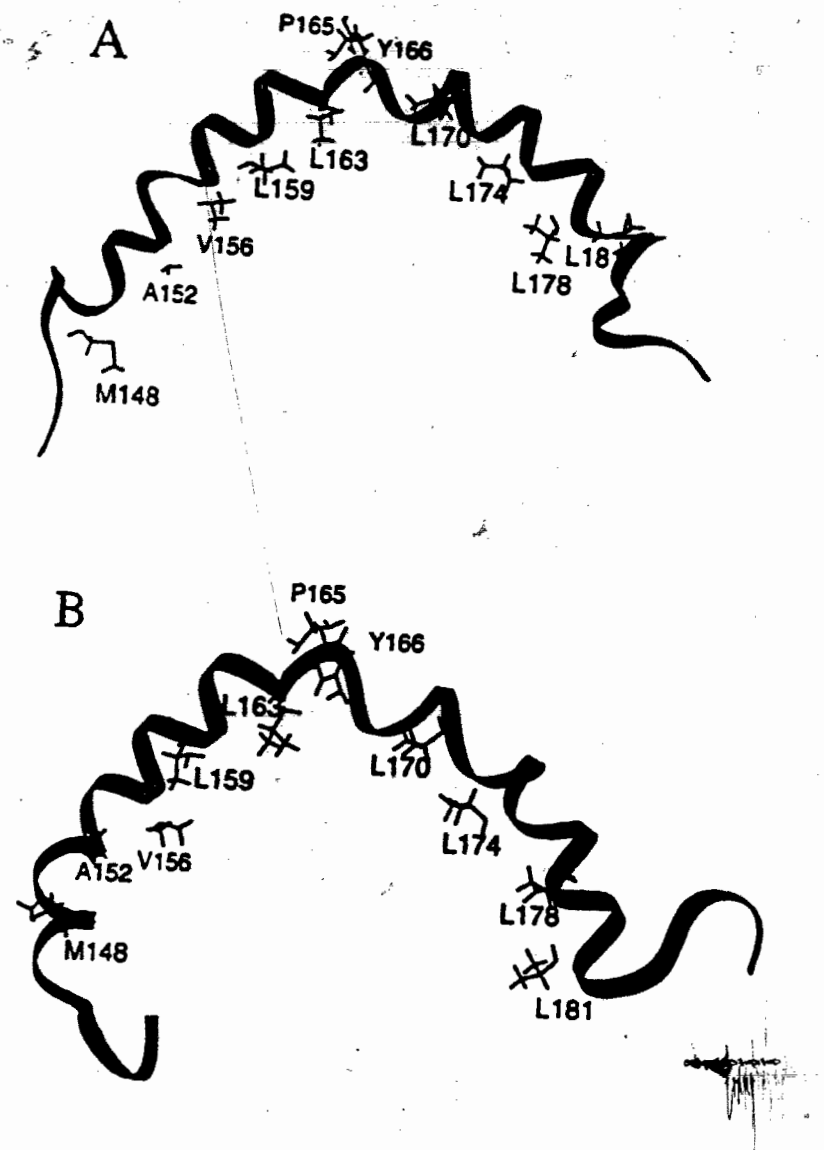

Fig. 6.24:. Ribbon representations of the structure most resembling the average of apoA-I(142-187) in DPC (A) and SDS (B). For clarity, only hydrophobic side-chains are shown.(From Wang *et al.*, 1997b).

Presented in Fig. 6.23 are similar structural regions of apoA-I(142-187) determined in SDS micelles based on 397 NOE distance restraints (195 inter- and 202 intra-residues). The Brookhaven PDB identification number for the 46mer in SDS is 1GW4. The RMSDs for superimposing the backbone atoms of the helical regions 146-162 (A) and 168-182 (B) are 2.43 ± 0.23 and 2.02 ± 0.21 Å, respectively. Superimposing the interhelical region, residues 163-168, gave a RMSD of 1.84 ± 0.20 Å (Fig. 6.23C). Therefore, the N-terminal helix in SDS is not as well defined as in DPC. This may relate

to the temperature at which the NOESY spectra were collected. More NOEs were obtained in DPC at 37 °C (450 NOEs) than in SDS at 50 °C (397 NOEs).

Fig. 6.24 shows the average structures of apoA-I(142-187) determined in DPC (A) and in SDS (B) micelles, respectively. Both are curved structures with the hydrophobic side chains on the concave face. It can also be seen that the aromatic ring of Y166 stacks with the ring of P165 with its hydroxyl group pointing toward the hydrophilic face. This local hydrophobic packing may explain why one of the H^{β} of P165 shifted upfield by approx. 1 ppm. Further investigation of the average structures showed that the dihedral angles (Φ and Ψ) for the residues 146-162 and 168-182 in general fall within the helical region (Fig. 6.25). However, the dihedral angles for residues from L163 to Y166 have the structural pattern of $\beta\alpha\gamma\beta$ in DPC, which has been classified as a half-turn (Efimov, 1993). A half-turn differs from a β-turn in that the former changes the helix direction by 90° while the latter changes it by 180°. In SDS, the same region was found to have $\beta\alpha\alpha\alpha$ structural pattern based on dihedral angles, which may be referred to as a helical bend.

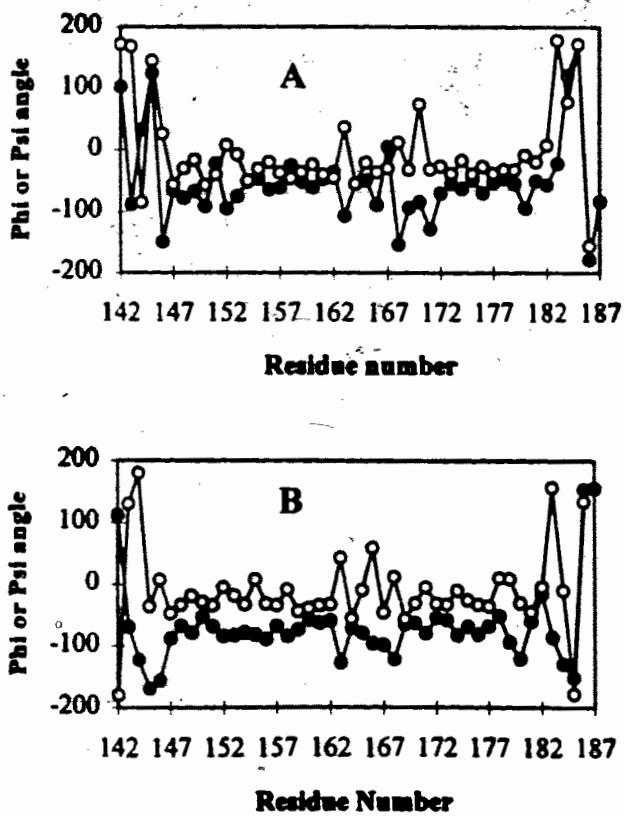

Fig. 6.25: Plots of the dihedral angles of the average structure of apoA-I(142-187) in SDS (A) and DPC (B). The solid and open circles correspond to phi and psi respectively.

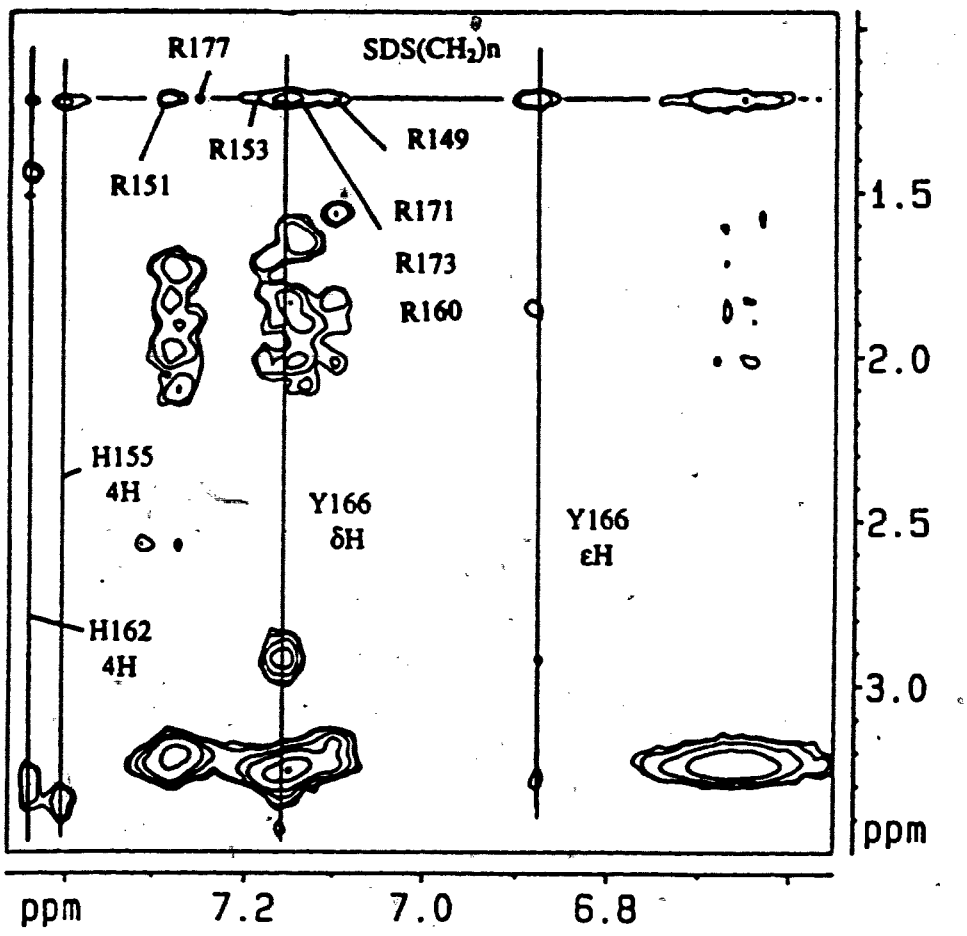

Fig. 6.26: Intermolecular NOEs between apoA-I(142-187) and SDS. The peptide/SDS-d_{25}/SDS ratio is 1:5:5 at pH 4.9, 37 °C. The SDS (CH2)n frequency is labled horizontally whereas the peptide signals such as H155, H166, and Y166 are labled vertically. At the cross are intermolecular NOEs. Intermolecular NOE peaks between SDS and arginine εH^N signals are labled directly along the SDS $(CH_2)n$ frequency.

6.2.4.4 Intermolecular NOEs between apoA-I(142-187) and SDS

In Sections 6.2.3.6 and 6.2.3.7, we showed that Y166 in apoA-I(166-185) interacts with lysoPC acyl chains and SDS alkyl chains, respectively. In Section 6.2.2, the fluorescence spectra of Y166 in apoA-I(142-187) suggest that Y166 moves to a

hydrophobic environment. To substantiate the lipid binding of the interhelical region of apoA-I(142-187) and to elucidate further structural information, intermolecular nuclear Overhauser effect observations were performed by adding protonated SDS to the apoA-I(142-187)/SDS-d_{25} sample. Fig. 6.26 shows a portion of the NOESY spectrum of the sample at pH 4.9 and 37 °C. Intermolecular NOEs from the side chains of arginines, M148, H155, H162, Y166, and K182 to SDS alkyl chains were identified. The identification and assignment of these intermolecular NOE peaks were possible since side chains of those residues have well-resolved proton resonances from other peptide signals. These NOE cross peaks were observed at a mixing time of 40 ms and were clearer at 80-120 ms. The NOEs of M148 and Y166 with SDS indicate hydrophobic interactions. In addition, the NOEs between Y166 and SDS confirmed the lipid binding of the interhelical region (Fig. 6.3). The NOEs between SDS and His, Arg, and Lys indicate that these amino acid residues are located in the interface of the apoA-I(142-187)/SDS complexes.

6.2.5 NMR study of apoA-I(122-187)

6.2.5.1 Signal assignment

As with apoA-I(142-187) (46mer), very few cross peaks from the amide protons to side chains appeared in the TOCSY spectrum of the 66mer. The fingerprint region of the NOESY of the 66mer is shown in Fig. 6.27. By comparison with the assignment achieved for the 46mer (Fig. 6.18), the signals for residues 146-182 were assigned as they appeared at the identical spectral regions. These assignments were subsequently confirmed by the identical NOE patterns. The assignment of residues 122-144 commenced with H135, which is readily recognized due to resonating to lower field of the water signal. From H135, residues Q132, E136, L137, and Q138 were assigned based on NOE connectivities. L144 and S142 were assigned since both amide protons showed cross peaks with the H^{δ} of P143 just as the NOE pattern formed by A164, P165, and Y166 (Section 6.2.4.2). Such a similarity indicates that P143 is also in a *trans*

conformation like P165. Some residues such as A124 and A130 were assigned by comparison with apoA-I(114-142) (Section 6.2.6) or by the process of elimination (POE). In this manner, approx. 90% H^{α} and 80% amide proton signals were assigned (Table 6.8).

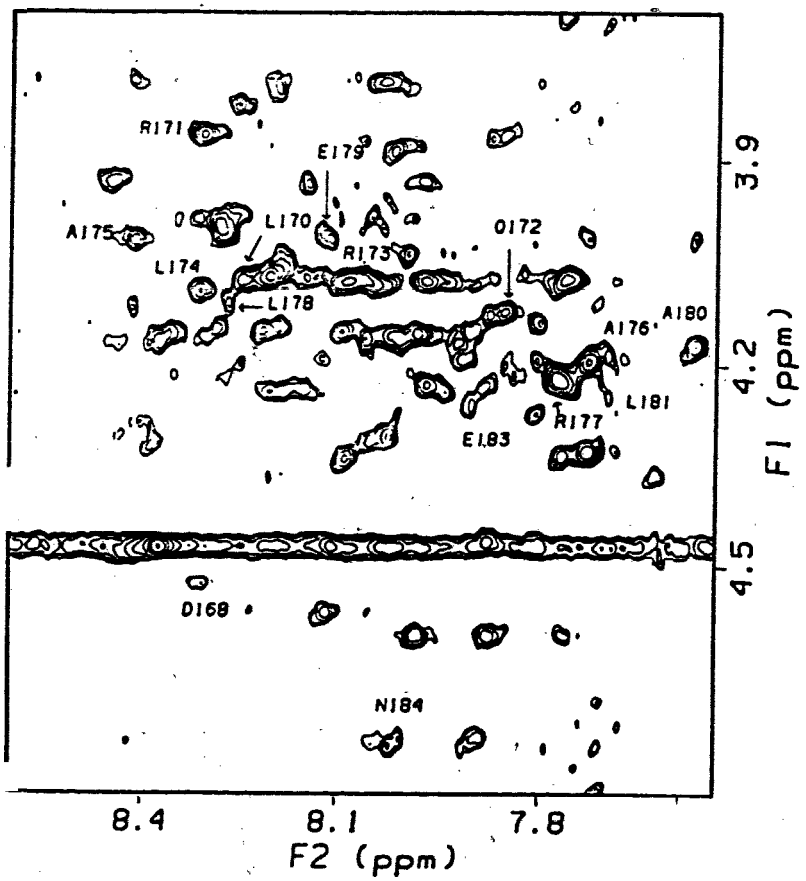

Fig. 6.27: Fingerprint region of the NOESY spectrum of apoA-I(122-187) in SDS-d_{25}-containing aqueous solution (H_2O/D_2O, 9:1, v/v), peptide/SDS ratio 1:60, pH 4.9 and 50 °C. For clarity and comparison with Figs. 6.18 & 6.20, only residues 168-184 are labeled.

Table 6.8: Proton Chemical Shifts (ppm) of ApoA-I(122-187) bound to SDS-d_{25} at the Peptide/SDS Ratio of 1:60, pH 4.9 and 50 °C[a]

Residue	H^N	H^{α}	CSI	H^{β}	H^{γ}	Others
Leu122		4.32	0			
Arg123	NA	4.30	0			
Ala124	8.37	4.27	0	1.38		
Glu125	8.29	4.31	0			

Leu126	NA	3.86	-1			
Gln127	NA	4.05	-1			
Glu128	NA	NA				
Gly129	NA	NA				
Ala130	NA	4.07	-1	1.49		
Arg131	NA	3.85	-1			
Gln132	7.99	4.14	-1			
Lys133	NA	4.18	-1			
Leu134	NA	4.08	-1			
His135	8.12	4.55	-1	3.44		
Glu136	8.07	4.12	-1			
Leu137	NA	4.14	-1			
Gln138	8.26	3.80	-1	2.14	2.46, 2.34	
Glu139	7.76	4.05	-1			
Lys140	NA	4.06	-1			
Leu141	NA	4.40	0	1.61		
Ser142	7.88	4.43	0	4.06, 4.12		
Pro143	-	4.49	0	2.39, 2.06	1.97, 1.84	H^{δ} 3.84, 3.59
Leu144	7.63	4.34	0	1.87, 1.73		H^{δ} 0.99, 0.91
Gly145	7.20	3.77	-1			
Glu146	NA	NA				
Glu147	8.17	4.22	0			
Met148	8.21	4.22	-1			
Arg149	8.15	3.91	-1			
Asp150	8.09	4.46	-1	2.88, 2.79		
Arg151	8.13	4.18	-1			
Ala152	8.37	4.13	-1	1.50		
Arg153	8.29	3.97	-1	2.00		
Ala154	7.76	4.22	-1	1.41		
His155	7.90	4.73	0	3.34, 3.25		2H -; 4H 7.46
Val156	8.04	3.76	-1	2.28	1.10, 1.04	
Asp157	8.42	4.47	-1	2.82, 2.78		
Ala158	7.81	4.25	-1	1.59		
Leu159	8.01	4.15	-1			H^{δ} 0.90
Arg160	8.45	3.91	-1			H^{δ} 3.24
Thr161	7.97	4.06	-1	4.22	1.21	

His162	7.88	4.58	-1	3.37, 3.30		
Leu163	7.99	4.58	+1	1.88, 1.69	-	H^{δ} 0.91
Ala164	7.77	4.32	0	1.56		
Pro165	-	4.35	0	2.16, 1.12	1.85	H^{δ} 3.67, 3.43
Tyr166	7.67	4.69	+1	3.30, 2.89		2,6H 7.16; 3,5H 6.89
Ser167	8.00	NA		4.01, 3.78		
Asp168	8.31	4.51	-1	2.72		
Glu169	8.13	4.18	-1			
Leu170	8.26	4.06	-1			
Arg171	8.31	3.84	-1	2.01		
Gln172	7.86	4.10	-1	2.19	2.56, 2.45	
Arg173	8.10	4.13	-1			
Leu174	8.31	4.07	-1	1.84	1.61	H^{δ} 0.90
Ala175	8.42	3.99	-1	1.49		
Ala176	7.73	4.17	-1	1.55		
Arg177	7.77	4.20	-1			
Leu178	8.27	4.10	-1		1.68	H^{δ} 0.91
Glu179	8.13	3.99	-1	2.18, 2.12		
Ala180	7.56	4.16	-1	1.54		
Leu181	7.72	4.18	-1	1.88, 1.83	1.69	H^{δ} 0.92
Lys182	7.80	4.12	-1			
Glu183	7.91	4.25	0			
Asn184	8.01	4.74	0	2.92, 2.85		
Gly185	8.04	3.93	0			
Gly186	8.12	3.97	0			
Ala187	-	4.20	-1	1.34		

a. Chemical shifts are referenced to internal standard DSS (0.00). NA = not assigned or not available.

6.2.5.2 Secondary structure of apoA-I(122-187)

Fig. 6.28 shows the CSI plot of apoA-I(122-187). As a comparison, the CSI for residues in apoA-I(166-185) (A) and (142-187) (B) are also included. Fig. 6.28C suggests that apoA-I(122-187) contains three helical regions, 126-140, 145-162, and 168-183. These helical segments are supported by the NOE pattern although sparse in the

region of 122-140 as a result of spectral overlap (Fig. 6.28D). The H^{α} chemical shifts for residues 166-185 in apoA-I(166-185), apoA-I(142-187), and apoA-I(122-187) in SDS at 50 °C are plotted in Fig. 6.29. It is evident that helix (168-182) found in the 20mer (Section 6.2.3.3) is maintained in the 46mer (Section 6.2.4.2) and 66mer. It can also be seen that the chemical shift similarity, especially for amide protons, between the 46mer and the 66mer is more striking than between the 20mer and either of the longer peptides (Fig. 6.29A). We may attribute this effect to end fraying (Shoemaker *et al.*, 1987; Rozek *et al.*, 1995), which is more pronounced in shorter peptides than in longer ones.

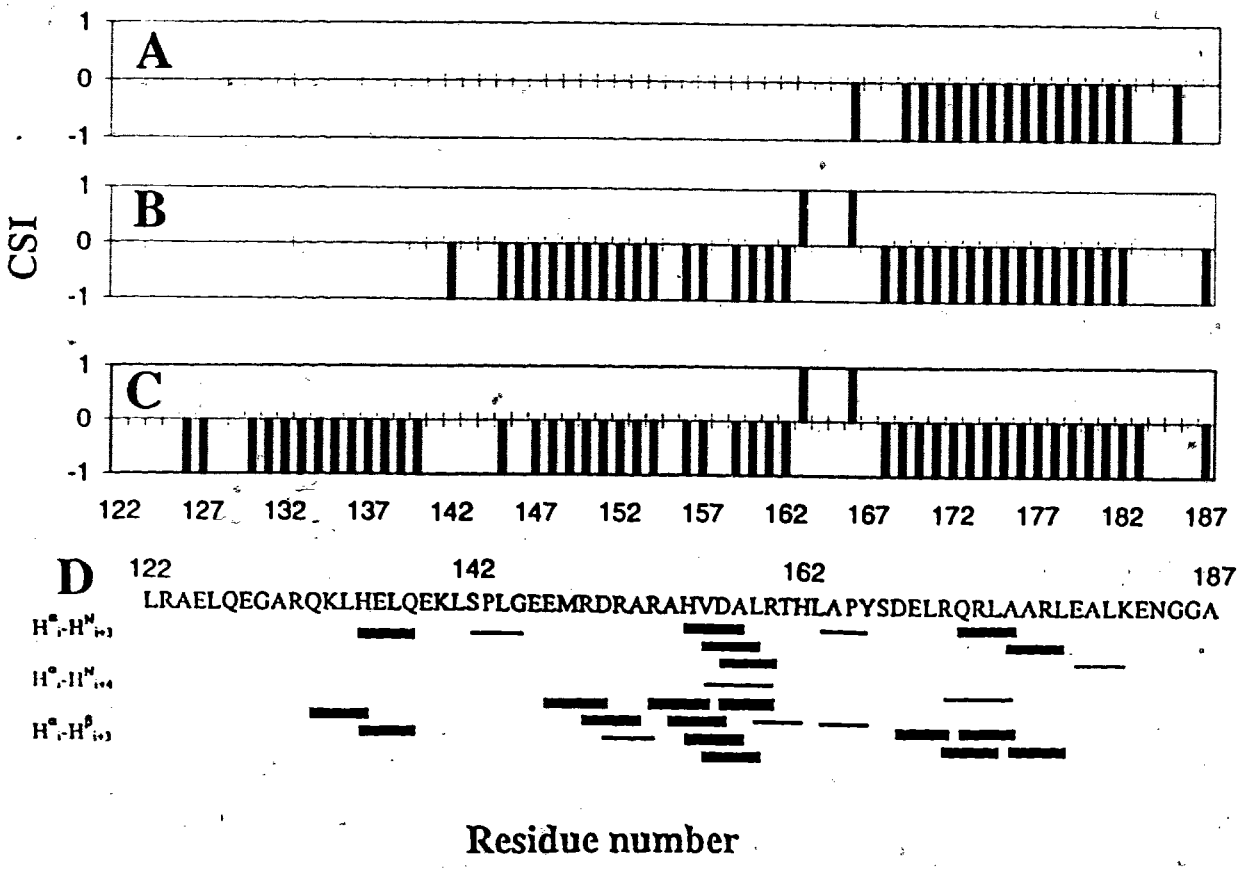

Fig. 6.28: H^{α} Chemical shift index plots of apoA-I(166-185) (A), apoA-I(142-187) (B) and apoA-I(122-187) (C) in SDS at pH 4.9 and 50 °C. CSIs were obtained relative to the random chemical shifts collected by Wishart *et al.* (1995). (D) The NOE connectivities of apoA-I(122-187) in SDS.

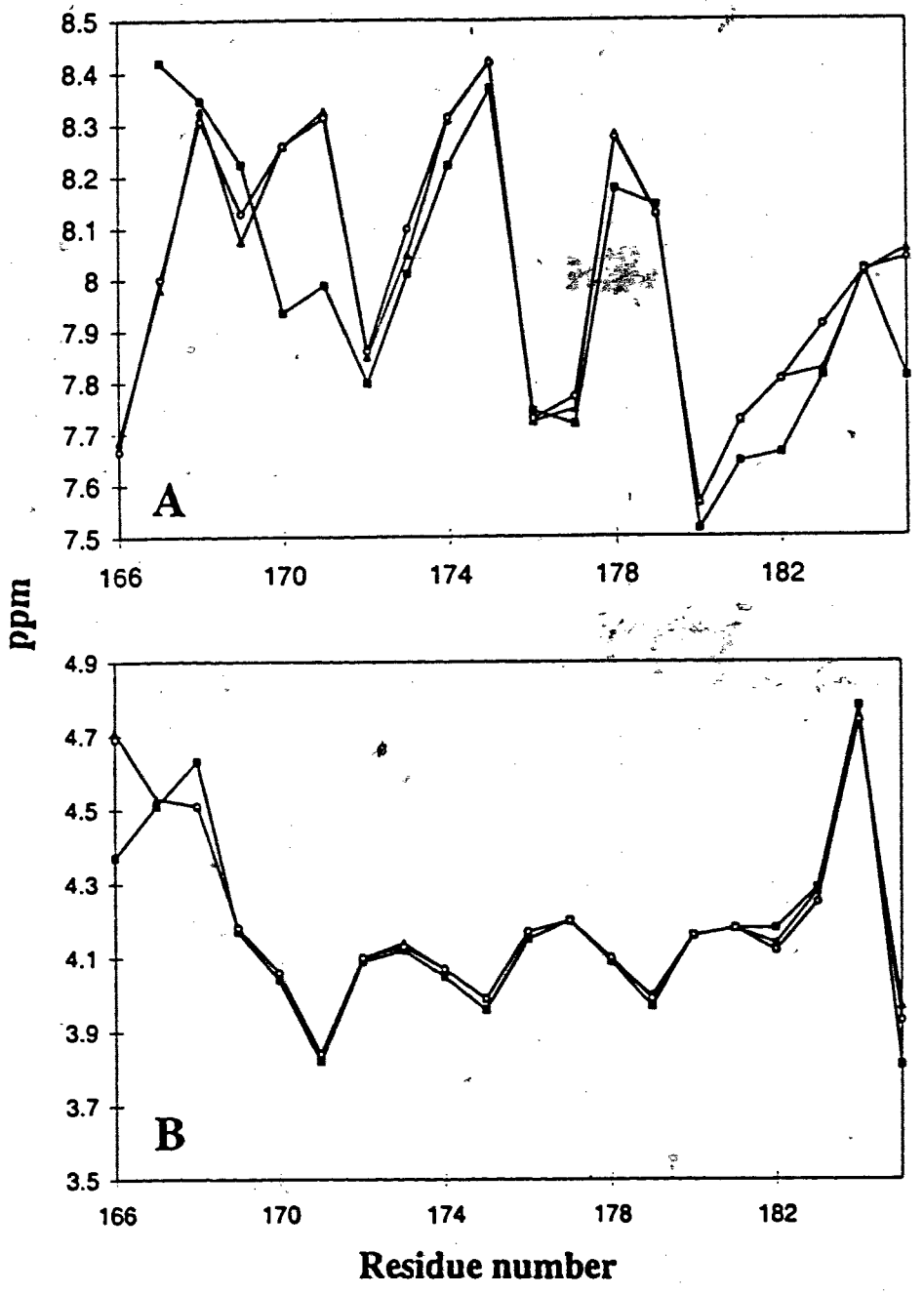

Fig. 6.29: Chemical shifts of amide (A) and α-protons (B) of residues 168-183 in apoA-I(166-185) (black squares), **apoA-I(142-187)** (solid triangles), **and apoA-I(122-187)** (open circles) **bound to SDS** at pH 4.9, 50 °C.

6.2.6 Structure of apoA-I(114-142) in SDS

6.2.6.1 Circular dichroism

In order to further confirm the helical structure for residues 124-140 in apoA-I(122-187), Dr. Sparrow also synthesized apoA-I(114-142) on our request based on our finding of the peptide-aided signal assignments (Figs. 6.28 & 6.29). The segment 124-140 was extended by eight residues to L114 to include a tyrosine for quantification of the peptide. ApoA-I(114-142) is predominantly random in water as evidenced by the strong negative CD band at ~200 nm (Fig. 6.20). The addition of SDS caused dramatic change in the CD spectrum. At the peptide/SDS ratio of 1:60, the helix content of the peptide was found to be 53% according to the 222 nm band (Eq. 3.3). However, the peptide appears to have lower affinity for DPC. It bound to DPC above the CMC and was not saturated until the peptide/DPC ratio of ~1:120. At the peptide/DPC ratio, the helix content is merely 41%, 10% lower than that in SDS.

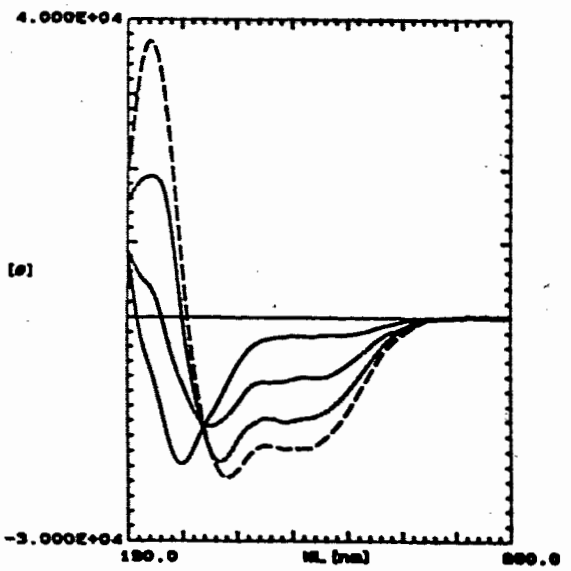

Fig. 6.30: CD spectra of apoA-I(114-142) (0.08 mM) in the absence and presence of SDS at pH 6 ± 1, 37 °C. The SDS/peptide ratio is 0:1 (solid), 5:1 (dash-dotted), 10:1 (dotted), and 60:1 (dashed).

6.2.6.2 NMR of apoA-I(114-142)

Based on the CD data, NMR studies of apoA-I(114-142) were performed in the presence of perdeuterated SDS. The signal assignment was achieved like apoE peptides (Chapter 4) and the chemical shifts are listed in Table 6.9. The amide signals for Y115 and R116 were not found probably due to fast exchange with water (Wüthrich, 1986). Based on the chemical shifts of H^{α}, the chemical shift indexes (CSI) (Wishart *et al.*, 1992; 1995) were assigned to all residues (Table 6.9). Except for G129, residues 122-140 have "-1" CSIs, thus supporting the helical structure of residues 124-140 observed in the 66mer (Fig. 6.28). Residues 115-119 have alternative CSIs of 0 and -1 but all shift upfield relative to the random shifts (Wishart *et al.*, 1995), suggesting a less helical structure (Rizo *et al.*, 1993; Chupin *et al.*, 1995). The residues in the middle of the sequence showed very weak or no TOCSY cross peaks from the amide proton to side chains whereas the residues at both ends, 117-119 and 139-142, have clear cross peak relays (Fig. 6.31), suggesting that only the middle region of the peptide is associated with the micelle. In addition, S142 gave two sets of peaks (Table 6.9). The helical region is supported by the strong H^{N}_{i}-H^{N}_{i+1} cross peaks in the NOESY spectrum (Fig. 6.32) (Wüthrich, 1986). The cross peaks between the amide proton of E120 and the δ-protons of P121 indicate that P121 is predominantly in a *trans* conformation (Wüthrich *et al.*, 1984). Similar proline conformations were observed previously for P143 and P165 in apoA-I(122-187) (Section 6.2.5), and P267 in apoE(263-286) (Chapter 4). Although this peptide contains only 29 residues heavy degeneracy occurred in the NOESY spectrum. For example, L134 & L137, A130 & K133 have almost the same H^{α} chemical shifts. As a consequence, NOEs of the (i, i+3) type are not available between these residues. The distance geometry calculation was thus not performed to prevent misleading structures. The difficulty met in the 29mer illustrates that residues 122-142 in the 66mer is a difficult sequence for homonuclear NMR studies.

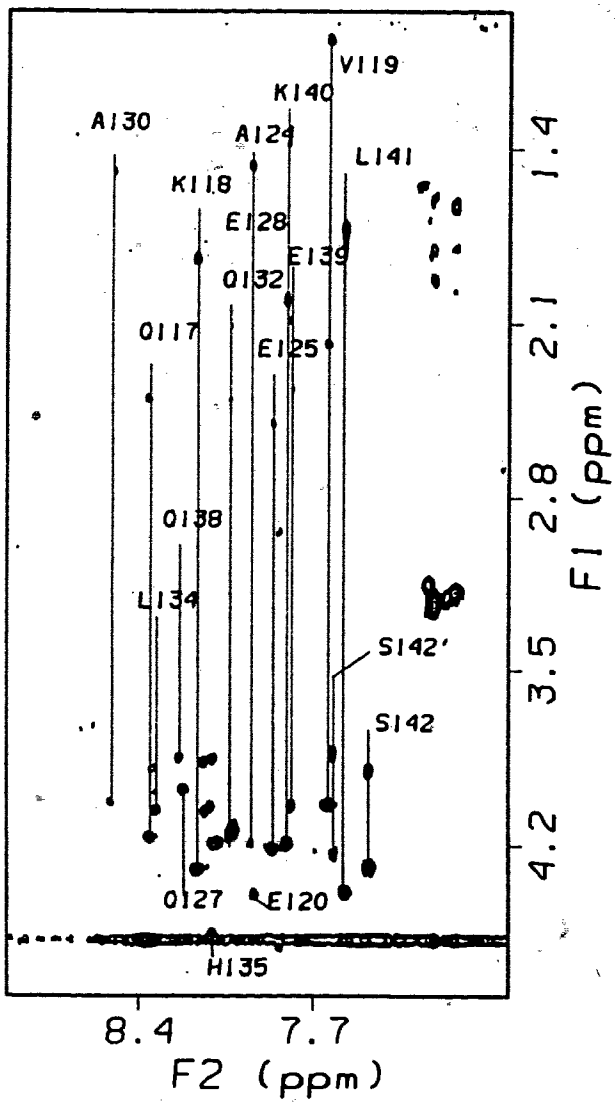

Fig. 6.31: Fingerprint region of the TOCSY spectrum of apoA-I(114-142) in SDS, peptide/SDS ratio 1:60, pH 4.9, 37 °C. Several peaks (R123, L126, R131, K133, E136, and L137) in the middle of the amide region are not labeled for clarity yet lack of TOCSY relay peaks is evident.

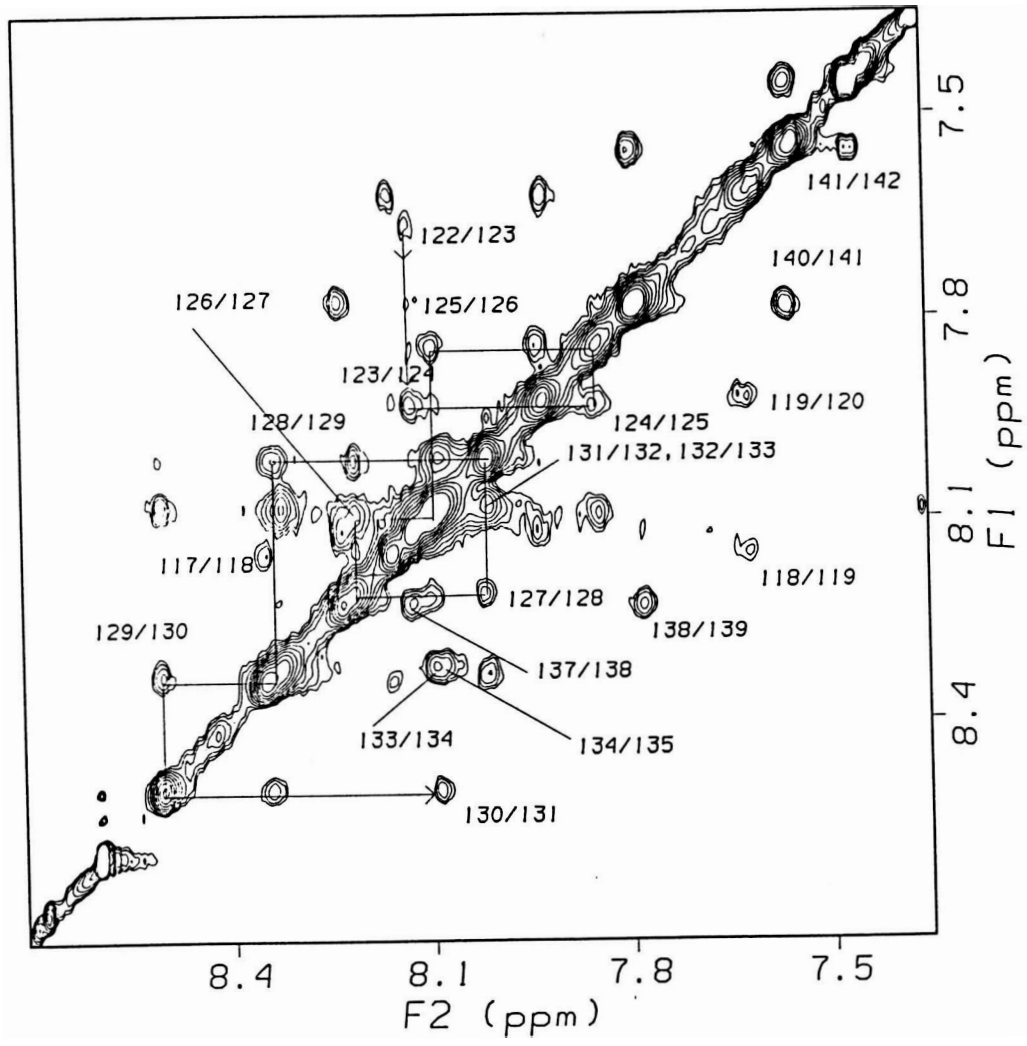

Fig. 6.32: Amide proton region of the NOESY spectrum (τ_m = 200 ms) of apoA-I(114-142) in SDS micelles. For clarity, only part of the H^N_i-H^N_{i+1} NOE connectivities from residues 122-131 are shown.

Table 6.9: Proton Chemical Shifts (ppm) of ApoA-I(114-142) in SDS-d_{25} at the Peptide/SDS Ratio of 1:60 at pH 4.9 and 37 °C[a]

Residue	H^N	H^α	CSI	H^β	H^γ	Others
Leu114	--	-	-		-	
Tyr115	-	4.34	-1	3.18, 3.10		2,6H 7.16; 3,5H 6.84
Arg116	-	4.33	0	1.97	1.63	H^δ 3.2?; εH^N 7.10
Gln117	8.35	4.16	-1	2.01	2.40	δH^N 7.44, 6.76
Lys118	8.16	4.30	0	1.84	1.52, 1.43	H^δ 1.71; H^ε 3.03
Val119	7.62	4.03	-1	2.18	0.96	
Glu120	7.92	4.39	0	2.08, 2.17	2.36	
Pro121	-	4.39	0	2.35, 1.87	2.00, 2.07	H^δ 3.72, 3.65
Leu122	7.67	4.22	-1	1.83	1.67	H^δ ??
Arg123	8.13	3.85	-1	1.98	1.67	H^δ 3.16; εH^N 7.22
Ala124	7.93	4.19	-1	1.46		
Glu125	7.85	4.21	-1	2.19, 2.23	2.51	
Leu126	8.10	4.21	-1	1.85, 1.71	1.71	H^δ 0.90
Gln127	8.22	3.97	-1	2.20	2.34, 2.52	δH^N 7.28, 6.71
Glu128	8.01	4.17	-1	2.12	2.42	
Gly129	8.34	3.98 3.89	0			
Ala130	8.51	4.02	-1	1.49		
Arg131	8.09	3.85	-1	1.91, 1.82	1.62	H^δ 3.23; εH^N 7.49
Gln132	8.01	4.12	-1	2.21	2.49	δH^N 7.55, 6.78
Lys133	8.11	4.06	-1	2.10	-	
Leu134	8.32	4.08	-1	1.87, 1.82	-?	H^δ 0.92
His135	8.10	4.55	-1	3.42		2H 8.6; 4H 7.25
Glu136	8.09	4.20	-1	2.01	2.42	
Leu137	8.10	4.07	-1	1.77	1.68	-
Gln138	8.23	3.88	-1	2.23	2.48, 2.32	δH^N 7.12, 6.67
Glu139	7.78	4.05	-1	2.27, 2.37	2.62	
Lys140	7.79	4.18	-1	2.00	1.59, 1.54	H^δ -
Leu141	7.55	4.39	0	1.79, 1.73	1.73?	H^δ 0.88
Ser142	7.45	4.29	-1	3.90		
Ser142'	7.62	4.24	-1	3.84		

[a]Chemical shifts are relative to internal DSS (0.00).

6.3 Discussion

6.3.1 Comparison of conformations of apoA-I peptides in SDS and DPC micelles

We have determined the structures of apoA-I(166-185) and apoA-I(142-187) in both SDS and DPC. The conformation of the N-terminus of apoA-I(166-185) is pH dependent. It becomes more helical at pH 6-7 (Figs. 6.7 & 6.9), where the acidic side chains are ionized according to pKa measurements (Fig. 6.5). The acidic side chains of D168 and E169, when ionized, tend to stay away from each other due to potential electrostatic repulsion. Alternatively, this pH effect may be interpreted by the so-called charge-helix dipole interaction (for a review, see Chakrabartty & Baldwin, 1995). Such an interaction refers to an electrostatic interaction between a charged group and the partial charges on the peptide backbone on NH and CO groups. The α-helix has a positive dipole at the N-end of the peptide and a negative dipole at the C-end. A typical example in the literature is the model peptide $(Glu)_{20}(Ala)_{20}$, which adopts a helical conformation more stable than that of $(Ala)_{20}(Glu)_{20}$ (Ihara *et al.*, 1982).

In the early amphipathic helix model, ion pairs were proposed between basic and acidic side chains (Segrest *et al.*, 1974). The N···O distance is within 3.5 Å when ion-paired (Baker & Hubbard, 1984). ApoA-I(166-185) has three potential ion pairs, D168-R171, E169-R173 and E179-K182. Distances measured between these pairs in the average structure in SDS or DPC are all greater than 6.5 Å in either SDS or DPC at pH 6-7. Thus, intrahelix ion pairs may not stabilize the amphipathic helical structures of apoA-I(166-185) bound to micelles.

The average amphipathic helix domains of apoA-I(166-185) determined in SDS and DPC micelles could be superimposed as shown in Fig. 6.12A. Similar results were obtained for LAP-20 (Buchko *et al.*, 1996b). In addition, apoA-I(142-187) was found to have similar curved helix-hinge-helix structures in both micelles (Fig. 6.24). These structures determined by different researchers for different peptides of different lengths strongly support that the hydrophobic effect dominates in the stabilization of the peptide/lipid complexes (Buchko *et al.*, 1996a,b; Wang *et al.*, 1996a,b; 1997b). In

addition, we demonstrated that SDS or DPC is a good mimic of lysoPC. It thus reinforces the notion that both SDS and DPC are useful as model lipids to study surface-active peptides (Inagaki *et al.*, 1989; Chupin *et al.*, 1995; Rozek *et al.*, 1995; Buchko *et al.*, 1996b; Dunne *et al.*, 1996; Seibal *et al.*, 1996a,b).

Local structural differences by D168 and E169 were observed at the N-terminus of apoA-I(166-185) in SDS and DPC micelles. Such a structural difference (Fig. 6.12A) could be true since differences in pKa values were also observed for D168 and E169 (Table 6.5). Moreover, the average structure in the interhelical region of apoA-I(142-187), residues 163-167, in the two micelles also showed difference, a helical bend in SDS and a half-turn in DPC. Hence, there might be electrostatic repulsion between anionic SDS head groups and the acidic residue pair, D168 and E169. Such potential electrostatic interactions may cause a preference of D168 and E169 for zwitterionic lipid DPC, thus leading to lipid selectivity. This speculation may explain the fact that peptide/SDS/DPC (1:40:40) complexes are more stable toward heat than either peptide/SDS (1:80) or peptide/DPC (1:80) complexes. The potential repulsions between SDS head groups and the acidic side chains in the interface of the amphipathic helix of apoE(263-286) may explain the fact that the peptide/SDS complexes are less stable toward heat than the peptide/DPC complexes. Indeed, there have been reports that protonation of interfacial acidic residues of a membrane-bound protein enhances lipid binding (Arnold & Cornell, 1996; Hanakam *et al.*, 1996).

6.3.2 Cationic side chains initiate and enhance anionic SDS binding

Sequence analysis revealed that the region 122-187 of apoA-I is rich in arginines, but contains few aromatic residues and no hydrophobic pairs (Refer to Chapter 4). Peptides ranging from 20 to 66 residues in the region 122-187 associated with anionic SDS below the CMC while they bind zwitterionic DPC near or above the CMC (Figs. 6.2 & 6.3), suggesting electrostatic interactions between anionic lipid head groups and cationic peptide side chains may initiate binding. Frank *et al.* (1997) also showed that deletion of either 122-165 or 144-186 from apoA-I decreases the initial association rate of

the protein mutants with lipid. These observations differ from the proposal that residues 44-65 and 220-241 in apoA-I initiate lipid binding (Palnugachari *et al.*, 1996).

In the solution structures of apoA-I(166-185), we found that cationic side chains cluster in the interface of the amphipathic helix (Fig. 6.13). The intermolecular NOEs between the cationic side chains of the peptide and SDS alkyl chains indicate that cationic side chains enhance SDS binding. The intermolecular NOEs between SDS C-1, C-2, C-3 and $(CH_2)_n$ protons and the aromatic ring protons of Y166 confirm the solution structure at pH 3.7, where Y166 bends toward the hydrophobic face to participate in lipid binding. The pKa difference observed in SDS and DPC supports salt bridge formation between Y166 and SDS (Fig. 6.5C) (Jardetzky & Roberts, 1981; Sem & Kasper, 1993; Pallaghy *et al.*, 1995). Since intermolecular NOEs between SDS C-1 protons and arginine εH^N protons were observed, we may extend the notion to other cationic side chains. Salt bridge formation between cationic side chains and SDS is further supported by several lines of evidence. First, these apoA-I peptides precipitated only at acidic pH during SDS titration but not during DPC titration. Second, apoA-I(142-187) complexed with SDS has a higher thermal stability than its complexes with DPC (Fig. 6.2D). Similar phenomenon was observed for apoA-I (Surewicz *et al.*, 1986) or synthetic peptide analogs (Mishra *et al.*, 1994) bound to lipids with different head groups. Third, the εH^N resonances of the arginine side chains in SDS showed upfield shifts by ~0.45 ppm relative to those in DPC (Tables 6.1, 6.3, 6.6, & 6.7). Fourth, SDS binds to apoA-I(166-185), apoA-I(142-187) or apoA-I(122-187) well below the CMC whereas DPC showed detectable binding only around the CMC (Fig. 6.2). Fifth, selective signal broadening was observed for apoA-I(166-185) upon addition of SDS (Fig. 6.14). The selective promotion of helix formation by anionic lipids has been observed for other membrane peptides (Backlund *et al.*, 1994; Johnson and Cornell, 1994). In some instances even anions of salts were found to be able to stabilize helix conformation of certain peptides probably due to charge neutralization (Rizo *et al.*, 1993; Agou *et al.*, 1995). Taken together, we propose that salt bridges as well as the hydrophobic interactions between cationic/hydrophobic side chains of apoA-I peptides and anionic lipid are the major interfacial stabilizing forces in the complex.

6.3.3 The curved helix-hinge-helix structure, lipid binding and a model for apoA-I(142-187)/lipid complexes

ApoA-I(142-187) associates with SDS and DPC as shown by CD and fluorescence spectroscopy. It appears that a micelle is required for apoA-I(166-185), apoA-I(142-187) or apoA-I(122-187) to bind DPC (Figs. 6.2 & 6.3). Other researchers have shown that the complexes of peptides or protein (< 20 kD) with SDS or DPC are only slightly larger than the micelle itself (Lauterwein *et al.*, 1979; Samsó *et al.*, 1995; Kallick *et al.*, 1995).

The NMR H^{α} secondary shifts of apoA-I(142-187) in both micelles suggest two helical regions: residues 146-162 and 168-182. These residues in helical regions correspond to 74% helix, which is similar to the values estimated by CCA (62% in SDS and 69% in DPC). The conformation of apoA-I(142-187), elucidated by distance geometry calculations, is a helix-hinge-helix structural motif ranging from the extended to the curved. In other words, the angle between the two helices is not fully determined. Hence, we use the term hinge as a general description of the interhelical structures in SDS and DPC. The reason for poorly defined interhelical structure may be attributed to fewer and weaker NOEs in the region (Fig. 6.21) and lack of long range NOEs as normally observed in globular proteins. In the average curved conformation, the hydrophobic residues of both amphipathic helices and the hinge are located on the concave face (Fig. 6.24), suggesting lipid-binding sites. Intermolecular NOE cross peaks between SDS alkyl chains and the arginines, histidines, M148, Y166, and K182 of the peptide confirmed that cationic side chains on both sides of the amphipathic helices are located in the interface of the peptide/SDS complexes. The involvement of Y166 in lipid binding is consistent with fluorescence spectroscopy (Fig. 6.2). Thus, these intermolecular NOEs substantiate that both amphipathic helices as well as the hinge structure all interact with the hydrophobic core of the micelle (Figs. 6.2 & 6.3). Taken together, we propose a model for the peptide/lipid complexes, wherein the amphipathic helix-hinge-helix straddles the micelle.

In the proposed structures for the tandem helical repeats found in apoA-I, the motifs are, almost without exception, anti-parallel linked by β-turn (Jonas *et al.*, 1989; Brasseur *et al.*, 1990). Sparks *et al.* (1992) showed that apoA-I conformation varies with the shape of the HDL particle. However, the parallel arrangement of helices is believed to be maintained from discoidal to spherical particles (Brasseur *et al.*, 1990; Talussot & Ponsin, 1994; Lins *et al.*, 1995). Since micelles with a diameter of ~50-60 Å are comparable in size to the smallest HDL_3, they may be regarded as a good mimic of the spherical HDL. In either SDS or DPC micelle models, no interhelix NOE was found in the spectrum of apoA-I(142-187), indicating that helix 146-162 and helix 168-182 may not be closely packed. The adjacent helix-helix interactions, which have been proposed to be additional stabilizing force in apoA-I (Brasseur *et al.*, 1990; Lins *et al.*, 1995), do not occur in apoA-I(142-187) bound to micelles. This is consistent with the fact that both helices in the peptide are typical class A1 amphipathic helices (Figs. 1.2 & 6.13) (Segrest *et al.*, 1994). These helices, if tightly packed, would place cationic side chains in the interhelical region, suggesting electrostatic repulsions rather than salt-bridge formation. In fact, these interfacial cationic side chains all interact with lipid. Our straddle model thus provides an alternative helix packing mode for helical repeats 5 & 6 of apoA-I in lipid.

6.3.4 Biological implications

We found that prolines P121, P143, and P165 are all in the *trans* conformation and located in the hinge regions. P209 and P220 also adopt *trans* conformations (Wang, Sparrow & Cushley, unpublished data). We predict that P66 & P99 in apoA-I have similar conformations (Fig. 1.1). The hinge structure near P165 is, on average, a helical bend or half-turn and also participates in lipid binding (Figs. 6.3 & 6.25). Hence, the major function of the proline may be to introduce a bend to the local sequence so that the hydrophobic faces of the two adjacent helices could be on the same side (Fig. 6.24), thus better conforming to the surface of the spherical HDL particles. Indeed, the P165R mutant of apoA-I is defective in promoting cholesterol efflux (von Eckardstein *et al.*,

1993). Our structural model for apoA-I(142-187) suggests that an arginine substitution would destroy the hydrophobic packing, e.g., between P165 and Y166, in the hinge structure (Fig. 6.24). As a consequence, the helix-hinge-helix motif in apoA-I(142-187) may become a longer helix as proposed by others (Epand *et al.*, 1995). If this is the case, the long helix, being unable to conform to the curved HDL surface as well as the helix-hinge-helix motif, would lead to an increased clearance of apoA-I and explain the lower HDL-cholesterol level in patients (Epand *et al.*, 1995). Similar conformation change in the hinge of the P143R mutant of apoA-I (Utermann *et al.*, 1984) or P143E mutation in hedgehog apoA-I (Sparrow *et al.*, 1995) may explain in part the lower LCAT activating ability of these mutants. We propose that the bend introduced by the proline may facilitate the transmission of the lipid-binding signal from helix i to the adjacent helix j via the hydrophobic residues in the hinge. Such a cooperative mode does not occur in the helix-break-helix motif when the break contains more than four hydrophilic or helix-breaking residues. Further research may be conducted to see whether the number of helix-breaking residues such as glycines between two helices influences biological functions such as LCAT activation.

It has been shown that the activity of LCAT also depends on the reconstituted HDL particle size, where the lipid ratio and number of protein molecules vary (Wald *et al.*, 1990; Jonas, 1992). Recently, Calabresi *et al.* (1997) found that apoA-I_{Milano}, where R173 is replaced by C173, promotes LCAT activity only 40 to 70% of the wild type. They proposed that LCAT activity is triggered by a specific conformation of apoA-I regulated by the environment (lipid, protein, size, pH, etc.). The flexibility offered by the hinge may be essential for apoA-I to adapt to the surface of HDL with various sizes and to achieve the active conformation. We showed that hydrophobic and cationic side chains are responsible for lipid binding. In addition, the cationic side chains do not form ion-pairs with acidic side chains in the same helix (Rozek *et al.*, 1995; Buchko *et al.*, 1996a,b). The binding and formation of helix led to a specific orientation for acidic side chains as noticed by Wang *et al.* (1996b). If the hydrophilic residues are involved in direct interaction with LCAT (Labeur *et al.*, 1997), the flexibility in the hinge may induce

a fit between the convex hydrophilic face of the helix-hinge-helix of apoA-I and LCAT, leading to decrease in flexibility of the hinge of apoA-I yet increase in LCAT activity.

Not all putative helices in human apoA-I are punctuated by prolines. As the C-terminus of apoA-I(142-187) is unstructured in either SDS or DPC micelles (Figs. 6.22B and 6.23B), such flexibility may not be due to purely end effects but may be due to G185 and G186. The flexibility in this region of apoA-I may explain why it is most susceptible to proteolysis (Ji & Jonas, 1995). As these glycines are highly conserved in the homologous sequences of apoA-I from other species, it seems that glycines signal an independent structural domain at the C-terminus of apoA-I, which is essential for rapid and strong lipid binding, but not for LCAT activation (Sparrow and Gotto, 1982; Ji & Jonas, 1995; Schmidt *et al.*, 1995; Holvoet *et al.*, 1996). The C-terminal strong lipid anchor of apoA-I, not directly involved in LCAT activation by itself, may facilitate the relatively weakly bound segment 122-185, an arginine-rich region, to interact somehow with LCAT. Interestingly, the LCAT-activating domain in apoE has been located at the C-terminal region 200-299 (De Pauw *et al.*, 1995), which can be divided into two functional domains: apoE(263-286), a strong lipid-binding segment (Chapter 4), and residues 200-262, an arginine-rich region. The arginine-rich region, having low lipid affinity (Sparrow *et al.*, 1992), may interact with LCAT similar to apoA-I(122-187) (above). Such a similarity in sequence between apoA-I and apoE may make it possible for apoA-I to play the role of apoE in chickens since apoE has not been found there (Lamon-Fava *et al.*, 1992).

CHAPTER 7: FT-IR BAND ASSIGNMENT OF APOLIPOPROTEIN FRAGMENTS IN LIPID-MIMETIC ENVIRONMENTS

7.1 Introduction

In previous chapters, we showed that apoA-I(166-185), apoA-II(18-30)+, and apoE(267-289) adopt class A1, A2, and G* amphipathic helices, respectively, in the presence of SDS. These helical structures are also supported by CD. In this chapter, we report the FT-IR study of these three peptides in the same milieu. The FT-IR work was done in cooperation with Drs. R.A. Shaw and H.H. Mantsch at the National Research Council (Shaw *et al.*, 1997). NMR-aided IR band assignment led to a new assignment for the IR band at ~1635 cm^{-1}.

7.2 Results

7.2.1 IR band assignment

Fig. 7.1 shows the amide I region (1600-1700 cm^{-1}) of the IR spectra of apoA-II(18-31)+, apoE(267-289), and apoA-I(166-185) in SDS. The spectral envelopes for apoA-I and E peptides are much broader than that of apoA-II(18-30)+, indicating that the conformations for the apoA-I and E peptides are more heterogeneous than the apoA-II peptide. The broad amide envelopes were deconvoluted into component bands and the deconvoluted bands were curve-fitted to the original spectra (Shaw *et al.*, 1997). Except the bands at 1673 cm^{-1} from TFA and below 1630 cm^{-1} from peptide side chains (Shaw *et al.*, 1997), two bands were found for apoA-II(18-30)+ at 1649 (80) and 1632 (20) cm^{-1}, respectively. Three bands were found for apoA-I(166-185) and apoE(267-289) each at 1654-1656 (40), 1645 (20), and 1636 (40) cm^{-1}, respectively. The numbers in the brackets following the wavenumbers are intensity of the band. The IR band at 1649-1656 cm^{-1} is usually assigned to helical conformations (Susi, 1972; Byler & Susi, 1986; Surewicz & Mantsch, 1988; Harris & Chapman, 1995; Zhang *et al.*, 1995). The band at

1645 cm^{-1} in only apoA-I and E peptides was assigned to the random structure. This assignment is in accord with the temperature studies (below) and the IR spectrum of apoC-I(7-24) in water (Shaw *et al.*, 1997), where it is unstructured (Rozek *et al.*, 1995). There is no consensus assignment for the band at 1632-1636 cm^{-1} (Surewicz & Mantsch, 1988;1996; Azpiazu *et al.*, 1993; Wolkers *et al.*, 1995; Zhang *et al.*, 1995).

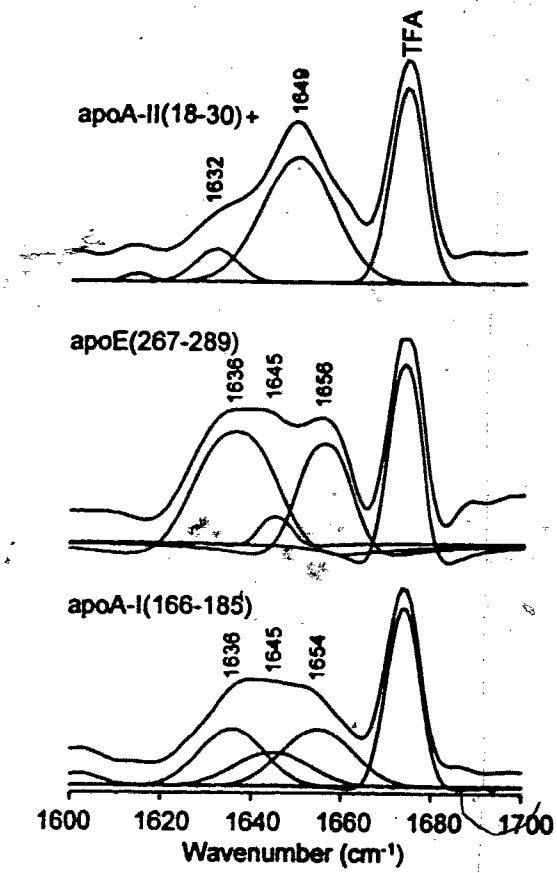

Fig. 7.1: FT-IR spectra and the deconvoluted bands of apoA-II(18-30)+, apoE(267-289), and apoA-I(166-185) bound to SDS in D_2O solutions (From Shaw *et al.*, 1997).

7.2.2 Effect of temperature

The temperature dependence of the IR spectra of the three peptides is depicted in Fig. 7.2. Little change occurred for apoA-II(18-30)+ upon raising temperature from 15 to 80°C whereas the 1632 band of apoE(267-289) decreases accompanied by an increase in intensity of the 1645 cm^{-1} band. From Fig. 7.3, it is evident that the increase of the random structure of the apoA-I peptide at 1645 cm^{-1} is at the expenses of the 1635 band while the 1654 band decreases only slightly.

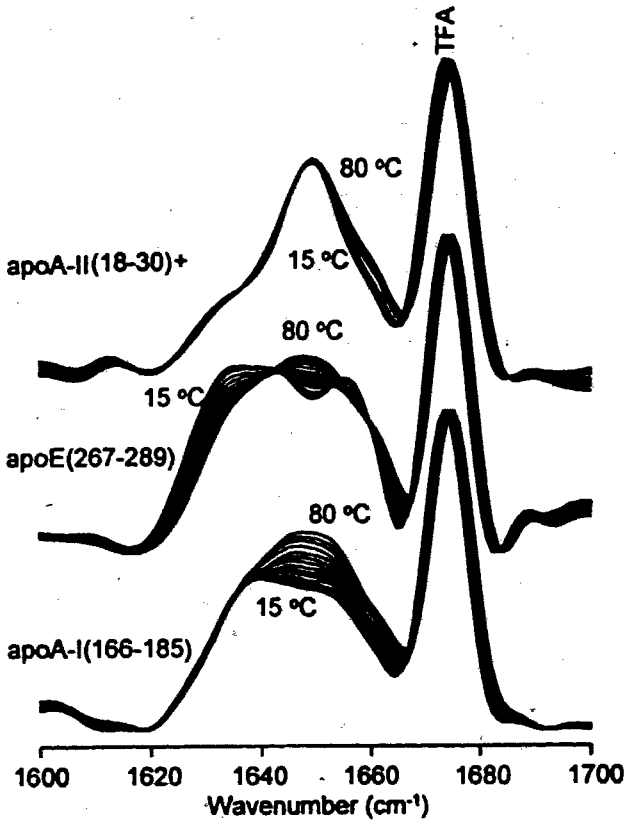

Fig. 7.2: Effect of temperature on the amide I band of the IR spectra of apoA-II(18-30)+, apoE(267-289), and apoA-I(166-185) in the SDS-bound state (From Shaw *et al.*, 1997).

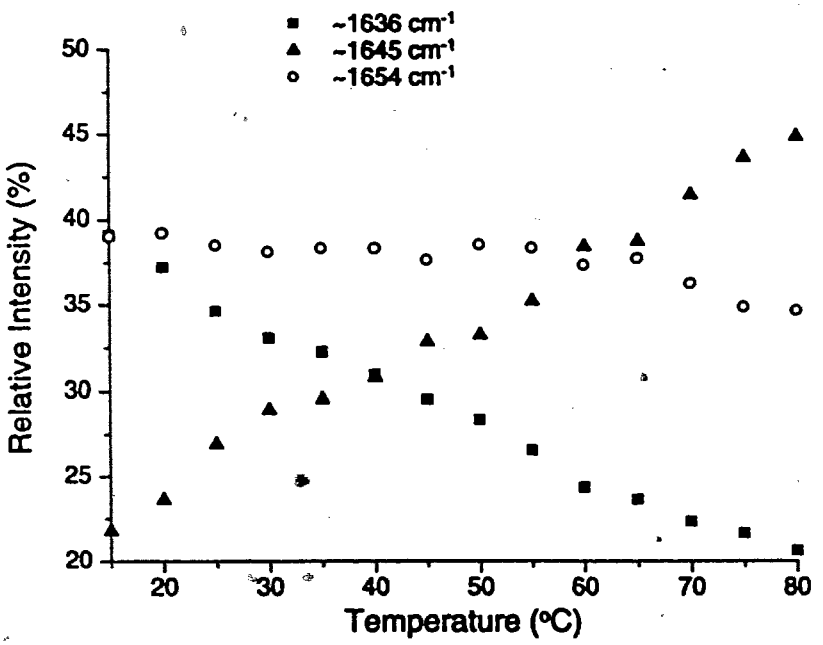

Fig. 7.3: Change of the intensity of deconvoluted bands of apoA-I(166-185) with temperature (From Shaw *et al.*, 1997).

7.2.3 Effects of pH on the IR spectra of apoA-I(166-185)

The IR spectra for apoA-I(166-185) at different pHs are presented in Fig. 7.4. The band pattern at pH 6.5 is similar to that at pH 10 but differs from that at pH 3. At and above pH 6.5, the 1638 band is more pronounced while at the acidic pH the intensity of 1642 band increases, indicating that the conformation of apoA-I(166-185) is pH-dependent.

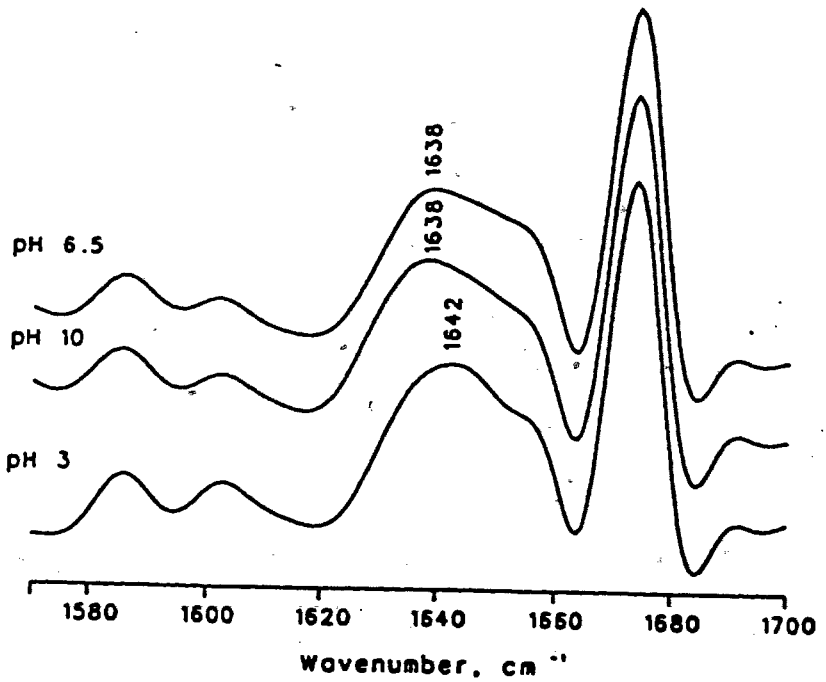

Fig. 7.4: IR spectra of apoA-I(166-185) at different pHs (From Shaw *et al.*, 1997).

7.3 Discussion

7.3.1 A novel assignment for the IR band at ~1635 cm^{-1}

Traditionally, the ~1635 band was assigned to β-sheet (Byler & Susi, 1986; Surewicz & Mantsch, 1988; Hirsh *et al.*, 1996). Based on this assignment, both apoE and

A-I peptides would contain 40% β-sheets, assuming that all IR bands have the same absorption coefficient. Such an assignment, however, is not consistent with the NMR structures nor chemical shifts for these two peptides, where helical structures were found to be dominant (Chapters 4-6). Hirsh *et al.* (1996) found 30% β-sheet based on the 1634 cm^{-1} band for an antimicrobial peptide magainin by FT-IR. However, both high resolution and solid-state NMR indicate that the peptide is all helical in lipid (Gesell *et al.*, 1997). A similar IR band was observed in the spectra of apoA-I/DMPC complexes (Yang et al., 1991) and in helical proteins such as hemoglobin and myoglobin (Byler & Susi, 1986). Recently, Zhang *et al.* (1995) also noticed this IR band for a transmembrane helical peptide in organic solvents, micelles, and bilayers and proposed an interconverting helix model to explain the absorption. Consistent with Zhang *et al.* (1995), the ~1635 band in lipoprotein model systems was shown to be neither lipid nor solvent dependent (Cushley *et al.*, 1994; Shaw *et al.*, 1997). With increase of temperature, the content of random structures (the 1645 cm^{-1} band) was found to increase for both apoE and A-I peptides whereas the band at ~1635 cm^{-1} decreased (Figs. 7.2 & 7.3), indicating that the latter may stem from one of the structured components in the peptide. Furthermore, the change of the IR spectra of apoA-I(166-185) with pH (Fig. 7.4) is reminiscent of our NMR study of the same peptide (Chapter 6). Both techniques indicate conformational change of apoA-I(166-185) from pH 3 to 6.5 whereas further increase of pH from 6.5 to 10 has little effect. Such a correlation led us to assign the IR band by comparison with NMR structures we determined. According to NMR, apoA-I(166-185) is more helical at physiological pH than at acidic pH regardless of lipid (Chapter 6). It appears that the more pronounced "structured component" at ~1635 cm^{-1} at pH 6 is coupled with the more helical conformation at the same pH. We propose that the band at ~1635 cm^{-1} may arise from the solvent-exposed helices, which form bifurcated hydrogen bonds with water or water and the peptide (Baker and Hubbard, 1984). Increase in temperature breaks up such hydrgen bonds, thereby leading to random structure. These solvent-exposed helices are evident at the N-terminus of apoE(267-289) NMR structures (Fig. 4.11B). In apoA-I(166-185) they are located at the termini, 3-4 residues each, and therefore are less

obvious to see (Fig. 6.9). This new assignment suggests that caution should be taken in interpreting the IR bands, especially when lacking high resolution protein structural data.

7.3.2 FT-IR and lipid-binding affinity

The 1649 cm^{-1} helical band of apoA-II(18-30)+ is 5-7 cm^{-1} lower than the similar bands of the apoE and apoA-I peptides, so is the band at 1632 cm^{-1}, which is 4 cm^{-1} less. The position of the amide I band reflects the strength of the hydrogen bond between the amide proton and the carbonyl group. Thus, it appears that the hydrogen bonds in apoA-II(18-30)+ are stronger than those in either apoE(267-289) or apoA-I(166-185). As helical conformations result from lipid association (Chapters 4-6), we propose that the A-II peptide binds lipid more tightly than either apoA-I(166-185) or apoE(267-289). Further support for this argument comes from the temperature experiments (Fig. 7.2). As both apoC-I(7-24) and apoC-I(35-53) (Shaw *et al.*, 1997) have the same IR spectra as apoA-II(18-30)+, these three peptides may be grouped together as the IR-group I. ApoA-I(166-185) and apoE(267-289) form the IR-group II. In the Segrest classification, apoA-II(18-30)+, apoA-I(166-185) and apoE(267-289) belong to class A2, A1, and G* amphipathic helices, respectively (Segrest *et al.*, 1990; 1994). Both molecular hydrophobicity potential calculations (Brasseur *et al.*, 1992) and peptide analogue studies by optical spectroscopy (Mishra and Palgunachari, 1996) suggest that the class A2 helices have a higher lipid affinity than class A1 or G* helices. These component helices appear to determine the protein properties. For example, apoA-I binds most weakly to DMPC compared to apoA-II, apoC-I, or apoC-III (Rosseneu *et al.*, 1976). In addition, apoA-I was shown to be displaced by apoA-II from the surface of lipoprotein particles (Lagocki and Scanu, 1980; Rosseneu *et al.*, 1981) whereas apoE can be displaced by apoC-I (Swaney and Weisgraber, 1994).

The weaker intensity of the ~1655 band for IR-group II further suggests that the lipid-binding helical domains in the IR-group II may be shorter than those in the IR-group I. Supporting this are the ratios of the molar ellipticity at 222 nm to that at 208 nm

of CD spectra. The values range from 0.88 to 0.93 for the IR-group I (Rozek *et al.*, 1995; Buchko *et al.*, 1996a,b) and 0.81-0.82 for the IR-group II (Wang & Cushley, unpublished data). A greater ratio corresponds to a more helical conformation (Rizo *et al.*, 1993; Fasman, 1996). The short lipid-binding domain lies in the middle region of apoA-I(166-185) (Chapter 6) but at the C-terminus of apoE(267-289) (Chapter 4). In Chapters 4-6, we showed that aromatic residues, hydrophobic pairs, and cationic side chains are important in lipid binding. Indeed, these elements are more abundant in the IR-group I than in the IR-group II. We, therefore, propose that the difference in the IR band position, relative intensity, and thermal stability may be utilized as an indicator for lipid affinity of apolipoprotein peptides (Shaw *et al.*, 1997). Stronger bands at shorter wave numbers and high thermal stability indicate longer amphipathic helices with higher lipid affinity. Therefore, a combined use of IR, CD, and NMR provides a more complete picture for the amphipathic helix model.

CHAPTER 8: HIGH RESOLUTION NMR SPECTRA OF HUMAN APOA-I AND APOA-II IN THE PRESENCE OF SDS

8.1 Introduction

In Chapters 5 & 6, we reported the NMR structures for apoA-II and apoA-I fragments in SDS. In this chapter, we present the NMR spectra of intact apoA-II and apoA-I in the presence of SDS. Some resonance assignments for intact apoA-I were made using the peptide-aided signal assignment strategy (Chapter 6).

8.2 Results

8.2.1 Isolation and purification of apolipoproteins

Fig. 8.1 shows that apoC-I, apoA-II in the reduced form, and apoA-I are eluted from PBE-94 at pH 7.7, 5.8, and 5.5, respectively. The proteins are pure as judged by SDS-PAGE (Fig. 8.2A).

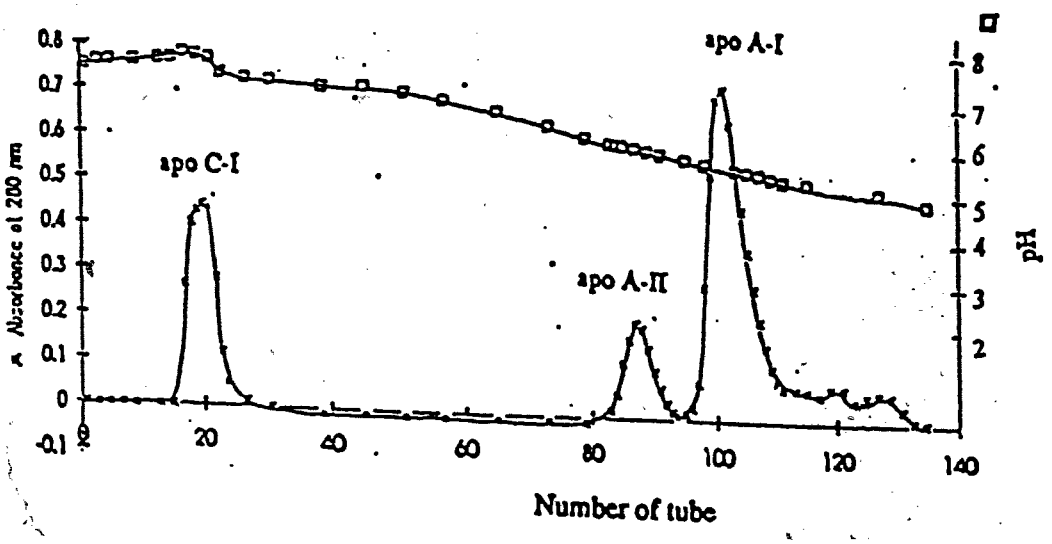

Fig. 8.1: Chromatogram of delipidated HDL on PBE-94 column. The peaks for pure proteins, apoA-I, reduced apoA-II and apoC-I, are labeled. Each tube contains 4.5 mL fraction collected at a flow rate of 25 mL/h. From 88 mg apolipoproteins loaded, 1 mg apoC-I, 8.6 mg reduced apoA-II and 18 mg of apoA-I were obtained.

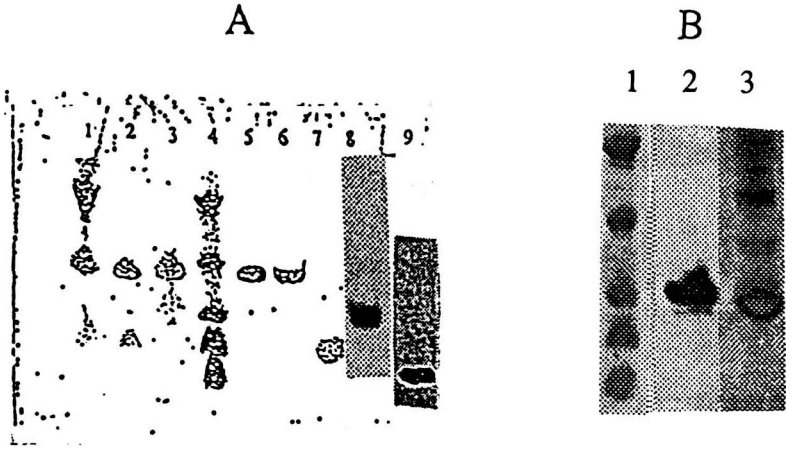

Fig. 8.2: SDS-PAGE of apolipoproteins. (A) Lanes 1, HDL; 2, washed HDL, reduced; 3, washed HDL, not reduced; 4, protein ladder (molecular weights from top to bottom are 66, 29, 14.3, 6.5, and 1.6, respectively); 5 & 6, apoA-I; 7, apoA-II, reduced; 8, apoA-II; 9, apoC-I; The protein gel was Coomassie blue stained. (B) Lanes 1, protein ladder; 2, apoA-II sample (peptide/SDS ratio, 1:80), prepared as described in Section 3.5.1; 3, NMR sample of reduced apoA-II (peptide/SDS ratio, 1:40). The gel was silver stained.

8.2.2 Apolipoprotein aggregates detected by SDS-PAGE

Purified apoC-I in polybuffer gave only one band (Fig. 8.2A, lane 9). However, three evenly spaced bands of almost the same intensity were observed after running through a HTP column. A similar gel pattern was observed for the reduced apoA-II (1.0 mg/mL) in 0.5 M sodium phosphate buffer (pH 6.8) containing 0.5% SDS. They were assigned as monomer (M_1), dimer (M_2), and trimer (M_3) of apoC-I or reduced apoA-II according to the estimated molecular masses. Teng *et al.* (1978) reported the same aggregation model for reduced apoA-II based on sedimentation studies. However, the dimer of apoA-I was not detected under the same conditions. Hence, the propensity to aggregate is:

$$\text{ApoC-I} \cong \text{reduced apoA-II} > \text{apoA-I.} \qquad (8.1)$$

Fig. 8.2B (lane 3) shows the SDS-PAGE for one NMR sample of reduced apoA-II, where aggregates of reduced apoA-II, ranging from M_2 to M_6, were detected even in

the presence of SDS (protein/SDS, 1:40) after storing the sample at room temperature for 40 days. M_1 was not detected probably due to the formation of the disulfide bond. However, only one band was detected for the NMR sample of apoA-II prepared using the procedure described in Section 3.5.1 (Fig. 8.2B, lane 2).

8.2.3 NMR spectra of apoA-II

Fig. 8.3 shows the NMR spectra of apoA-II in SDS before (A) and after (B) reduction of the disulfide bond. Over the envelope of the amide region, a few peaks showed clear splitting (Fig. 8.3A). The coupling constants, $^3J_{HNH\alpha}$, were measured to be 7.7 Hz (8.02 ppm, T76), 7.3 Hz (7.88 ppm, Q77) and 6.7 Hz (7.72 ppm, T72), respectively. These values are typical of conformational averaging (Wüthrich, 1986). The addition of β-mercaptoethanol caused spectral change mainly in the amide region near 8 ppm, suggesting that reduction induces a local conformational change. Most evidently, a new peak appeared at 8.35 ppm.

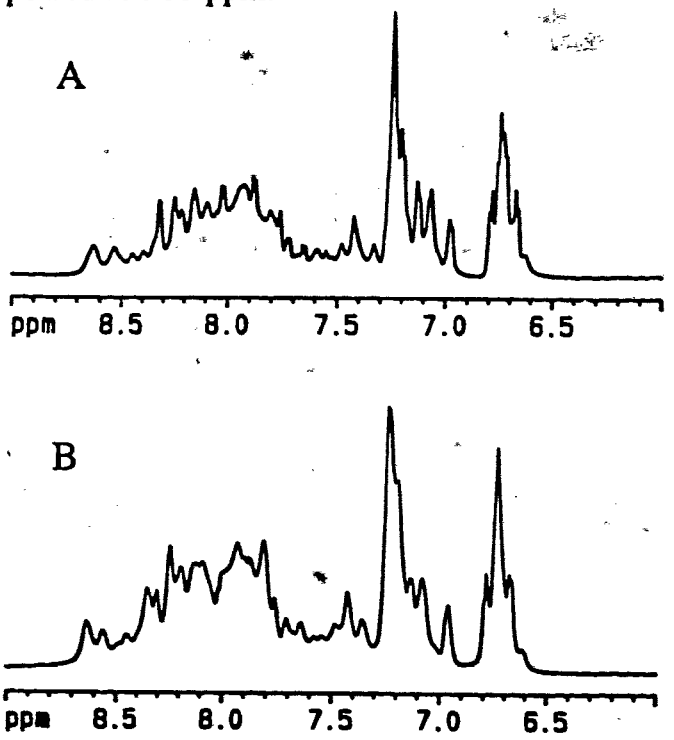

Fig. 8.3: NMR spectra of intact apoA-II (A) and reduced apoA-II (B) in the presence of SDS (protein/SDS, 1:80) at pH 5.7, 37 °C. Intact apoA-II was purified using FPLC in cooperation with Dr. Buchko (Mezdour *et al.*, 1987) from delipidated HDL, isolated from human blood plasma by the author (Section 3.1.2). Both spectra are the average of 128 scans over the spectral width of 6250 Hz.

Fig. 8.4A shows the fingerprint region of the 2D TOCSY of apoA-II, a protein of 17 kD consisting of two identical peptide chains. The broad lines and spectral overlap made it impossible to fully assign the spectrum yet terminal residues Q1, A2, K3, and T72 to Q77 were assigned since they give very strong TOCSY relay peaks. The same spectral region of apoA-II in SDS under the reducing condition is given in Fig. 8.4B. As anticipated, the TOCSY peaks for the reduced apoA-II (Fig.8.4B) are much narrower than those for the intact apoA-II (Fig. 8.4A) as a result of the decrease in molecular weight. Superposing the TOCSY spectra of apoA-II before and after reduction revealed that all the peaks in the spectrum of intact apoA-II recurred in the same spectral positions of the reduced apoA-II. This is strong evidence for symmetry of the native dimer. Such symmetry explains the observation that reduction of apoA-II influences neither structure nor lipid binding (Jackson *et al.*, 1973; Calabresi *et al.*, 1996). Some extra peaks can be seen upon reduction. Most evidently, a single peak appeared at (8.35, 4.74) ppm in Fig. 8.4B. Corresponding to this peak a pair of H^{β} protons at 3.21 and 3.13 ppm was clear. Thus, this new peak is assigned to Cys6 as the set of chemical shifts matches the random chemical shifts for this residue (Table 2.1), indicating Cys6 is unstructured. This observation is consistent with early electron spin resonance (ESR) spectra, which indicate that this region of apoA-II is not involved in lipid binding (Jackson *et al.*, 1973). We attribute the extra peaks to the increased flexibility because of breaking up the disulfide bond.

Portions of the NOESY spectra of apoA-II in SDS are shown in Fig. 8.5. Most of the H^{α} signals resonate upfield of the water signal at 4.6 ppm (Fig. 8.5A), indicating a predominant helical conformation. This is supported by NOE connectivities such as H^{α}_{i}-H^{N}_{i+j} (Fig. 8.5A) and H^{N}_{i}-H^{N}_{i+1} (B). Some resonances at the border of the spectrum were tentatively assigned, for example, Y14 (8.27 ppm) and F15 (8.66 ppm). In addition, the (i, i+4) NOEs of these aromatic side chains with the side chains of another hydrophobic pair L10V11 were found. These interactions are reminiscent of those between W264F265 and L268V269 observed for apoE(263-286) (Chapter 4), indicating the formation of a hydrophobic cluster and local helical structure.

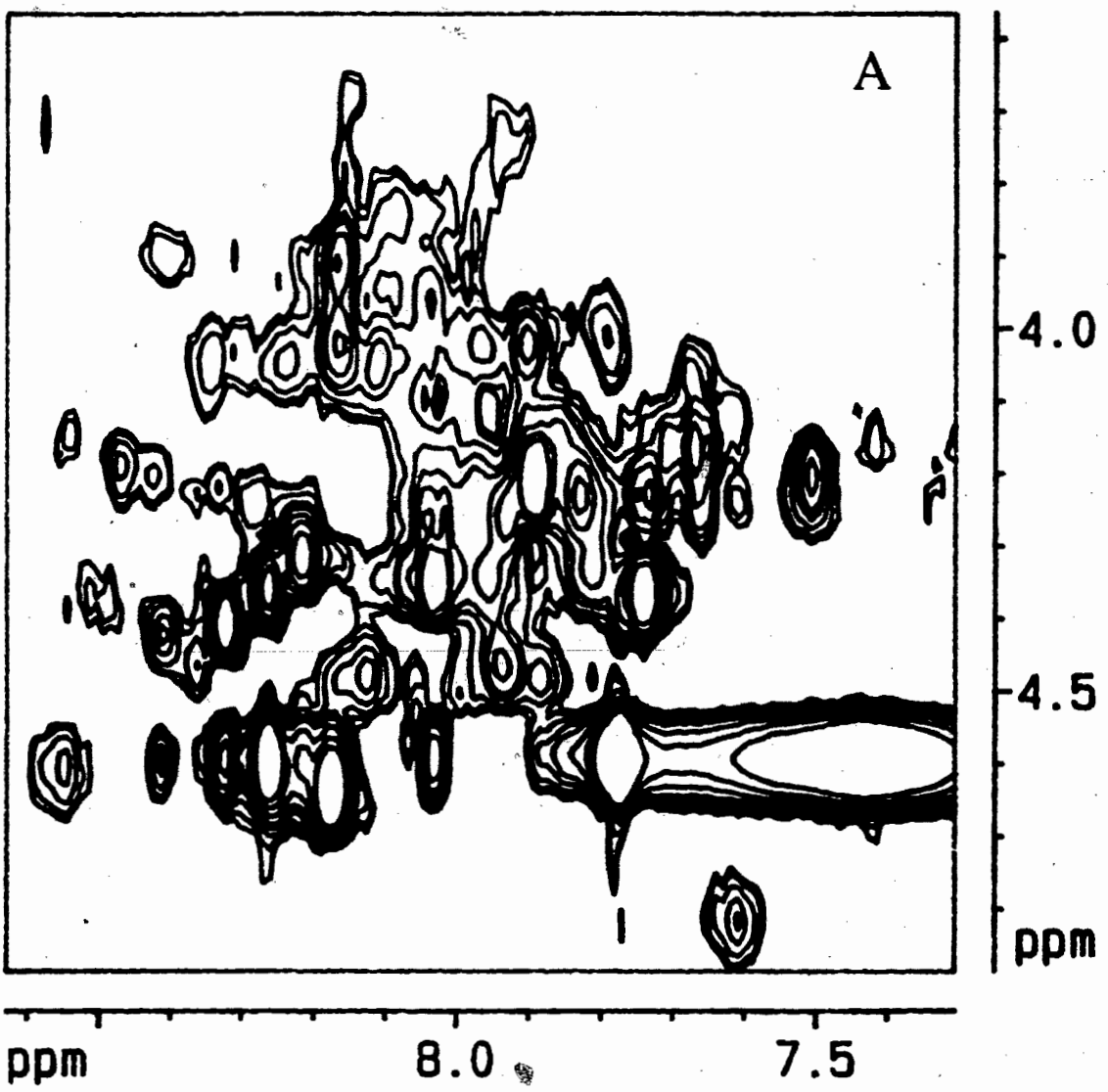

Fig. 8.4: Fingerprint regions of the TOCSY spectra of apoA-II in SDS before (A) and after (B) reduction, pH 5.7, 37 °C, and protein/SDS molar ratio of 1:80. For both (A) and (B), 640 increments were collected in t_1 with 32 scans each over the spectral width of 6250 Hz.

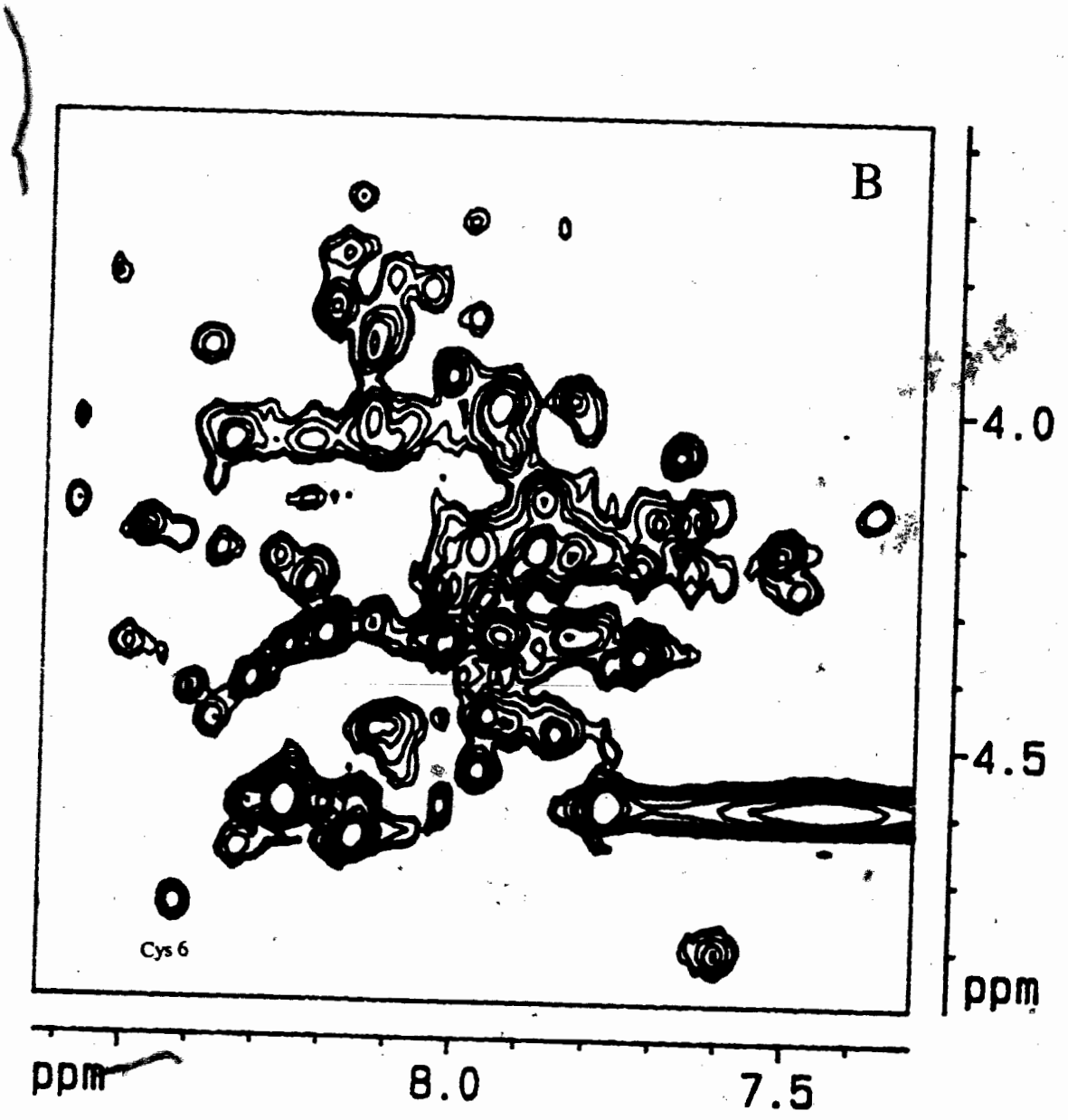

Fig. 8.4 (Continued)

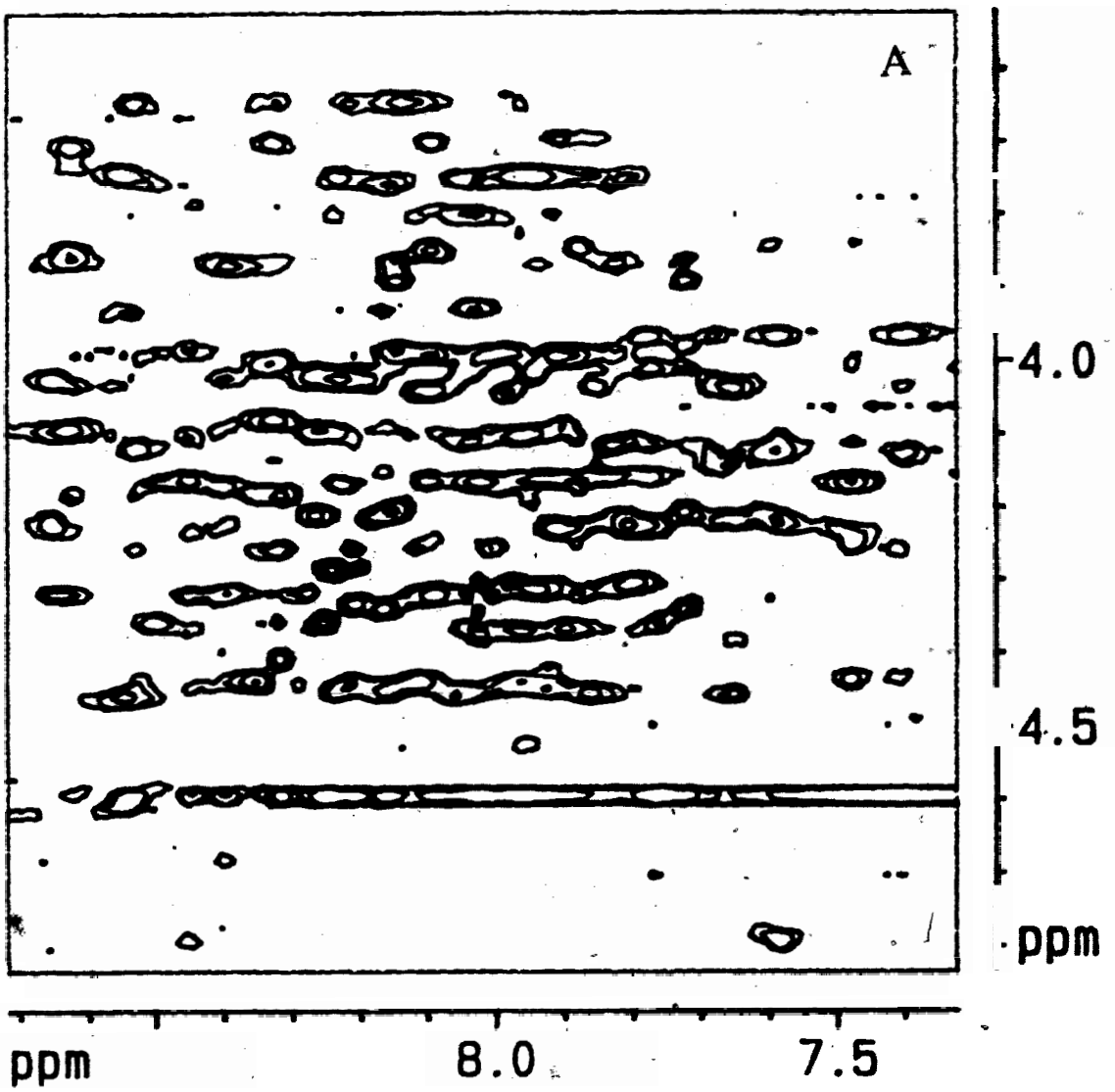

Fig. 8.5: Fingerprint (A) and amide proton (B) regions of the NOESY spectrum (τ_m = 100 ms) of apoA-II in SDS at pH 5.7, 37 °C, protein/SDS molar ratio 1:80.

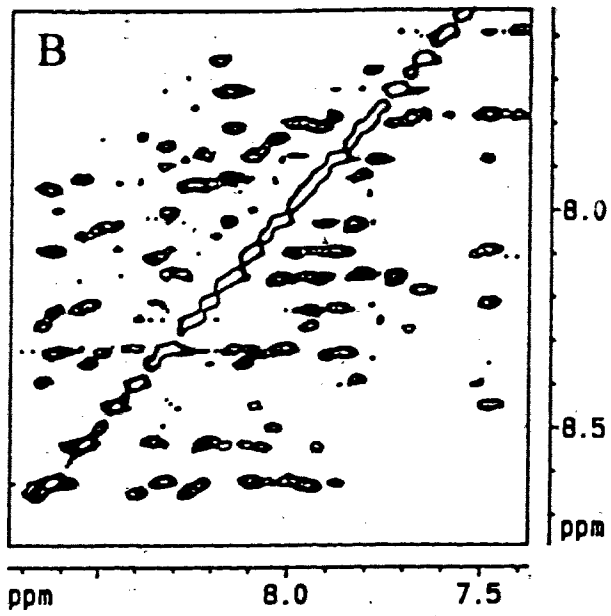

Fig. 8.5 (Continued)

8.2.4 NMR spectra of apoA-I

Fig. 8.6 shows the NMR spectra of apoA-I in the absence (A) and presence (B) of SDS. In the absence of SDS, NMR lines are very broad and more than four Trp resonances were observed (Fig. 8.6A), suggesting protein aggregation. In the presence of SDS, three Trp N1 proton signals at 9.62, 9.82 and 9.89 ppm were found in Fig. 8.6B. Two-dimensional NMR spectra at 25°C confirmed that the absorption at 9.82 ppm results from two Trp N1 protons. The four Trp N1 resonances are consistent with the notion that apoA-I is in the monomer state at the saturating level of SDS (Reynolds, 1982). Several valine spin systems were found in the TOCSY spectrum with H^{α} below 4 ppm. Relative to the random chemical shift (Table 2.1), the H^{α} of these valines all shifted upfield by greater than 0.1 ppm, suggesting locations in helical regions. The NOESY spectrum of intact apoA-I, M_r = 28,083, in SDS at pH 6.4 and 37 °C is shown in Fig. 8.7. Most of the H^{α} signals of apoA-I in SDS appear to high field of water at 4.6 ppm, indicating that the main secondary structure is helical. This is supported by CD, which suggests 50% helix

in SDS. Two prolines were found to have H^{α} chemical shifts of ~4.7 ppm. As these shifts differ from those found for prolines in the interhelical regions, where H^{α} chemical shifts are ~4.4 ppm (refer to Section 6.3.4), they may suggest the existence of β-structures, most probably at the N-terminus of apoA-I, residues 1-7.

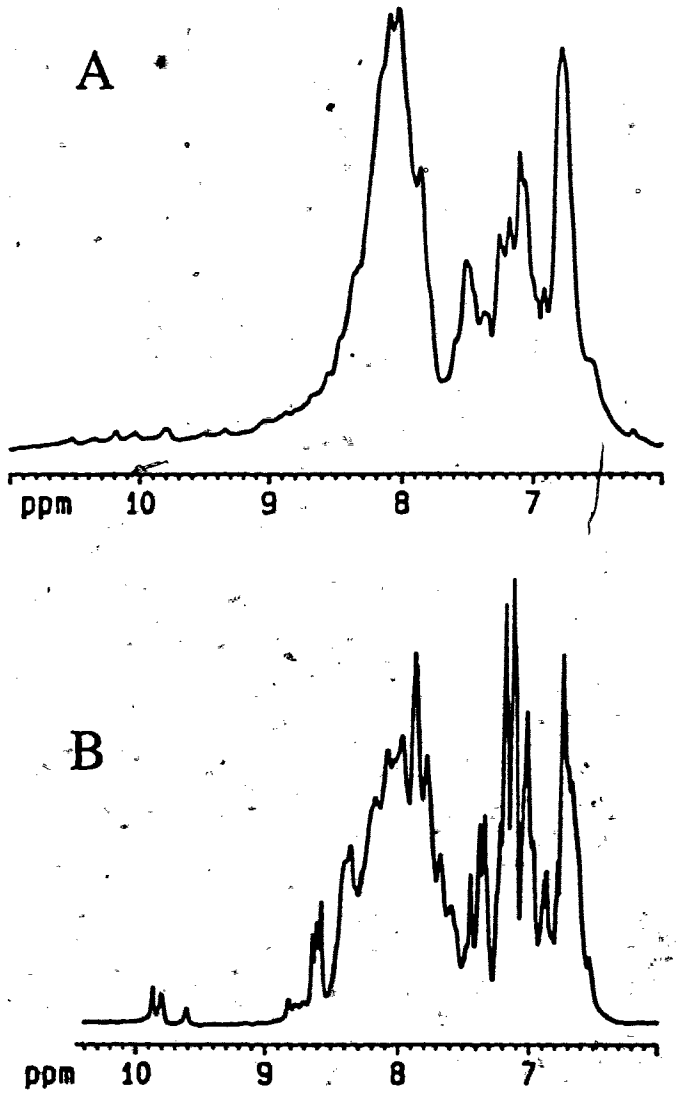

Fig. 8.6: NMR spectra of apoA-I in the absence (A) and presence (B) of SDS. The protein concentration was 0.36 mM in aqueous solution and 3.0 mM in SDS (protein/SDS, 1:140), pH 6.4, 37 °C. The spectrum in water is the average of 2000 scans over spectral width 8064.5 Hz whereas 32 scans were collected for the spectrum in SDS.

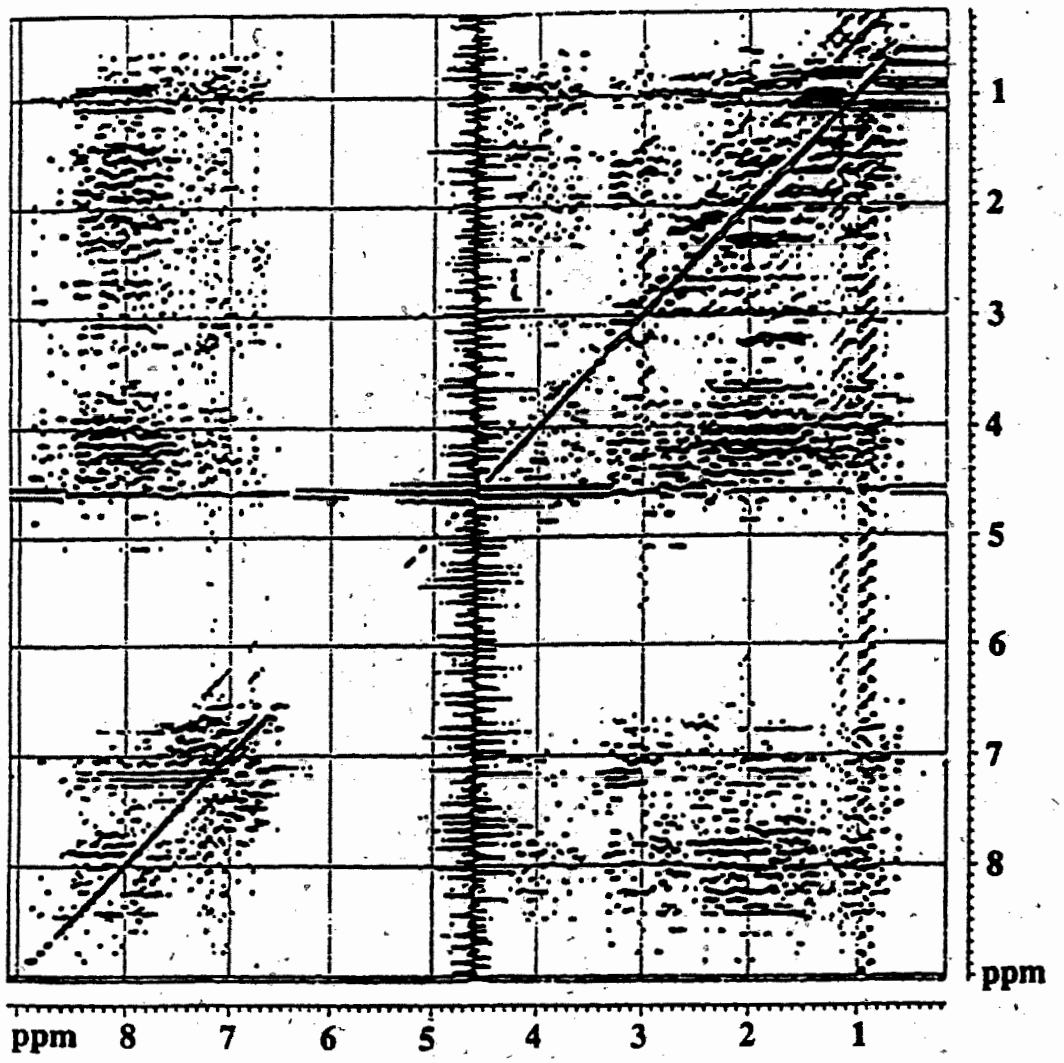

Fig. 8.7: NOESY spectrum of human apoA-I in the presence of SDS at pH 6.4, 37 °C, protein/SDS ratio of 1:140.

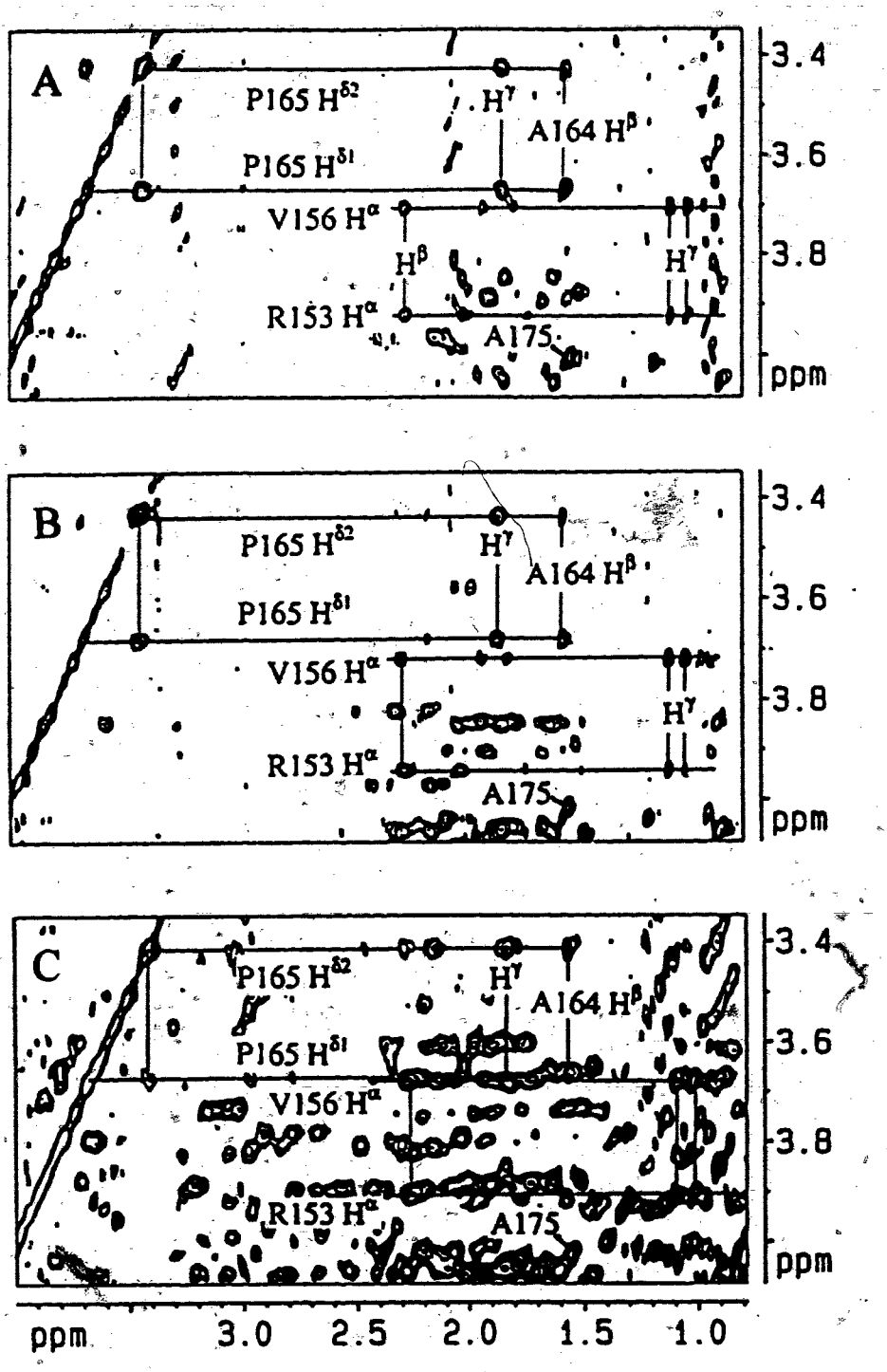

Fig. 8.8: Portions of the NOESY spectrum of (A) apoA-I(142-187), peptide/SDS molar ratio 1:60, at pH 6.9 and 50 °C (τ_m = 150 ms), (B) apoA-I(122-187), peptide/SDS ratio 1:60, at pH 6.2 and 50 °C (τ_m = 300 ms), and (C) apoA-I, protein/SDS ratio 1:140, at pH 6.4 and 37 °C (τ_m = 150 ms). In each spectrum the NOE connectivities for R153, V156, A164, P165 and A175 were labeled (From Wang *et al.*, 1997b).

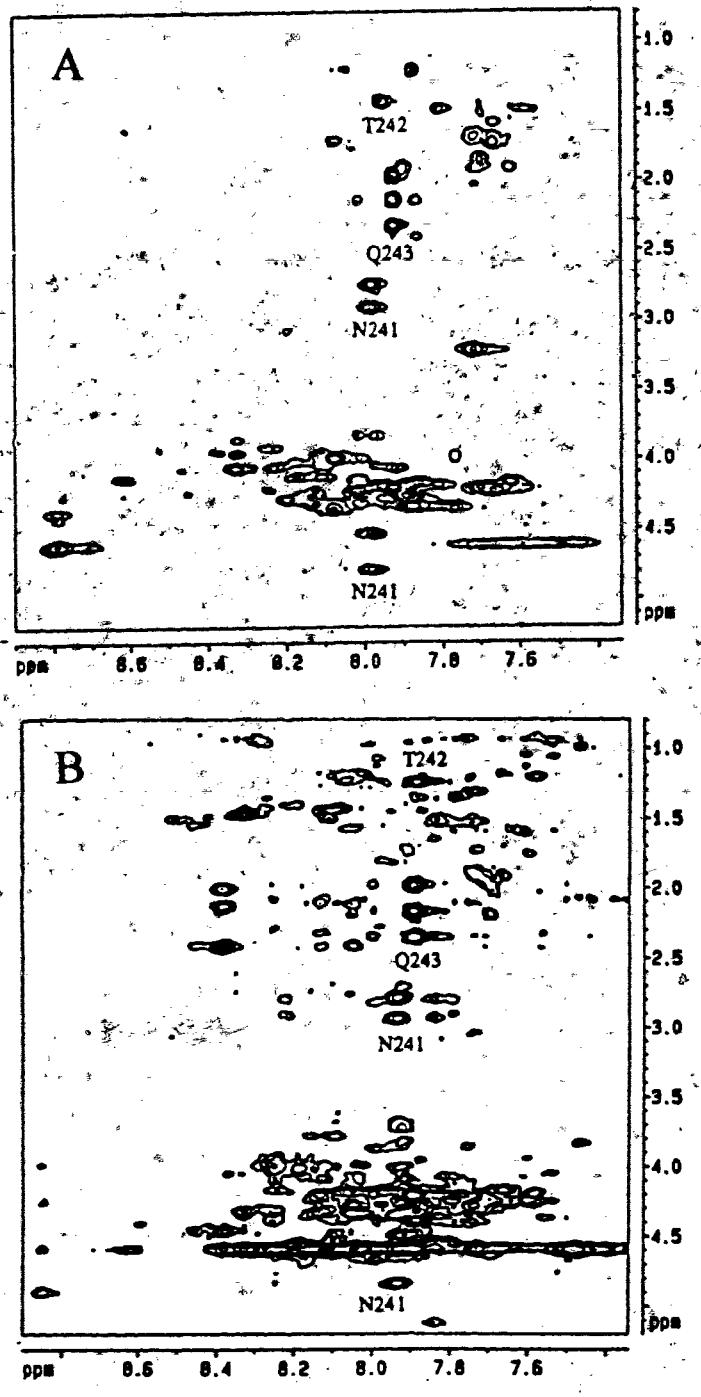

Fig. 8.9: H^{α}-H^{N} regions of the TOCSY spectra of (A) apoA-I(201-243) in DPC, peptide/DPC ratio 1:80, at pH 4.4, 37 °C; and (B) **apoA-I** in SDS as in Fig. 8.8.

Based on the assignments for apoA-I(142-187) and apoA-I(122-187) (Chapter 6), several resonances were found in the similar region of the apoA-I spectrum, where overlap is not severe (Fig. 8.8C). As shown, the chemical shifts for R153, V156, A164, P165, and A175 (labeled) are essentially identical to those measured in peptides under similar conditions. Such assignments suggest that the helix-hinge-helix motif found in apoA-I(142-187) and apoA-I(122-187) is very likely maintained in intact apoA-I.

Fig. 8.9 shows the same spectral regions of the TOCSY spectra of apoA-I(201-243) in DPC (A) and intact apoA-I in SDS (B). Although the spectra were recorded in different model lipids at different pHs, the three C-terminal residues, N241, T242, and Q243, appear at similar spectral regions. Hence, these residues in intact apoA-I were assigned using peptide-aided signal assignment strategy (PASA) (Fig. 8.9). Both the strong TOCSY peaks and the chemical shifts indicate that these three residues do not form helical structure and probably not participate in lipid binding.

8.2.5 Heteronuclear apoA-I spectra

As only limited information is available from 2D ^{1}H-NMR spectra as a result of severe spectral overlap (Fig. 8.7), the laboratory is currently switching to heteronuclear multidimensional NMR techniques in cooperation with other laboratories that produce isotope-labeled apoA-I or its fragments. The heteronuclear 2D (^{1}H, ^{15}N) HMQC spectrum of intact apoA-I is given in Fig. 8.10. A preliminary 3D (^{1}H, ^{15}N) HMQC-NOESY spectrum is shown in Fig. 8.11. A brief investigation of 2D slices shows that even in the ^{15}N-edited 3D spectra there is still significant peak overlap and missing signals. The difficulty can be attributed to the large size, formation of complexes with SDS and predominantly helical conformation of apoA-I.

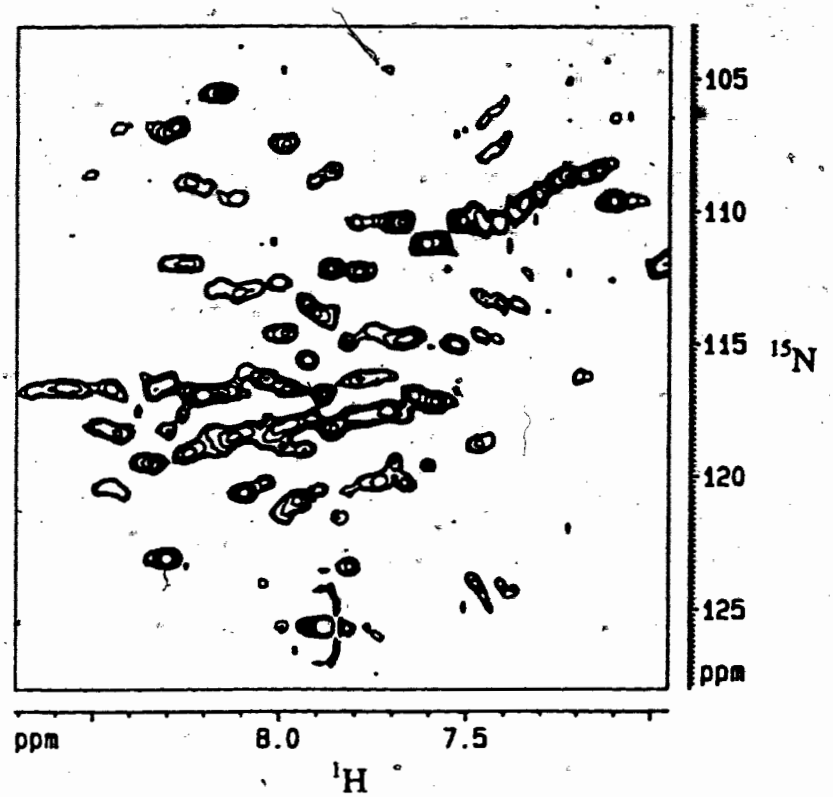

Fig. 8.10: HMQC spectrum of ^{15}N-labeled apoA-I (~2 mM), protein/SDS-d_{25} ratio, 1:140, at pH 6.4, 37°C. The carrier frequency for ^{1}H is set at 600.1300 MHz while it is 60.8100 MHz for ^{15}N. The spectral width is 12 ppm for ^{1}H and 50 ppm for ^{15}N. The J-modulated coherence transfer time between between ^{1}H and ^{15}N is set to 1/(2J), where J = 95 Hz for ^{1}H-^{15}N. 2K data points in t_2 and 512 increments in t_1 were collected.

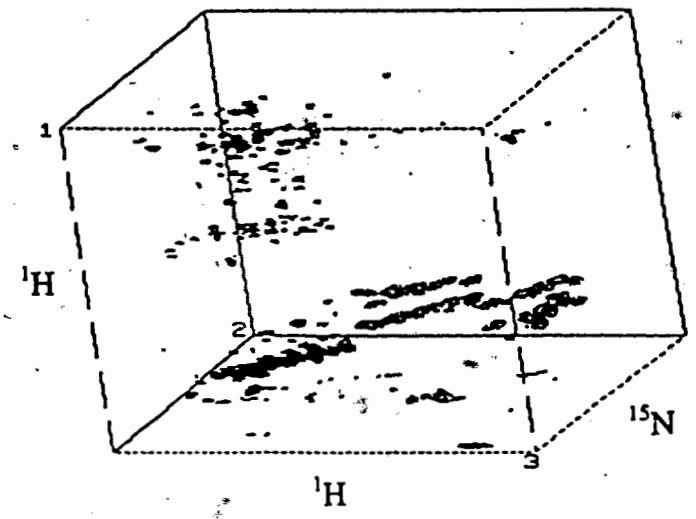

Fig. 8.11: 3D (^{1}H, ^{15}N) HMQC-NOESY spectrum of apoA-I. The protein contains 11 more residues at the N-terminus, MRGSHHHHHHM, to facilitate purification (Bergeron *et al.*, 1997). This spectrum was collected with the aid of D.G. Naugler under the same conditions as in Fig. 8.10. The data size is 128 (t1) × 64 (t2) × 1024 (t3). The water signal was presaturated prior to data collection.

8.3 Discussion

8.3.1 Apolipoprotein oligomerization, molecular basis, and NMR study

Apolipoproteins have a strong tendency to self-associate or aggregate (Gwynne *et al.*, 1974; Osborne & Brewer, 1977; Scanu, 1978; Teng *et al.*, 1978; Donovan *et al.*, 1987). Aggregation is usually accompanied by increase in helicity of the protein but decrease in the ability to bind lipids, suggesting hydrophobic interactions between proteins (Scanu, 1978). We showed that aggregates could be monitored by SDS-PAGE plus silver-staining. The aggregation trend described in Eq. 8.1 is correlated with apolipoprotein lipid-binding affinity observed by others (Lagocki & Scanu, 1980; Rosseneu *et al.*, 1981; Swaney & Weisgraber, 1994). In Chapter 4, we proposed that aromatic residues and hydrophobic pairs are important lipid anchors. It appears that these elements also play an important role in protein aggregation since removal of the strong lipid-binding C-terminal segments from apoA-I or apoE greatly inhibited aggregation (Westerlund & Weisgraber, 1993; Ji & Jonas, 1995). In fact, the oligomerization of apoE(263-286) was observed. This correlation reinforces our notion that synthetic peptide studies and site-directed mutagenesis studies may provide complementary information about the protein (Section 1.4).

It has long been known that the NMR sample preparation is crucial for membrane protein studies (McDonnell & Opella, 1993; Opella & Marassi, 1996). The problem of apolipoprotein aggregation is more serious here since the protein concentrations in NMR samples are much higher than those used in biochemical studies. Previous studies did not offer a solution to the aggregation problem (Osborne & Brewer, 1977; Scanu, 1978). Because it is extremely difficult to remove the aggregates once formed, the best policy is to block their formation. The main strategies employed by the author to prepare apolipoprotein NMR samples without detectable aggregates include keeping the protein in a dilute solution (< 1 mg/mL) and at pH < 3.5, minimizing the storage time, adding sufficient amounts of detergents so as to saturate the hydrophobic domains, and

lyophilizing the solution for storage. For apoA-II, there is a great advantage to prepare the apoA-II sample first and then reduce the disulfide bond to improve resolution of NMR spectra (Fig. 8.2B). ApoA-II and apoA-I samples prepared in this manner are in the monomer state and are stable for at least three months at room temperature. The high quality of apoA-I and apoA-II spectra presented in the thesis illustrates that NMR studies of apolipoprotein conformations in lipid-mimetic environments are promising. The final assignment of apoA-I (243 residues) spectra would require isotopically labeled samples enriched with ^{13}C, ^{15}N, and/or ^{2}H (Zhang *et al.*, 1994; Shan *et al.*, 1996; Garrett *et al.*, 1997). Deuteration suppresses line broadening arising from spin-spin interactions and improves sensitivity due to a longer T_2 relaxation times (Markley *et al.*, 1968; Torchia *et al.*, 1988; LeMaster & Richards, 1988; Venters *et al.*, 1995).

8.3.2 Peptide-aided signal assignment of apoA-I

Before we had access to isotope-labeled samples, we studied several apolipoprotein segments of potential biological importance (Chapters 4-7). We found that the assignment of apoA-I(166-185) was useful in the assignment of apoA-I(142-187) since the same conformation was found for residues 168-182 in the two peptides (Chapter 6). The chemical shift identity for residues 146-182 between apoA-I(142-187) and apoA-I(122-187) is striking (Fig. 8.8, A & B). Using the general similarity of chemical shifts, the author was able to assign several resonances in apoA-I (243 residues) (Figs. 8.8 & 8.9). We, therefore, propose that such a peptide-aided signal assignment (PASA) may be useful in NMR studies of apoA-I and other members in the exchangeable apolipoprotein family (Wang *et al.*, 1997a,b). A similar strategy has also been proposed for modular proteins (McEvoy *et al.*, 1997) at approximately the same time. We believe that a combined study of intact protein and the segments by NMR will ultimately lead to a complete structural understanding of apoA-I.

8.3.3 The structural and functional domains of apoA-I

In Section 4.3.4, we proposed to locate strong lipid-binding regions based on the density of hydrophobic pairs and aromatic residues in the protein sequence. Here we have plotted the hydrophobic residue marks against the residue number in apoA-I sequence. Although simple, some key features of this hydrophobic plot are interesting since they appear to explain many experimental data of apoA-I.

(1) Each vertical bar stands for a hydrophobic residue, which appears regularly in the sequence separated by every 2-3 residues, suggesting helical structure. Note that such a periodicity can encompass proline-containing regions (Section 6.3.4). Also, three hydrophobic residues, V19, L44, and V227 in the vicinity of hydrophobic pairs, are predicted to be on the hydrophilic face and thus may not participate in lipid binding. The potential helical structures in such regions remain to be proved. Except at the termini, only four helix-breaking regions were found, namely residues 23-28, 34-37, 76-81, and 182-188 (Fig. 8.12). The helix-breaking regions have four or more hydrophilic residues in a row. Therefore, the putative helix 0, residues 7-34, in Fig. 1.1 may be a helix(7-22)-break(23-28)-helix(29-34) motif rather than a continuous helix. The putative helix 2 may be another helix(66-75)-break(76-81)-helix(82-98) motif. The breaks near G35 and G185G186 may form loop regions, which separate the independent structural and functional domains at the C- and N-termini from the central domain of apoA-I (Ji & Jonas, 1995; Rogers *et al.*, 1997). This may explain why both regions nearby are highly susceptible to proteolysis as mentioned in Sections 6.1 and 6.3.4.

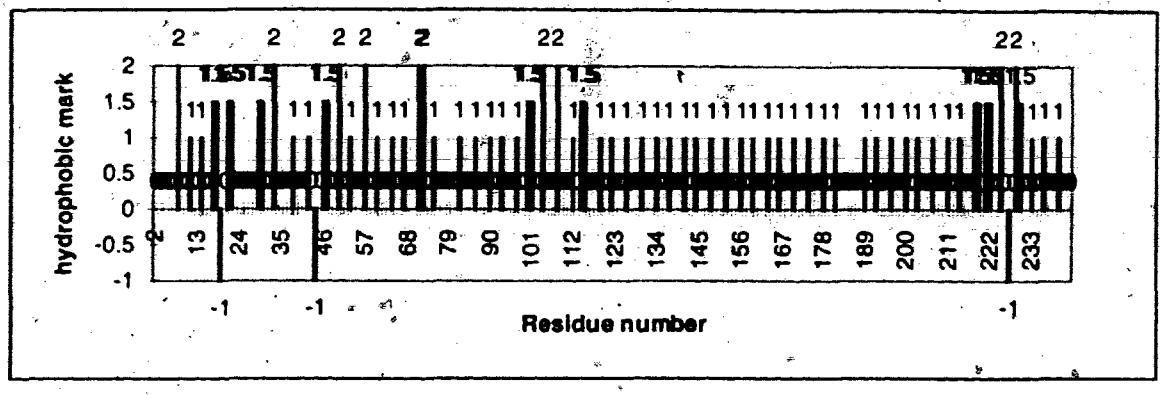

Fig. 8.12: A hydrophobic plot of human apoA-I. In the hydrophobic plot, residues Y, L, V, M, and A have been assigned a hydrophobic mark of 1's while aromatic residues, F and W, are given 2's and hydrophobic pairs such as VY, VL, LL, FW, YL, and FL two 1.5's. The higher arbitrary marks for the hydrophobic pairs and aromatic residues reflect their importance in lipid binding (Chapter 4). Alanines will be assigned as hydrophobic only when there are no other larger hydrophobic residues in the vicinity. Examples are and may be A130, A152, A196, and A207.

(2) As depicted by bars with 1.5's and 2's in Fig. 8.12, there are five regions in apoA-I (helices 0, 1, 2, 3, and 8 in Fig. 1.1) that are relatively rich in aromatic residues and hydrophobic pairs. Srinivas *et al.* (1991) showed that apoA-I(1-33) (helix 0 in Fig. 1.1) associated with DMPC but apoA-I(8-33) did not. Palgunachari *et al.* (1996) found that among the eight putative helices (helices 1 to 8 in Fig. 1.1) only the first and the last bound to DMPC but all associated with lysoPC except helix 2. The failure of the helix 2 in binding lipid may be due to synthesizing only residues 66-87 instead of complete repeat residues 66-99. Therefore, all nine putative helical regions will bind lipid, in agreement with the hydrophobic plot (Fig. 8.12). Frank *et al.* (1997) showed that helix 3 is important in stabilizing protein-lipid complexes. The importance of the C-terminus of apoA-I in lipid binding has been demonstrated by several studies (Sparrow & Gotto, 1982; Schmidt *et al.*, 1995; Holvoet *et al.*, 1996; Davidson *et al.*, 1996). Sorci-Thomas *et al.* (1997) showed that substituting residues 143-164 by another copy of residues 220-241 increased the stability of protein-lipid complexes. Therefore, the major role of these aromatic-rich regions is to stabilize the structure of apoA-I in lipid (Chapter 4). The N-terminal helices 0-3 may also play a role in stabilizing the structure of apoA-I in the lipid-free state (Palgunachari *et al.*, 1996; Davidson *et al.*, 1996; Rogers *et al.*, 1997), probably

by forming a helix bundle structure similar to apoE (Wilson *et al.*, 1991). Finally, different from the region 122-187 (below), these aromatic regions are accompanied mostly by lysines rather than arginines. As the side chains of lysines are more hydrophobic than arginines, these lysines may be an extra determinant for the structural and functional role of these aromatic domains of apoA-I.

(3) The region covering residues 122-185 is very smooth in the hydrophobic plot (Fig. 8.12) as a result of containing neither aromatic residues (W & F) nor hydrophobic pairs. It is anticipated that such a region will not bind lipid tightly. However, the implication of this region in LCAT activation is evident (Sparrow & Gotto, 1980; Fukushima *et al.*, 1980; Minnich *et al.*, 1992; Sorci-Thomas *et al.*, 1993, 1997; Holvoet *et al.*, 1995). The helix-hinge-helix-hinge-helix secondary structural pattern of apoA-I(122-187) (Fig. 6.28) corresponds exactly to the sequence periodicity, indicating that helix-hinge-helix motifs are structural units in apoA-I (Fig. 8.8).

CHAPTER 9: CONCLUDING REMARKS

In the thesis, we have employed several biophysical techniques to study the conformation of apolipoprotein segments. Optical techniques are not capable of providing structural details at atomic level. They, however, are usually not limited by protein size or lipid type. The data obtained in the same lipid model by various techniques (Chapter 7) or in different lipid models by the same technique may provide complementary information (Cann *et al.*, 1994; Sejbal *et al.*, 1996a). For example, apoE(267-289) does not bind DMPC but associates with SDS or DPC. NMR structural differences between apoE(263-286) and apoE(267-289) suggest that one hydrophobic cluster is sufficient to bind to micelles but two or more are required to bind vesicles (Chapter 4). The similar helical conformations and blue shifts of apoE(263-286) in both SDS (Chapter 4) and DMPC (Sparrow *et al.*, 1992) suggest that the hydrophobic packing found in micelles may apply to the peptide/DMPC complexes. In micelles, the determined interhelical structures for apoA-I(142-187) are in support of lipid binding of Y166, which is further substantiated by intermolecular NOEs between SDS and Y166. The fluorescence of Y166 has been observed in both SDS and DPC for apoA-I(142-187) (Chapter 6), and also in DMPC for apoA-I(145-183) (used for quantifying the peptide) (Vanloo *et al.*, 1995), indicating that the interhelical region by P165 is bound to lipid regardless of lipid models.

9.1 General structural features of apolipoprotein segments

The amphipathic helix (Segrest *et al.*, 1974) is characterized by clustering of hydrophobic side chains on one face and hydrophilic side chains on the opposite face. The hydrophobic face of the helix was proposed to interact with the acyl chains of lipids, thus explaining why these proteins serve as vehicles in human blood to transport water-insoluble lipids. Although the hypothesis is supported by many facts (Sparrow & Gotto, 1982; Segrest *et al.*, 1994), there was no detailed structure in the lipid-bound state. Thus, this thesis represents one of the first high resolution structure determinations of

apolipoprotein fragments in lipid-mimetic environments. The features of NMR structures for the peptides of 18-24 residues reported here can be summarized below:

(1) According to Segrest's classification (Segrest *et al.*, 1990; 1994), apoA-I(166-185), apoA-II(18-30)+, and apoE(267-289) belong to class A1, A2, and G* amphipathic helices (Fig. 1.2), respectively. The NMR structures (Figs. 6.11, 5.6, & 4.13B) for those three peptides are consistent with such a classification and also revealed additional new structural features (Chapters 4-6). Other examples of class A2 amphipathic helical structures determined by NMR are from apoC-I and LAP-20 (Rozek *et al.*, 1995; Buchko *et al.*, 1996b). We conclude that amphipathic helices are indeed a common structural motif in exchangeable apolipoproteins, at least in micelles.

(2) ApoA-I(166-185) possesses similar conformations in SDS, DPC or lysoPC with localized differences at the N-termini (Chapter 6). Similar conformations were also found for LAP-20 in either SDS or DPC (Buchko *et al.*, 1996b). We, therefore, conclude that hydrophobic interactions dominate in determining the lipid-bound conformation. As SDS and DPC mimic lysoPC well, we propose that both can be used to model lipid environments for conformational studies of apolipoprotein peptides (Rozek *et al.*, 1995; Buchko *et al.*, 1996b; Dunne *et al.*, 1996; Sejbal *et al.*, 1996a; Opella *et al.*, 1997).

(3) Contrary to the proposal made by Segrest *et al.* (1994), cationic side chains in both class A1 and A2 amphipathic helices are extended in the interface and, therefore, do not preferentially "snorkel", at least in micelles (Chapters 5-6) (Rozek *et al.*, 1995; Buchko *et al.*, 1996a,b).

(4) Contrary to an earlier proposal of ion pair formation between acidic and basic side chains in lipoproteins (Segrest *et al.*, 1974), the intrahelix ion pairs do not occur in the NMR structures of the peptides in association with either SDS or DPC (Chapters 5-6) (Rozek *et al.*, 1995; Buchko *et al.*, 1996a,b). Instead, it is more likely that cationic side chains form ion pairs with anionic lipid head groups (Chapter 6).

9.2 Important apoA-I fragments

In this thesis, the author has investigated segments of different lengths from the same protein, apoA-I. We showed that the helix 168-182 found in apoA-I(166-185), a 20mer, is retained in apoA-I(142-187), a 46mer, and in apoA-I(122-187), a 66mer (Chapter 6). In addition, the helix-hinge-helix motif found in apoA-I(142-187) is retained in the 66mer, and most likely in intact apoA-I (Chapter 8). These structural motifs lend support to the predicted secondary structures of apoA-I (Segrest *et al.*, 1994) except the hinge near P165, which is, on average, a helical bend or half-turn rather than a β-turn. The predominance of helical structures is in agreement with the NOESY spectrum of apoA-I (243 residues) (Fig. 8.7). The NOESY spectra of human apoA-II (154 residues) in SDS (Fig. 8.5) and apoC-III (79 residues) in DPC (Buchko *et al.*, 1997) also suggest predominant helical conformations. The preliminary NMR structure of apoC-I (57 residues) was shown to contain two helices separated by an extended linker region (Rozek *et al.*, 1996). All these NMR studies strongly support the predicted secondary structures of apolipoproteins. This is fortunate because, unlike hydrophobic transmembrane helices, which can be predicted quite accurately (Engleman *et al.*, 1982; Aloy *et al.*, 1997), sequences with the periodicity of an amphipathic helix have been found in β-sheet proteins (Parker & Stezowski, 1996).

9.3 Lipid-binding elements

It has long been proposed that hydrophobic interactions are responsible for lipid binding (Stoffel *et al.*, 1974; Assmann *et al.*, 1974; Sparrow & Gotto, 1982; Subbaro *et al.*, 1988). From the NMR structures, we found that aromatic-aromatic and aromatic-hydrophobic side-chain interactions led to formation of hydrophobic clusters, providing lipid-binding sites (Chapter 4). In addition, while electrostatic interactions between apolipoprotein segments and DPC play little role (Chapter 6), consistent with earlier observations (Stoffel *et al.*, 1974; Assmann *et al.*, 1974; Reijngoud *et al.*, 1982), interfacial cationic side chains do interact with anionic SDS (Chapter 6). The functions

of the cationic side chains are two-fold. First, cationic side chains may initiate anionic lipid binding to peptides or proteins. Second, upon formation of the helix, cationic side chains further enhance anionic lipid binding by (1) hydrophobic interactions between SDS alkyl chains and the cationic side chains, and (2) salt bridges between SDS head groups and positively charged moieties of the cationic side chains (Chapters 5 & 6).

In conclusion, our NMR structures (Chapters 4-6) illustrate that there are three major hydrophobic lipid-binding elements: hydrophobic side chains, hydrophobic pairs, and cationic side chains and one lipid affinity modulator: acidic or polar side chains. A semi-quantitative assessment of the lipid affinity is to count the number of hydrophobic pairs, aromatic residues, and cationic side chains (in the interface). We may, therefore, establish a new classification of amphipathic helices based on these lipid-binding elements. An amphipathic helix consists of any combination of the three classes of hydrophobic clusters listed below:

Class I, hydrophobic residues, hydrophobic pairs, very few or no cationic side chains;

Class II, hydrophobic residues, no hydrophobic pairs, several cationic side chains (mainly arginines)

Class III, hydrophobic residues, hydrophobic pairs, several cationic side chains (mainly lysines)

The concept of hydrophobic cluster may be harnessed as a new tool in search for lipid-binding segments in apolipoproteins and in *de novo* peptide design. Such an NMR-structure-based classification adds to our knowledge on amphipathic helices, especially in binding lipids. From such a classification, it is evident that hydrophobic interactions dominate according to class I, where usually aromatic residues and hydrophobic pairs exist, which are good lipid anchors. Examples are segments near the C-terminus of apolipoproteins such as apoE and apoA-I (Chapters 4 & 6).

A typical example for class II is apoA-I(166-185). The four leucines in this peptide have a ΔG_{hb} = -11.6 kcal/mol, equivalent to only one hydrophobic cluster (cf.,

Table 4.4). It is thus not surprising to observe that the hydrophobic moieties of the cationic side chains participate in lipid binding (Chapter 6). Class III, corresponding to IR-group I peptides (Chapter 7), binds lipid tightly since they contain all lipid-binding elements above. Examples are segments in apoA-II, apoC-I and apoC-III. The potential lipid-binding affinity (Chapter 7) may be a good parameter in judging the possible biological function. High lipid affinity would mainly limit the function of the segment to lipid binding (Chapters 4-5) whereas segments with weak to medium lipid affinity may be potential candidates for other functions such as lipolysis enzyme activation.

9.4 Structural models for the peptide/lipid complexes

Amphipathic helices, proposed for apolipoproteins by Segrest *et al.* (1974), have now been recognized as one of the key protein structural units in nature (Perutz *et al.*, 1965; Segrest *et al.*, 1990; McDonnell *et al.*, 1993; Papavoine *et al.*, 1994; Haltia & Freire, 1994; Dunne *et al.*, 1996). Based on the NMR structures, intermolecular NOEs between apoA-I peptides and SDS, and lipid-binding studies, we propose two models for apoA-I peptides/SDS complexes: (1) the paddle model, where a single amphipathic helix is bound to the micelle and (2) the straddle model, where the helix-hinge-helix structural motif straddles the micelle. The paddle model applies if the helix is a class A amphipathic helix since the "pairs" of cationic side chains in the interface of the class A helix resemble pairs of paddles on a canoe. It differs from the snorkel model (Segrest *et al.*, 1990; 1994) in at least two aspects. First, the ensemble of interfacial cationic side chains is extended in the interface in the shape of cone rather than preferentially "snorkeling" (Chapter 5). Second, our model is deduced from NMR data whereas the snorkel model remains a hypothesis.

The helix-hinge-helix structures found in apoA-I(142-187) would conform to the curvature of a spherical particle well and provide an alternative mode for helix packing on lipoprotein particles (Chapter 6). A prominent feature of our models is the complement of both hydrophobic (SDS alkyl chains with peptide hydrophobic and cationic side chains) and electrostatic interactions (anionic SDS with peptide cationic side

chains) in the interface. The significance of the straddle model may be that the amphipathic helix-hinge-helix (Chapter 6) or helix-bend-helix (Chapter 4) structural motif could have been one of the major determinants for the formation of spherical particles of lipoproteins. As lipoproteins are good model systems to study protein-lipid interactions (Morrisett *et al.*, 1977), our models not only contribute to the understanding of lipoprotein systems but also to other membrane binding peptides such as antibacterial peptides, peptide hormones, and lytic peptides (Kaiser & Kézdy, 1984; Segrest *et al.*, 1990).

REFERENCES

Abragam, A. (1961) *The Principles of Nuclear Magnetism* Oxford University Press, Oxford.

Acton, S., Rigotti, A., Landschulz, K.T., Xu, S., Hobbs, H.H., & Krieger, M. (1996) *Science* **271**, 518-520.

Agou, F., Yang, Y., Gesquiere, J.-C., Waller, J.-P., & Guittet, E. (1995) *Biochemistry* **34**, 569-576.

Alaupovic, P. (1996) *Methods Enzymol.* **263**, 32-60.

Aloy, P., Cedano, J., Oliva, B., Aviles, F.X., & Querol, E. (1997) *Comput. Appl. Biosci.* **13**, 231-234.

Anantharamaiah, G.M., Jones, J.L., Brouillette, C. G., Schmidt, C.F., Chung, B.H., Hughes, T.A., Bhown, A.S., & Segrest, J.P. (1985) *J. Biol. Chem.* **260**, 10248-10255.

Anantharamaiah, G.M., Venkatachalapathi, Y.V., Brouillette, C.G., & Segrest, J.P. (1990) *Arteriosclerosis* **10**, 95-105.

Anfinsen, C.B. (1973) *Science* **181**, 223-230.

Arnold, R.S. & Cornell, R.B. (1996) *Biochemistry* **35**, 9917-9924.

Assmann, G., Highet, R.J., Sokoloski, E.A., & Brewer, H.B., Jr. (1974) *Pro. Nat. Acad. Sci. U.S.A.* **71**, 3701-3705.

Austin, K., Brown, L.R. & Stewart, P.R. (1975) *J. Membrane Biol.* **24**, 55-69.

Azpiazu, I., Gomez-Fernandez, J.C., Chapman, D. (1993) *Biochemistry* **32**, 10720-10726.

Backlund, B-M., Wikander, G., Peeters, T.L., & Gräslund, A. (1994) *Biochim. Biophys. Acta* **1190**, 337-344.

Bairaktari, E., Mierke, D.F., Mammi, S., & Peggion, E. (1990) *Biochemistry* **29**, 10090-10096.

Baker, E.N. & Hubbard, R.E. (1984) *Prog. Biophys. Molec. Biol.* **44**, 97-179.

Baker, H.N., Delahunty, T., Gotto, A.M., Jr., & Jackson, R.L. (1974) *Proc. Natl. Acad. Sci. U.S.A.* **71**, 3631-3634.

Banka, C.L., Bonnet, D.J., Black, A.S., Smith, R.S. & Curtiss, L.K. (1991) *J. Biol. Chem.* **266**, 23886-23892.

Barany, G. and Merrifield, R.B.(1980) in *The Peptides: Analysis, Synthesis, Biology* (E. Gross and J. Meienhofer, Eds.), pp. 3-284, Academic Press, New York.

Barker, W.C. & Dayhoff, M.O. (1977) *Comp. Biochem. Physiol.* **57B**, 309-315.

Barkia, A., Puchois, P., Ghalim, N., & Torpier, G. (1991) *Atherosclerosis* **87**, 135-146.

Barlow, D.J. & Thornton, J.M. (1988) *J. Mol. Biol.* **201**, 610-619.

Barrans, A., Jaspard, B., Barbaras, R., Chap, H., Perret, B. & Collet, X. (1996) *Biochim. Biophys. Acta* **1300**, 73-85.

Barter, P.J. & Rye, K.A. (1996) *Atherosclerosis* **121**, 1-12.

Basu, G., Bagchi, K. & Kuki, A. (1991) *Biopolymers* **31**, 1763-1774.

Bax, A. & Davis, D.G. (1985) *J. Magn. Reson.* **65**, 355-360.

Bax, A. & Grzesiek, S. (1993) *Acc. Chem. Res.* **26**, 131-138.

Bazzo, R., Tappin, M.J., Postore, A., Harvey, T.S., Carver, J.A., & Campbell, I.D. (1988) *Eur. J. Biochem.* **173**, 139-146.

Bergeron, J., Frank, P.G., Emmanuel, F., Latta, M., Zhao, Y., Sparks, D.L., Rassart, E., Denèfle, P., & Marcel, Y.L. (1997) *Biochim. Biophys. Acta* **1344**, 139-152.

Berndt, K.D., Güntert, P., & Wüthrich, K. (1996) *Proteins: Struct. Funct. Genet.* **24**, 304-313.

Bloch, F. (1946) *Phys. Rev.* **70**, 460-474.

Boguski, M.S., Elshourbagy, N., Taylor, J.M., & Gordon, J.I. (1984) *Proc. Natl. Acad. Sci. U.S.A.* **81**, 5021-5025.

Boucher, W., Laue, E.D., Campbell-Burk, S. & Domaille, P.J. (1992) *J. Am. Chem. Soc.* **114**, 2262-2264.

Branden, C. & Tooze, J. (1991) *Introduction to Protein Structure* Garland Publishing, Inc., New York & London.

Brasseur, R., De Meutter, J., Vanloo, B., Goormaghtigh, E., Ruysschaert, J.M. & Rosseneu, M. (1990) *Biochim. Biophys. Acta* **1043**, 245-252.

Brasseur, R., Lins, L., Vanloo, B., Ruysschaert, J.-M., & Rosseneu, M. (1992) *Proteins: Struct. Funct. Genet.* **13**, 246-257.

Braunschweiler, L. & Ernst, R.R. (1983) *J. Magn. Reson.* **53**, 521-528.

Breiter, D.R., Kanost, M.R., Benning, M.M., Wesenberg, G., Kaw, J.H., Wells, M.A., Rayment, I., & Holden, H.M. (1991) *Biochemistry* **30**, 603-608.

Breslow, J.L. (1996) *Science* **272**, 685-688.

Breslow, J.L., McPherson, J., Nussbaum, A.L., Williams, H.W., Lofquist-Kahl, F., Karathanasis, S.K., & Zannis, V.I. (1982) *J. Biol. Chem.* **257**, 14639-14641.

Brewer, H.B., Jr., Fairwell, T., LaRue, A., Ronan, R., Houser, A., & Bronzert, T.J. (1978) *Biochem. Biophys. Res. Commun.* **80**, 623-630.

Brewer, H.B., Jr., Lux, S.E., Ronan, R. & John, K.M. (1972) *Proc. Natl. Acad. Sci. U.S.A.* **69**, 1304-1308.

Brewer, H.B., Jr., Shulman, R., Herbert, P., Ronan, R. & Wehrly, K. (1974) *J. Biol Chem.* **249**, 4975-4984.

Brouillette, C.G. & Anantharamaiah, G.M. (1995) *Biochim. Biophys. Acta* **1256**, 103-129.

Brown, L.R. (1979) *Biochim. Biophys. Acta* **557**, 135-148.

Brown, L.R., & Wüthrich, K. (1977) *Biochim. Biophys. Acta* **468**, 389-410.

Brown, L.R., & Wüthrich, K. (1981) *Biochim. Biophys. Acta* **647**, 95-111.

Bruix, M., Parello, M., Herranz, J., Rico, M. & Nieto, J.L. (1990) *Biochem. Biophys. Res. Commun.* **167**, 1009-1014.

Buchko, G.W., Rozek, A., Wang, G., Frohlich, J.J. & Cushley, R.J. (1997) *Protein Pept. Lett.* **4**, 47-54.

Buchko, G.W., Rozek, A., Zhong, Q., & Cushley, R.J. (1995) *Pept. Res.* **8**, 86-94.

Buchko, G.W., Treleaven, W.D., Dunne, S.J., Tracey, A.S. & Cushley, R.J. (1996b) *J. Biol. Chem.* **271**, 3039-3045.

Buchko, G.W., Wang, G., Pierens, G.K., & Cushley, R.J. (1996a) *Int. J. Peptide Protein Res.* **48**, 21-30.

Burley, S.K. & Petsko, G.A. (1985) *Science* **229**, 23-28.

Burley, S.K. & Petsko, G.A. (1988) *Adv. Protein Chem.* **39**, 125-189.

Byler, D.M. & Susi, H. (1986) *Biopolymers* **25**, 469-487.

Calabresi, L., Franceschini, G, Burkybile, A., & Jonas, A. (1997) *Biochem. Biophys. Res. Commun.* **232**, 345-349.

Calabresi, L., Lucchini, A., Vecchio, G., Sirtori, C.R., & Franceschini, G. (1996) *Biochim. Biophys. Acta* **1304**, 32-42.

Calabresi, L., Meng, Q.-H., Castro, G.R., and Marcel, Y.L. (1993) *Biochemistry* **32**, 6477-6484.

Cann, J.R., Liu, X., Stewart, J.M., Gera, L., & Kotovych, G. (1994) *Biopolymers* **34**, 869-878.

Carpenter, K.A., Wilkes, B.C., Weltrowska, G. & Schiller, P.W. (1996) *Eur. J. Biochem.* **241**, 756-764.

Castro, G.R. & Fielding, C.J. (1988) *Biochemistry* **27**, 25-29.

Castro, G., Nihoul, L.P., Dengremont, C., de Geitère, C., Delfly, B., Tailleux, A., Fievet, C., Duverger, N., Denèfle, P., Fruchart, J.-C., & Rubin, E.M. (1997) *Biochemistry* **36**, 2243-2249.

Cavanagh, J., Fairbrother, W. J., Palmer III, A. G., & Skelton, N. J. (1996) *Protein NMR Spectroscopy* Academic Press, New York.

Chakrabartty, A. & Baldwin, R.L. (1995) *Adv. Protein Chem.* **46**, 141-176.

Chen, S.-H., Yang, C.Y., Chen, P.-F., Setzer, D., Tanimura, M., Li, W.-H., Gotto, A.M., Jr., & Chan, L. (1986) *J. Biol. Chem.* **261**, 12918-12921.

Chen, T.C., Sparrow, J.T., Gotto, A.M., Jr., & Morrisett, J.D. (1979) *Biochemistry* **18**, 1617-1622.

Chen, Y.-H., Yang, J.T., & Martinez, H.M. (1972) *Biochemistry* **11**, 4120-4131.

Cheung, M.C. & Albers, J.J. (1977) *J. Clin. Invest.* **60**, 43-50.

Cheung, M.C., Segrest, J.P., Albers, J.J., Cone, J.T., Brouillette, C.G., Chung, B.H., Kashyap, P.M., Glasscock, M.A., & Anantharamaiah, G.M. (1987) *J. Lipid Res.* **28**, 913-929.

Cheung, P. & Chan, L. (1983) *Nucleic Acids Res.* **11**, 3703-3715.

Chupin, V., Killian, J.A., Breg, J., De Jongh, H.H.J., Boelens, R., Kaptein, R., & De Kruijff, B. (1995) *Biochemistry* **34**, 11617-11624.

Clark-Lewis, I., Aebersold, R.A., Ziltner, H., Schrader, J.W., Hood, L.A., & Kent, S.B.H. (1986) *Science* **231**, 134-139.

Clore, G. & Gronenborn, A (1989) *CRC Crit. Rev. Biochem. Mol. Biol.* **24**, 479-564.

Clore, G. & Gronenborn, A (1991) *Prog. NMR Spectrosc.* **23**, 43-92.

Clore, G. & Gronenborn, A (1991) *Science* **252**, 1390-1399.

Clore, G., Gronenborn, A., Nilges, M., & Ryan, C. (1987) *Biochemistry* **26**, 8012-8023.

Cordier-Ochsenbein, F., Guerois, R., Baleux, F., Huynh-Dinh, T., Chaffotte, A., Neumann, J.-M., & Sanson, A. (1996) *Biochemistry* **35**, 10347-10357.

Cowan, S.W.,Schirmir, T., Rummel, G., Steiert, M., Ghosh, R., Pauptit, R.A., Jansonius, J.N. & Rosenbusch, J.P. (1992) *Nature* **358**, 727-733.

Crespi, H.L., Rosenberg, R.M., & Katz, J.J. (1968) *Science* **161**, 795-796.

Crippen, G.M. (1977) *J. Comput. Phys.* **24**, 96-107.

Crippen, G.M. (1981) *Distance Geometry and Conformational Calculations*, Research Studies Press, Wiley, New York.

Crippen, G.M. & Havel, T.F. (1978) *Acta Cryst.* **A34**, 282-284.

Crippen, G.M. and Havel, T.F. (1988) *Distance Geometry and Molecular Conformation* Research Studies Press Ltd., Taunton, Somerset, England.

Cushley, R.J., Tracey, A.S., Zhong, Q., Treleaven, W.D., & Wang, G. (1994) in *Peptide: Chemistry, Structure and Function* (R.S. Hodges and J.A. Smith, Eds.), pp. 774-776, ESCOM, Leiden, The Netherlands.

Davidson, W.S., Hazlett, T., Mantulin, W.W., & Jonas, A. (1996) *Proc. Natl. Acad. Sci. U.S.A.* **93**, 13605-13610.

De Backer, G., Rosseneu, M., & Deslypere, J.P. (1982) *Atherosclerosis* **42**, 197-203.

Deisenhofer, J., Epp, O., Miki, K., Huber, R., & Michel, H. (1985) *Nature* 318, 618-624.

Déméné, H., Jullian, N., Morellet, N., De Rocquigny,H., Cornille, F., Maigret, B., & Roques, B.P. (1994) *J. Biomol. NMR* **4**, 153-170.

De Pauw, M., Vanloo, B., Weisgraber, K., & Rosseneu, M. (1995) *Biochemistry* **34**, 10953-10960.

Di Stefano, D.L. & Wand, A.J. (1987) *Biochemistry* **26**, 7272-7281.

Doak, D.G., Mulvey, D., Kawaguchi, K., Villalain, J. & Campbell, I.D. (1996) *J. Mol. Biol.* **258**, 672-687.

Donovan, J.M., Benedek, G.B., & Carey, M.C. (1987) *Biochemistry* **26**, 8116-8125

Doucet, J.-P. & Weber, J. (1996) *Computer-Aided Molecular Design Theory and Applications* Academic Press, London, San Diego, New York.

Drayna, D., Fielding, C., Mclean, J., Baer, B., Castro, G., Chen, E., Comstock, L., Henzel, W., Kohr, W., Rhee, L., *et al.* (1986) *J. Biol. Chem.* **261**, 16535-16539.

Dunne, S.J., Cornell, R.B., Johnson, J.E., Glover, N.R., & Tracey, A.S. (1996) *Biochemistry* **35**, 11975-11984.

Dwek, R.A. (1973) *Nuclear Magnetic Resonance in Biochemistry* Clarendon Press, Oxford.

Dyer, C.A., Cistola, D.P., Parry, G.C., & Curtiss, L.K. (1995) *J. Lipid Res.* **36**, 80-88.

Dyson, H.J., Merutka, G., Waltho, J.P., Lerner, R.A., & Wright, P.E. (1992) *J. Mol. Biol.* **226**, 795-817.

Dyson, H.J., Rance, M., Houghten, R.A., Wright, P.E., & Lerner, R.A. (1988) *J. Mol. Biol.* **201**, 201-217.

Easthope, P.L. & Havel, T.F. (1989) *Bull. math. Biol.* **51**, 173-194.

Edelstein, C., Kezdy, F.J., Scanu, A.M. & Shen, B.W. (1979) *J. Lipid Res.* **20**, 143-153.

Efimov, A.V. (1993) *Prog. Biophys. molec. Biol.* **60**, 201-239.

Eisenberg, D., Weiss, R.M., Terwilliger, T.C. & Wilcox, W. (1982) *Faraday Symp. Chem. Soc.* **17**, 109-120.

Elliot, A. & Ambrose, E.J. (1950) *Nature* **165**, 921-922.

Elshourbagy, N.A., Walker, D.W., Boguski, M.S., Gordon, J.I., & Taylor, J.M. (1986) J. Biol. Chem. **261**, 1998-2002.

Emmanuel, F., Steinmetz, A., Rosseneu, M., Brasseur, R., Gosselet, N., Attenot, F., Cuine, S., Seguret, S., Latta, M., Fruchart, J.C. *et al.* (1994) *J. Biol. Chem.* **269**, 29883-29890.

Englander, S.W. & Kallenbach, N.R. (1983) *Q. Rev. Biophys.* **16**, 521-655.

Englander, S.W. & Wand, A.J. (1987) *Biochemistry* **26**, 5953-5958.

Engleman, D.M., Goldman, A., & Steitz, T.A. (1982) *Methods Enzymol.* **88**, 81-88.

Epand, R.M., Shai, Y., Segrest, J.P., & Anantharamaiah, G.M. (1995) *Biopolymers* **37**, 319-338.

Ernst, R.R. (1994) *Bull. Magn. Reson.* **16**, 5-32.

Ernst, R.R. (1996) in "*Encyclopedia of Nuclear Magnetic Resonance*" (D.M. Grant & R.K. Harris, Eds.), pp. 293-305, John Wiley & Sons, Chichester, New York.

Ernst, R.R., Bodenhausen, G.B., and Wokaun, A. (1987) *Pricinples of Nuclear Magnetic Resonance in One and Two Dimensions* Oxford University Press, Oxford.

Evans, J.N.S. (1995) *Biomolecular NMR Spectroscopy* Oxford University Press, Oxford.

Fasman, G.D. (1996) in *Circular Dichroism and the Conformational Analysis of Biomolecules* (G.D. Fasman, Ed.), pp. 381-412, Plenum Press, New York.

Feigenson, G.W., Meers, P.R. & Kingsley, P.B. (1977) *Biochim. Biophys. Acta* **471**, 487-491.

Fenske, D.B., Chana, R.S., Parmar, Y.I., Treleaven, W.D. & Cushley, R.J. (1990) *Biochemistry* **27**, 4491-4500.

Fielding, C.J., Shore, V.G., & Fielding, P.E. (1972) *Biochem. Biophys. Res. Commun.* **46**, 1493-1498.

Fielding, P.E., Kawano, M., Catapano, A.L., Zoppo, A., Marcovina, S., & Fielding, C.J. (1994) *Biochemistry* **33**, 6981-6985.

Finucane, M.D. & Jardetzky, O. (1996) *Protein Sci.* **5**, 653-662.

Fitch, W.M. (1977) *Genetics* **86**, 623-644.

Fogh, R.H., Schipper, D., Boelens, R., & Kaptein, R. (1994) *J. Biomol. NMR* **4**, 123-128.

Folkers, P.J.M., Clore, G.M., Driscoll, P.C., Dodt, J., Köhler, S., & Gronenborn, A.M. (1989) *Biochemistry* **28**, 2601-2617.

Forrest, B.J. & Cushley, R.J. (1977) *Atherosclerosis* **28**, 309-318.

Frank, P.G., Bergeron, J., Emmanuel, F., Lavigne, J.-P., Sparks, D.L., Denèfle, P., Rassart, E., & Marcel, Y.L. (1997) *Biochemistry* **36**, 1798-1806.

Freeman, R. (1994) in *Nuclear Magnetic Resonance in Modern Technology* (G.E. Maciel, Ed.), pp. 23-56, Kluwer Academic Publishers, Dordrecht, Boston & London.

Freifelder, D. (1976) *Physical Biochemistry Application to Biochemistry and Molecular Biology*, pp. 410-443, W.H. Freeman and Company, San Francisco.

Friebolin, H. (1991) *Basic One- and Two-Dimensional NMR spectroscopy* VCH Verlagsgesellschaft, Weinheim, Germany.

Frishman, D. & Argos, P. (1997) *Proteins, Struct. Funct. & Genet.* **27**, 329-335.

Fukushima, D., Yokoyama, S., Kroon, D.J., Kézdy, F.J., & Kaiser, E.T. (1980) *J. Biol. Chem.* **255**, 10651-10657.

Garrett, D.S., Seok, Y.-J., Liao, D.-I., Peterkofsky, A., Gronenborn, A.M., & Clore, G.M. (1997) *Biochemistry* **36**, 2517-2530.

Gesell, J., Zasloff, M. & Opella, S.J. (1997) *J. Biomol. NMR* **9**, 127-135.

Gibbons, W.A., Crepaux, D., Delayre, J., Dunand, J.-J., Hajdukovic, & Wyssbrod, H.R. (1976) in *Peptides: Chemistry, Structure and Biology* (R. Walter & J. Meienhofer, Eds.), pp. 127-137, Ann Arbor, New York.

Gierasch, L.M., Lacy, J.E., Thompson, K.F., Rockwell, L. & Watnick, P.I. (1982) *Biophys. J.* **37**, 275-284.

Gill, S.C. & von Hippel, P.H. (1989) *Anal. Biochem.* **182**, 319-326.

Glomset, J.A. (1968) *J. Lipid Res.* **9**, 155-167.

Gofman, J.W., Lindgren, F.T., & Elliott, H. (1949) *J. Biol. Chem.* **179**, 973.

Griesinger, C., Sorensen, O.W., & Ernst, R.R. (1989) *J. Magn. Reson.* **84**, 14-63.

Gronenborn, A.M., & Clore, G.M. (1995) *CRC Crit. Rev. Biochem. Mol. Biol.* **30**, 351-385.

Gwynne, J., Brewer, H.B., Jr. and Edelhoch, H. (1974) *J. Biol. Chem.* **249**, 2411-2416.

Haltia, T. & Freire, E. (1995) *Biochim. Biophys. Acta* **1228**, 1-27.

Hanakam, F., Gerisch, G., Lotz, S., Alt, T. & Seelig, A. (1996) *Biochemistry* **35**, 11036-11044.

Harris, P.I. & Chapman, D. (1995) *Biopolymers* **37**, 251-263.

Havel, R.J., Eder, H.A. & Bragdon, J.H. (1955) *J. Clin. Invest.* **34**, 1345-1354.

Havel, T.F. (1990) *Biopolymers* **29**, 1565-1585.

Havel, T.F. (1991) *Prog. Biophys. Molec. Biol.* **56**, 43-78.

Havel, T.F. (1996) in *Encyclopedia of Nuclear Magnetic Resonance* (D.M. Grant & R.K. Harris, Eds.), pp. 1701-1710, John Wiley & Sons, Chichester, New York.

Havel, T.F., Kuntz, I.W., & Crippen, G.M. (1983) *Bull. math. Biol.* **45**, 665-720.

Havel, T.F. & Wüthrich, K. (1984) *Bull. math. Biol.* **46**, 673-698.

Havel, T.F. & Wüthrich, K. (1984) *J. Mol. Biol.* **182**, 281-294.

Helenius, A., McCaslin, D.R., Fries, E., & Tanford, C. (1979) *Methods Enzymol.* **56**, 734-749.

Henry, G.D. & Sykes, B.D. (1994) *Methods Enzymol.* **239**, 515-535.

Heukeshoven, J. & Dernick, R. (1985) *Electrophoresis* **6**, 103-112

Hirsh, D.J., Hammer, J., Maloy, W.L., Blazyk, J., & Schaefer, J. (1996) *Biochemistry* **35**, 12733-12741.

Holvoet, P. Zhao, Z., Deridder, E., Dhoest, A., & Collen, D. (1996) *J. Biol. Chem.* **271**, 19395-19401.

Holvoet, P. Zhao, Z., Vanloo, B., Vos, R., Deridder, E., Dhoest, A., Taverrne, J., Brouwers, E., Demarsin, E., Engelborghs, Y., Rosseneu, M., Collen, D., & Brasseur, R. (1995) *Biochemistry* **34**, 13334-13342.

Holzwarth, G.M. & Doty, P. (1965) *J. Am. Chem. Soc.* **87**, 218-228.

Ihara, S., Ooi, T., & Takahashi, S. (1982) *Biopolymers* **21**, 131-145.

Ikura, M., Kay, L.E., Bax, A. (1990) *Biochemistry* **29**, 4659-4667.

Inagaki, F., Shimada, I., Kawaguchi, K., Hirano, M., Terasawa, I., Ikura, T., & Go, N. (1989) *Biochemistry* **28**, 5985-5991.

Innerarity, T.L., Friedlander, E.J., Rall, R.L., Jr., Weisgraber, & K.H., Mahley, R.W. (1983) *J. Biol. Chem.* **258**, 12341-12347.

Innerarity, T.L., Pitas, R.E., & Mahley, R.W. (1979) *J. Biol. Chem.* **254**, 4186-4190.

Jackson, R.L., Baker, H.N., Gilliam, E.B., & Gotto, A.M., Jr. (1977) *Proc. Natl. Acad. Sci. U.S.A.* **74**, 1942-1945.

Jackson, R.L., Morrisett, J.D., Pownall, H.J., & Gotto, A.M., Jr. (1973) *J. Biol. Chem.* **248**, 5218-5224.

Jacobs, R.E. & White, S.H. (1989) *Biochemistry* **28**, 3421-3437.

Jahn, C.E., Osborne, J.O., Schaefer, E.J. & Brewer, H.B., Jr. (1983) *Eur. J. Biochem.* **131**, 25-29.

Jardetzky, O. & Roberts, G.C.K. (1981) *NMR in Molecular Biology* Academic Press, New York.

Jardetzky, O., Wade, N.G., & Fisher, J.J. (1963) *Nature* **197**, 183-184.

Jeener, J., Meier, B.H., Bachmann, P., & Ernst, R.R. (1979) *J. Chem. Phys.* **71**, 4546-4553.

Ji, Y. & Jonas, A. (1995) *J. Biol. Chem.* **270**, 11290-11297.

Jimenez, M.A., Nieto, J.L., Herranz, J., Rico, M., & Santoro, J. (1987) *FEBS Lett.* **221**, 320-324.

Johnson, B.A., Stevens, S.P., & Williamson, J.M. (1994) *Biochemistry* **33**, 15061-15070.

Johnson, C.E. & Bovey, F.A. (1958) *J. Chem. Phys.* **29**, 1012-1014.

Johnson, J.E. & Cornell, R.B. (1994) *Biochemistry* **33**, 4327-4335.

Johnson, P.E., Joshi, M.D., Tomme, P., Kilburn, D.G., & McIntosh, L.P. (1996) Biochemistry **35**, 14381-14394.

Johnson, W.C., Jr. (1990) *Proteins: Struct., Funct., Genet.* **7**, 205-214.

Jonas, A. (1986) *Methods Enzymol.* **128**, 553-582.

Jonas, A. (1992) in *Structure and Function of Apolipoproteins* (M. Rosseneu, Ed.), pp. 217-250, CRC Press, Boca Raton, Ann Arbor, London, Tokyo.

Jonas, A., Steinmetz, A., & Churgay, L. (1993) *J. Biol. Chem.* **268**, 1596-1602.

Jonas, A., Kézdy, K.E., & Wald, J.H. (1989) *J. Biol. Chem.* **264**, 4818-4824.

Kaiser, R. (1965) *J. Chem. Phys.* **42**, 1838-1839.

Kaiser, E.T. & Kézdy, F.J. (1984) *Science* **223**, 249-255.

Kallick, D.A., Tessmer, M.R., Watts, C.R., & Li, C.-Y. (1995) *J. Magn. Res.* **B109**, 60-65.

Kanellis, P., Romans, A.Y., Johnson, B.J., Kercret, H., Chiovetti, R., Jr., Allen, T.M., & Segrest, J.P. (1980) *J. Biol. Chem.* **255**, 11464-11472.

Karathanasis, S.K., Zannis, V.I., & Breslow, J.L. (1983) *Proc. Natl. Acad. Sci. U.S.A.* **80**, 6147-6151.

Karplus, P.A. (1997) *Protein Science* **6**, 1302-1307.

Karplus, R. (1963) *J. Am. Chem. Soc.* **85**, 2870-2871.

Kay, L.E. (1995) *Curr. Opin. Struct. Biol.* **5**, 674-681.

Kay, L.E., Clore, G.M., Bax, A. & Gronenborn, A.M. (1990) *Science* **249**, 411-414.

Keeler, J., Clowes, R.T., Davis, A.L., Laue, E. (1994) *Methods Enzymol.* **239**, 145-207.

Kohda, D., Sawada, T., & Inagaki, F. (1991) *Biochemistry* **30**, 4896-4900.

Kuntz, I.D., Kosen, P.A., & Craig, E.C. (1991) *J. Am. Chem. Soc.* **113**, 1406-1408.

Kuntz, I.D., Thomason, J.F., & Oshiro, C.M. (1989) *Methods Enzymol.* **177**, 159-204.

Labeur, C., Lins, L., Vanloo, B., Baert, J., Brasseur, R., Rosseneu, M. (1997) *Arterioscler. Thromb. Vasc. Biol.* **17**, 580-588.

Lagocki, P.A. & Scanu, A.M. (1980) *J. Biol. Chem.* **255**, 3701-3706.

Lakowicz, J.R. (1983) *Priciples of Fluorescence Spectroscopy* Plenum Press, New York.

Lamon-Fava, S., Sastry, R., Ferrari, S., Rajavashisth, T.B., Lusis, A.J., & Karathanasis, S.K. (1992) *J. Lipid. Res.* **33**, 831-842.

Landolt-Marticorena, C., Williams, K.A., Deber, C.M. & Reithmeier, R.A.F. (1993) *J. Mol. Biol.* **229**, 602-608.

Lauterwein, J., Bösch, C., Brown, L.R., & Wüthrich, K (1979) *Biochim. Biophys. Acta* **556**, 244-264.

LeMaster, D.M. & Richards, F.M. (1988) *Biochemistry* **27**, 142-150.

Li, W.H., Tanimura, M., Luo, C.C., Datta, S., Chan, L. (1988) *J. Lipid Res.* **29**, 245-271.

Linderström-Lang, K.U. & Schellman, J.A. (1959) *The Enzymes* **1**, 443-510.

Lins, L., Brasseur, R., De Pauw, M., Van Biervliet, J.P., Ruysschaert, J.-M., Rosseneu, M., & Vanloo, B. (1995) *Biochim. Biophys. Acta* **1258**, 10-18.

Lins, L., Rosseneu, M., Ruysschaert, J.-M., & Brasseur, R. (1992) in *Structure and Function of Apolipoproteins* (Rosseneu, M., Ed.), pp. 251-268, CRC Press, Boca Raton, Ann Arbor, London, Tokyo

Liu, X., Stewart, J.M., Gera, L., & Kotovych, G. (1993) *Biopolymers* **33**, 1237-1247.

Lowe, J.P. (1993) *Quantum Chemistry* (2nd Ed.) Academic Press, Inc., Boston, San Diego, New York, London, Sydney, Tokyo, Toronto.

Lowry, H.O., Rosebrough, N.J., Farr, A.L., & Randall, R.J. (1951) *J. Biol. Chem.* **193**, 265-275.

Luc, G., Bard, J.M., Poulain, P., Arveiler, D., Evans, A.E., Cambien, F., Fruchart, J.C., Ducimetiere, P. (1997) *Eur. J. Clin. Invest.* **27**, 242-247.

Luidens, M.K., Figge, J., Breese, K., & Vajda, S. (1995) *Biopolymers* **39**, 367-376.

Lund-Katz, S., Ibdah, J.A., Letizia, J.Y., Thomas, M.T. & Phillips, M.C. (1988) *J. Biol. Chem.* **263**, 13831-13838.

Lund-Katz, S., Weisgraber, K.H., Mahlay, R.W. & Phillips, M.C. (1993) *J. Biol. Chem.* **268**, 23008-23015.

Lycksell, P.-O., Öhman, A., Bengtsson-Olivecrona, G., Johansson, L.B., Wijmeng, S.S., Wernic, D., Gräslund, A. (1992) *Eur. J. Biochem.* **205**, 223-231.

McDonnell, P.A. & Opella, S.J. (1993) *J. Magn. Reson.* **B102**, 102-125.

McDonnell, P.A., Shon, K., Kim, Y., & Opella, S.J. (1993) *J. Mol. Biol.* **233**, 447-463.

McEvoy, M.M., de la Cruz, A.F.A. & Dahlquist, F.W. (1997) *Nature Struct. Biol.* **4**, 9.

McLachlan, A.D. (1977) *Nature* **267**,465-466.

McLean, L.R., Hagaman, K.A., Owen, T.J., & Krstenansky, J.L. (1991) *Biochemistry* **30**, 31-37.

Mcleod, R., Lacko, A.G., Pritchard, P.H. & Frohlich, J. (1986) *J. Chromatogr.* **381**, 271-283.

Macquaire, F., Baleux, F., Huyhn-Dinh, T., Rouge, D., Neumann, J.-M., & Sanson, A. (1993) *Biochemistry* **32**, 7244-7254.

Maguire, G.F., Lee, M., & Connelly, P.W. (1989) *J. lipid Res.* **30**, 757-761

Mahley, R.W. & Innerarity, T.L. (1983) *Biochim. Biophys. Acta* **737**, 197-222.

Mao, S.J.T., Jackson, R.L., Gotto, A.M., Jr., & Sparrow, J.T. (1981) *Biochemistry* **20**, 1676-1680.

Marcel, Y.L., Provost, P.R., Koa, H., Raffai, E., Dac, N.V., Fruchart, J-C., & Rassart, E. (1991) *J. Biol. Chem.* **266**, 3644-3653.

Marion, D., Driscoll, P.C., Kay, L.E., Wingfield, P.T., Bax, A., Bronenborn, A.M. & Clore, G.M. (1989) *Biochemistry* **28**, 6150-6156.

Marion, D., Ikura, M., & Bax, A. (1989) *J. Magn. Reson.* **84**, 425-430.

Marion, D. & Wüthrich, K. (1983) *Biochem. Biophys. Res. Commun.* **113**, 967-974.

Markley, J.L., Meadows, D.H. & Jadetzky, O. (1967) *J. Mol. Biol.* **27**, 25-40.

Markley, J.L., Putter, I., & Jadetzky, O. (1968) *Science* **161**, 1249-1251.

Meng, Q.-H., Calabresi, L., Fruchart, J.-C., & Marcel, Y.L. (1993) *J. Biol. Chem.* **268**, 16966-16973.

Merutka, G. & Stellwagen, E. (1991) *Biochemistry* **30**, 1591-1594.

Mezdour, H., Clavey, V., Kora, I., Koffigan, M., Barkia, A. & Fruchart, J.-C. (1987) *J. Chromatogr.* **414**, 35-45.

Miller, N.E. (1987) *Am. Heart J.* **113**, 589-597.

Minnich, A., Collet, X., Roghani, A., Cladaras, C., Hamilton, R.L., Feilding, C.J., & Zannis, V.I. (1992) *J. Biol. Chem.* **267**, 16553-16560.

Mishra, V.K., & Palgunachari, M.N. (1996) *Biochemistry* **35**, 11210-11220.

Mishra, V.K., Palgunachari, M.N., Segrest, J.P., & Anantharamaiah, G.M. (1994) *J. Biol. Chem.* **269**, 7185-7195.

Momany, F.A., McGuire, R.F., Burgess, A.W. & Scheraga, H.A. (1975) *J. Phys. Chem.* **79**, 2361-2381.

Morrisett, J.D., Jackson, R.L., & Gotto, A.M., Jr. (1977) *Biochim. Biophys. Acta* **472**, 93-133.

Mowri, H.-O., Patsch, J.R., Gotto, A.M., Jr., & Patsch, W. (1996) *Arterioscler. Thromb. Vasc. Biol.* **16**, 755-762.

Munoz, V., Blanco, F.J., & Serrano, L. (1995) *Nature Struct. Biol.* **2**, 380-385.

Narayanaswami, V., Kay, C.M., Oikawa, K. & Ryan, R.O. (1993) *Biochemistry* **33**, 13312-13320.

Nakagawa, S.H., Lau, H.S.H., Kézdy, F.J., & Kaiser, E.T. (1985) *J. Am. Chem. Soc.* **107**, 7087-7092.

Nelson, J.W. & Kallenback, N.R. (1989) *Biochemistry* **28**, 5256-5261.

Nichols, A.V. (1990) In *Advances In Cholesterol Ressearch* (M. Esfahani & T.B. Swaney, Eds.), pp. 313-365, The Telford Press, New Jersey.

Nicholson, H., Anderson, D.E., Dao-pin, S., & Matthews, B.W. (1991) *Biochemistry* **30**, 9816-9828.

Niles, M., Clore, G.M. & Gronenborn, A.M. (1988) *FEBS. Lett.* **239**, 129-136.

Noggle, J.H. & Schirmer, R.E. (1971) *The Nuclear Overhauser Effect* Academic Press, New York & London.

Nolte, R.T. & Atkinson, D. (1992) *Biophys. J.* **63**, 1221-1239.

Nozaki, Y. & Tanford, C. (1971) *J. Biol. Chem.* **246**, 2211-2217.

Öhman, A., Lycksell, P.-O., & Gräslund, A. (1993) *Eur. Biophys. J.* **22**, 351-357.

O'Neil, J.D.J. & Sykes, B.D. (1989) *Biochemistry* **28**, 699-707.

Opella, S.J., Chirlian, L.E., & Bechinger, B. (1997) in *Biological NMR Spectroscopy* (J. L. Markley & S.J. Opella, Eds.), pp. 139-156, Oxford University Press, New York, Oxford.

Opella, S.J. & Marassi, F.M. (1996) in *Encyclopedia of Nuclear Magnetic Resonance* (D.M. Grant & R.K. Harris, Eds.), pp. 2994-3003, John Wiley & Sons, Chichester, New York.

Ösapay, K. & Case, D.A. (1991) *J. Am. Chem. Soc.* **113**, 9436-9444.

Ösapay, K. & Case, D.A. (1994) *J. Biomol. NMR* **4**, 215-230.

Osborne, J.C., Jr. & Brewer, H.B., Jr. (1977) *Adv. Protein Chem.* **31**, 253-327.

Oschkinat, H., Müller T. & Dieckman (1994) *Angew Chem. Int. Ed. Engl.* **33**, 277-293.

Oschkinat, H., Griesinger, C., Kraulis, P.J., Sorensen, O.W., Ernst, R.R., Gronenborn, A.M., & Clore, G.M. (1988) *Nature* **332**, 374-376.

Otter, A., Scott, P.G., Cann, J.R., Vavrek, R.J., Stewart, J.M., & Kotovych, G. (1989) *J. Biomol. Struct. Dyn.* **6**, 609-625.

Otter, A., Scott, P.G., Liu, X., & Kotovych, G. (1989) *J. Biomol. Struct. Dyn.* **7**, 455-475.

Otting, G., Widmer, H., Wagner, G., & Wüthrich, K. (1986) *J. Magn. Reson.* **66**, 187-193.

Paananen, K., Saarinen, J., Annila, A., & Kovanen, P.T. (1995) *J. Biol. Chem.* **270**, 12257-12262.

Palgunachari, M.N., Mishra, V.K., Lund-Katz, S., Phillips, M.C., Adeyeye, S.O., Alluri, S., Anantharamaiah, & G.M., Segrest, J.P. (1996) *Arterioscler. Thromb. Vasc. Biol.* **16**, 329-338.

Pallaghy, P.K., Scanlon, M.J., Monks, S.A. & Norton, R.S. (1995) *Biochemistry* **34**, 3782-3794.

Papavoine, C.H.M., Konings, R.N.H., Hilbers, C.W., & van de Ven, F.J.M. (1994) *Biochemistry* **33**, 12990-12997.

Parker, W. & Stezowski, J.J. (1996) *Proteins: Struct. Funct. & Genet.* **25**, 253-260.

Parmar, Y.I., Gorrissen, H., Wassall, S.R. & Cushley, R.J. (1985) *Biochemistry* **24**, 171-176.

Pastore, A. & Saudek, V. (1990) *J. Magn. Reson.* **90**, 165-176.

Patsch, W. & Gotto, A.M., Jr. (1996) *Method Enzymol.* **263**, 3-32.

Peitsch, M.C., Kress, A., Lerch, P.G., Morgenthaler, J.-J., Isliker, H., & Heiniger, H.-J. (1989) *Anal. Biochem.* **178**, 301-305.

Perczel, A., Hollósi, M., Tusnády, G., & Fasman, G.D. (1991) *Protein Engineering* **4**, 669-679.

Perczel, A., Park, K. & Fasman, G.D. (1992) *Anal. Biochem.* **203**, 83-93.

Perrin, C.L., Dwyer, T.J., Rebek, J., Jr., Duff, R.J. (1990) *J. Am. Chem. Soc.* **112**, 3122-3125.

Perutz, M.F., Kendrew, J.C. & Watson, H.C. (1965) *J. Mol. Biol.* **13**, 669-678.

Pierens, G.K., Buchko, G.W., Wang, G., Treleaven, W.D., Rozek, A. & Cushley, R.J. (1995) *Bull. Magn. Reson.* **17**, 292-293.

Piotto, M., Saudek, V., & Sklenár, V. (1992) *J. Biomol. NMR* **2**, 661-665.

Plateau, P. & Guéron, M. (1982) *J. Am. Chem. Soc.* **104**, 7310-7311.

Plesniak, L.A., Wakarchuk, W.W., McIntosh, L.P. (1996) *Protein Sci.* **5**, 1118-1135.

Poirier, J., Minnich, A. & Davignon, J. (1995) *Ann. Med.* **27**, 663-670.

Ponsin, G., Sparrow, J.T., Gotto, A.M., Jr., & Powall, H.J. (1986) *J. Clin. Invest.* **77**, 559-567.

Poole, C.P., Jr. & Farach, H.A. (1987) *Theory of Magnetic Resonance* (2nd Ed.) John Wiley & Sons, New York.

Pownall, H.J. & Gotto, A.M., Jr. (1992) in *Structure and Function of Apolipoproteins* (Rosseneu, M., Ed.), pp. 1-32, CRC Press, Boca Raton, Ann Arbor, London, Tokyo.

Pownall, H.J., Hu, A., Gotto, A.M., Jr., Albers, J.J., & Sparrow, J.T., & (1980) *Proc. Natl. Acad. Sci. U.S.A.* **77**, 3154-3158.

Pownall, H.J., Massey, J.B., Sparrow, J.T., & Gotto, A.M., Jr. (1987) In *Plasma Lipoproteins* (A.M. Gotto, Jr., Ed.), pp. 95-127, Elsevier (Biomed. Div.), New York.

Raj, P.A., Soni, S.-D., & Levine, M.J. (1994) *J. Biol. Chem.* **269**, 9610-9619.

Rajan, R. & Balaram, P. (1996) *Int. J. Peptide Protein Res.* **48**, 328-336.

Rall, S.C., Jr., Weisgraber, K.H., & Mahley, R.W. (1982) *J. Biol. Chem.* **257**, 4171-4178.

Rance, M., Sørensen, O.W., Bodenhausen, G., Wagner, G. Enrst, R.R., & Wüthrich, K. (1983) *Biochem. Biophys. Res. Commun.* **117**, 479-485.

Raymond, S. & Weinstraub, L. (1959) *Science* **130**, 711.

Redfield, A.G. & Kuntz, S.D. (1975) *J. Magn. Reson.* **19**, 250-254.

Reijnggoud, D.J., Lund-Katz, S., Hauser, H., & Phillips, M.C. (1982) *Biochemistry* **21**, 2977-2983.

Remerowski, M.L., Domke, T., Groenewegen, A., Pepermans, H.A.M., Hilbers, C.W. & van de Ven, F.J.M. (1994) *J. Biomol. NMR* **4**, 257-278.

Revington, M.J., Lee, W., & Arrowsmith, C.H. (1997) in *Biological NMR Spectroscopy* (J.L. Markley & S.J. Opella, Eds.), pp. 50-66, Oxford University Press, New York Oxford.

Reynolds, J.A. (1982) in *Lipid-Protein Interactions Vol. 2* (P.C. Jost & O.H. Griffith, Eds.), pp. 193-224, Wiley, New York.

Ribeiro, A.A., Wemmer, D., Bray, R.P. & Jardetzky, O. (1981) *Biochem. Biophys. Res. Commun.* **99**, 668-674.

Rizo, J., Blanco, F.J., Kobe, B., Bruch, M.D., & Gierasch, L.M. (1993) *Biochemistry* **32**, 4881-4894.

Rogers, D.P., Brouillette, C.G., Engler, J.A., Tendian, S.W., Roberts, L., Mishra, V.K., Anantharamaiah, G.M., Lund-Katz, S., Phillips, M.C., & Ray, M.J. (1997) *Biochemistry* **36**, 288-300.

Rosseneu, M. (1992) *Structure and Function of Apolipoproteins* CRC Press, Boca Raton, Ann Arbor, London, Tokyo.

Rosseneu, M., Soetewey, F., Blaton, V., Lievens, J., & Peeters, H. (1976) *Chem. Phys. Lipids* **17**, 38-56.

Rosseneu, M., Van Tornout, P., Lievens, M.-J., & Assmann, G. (1981) *Eur. J. Biochem.* **117**, 347-352.

Rozek, A., Buchko, G.W., & Cushley, R.J. (1995) *Biochemistry* **34**, 7401-7408.

Rozek, A., Buchko, G.W., Kanda, P., & Cushley, R.J. (1997) *Protein Science* **In press.**

Rozek, A., Kanda, P. Weisgraber, K.H., & Cushley, R.J. (1996) in *XVIIth ICMRBS (International Conference on Magnetic Resonance in Biological System)* Keystone, Colorado.

Rubin, E.M., Kruss, R.M., Spangler, E.A., Verstuyft, J.G., & Clift, S.M. (1991) *Nature* **353**, 265-267.

Samsó, M., Daban, J.-R., Hansen, S. & Jones, G.R. (1995) *Eur. J. Biochem.* **232**, 818-824.

Scanu, A.M. (1978) In *Physical Aspects of Protein Interaction* (N. Catsimpoolas, Ed.), pp. 171-179, Elsevier, New York, Amsterdam & Oxford.

Scanu, A.M. & Edelstein, C. (1971) *Anal. Biochem.* **44**, 576-588.

Schiffer, C.A., Huber, R., Wuthrich, K., van Gunsteren, W.F. (1994) *J. Mol. Biol.* **241**, 588-599.

Schmidt, H.H.-J., Remaley, A.T., Stonik, J.A., Ronan, R., Wellmann, A., Thomas, F., Zech, L.A., Brewer, H.B., Jr. & Hoeg, J.M. (1995) *J. Biol. Chem.* **270**, 5469-5475.

Schulz, G.E. & Schirmer, R.H. (1979) *Principles of Protein Structure* Springer-Verlag, New York, Heidelberg, Berlin.

Schumaker,V.N. & Puppione, D.L. (1986) *Methods Enzymol.* **128**, 155-170.

Segrest, J.P., De Loof, H., Dohlman, J.G., Brouillette, C.G., & Anantharamaiah, G.M. (1990) *Proteins: Struct. Funct. Genet.* **8**, 103-117.

Segrest, J.P., Garber, D.W., Brouillette, C.G., Harvey, S.C., & Anantharamaiah, G.M (1994) *Adv. Protein Chem.* **45**, 303-369.

Segrest, J.P., Jackson, R.L., Morrisett, J.D., & Gotto, A.M., Jr. (1974) *FEBS lett.* **38**, 247-253.

Segrest, J.P., Jones, M.K., De Loof, H., Brouillette, C.G., Venkatachalapathi, Y.V., & Anantharamaiah, G.M. (1992) *J. Lipid Res.* **33**, 141-166.

Sejbal, J., Cann, J.R., Stewart, J.M., Gera, L., & Kotovych, G. (1996a) *J. Med. Chem.* **39**, 1281-1292.

Sejbal, J., Cann, J.R., Stewart, J.M., Gera, L., & Kotovych, G. (1996b) *Immunopharmacology* **33**, 198-200.

Sem, D.S. & Kasper, C.B. (1993) *Biochemistry* **32**, 11548-11558.

Serrano, L., Bycroft, M., & Fersht, A.R. (1991) *J. Mol. Biol.* **218**, 465-475.

Shan, X., Hardner, K.H., Muhandiram, D.R., Rao, N.S., Arrowsmith, C.H. & Kay, L.E. (1996) *J. Am. Chem. Soc.* **118**, 6570-6579.

Shanno, D.F. (1978) *Math. Oper. Res.* **3**, 244-256.

Shaw, D. (1984) *Fourier Transform N.M.R. Spectroscopy* (2nd Ed.) Elsevier, Amsterdam, Oxford, New York, Tokyo.

Shaw, R.A., Mantsch, H.H., Wang, G., Rozek, A., Buchko, G.W., Treleaven, W.D., & Cushley, R.J. (1997) *Biochemistry* **In revision**.

Shen, B.W., Scanu, A.M., & Kezdy, F.J. (1977) *Proc. Natl. Acad. Sci. U.S.A.* **74**, 837-841.

Shiffer, J. & Edmundson, A.B. (1967) *Biophys. J.* **7**, 121-135.

Shoemaker, K.R., Kim, P.S., York, E.J., Stewart, J.M., & Baldwin, R.L. (1987) *Nature* **326**, 563-567.

Shulman, R., Herbert, P., Wehrly, K., & Fredrickson, D.S. (1974) *J. Biol. Chem.* **250**, 182-190.

Shuker, S.B., Hajduk, P.J., Meadows, R.P., & Fesik, S.W. (1996) *Science* **274**, 1531-1534.

Siemion, I.Z., Cebrat, M., Jankowski, A., Lisowski, M., Pedyczak, A & Wyslouch, A. (1994) *Int. J. Peptide Protein Res.* **44**, 61-69.

Sklenár, V., Piotto, M., Leppik, R., & Saudek, V. (1993) *J. Magn. Reson.* **A102**, 241-245.

Solomon, I. (1955) *Phys. Rev.* **99**, 559-565.

Sorci-Thomas, M., Curtiss, L., Parks, J.S., Thomas, M.J. & Kearns, M.W. (1997) *J. Biol. Chem.* **272**, 7278-7284.

Sorci-Thomas, M., Kearns, M.W., & Lee, J.P. (1993) *J. Biol. Chem.* **268**, 21403-21409.

Sørensen, O.W., Eich, G.W., Levitt, M.H., Bodenhausen, G. & Ernst, R.R. (1983) *Prog. NMR Spectrosc.* **16**, 163-192.

Soutar, A.K., Garner, C.W., Baker, H.N., Sparrow, J.T., Jackson, R.L., Gotto, A.M., Jr. & Smith, L.C. (1975) *Biochemistry* **14**, 3057-3064.

Sparks, D.L., Davidson, W.S., Lund-katz, S., & Phillips, M.C. (1993) *J. Biol. Chem.* **268**, 23250-23257.

Sparks, D.L., Lund-katz, S., & Phillips, M.C. (1992) *J. Biol. Chem.* **267**, 25839-25847.

Sparrow, D.A., Laplaud, P.M., Saboureau, M., Zhou, G., Dolphin, P.J., Gotto, A.M., Jr., & Sparrow, J.T. (1995) *J. Lipid Res.* **36**, 485-495.

Sparrow, J.T. & Gotto, A.M. Jr. (1980) *Ann. N.Y. Acad. Sci.* **348**, 187-211.

Sparrow, J.T. & Gotto, A.M., Jr. (1982) *CRC Crit. Rev. Biochem.* **13**, 87-107.

Sparrow, J.T. & Monera, O.D. (1996) *Peptide Res.* **9**, 218-222.

Sparrow, J.T., Sparrow, D.A., Culwell, A.R., & Gotto, A.M., Jr. (1985) *Biochemistry* **24**, 6984-6988.

Sparrow, J.T., Sparrow, D.A., Fernando, G., Culwell, A.R., Kovar, M., & Gotto, A.M., Jr. (1992) *Biochemistry* **31**, 1065-1068.

Spuhler, P., Anantharamaiah, G.M., Segrest, J.P. & Seelig, J. (1994) *J. Biol. Chem.* **269**, 23904-23910.

Srinivas, R.V., Venkatachalapathi, Y.V., Rui, Z., Owens, R.J., Gupta, K.B., Srinivas, S.K., Anantharamaiah, G.M., Segrest, J.P., & Compans, R.W. (1991) *J. Cell. Biochem.* **45**, 224-237.

Stoffel, W., Zierenberg, O., Tunggal, B., & Schreiber, E. (1974) *Proc. Natl. Acad. Sci. U.S.A.* **71**, 3696-3700.

Stuart, D.I. & Jones, E.Y. (1997) *Nature* **386**, 437-438 (Comments on the largest protein complex published in the same issue).

Subbarao, N.K., Fielding, C.J., Hamilton, R.L., & Szoka, F.C. (1988) *Proteins Struct. Funct. Genet.* **3**, 187-198.

Sugiura, M., Maccioni, R.B., Cann, J.R., York, E.J., Stewart, J.M., & Kotovych, G. (1987) *J. Biomol. Struct. Dyn.* **4**, 1105-1117.

Surewicz, W.K., Epand, R.M., Pownall, H.J., & Hui, S.-W. (1986) *J. Biol. Chem.* **261**, 16191-16197.

Surewicz, W.K. & Mantsch, H.H. (1988) *Biochim. Biophys. Acta* **952**, 115-130.

Surewicz, W.K. & Mantsch, H.H. (1996) In *Spectroscopic Methods for Determinating Protein Structure in Solution* (H.A. Havel, Ed.), pp. 135-162, VCH Publishers, Inc., New York.

Susi, H. (1972) *Methods Enzymol.* **26**, 455-472.

Sviridov, D., Pyle, L., & Fidge, N. (1996) *Biochemistry* **35**, 189-196.

Swaney, J.B. & Weisgraber, K.H. (1994) *J. Lipid Res.* **35**, 134-142.

Szilágyi, L. (1995) *Prog. NMR Spectrosc.* **27**, 325-443.

Szilágyi, L. & Jardetzky, O. (1989) *J. Magn. Res.* **83**, 441-449.

Talussot, C. & Ponsin, G. (1994) *J. Theor. Biol.* **169**, 143-152.

Tanford, C. (1980) *The hydrophobic effect* (2nd Ed.), Wiley, New York.

Tanford, C. and Reynolds, J.A. (1976) *Biochim. Biophys. Acta* **457**, 133-170.

Teng, T., Barbeau, D.L., & Scanu, A.M. (1978) *Biochemistry* **17**,17-21.

Terwilliger, T.C., Weissman, L., & Eisenberg, D. (1982) *Biophys. J.* **37**, 353-361.

Thewalt, J.L. & Cushley, R.J. (1987) *Biochim. Biophys. Acta* **905**, 329-338.

Thewalt, J.L., Tulloch, A.P. & Cushley, R.J. (1986) *Chem. Phys. Lipids* **39**, 93-107.

Torchia, D.A., Sparks, S.W., & Bax, A. (1988) *J. Am. Chem. Soc.* **110**, 2320-2321.

Treleaven, W.D., Wassall, S.R. & Cushley, R.J. (1983) *Chem. Phys. Lipids* **33**, 223-231.

Uboldi, P., Spoladore, M., Fantappiè, S., Marcovina, S., & Catapano, A.L. (1996) *J. Lipid Res.* **37**, 2557-2568.

Utermann, G., Haas, J., Steinmetz, A., Pattzold, R., Rall, S.C., Weisgraber, K.H., & Mahley, R.W. (1984) *Eur. J. Biochem.* **144**, 326-331.

van de Ven, F.J.M. (1995) *Multidimensional NMR in liquids* VCH Publishers, Inc., New York.

Vanloo, B., Demoor, L., Boutillon, C., Lins, L., Brasseur, R., Baert, J., Fruchart, J.C., Tartar, A., & Rosseneu, M. (1995) *J. Lipid Res.* **36**, 1686-1696.

Vanloo, B., Morrison, J., Fidge, N., Lorent, G., Lins, L., Brasseur, R., Ruysschaert, J.M. & Rosseneu, M (1991) *J. Lipid Res.* **32**, 1253-1264.

Venters, R.A., Metzler, W.J., Spicer, L.D., Mueller, W.J., & Farmer, B.T., II (1995) *J. Am. Chem. Soc.* **117**, 9592-9593.

von Eckardstein, A., Castro, G., Wybranska, I., Theret, N., Duchateau, P., Duverger, N., Fruchart, J.C., Ailhaud, G. & Assman, G. (1993) *J. Biol. Chem.* **268**, 2616-2622.

Vuister, G.W., Boelens, R., Kaptein, R. (1988) *J. Magn. Reson.* **80**, 176-185.

Wagner, G., Braun, W., Havel, T.F., Schaumann, T., Go, N., Wüthrich, K. (1987) *J. Mol. Biol.* **196**, 611-639.

Wald, J.H., Krul, E.S., & Jonas, A. (1990) *J. Biol. Chem.* **265**, 20037-20043.

Wang, G., Pierens, G.K., Treleaven, W.D., Sparrow, J.T., & Cushley, R.J. (1996a) *Biochemistry* **35**, 10358-10366.

Wang, G., Sparrow, J.T., Naugler, D.G., Marcel, Y.L., & Cushley, R.J. (1997a) in *Frontiers of NMR in Molecular Biology-V*, p. 27, Taos, New Mexico.

Wang, G., Sparrow, J.T., & Cushley, R.J. (1997b) *Biochemistry* **In revision**.

Wang, G., Treleaven, W.D., & Cushley, R.J. (1996b) *Biochim. Biophys. Acta* **1301**, 174-184.

Warden, C., Hedrick, C.C., Qiao, J.-H., Castellani, L.W., & Lusis, A.J. (1993) *Science* **261**, 469-471.

Weisgraber, K.H. (1994) *Adv. Protein Chem.* **45**, 249-302.

Weisgraber, K.H. & Mahlay, R.W. (1996) *FASEB. J.* **10**, 1485-1494.

Weisgraber, K.H., Newhouse, Y.M. & McPherson, A. (1994) *J. Mol. Biol.* **236**, 382-384.

Westerlund, J.A. & Weisgraber, K.H. (1993) *J. Biol. Chem.* **268**, 15745-15750.

Wetterau, J.R., Aggerbeck, L.P., Rall, S.C., Jr., & Weisgraber, K.H. (1988) *J. Biol. Chem.* **263**, 6240-6248.

Williams, K.A., Farrow, N.A., Deber, C.M., Kay, L.E. (1996) *Biochemistry* **35**, 5145-5157.

Williamson, M.P. (1990) *Biopolymers* **29**, 1423-1431.

Williamson, M.P., Havel., T.F., & Wüthrich, K. (1985) *J. Mol. Biol.* **182**, 295-315.

Wilson, C., Wardell, M.R., Weisgraber, K.H., Mahley, R.W., & Agard, D.A. (1991) *Science* **252**, 1817-1822.

Wishart, D.S., Bigam, C.G., Holm, A., Hodges, R.S. & Sykes, B.D. (1995) *J. Biomol. NMR* **5**, 67-81.

Wishart, D.S., Sykes, B.D., & Richards, F.M. (1991) *J. Mol. Biol.* **222**, 311-333.

Wishart, D.S., Sykes, B.D., & Richards, F.M. (1992) *Biochemistry* **31**, 1647-1651.

Wolfe, S., Weaver, D.F., & Yang, K. (1988) *Can. J. Chem.* **66**, 2687-2702.

Wolkers, W.F., Haris, P.I., Pistorius, A.M., Chapman, D., Hemminga, M.A. (1995) *Biochemistry* **34**, 7825-7833.

Woody, R.W. (1995) *Methods Enzymol.* **246**, 34-71.

Wüthrich, K. (1986) *NMR of Proteins and Nucleic Acids*, Wiley, New York.

Wüthrich, K., Billeter, M., & Braun, W. (1983) *J. Mol. Biol.* **169**, 949-961.

Wüthrich, K., Billeter, M., & Braun, W. (1984) *J. Mol. Biol.* **180**, 715-740.

Yancey, P.G., Bielicki, J.K., Johnson, W.J., Lund-Katz, S., Palgunachari, M.N., Anantharamaiah, G.M., & Segrest, J.P. (1995) *Biochemistry* **34**, 7955-7965.

Yang, C.-Y., Chen, S.H., Gianturco, S.H., Bradley, W.A., Sparrow, J.T., Tanimura, M., Li, W.H., Sparrow, D.A., Deloof, H., & Rosseneu, M. (1986a) *Nature* **323**, 738-742.

Yang, C.Y., Gu, Z.W., Blanco-Vaca F., Gaskell, S.J., Yang, M., Massey, J.B., Gotto, A.M., Jr., & Pownall, H.J. (1994) *Biochemistry* **33**, 12451-12455.

Yang, C.-Y. & Pownall, H.J. (1992) in *Structure and Function of Apolipoproteins* (M. Rosseneu, Ed.), pp. 63-84, CRC Press, Boca Raton, Ann Arbor, London, Tokyo.

Yang, J.T., Wu, C.-S. C., & Martinez, H.M. (1986b) *Methods Enzymol.* **130**, 208-269.

Yang, Y.N.J., Treleaven, W.D. & Cushley, R.J. (1991) *Biochem. Int.* **25**, 1077-1086.

Yee, A.A., Babiuk, R., & O'Neil, J.D.J. (1995) *Biopolymers* **36**, 781-792.

Yuan, T., Mietzner, T.A., Montelaro, R.C., & Vogel, H.J. (1995) *Biochemistry* **34**, 10690-10696.

Yun, R.H., Anderson, A., & Hermans, J. (1991) *Proteins: Struct. Funct. Genet.* **10**, 219-228.

Zhang, L.-H., Kotite, L., & Havel, R.J. (1996) *J. Biol. Chem.* **271**, 1776-1783.

Zhang, Y.-P., Lewis, R.N.A.H., Henry, G.D., Sykes, B.D., Hodges, R.S., & McElhaney, R.N. (1995) *Biochemistry* **34**, 2348-2361.

Zhang, H., Zhao, D., Revington, M., Lee, W., Jia, X., Arrowsmith, C. & Jardetzky, O. (1994) *J. Mol. Biol.* **238**, 592-614 (The structure of 37 kD *trp* Repressor-Operator Complex).

Zhao, Y., Sparks, D.L., & Marcel, Y.L. (1996) *J. Biol. Chem.* **271**, 25145-25151.

Zhong, Q. (1992) *Ph.D. Thesis*, Simon Fraser University.

Zhong, Q., Clark-Lewis, I., & Cushley, R.J. (1994) *Pept. Res.* **7**, 99-106.

Zhou, N.E., Zhu, B.-Y., Sykes, B.D. & Hodges, R.S. (1992) J. Am. Chem. Soc. 114, 4320-4326.

Zubay, G. (1993) *Biochemistry,* Wm. C. Brown Publishers, Iowa, USA; Melbourne, Australia; Oxford, England.